ISSN 2071-4726
2071-0305

Инженерно-строительный журнал

НАУЧНОЕ ИЗДАНИЕ

№6(74) 2017

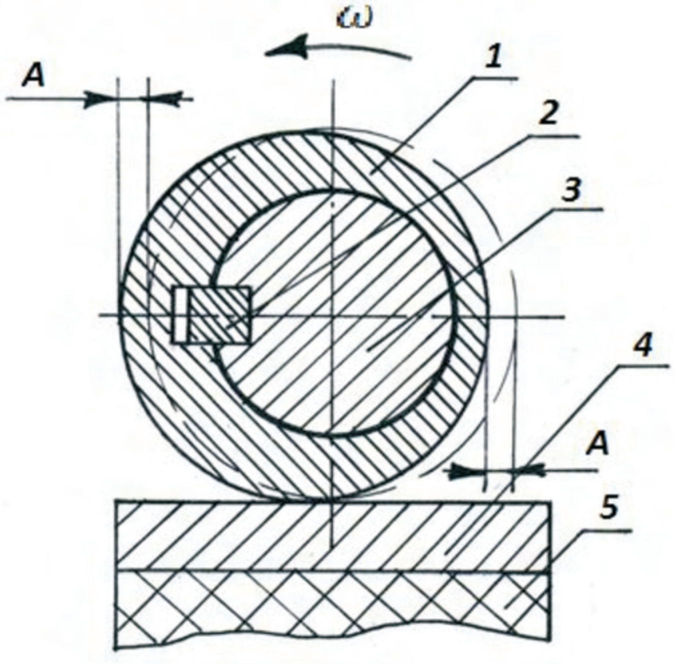

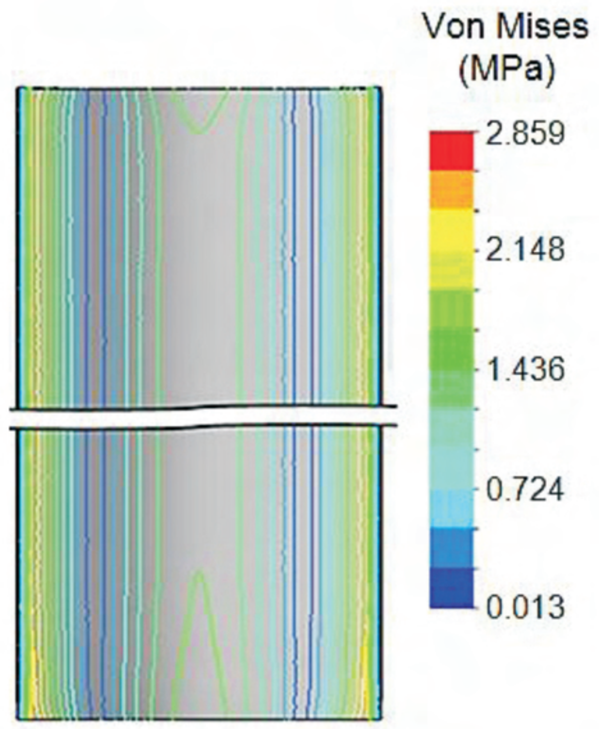

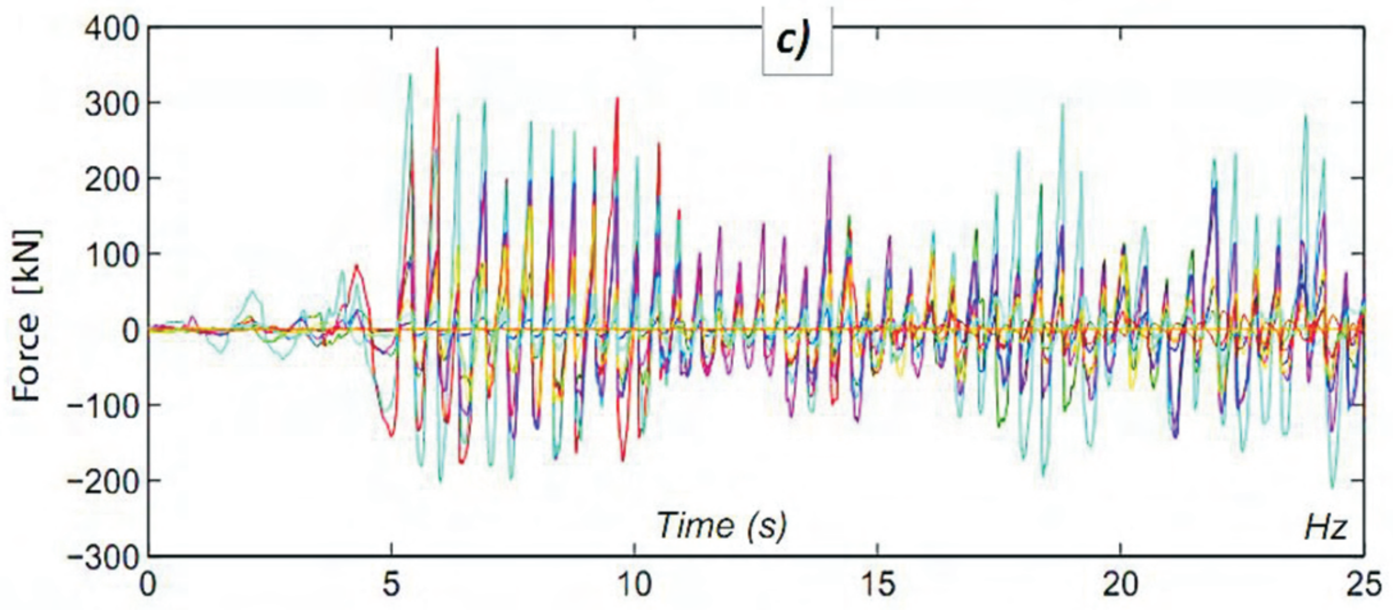

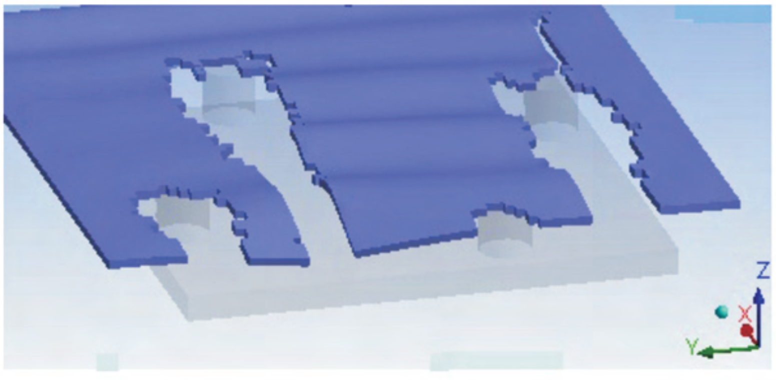

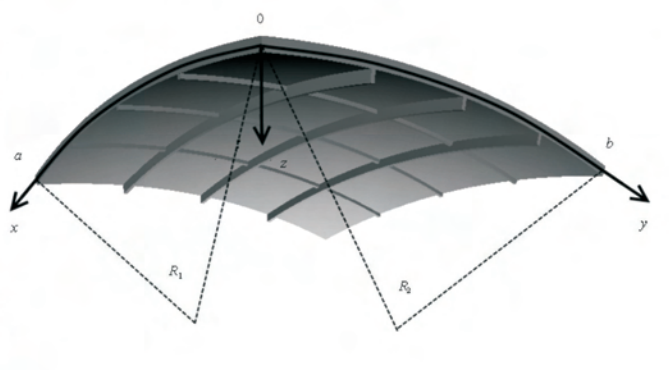

http://www.engstroy.spbstu.ru – полнотекстовая версия журнала в сети Интернет.
Бесплатный доступ, обновление с каждым новым выпуском

Инженерно-строительный журнал
НАУЧНОЕ ИЗДАНИЕ

ISSN 2071-4726, 2071-0305

Свидетельство о государственной регистрации: ПИ №ФС77-38070, выдано Роскомнадзором

Специализированный научный журнал. Выходит с 09.2008.

Включен в Перечень ведущих периодических изданий ВАК РФ

Периодичность: 8 раз в год

Учредитель и издатель:

Санкт-Петербургский политехнический университет Петра Великого

Адрес редакции:

195251, СПб, ул. Политехническая, д. 29, Гидрокорпус-2, ауд. 227А

Содержание

На обложке: иллюстрации авторов к статьям номера

Контакты:
Тел. +7(812)535-52-47 E-mail: mce@spbstu.ru
Web: http://www.engstroy.spbstu.ru

http://www.engstroy.spbstu.ru – full-text open-access version in Internet. It is updated immediately with each new issue.

Magazine of Civil Engineering
SCHOLAR JOURNAL

ISSN 2071-4726
Peer-reviewed scientific journal
Start date: 2008/09
8 issues per year

Publisher:
Peter the Great St. Petersburg Polytechnic University

Indexing:
Scopus, Russian Science Citation Index (WoS), Compendex, DOAJ, EBSCO, Google Academia, Index Copernicus, ProQuest, Ulrich's Serials Analysis System

Corresponding address:
227a Hydro Building, 29 Polytechnicheskaya st., Saint-Petersburg, 195251, Russia

Contents

On the cover: authors' illustrations

+7(812) 535-52-47
E-mail: mce@spbstu.ru
Web: http://www.engstroy.spbstu.ru/eng/index.html

doi: 10.18720/MCE.74.1

Strength and deformation characteristics of ash and slag mixture

Прочностные и деформационные характеристики золошлаковой смеси

V.V. Sirotyuk,
A.A. Lunev,
Siberian State Automobile and Highway University, Omsk, Russia

Д-р техн. наук, профессор В.В. Сиротюк,
аспирант А.А. Лунёв,
Сибирский государственный автомобильно-дорожный университет, Омск, Россия

Key words: ashes; construction; civil engineering; engineering properties; shear strength; embankments; leveling operation

Ключевые слова: золошлаковая смесь; строительство; гражданское строительство; деформационные характеристики; прочностные характеристики; земляное полотно; вертикальная планировка

Abstract. Burning of coal and brown coals at thermal power plants (TPP) is the main method of generating electric and heat energy in the Russian Federation. Inasmuch as a result of coal combustion a considerable amount of waste is produced (up to 50% of the whole mass of base coal) the quantity of the gained ash slag in a landfill is measured with hundreds of millions of tons. Insufficient level of knowledge about strength and deformation properties of these artificially-produced soils for building motor roads' roadbeds and embankments substantially limits the scope of using the ASM in the Russian Federation. In this connection, the purpose of the research is to study a complex of the ASM's engineering properties for evaluating its use as a soil material for building embankments of motor roads' roadbeds and leveling operations. In the frames of the research, there have been tested the ASM samples, obtained from burning Ekibastuz coal in boilers with dry ash removal. Samples were made with different density and humidity. For each density value, there were determined the modulus of deformation and the elastic modulus. The authors have determined the values of the angle of internal friction and specific cohesion of the ASM depending on the moisture and normal pressure. Consolidated and drained tests in triaxial compression devices have allowed to determine the values of the secant elastic modulusand the Poisson's ratio of the ASM's with different density. As a result, it was found that an increase in the ASM's density significantly increases the elastic and deformation modulus, the angle of internal friction, and the cohesion of this artificially-produced soil. However, after a certain degree of compaction, the cohesion value begins to decrease. Increasing the moisture content of the ASM samples decreases the modulus of elasticity and general deformation, but it has an ambiguous effect on the angle of internal friction and cohesion.

Аннотация. Сжигание каменных и бурых углей на тепловых электростанциях (ТЭС, ТЭЦ) является основным способом генерации электрической и тепловой энергии в Российской Федерации. Поскольку в результате сгорания угля, образуется большое количество отходов (до 50% от массы исходного угла), объем накопленных в отвалах золошлаков, измеряется сотнями миллионов тонн. Недостаточный уровень знаний о прочностных и деформационных свойствах золошлаковых смесей (ЗШС) при сооружении земляного полотна автомобильных дорог и планировочных насыпей существенно ограничивает сферу применения ЗШС в РФ. В связи с этим, целью исследования является изучение комплекса инженерных свойств ЗШС для оценки их применения в качестве грунтового материала для возведения насыпей земляного полотна автомобильных дорог и вертикальных планировок. В рамках исследования проведены испытания образцов ЗШС от сжигания Экибастузских каменных углей в котлах с сухим шлакоудалением. Образцы изготавливали с различной плотностью и влажностью. Для каждого значения плотности определен модуль общей деформации на приборе компрессионного сжатия и модуль упругости по адаптированной методике рычажного пресса. Определены значения угла внутреннего трения и удельного сцепления ЗШС в зависимости от влажности и нормального давления с применением метода одноплоскостного прямого (медленного) среза. Консолидированно-дренированные

Сиротюк В.В., Лунёв А.А. Прочностные и деформационные характеристики золошлаковой смеси // Инженерно-строительный журнал. 2017. № 6(74). С. 3–16.

испытания в приборах трехосного сжатия позволили определить значения секущего модуля упругости и коэффициента Пуассона при значениях плотности. В результате установлено, что увеличение плотности ЗШС существенно повышает модуль упругости и деформации, угол внутреннего трения и сцепление этого техногенного грунта. Однако после определенной степени уплотнения начинается снижение величины сцепления. Увеличение влажности образцов ЗШС понижает модуль упругости и общей деформации, но имеет неоднозначное влияние на угол внутреннего трения и сцепление.

Introduction

The vast majority of thermal power plants (TPP) in the Siberian and Far Eastern Federal Districts, some TPP in the European part of Russia are coal and brown coal-fired and more over, this tendency will have been sustaining for decades. From 10 % to 50 % of ash and slag wastes (ASW) are formed, including finely dispersed fly ash and ash-and-slag mixture (ASM), when burning each ton of coal. Ash and slag are jointly transported to ash dumps, forming the ASM. Almost 1.6 billion tons of the ASM have been accumulated on the territory of the Russian Federation. Only in the city of Omsk, about 73 million tons of the ASM have been accumulated and this figure increases by an additional 1.6 million tons annually.

But another problem is escalating in cosmopolitan cities: hundreds of millions of cubic meters of soil are required to construct an earth roadbed, a layout road embankment, to correct in arable and highly cost rural lands.

The use of the ASW is possible in many industries. This is production of rare-earth elements, creation of composites using fly ash, soil melioration, production of ceramic products and bricks, catalysis and, of course, in the construction industry [1–3]. Among the listed methods of recycling, the large-tonnage use of the ASM for building embankments is the most prospective since it allows solving both problems mentioned above with low additional cost.

Publications [4–8] reflect studies confirming the possibility of building motor roads' embankments of the ASM. The main obstacle, hampering the full-scale use of the ASM, is insufficient knowledge base of their physical and mechanical properties, strength and deformation characteristics when changing humidity and density for designing engineering structures.

Studies of the fly ash's mechanical properties abroad were carried out in 1972 by A.M. DiGioia and W.L. Nuzzo. During experiments, they conducted tests on direct cut and triaxial compression devices at different dry soil densities (from 60 to 80 pounds per cubic foot). The influence of vibrational loads of different frequencies on the ash compactibility was also investigated. However, these studies were typical not for dump ash and slag, but for the fly ash of western Pennsylvania. In addition, the study did not investigate the influence of moisture on the material's properties [9].

The studies of Gray and Lin (1972) focus on the dependence of the particles' shape, granulometric and chemical composition on the change of the specific weight of coal ash and its effect on strength characteristics of the material. The results of this researching cannot be fully used widespread because the ash from Michigan state was tasted which has much higher concentration of free lime than in inert ash of Russia [10]. Like Gray and Lin, B. Indraratna et al. (1990) in their paper [11] studied granulometric and mineralogical compositions, pozzolanic properties, compactibility and strength characteristics of C class ashes, selected from the Mae Moh power plant in northern Thailand.

In our experiments we have taken into consideration the researching by J.P. Martin [12] for fly ash of F class (non-cement) for evaluating of their use in a road embankment. The article evaluates the shear strength, compressibility, water-permeability and compactibility of the ASM in comparison with earlier works of other authors.

Singh and Panda (1996), having tested the strength characteristics on freshly compacted samples with different moisture, concluded, that the main part of the shear resistance is due to the angle of shear resistance [13].

The justification of stability for a road embankment which was made from ASM was made by R. Ossowski и K. Gwizdala [14] on the basis of the results of monitoring of an experimental road embankment subject to flooding. And also the parameters for these materials were taken from the results of their coworkers` researchings by Dredg Dikes, L. Balochowski Z. Sikora [15], and the rest – from the work by Ossowski и Sikora[16].

N.S. Pandian did research of ASM, clinker and flue ash under various conditions using three-axis compression. He considers that cohesion in ASM appears only in thick and humid mixture and disappears at water saturation or destruction of compact structure [17]. The results of sample testing with various ash combination and clinker are also displayed in the article by B. Kim et al. [18].

S.K. Pal and A. Ghost investigated the shear strength of the ASM samples, selected from nine TPP. The tests were carried out in triaxial compression devices according to the scheme of unconsolidated-undrained test [19]. The strength characteristics of the ASM in three-axis compression devices were also evaluated by Jakka et al. In these experiments, the ASM from three different sources have been tested in a friable and compacted state, which makes it impossible to predict the roadbed's stability under real operating conditions [20].

The work of S.K. Tiwari reflects the influence of water saturation of samples, designed in a laboratory, on their strength characteristics. The author has stated that the ASM's strength did not decrease to zero as in Pandian's experiments [21].

Studies of the physical and mechanical properties of the ASW and directions of their effective utilization have been intensively developed in Russia in the 1970–80s. Complex studies of ash and slag, conducted in the SouzDorNii, SibADI, Giprodornia, and the scientific centers of Belarus, Ukraine, Kazakhstan and Uzbekistan are reflected in the construction standards VSN 185-75. The requirements for the ASM for building a roadbed in this first document were limited only to the amount of frost heaving. The calculated strength and deformation parameters of the ASM are absent there.

In 1978 the article [22] was published in which V.A. Melentjev and others summarized the considerable amount of information about the properties of ASM of various CHPs. This is review paper which poorly takes into account the problems of using the ASM as artificially-produced soils.

Information on the ASM mechanical properties, depending on the moisture and porosity of this material, is presented in the work of P.Y. Dyakonov [23]. However, as in other authors` works, the limited amount of researching gives no opportunity to draw a conclusion upon the dependency for different conditions of earth roadbed maintenance.

Specialists from TSUAB, M.V. Balyura and V.V. Fursov , have analyzed the physical and mechanical properties of the ASM from the dumps of the Tomsk state district power plant (SDPP)-2, Severskaya TPP, Kemerovskaya TPP, Novokemerovskaya TPP [8,24]. These studies had a dotted character, without an analysis of cause-effect relationships. Therefore, it is impossible to determine reliable calculated parameters for designing embankments of the ASM on their basis.

Some strength properties of the ASM from the dump of the Kashirskaya SDPP - 4, which we used to calculate the stability of high embankments at the traffic junction near Kashira, Moscow Region, were investigated in the laboratory of the geological department of the Moscow State University [6].

The researching of ASM as man-made soils has been conducted in SibADI since 1973. These data and also some results of other researching in the Russian Federation and abroad were reflected in the road construction standard (218.2.031-2013) which is the principal document regulating the use of ASM in road construction of the Russian Federation nowadays. The calculating rates of durability and deformation figures, shown in the road construction standard have been deliberately underestimated because of the limited data during the development of this document. Therefore, when designing the ASM embankments only on the basis of the data from this document, a significant and sometimes unreasonably inflated margin of safety is possible.

Attempts to use foreign and domestic data on the strength and deformation parameters of the ASM during the elaboration of the above mentioned normative and guidance document have failed to give positive results due to a number of reasons:

- the majority of publications do not contain the necessary information on the methods for determining the indicators that interest us;
- methods of the ASM testing are so diverse that they often do not allow to compare the results obtained;
- the majority of publications do not reflect the entire range of the ASM's mechanical properties in the range of possible impact of natural factors, that change during the operation of motor roads in the Russian Federation;
- all mechanical properties of ASM depend on technique of burning coal and his genesis and for coal ash which was formed after combustion Ekibastuz coal similar research was not carried out;

– the authors of some publications do not give specific data on test results.

Therefore, the purpose of the research is to study a complex of the ASM's engineering properties for assessing their use as a soil material for building embankments of motor roads' roadbeds and leveling operations.

Methods

In the frames of the research, there was prepared a test program, which included a series of one-factor experiments. The choice of experimental conditions reflected the most probable embankments' states in the process of their operation throughout the life cycle. The research program is presented in the Table 1.

Table 1. Test program

Series number	Changing parameter of the ASM	Range of change	Value of unchangeable parameter	Purpose of a series of experiments
1	Density of a maximum dry density	90 %–105 %	optimal moisture	to determine the regularities of changing the ASM mechanical properties depending on moisture and compaction degree
2	moisture	12 %–33 % (total saturation)	MDD – 95 %	

Before producing the samples, the value of maximum dry soil's density and optimal moisture of the ASM were determined. For these purposes, there was used a form of a large device for standard compaction of the SoyuzDorNii design, which is an analogue of the testing form by Proctor's method.

Research of strength characteristics of the ASM was performed on the direct cut devices PSG-3M in accordance with the technique, similar to the method of ASTM D3080. Samples of the ASM were formed in a large device for standard compaction, varying the degree of compaction by the number of weight impacts. When achieving the required value of density, a ring, with 40 cm^2 cross-section, was pressed into the ASM for the direct cut test in the PSG-3M device.

The tests were carried out according to the scheme of consolidated and drained cut of artificial composition's samples. The experiments were carried out by successive shearing of the samples at three vertical load stages of 100, 200, 300 kPa. The samples' manufacture was originally conducted with the moisture of 33 % (maximum water saturation). The prepared sample at the optimum moisture was placed in a direct cut device, a load of 50 kPa was applied to it, after that 10 ml of water was poured into the top part until it appeared from the lower part of the sample.

The determination of the ASM's deformation modulus was carried out on compression devices KPr-1M. Samples were made in a manner similar to the method of manufacturing samples for direct cut tests. After manufacture, circular samples with a diameter of 87.4 mm and a height of 25 mm were placed in a compression device (not allowing lateral expansion), both sides were interleaved with filter paper, indicators of vertical displacement were installed and pressure stages of 100, 200, 300 kPa were successively applied. After each loading, vertical settling was expected and fixed. Upon reaching the 300 kPa stage and stabilizing the settling, a stepped unloading of the sample was carried out with the control of elastic deformations. After the load was removed, the load was repeated similarly to one at the beginning of the experiment. Abroad, a similar test method is described in ASTM D 2435-04 and is a remote analogue of compression tests.

The dependence of the ASM's elastic modulus on the degree of moisture and compaction was determined using the method of the lever press. The compaction of the sample in a form was implemented with a weight from a large standard compaction device. The form for testing had a height of 150 mm and internal diameter of 150 mm. Since the diameter of the form was bigger than the diameter of the anvil, the soil was compacted layer by layer, moving the anvil according to the scheme, used in "A" test of Proctor's method.

The soil was compacted into three layers, each layer was compacted with a number of impacts predetermined during pre-compaction. The finished sample was cut up to the brims of the form, a stamp with a diameter of 50 mm was placed on the center of the sample's surface. Further, a stepwise load application was carried out through a stamp of 0 to 500 kPa at 100 kPa interval. After stabilizing the settlings at each stage, the stamp's settling was fixed by means of two time-type sensors. Stepwise unloading of the sample was carried out with the interval of 100 kPa with the control of deformation restoration. Then the sample was loaded again. If the branch of the compression curve of unloading and secondary loading coincided, the tests were terminated. The closest analogue of this method in foreign practice is the method for determining CBR, described in ASTM D1883-16 (this standard uses only the primary loading branch and the kinematic loading scheme).

Testing of the ASM for triaxial compression was carried in triaxial compression devices ASIS. The samples production was carried out by forming the soil's monolith in a large device for standard compaction and subsequent plugging of a cylinder into the massif (Fig. 1a). Density and moisture control was carried out by weighing a form, filled with soil, and sampling for determining moisture.

a. 

b. 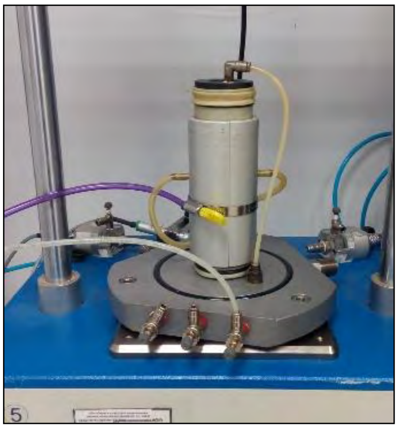

Figure 1. Testing of the ASM in the triaxial compression device:
a – a cylinder plugged into the massif; b – a rubber-covered sample

The extracted sample, with the diameter of 50 mm and the height of 100 mm was covered in a hermetically sealed rubber (Fig. 1b), then there was installed a camera of the device which was filled with distilled deaerated water and lateral pressure was fed. In the frames of the experiment, the tests were carried out only at the lateral pressure of 100 kPa, which was required to determine the Poisson's ratio and the secant elastic modulus, with a relatively low lateral pressure. Determination of characteristics was carried out on a consolidated and drained scheme, which is almost similar to ASTM D7181-11 tests.

Results and Discussion

The peculiarities of the ASM structure. The optimal moisture of the ASM and the maximum dry soil's density were determined before testing the samples (Fig. 2).

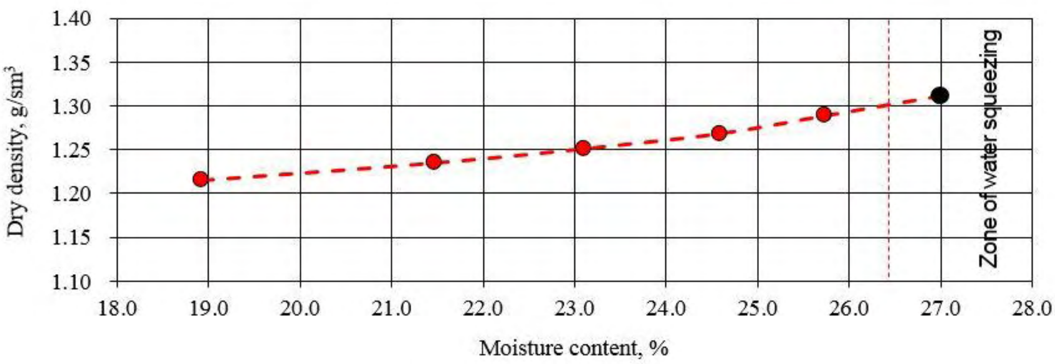

Figure 2. Dependence of the dry soil's density (the ASM) on moisture

The graph of standard compaction of the ASM usually does not have an extremum, characteristic for clay soils (similar data given in the works of Pandian, Jakka, Balachowski, Tiwary [12, 17, 19, 20]). As Singh et al. recommended, the concept of optimum moisture for this artificially-produced soil is assigned by the limiting value of the density to the zone of water squeezing [13].

The analysis of the curve in Figure 2 indicates that the change in the ASM's density indicator does not exceed 7 % with a change in moisture by 42 %, therefore, this artificially-produced soil has a wide interval of possible moisture for compaction. The value of optimal moisture for the ASM is twice and more times higher than the similar parameter for pulverscent sands and light sandy loams, although the granulometric composition of these natural soils and the ASM has similar features [7, 17]. The abnormally high values of water absorption of the ASM are explained by the peculiarities of their microstructure, that is confirmed by Kim at al [18].

Unlike most natural dispersed soils, the real value of the ASM’s specific surface doesn’t have direct relation with granulometric composition. Particles of the grinded "barren rock" of the soil (entered in coal) are subjected to the thermal effect, passing through the flame of a boiler unit, having the temperature of 1400-1600 C^o. These particles undergo a stage of pyroplastic state with emitting a complex gaseous phase. Therefore, the ash particles have significant microporosity (Fig. 3, microphotographs are made in LLC "Institute of Applied Ecology and Hygiene").

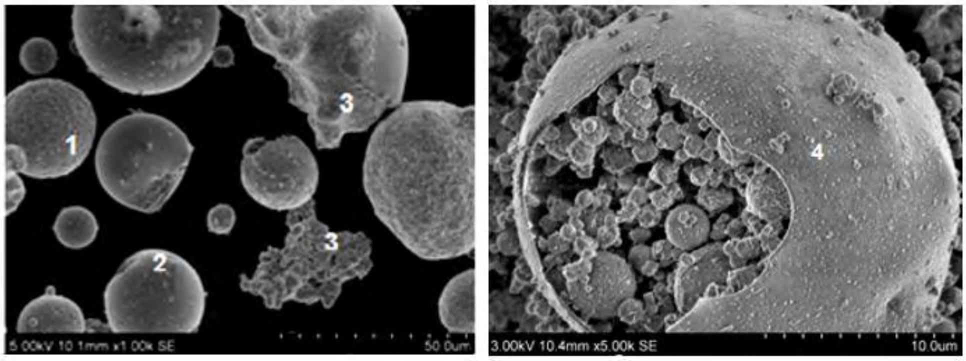

Figure 3. Morphological elements of ash: spheres with a rough and grumous surface (1); with a smooth and vitrified surface (2); fragments of particles and aggregates of irregular shape (3); pleurosphere with a broken shell (4)

According to our data, the specific surface of the ASM, determined by the standard air-permeability method, varies from 0.8 to 2.5 thousand cm^2/g (fly ash – up to 6.0 thousand cm^2/g), depending on the sampling site in ash dump. The presence of open and closed microporosity is the reason that the value of the actual specific surface of ash particles (determined by the method of low-temperature adsorption of nitrogen or desorption of argon) reaches 50,000 cm^2/g and more. In the work [25], Zabielska-Adamska gives a reference to studies that indicate the high adsorption capacity of the ASM, which is related to the value of the specific surface.

A significant value of the specific surface area of highly dispersed ash particles is the main reason for the abnormally high water retentivity of all ash and slag, whichis confirmed at the work of Huang [26]. The same reason explains the comparatively small value of the bulk density of the ASM, which usually varies from 0.8 to 1.3 g / cc. Although, the true density of vitreous substance of ash particles reaches 2.5-3.2 g /cc.

Strength parameters. The forces separation of soils shear strength on the forces of internal friction and cohesion is conditional. In the process of shear, it is impossible to purely separate elements, associated with the deformation of water films, overcoming the forces of molecular interaction, mutual blocking and mechanical engagement of particles. Consequently, it is not always possible to establish the exact mathematical dependencies of changing these parameters.

The generally accepted strength parameters of soils - the angle of internal friction φ and the specific cohesion c are not true in these engineering experiments, but the apparent cohesion and the angle of shear resistance, which have been determined by many researches in their works [11, 12, 17]. Nevertheless, these conditional values are accepted as the main criteria for calculating soil structures. The φ and c values are calculated by plotting a straight line with the best approximation to experimental points by the least squares method. Figure 4 shows the results of determining the angle of internal friction, specific cohesion and general shear resistance in the samples of the ASM, depending on the compaction coefficient.

It follows from the graphs that the density of the ASM has a significant effect on the strength characteristics of this artificially-produced soil. As Huang describes, with increasing density, the particles are increasingly getting closer, the number of contacts, jamming and blocking depth of separate particles is growing [26]. Thus, with increasing density, the angle of friction will be higher because of more jamming and blocking. The cohesion decreases with an increase of the ASM’s compaction coefficient from 1.0 to 1.05. The similar effect is considered by Padam in his thesis. In his experiments, when the work on compaction increases the cohesion value also decreases [27]. Presumably, this is explained by the destruction of large porous aggregates of the ASM, occurring during compaction, which has been described earlier by Kim et al. and observed by us (Figure 5).

When the work on compaction increases, the arising contact stresses destroy the mechanical linkages of the ASM's particles, as it happens in sands and is described by Roberts и De Souza [28], and reduce this component of resistance to shear. At the same time, there is maintained the cohesion caused by the interaction of water films around the particles and described by Martin et al. [12].

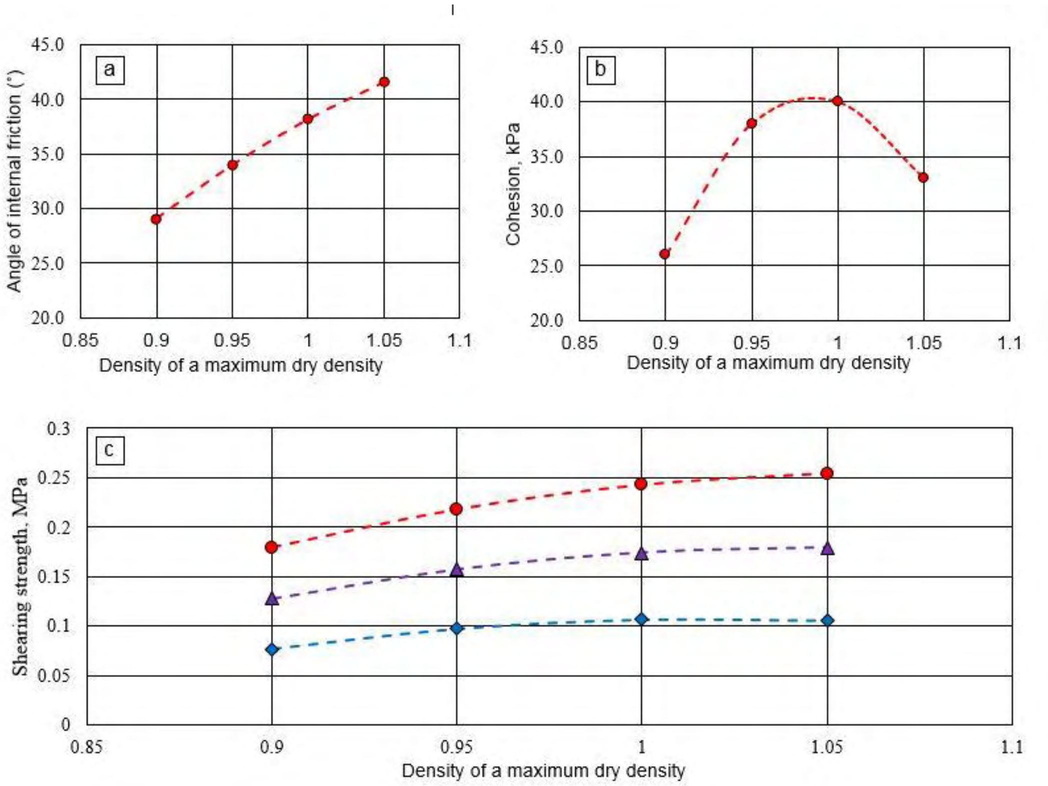

Figure 4. Dependences of the angle of internal friction (a), specific cohesion (b) and shear strength (c) from the compaction coefficient. Shear strength at normal pressure: ◆–100 kPa; ▲– 200 kPa; ■– 300 kPa

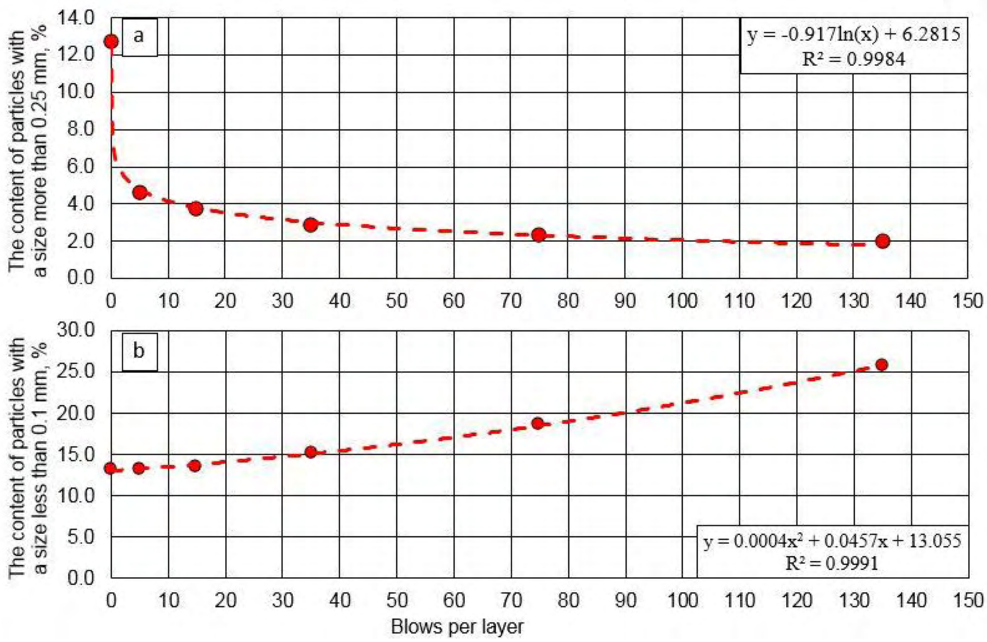

Figure 5. Content change of the fraction with the size over 0.25 mm (a) and less than 0.1 mm (b) during the ASM compaction

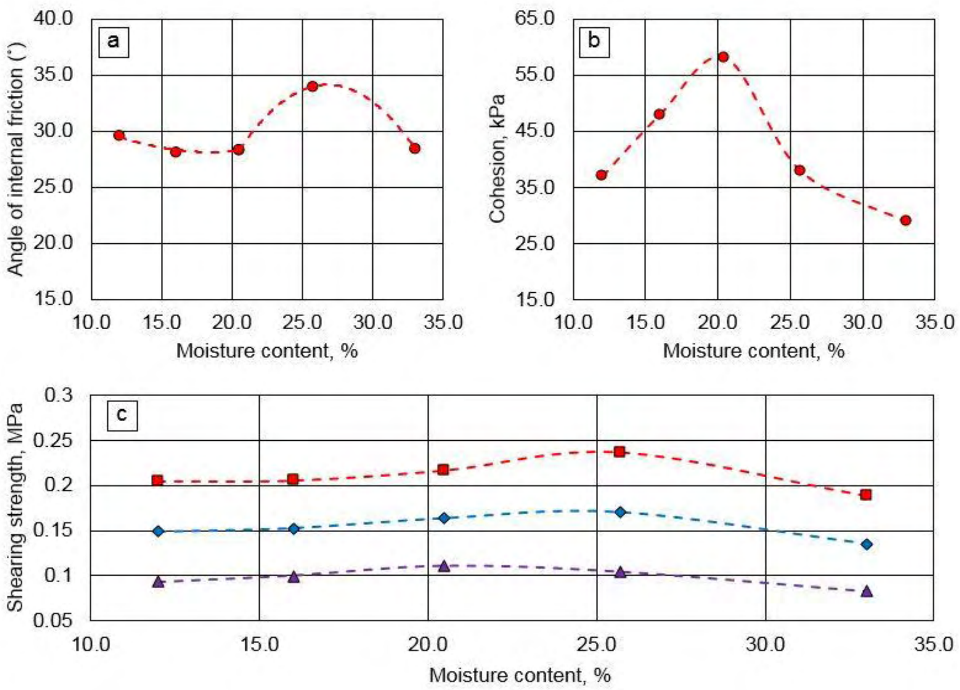

Figure 6. Dependences of the angle of internal friction (a), cohesion (b) and shear strength (c) on moisture. Shear strength at normal pressure: ▲–100 kPa, ◆ – 200 kPa, ■– 300 kPa

The tests of the ASM with different moisture were carried out at 0.95 compaction coefficient, which usually corresponds to the so-called common soil density. At the same time, the moisture of a roadbed can vary over a life cycle within a wide range. The maximum moisture value of 33 % corresponds to the total water saturation of the ASM at a normal pressure of 100 kPa. Figure 6 shows the results of determining the ASM strength characteristics depending on its moisture.

During multiple testing of samples with different moisture, there have been obtained non-standard dependences of changing the angle of internal friction on moisture. As in the experiments of Lamb et al. the maximum shear strength was obtained at optimal moisture of the ASM [29]. On the whole, it has been determined that shearing stresses, necessary for the destruction of the sample, increase with a rise of moisture up to the optimal value.

It is known from the work of DiGioia and Nuzzo that the most part of shear strength the ASM has in wet condition [9]. Strengthening of water films' confining force when the moisture increases is apparently explains the increase of cohesion with the same degree of compaction. After the appearance of redundant moisture (20.5 %), the cohesion decreases. At total saturation the value of cohesion and general shear resistance was minimal, as in Pandian's experiments [17]. The values' intervalsof the angle of internal friction and cohesion do not fall outside the limits, obtained by Pal et al. [19].

Besides two strength parameters in calculations using software complexes for modeling, based on finite elements method (Mohr-Coulomb, Drucker-Prager, Herdering soil), an additional parameter, the dilatancy angle (ψ) [30-33], is introduced. For the approximate dilatancy angle determination there is used an empirical dependence which links this parameter to the angle of internal friction: $\psi \approx \varphi - 30°$. At a value of φ less than 30°, the dilatancy angle is equated to zero [34].

Strength parameters of the ASM, determined by the results of the research, are presented in the Table 2.

Table 2. Strength parameters of the ASM

Parameters	Influencing factors and their values								
	Density of a maximum dry density				Moisture, % by mass				
	0.90	0.95	1.00	1.05	12.0	16.0	20.5	25.7	33.0
Angle of internal friction, degree	29.1 26.4	34.0 29.8	38.2 35.8	41.6 40.4	29.6 27.7	28.2 26.5	28.3 26.1	34.0 29.8	28.4 24.9
Specific cohesion, kPa	26 24	38 33	40 37	33 32	37 35	48 45	58 54	38 33	29 26
Dilatancy angle, degree	0	4	8.2	10.2	0	0	0	4	0
Note: standard value of the parameter is above the line, calculated value of the parameter is under the line, considering processing by methods of mathematical statistics.									

The strength parameters of the ASM, determined by us, have been compared with natural soils prevailing in the SFD (numerical values of the natural soil parameters are not presented due to limitations in the volume of publication). A comparison has showed that the ASM is an artificially-produced soil, which is not inferior in strength parameters to natural soils. Moreover, the ASM is superior to the most part of natural sediments on shear strength.

Deformation parameters. The main characteristics of the soils compressibility are the general deformation modulus $E_{general}$, the elastic modulus E and the coefficient of lateral expansion (Poisson's ratio) *v*. Both moduli are parameters of the stress diagram – deformation, and as a rough approximation, represent the proportionality coefficient of this dependence at the required stress level. The differences are that the elastic modulus describes only elastic (restoring) deformations, and the general deformation modulus – both elastic and plastic.

Figure 7 shows the results of determining deformation modulus of the ASM samples in the compression device, depending on the compaction coefficient and moisture content of this material.

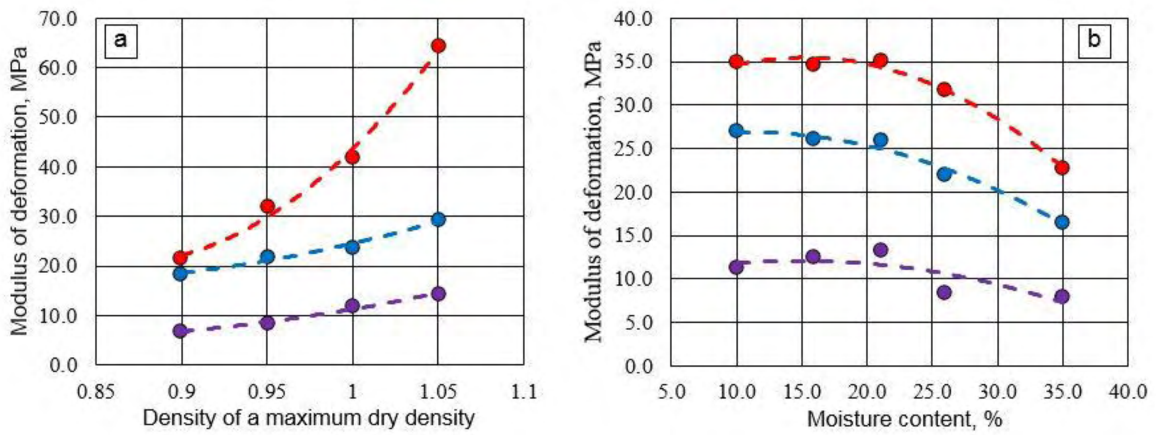

Figure 7. Dependence of the deformation modulus of the ASM on the compaction coefficient (a) and moisture (b), at normal pressure: ▲–100 kPa; ◆ – 200 kPa; ■– 300 kPA

The graph (Fig. 7a) shows a significant growth of the deformation modulus at increase of the density of a soil skeleton. A quick increase of the modulus under the conditions of the compression device at the pressure of 300 kPa is connected with a state of soil in which there is no particles repacking due to slip of aggregates, and the settling can be explained by the destruction of particles tightly clamped in their positions. Such changes in the ASM's structure have been described earlier by Kim at al. [18].

The results of the research (Fig. 7b) indicate a decrease of the constrained modulus of deformation with an increase of the ASM moisture. When increasing the moisture, the water expands the particles, which weakens the structure of the ASM. The results of testing the ASM, considering the statistical processing, are shown in the Table 3.

Table 3. The modulus of the ASM deformation

The deformation modulus at normal pressure	Influencing factors and their values								
	Density of a maximum dry density				Moisture, % by mass				
	0.90	0.95	1.00	1.05	10.0	16.0	20.5	25.7	33.0
100 kPa	6.79 5.93	8.46 7.16	11.86 8.30	14.25 13.74	11.35 10.95	12.52 11.99	13.28 12.33	8.46 7.16	7.81 6.22
200 kPa	18.30 17.50	20.92 17.89	23.75 18.93	29.22 27.64	26.86 25.14	26.10 25.13	25.91 24.94	20.92 17.89	16.44 15.88
300 kPA	21.53 19.76	31.66 27.14	41.81 38.24	64.11 63.84	34.92 32.85	34.55 32.53	35.04 33.30	31.66 26.15	22.73 22.05
Note: standard value of the parameter is above the line, calculated value of the parameter is under the line, considering processing using the methods of mathematical statistics.									

Determination of the elastic modulus was carried out with the replacement of the lever press for the universal machine AL-7000LA10, which makes it possible to apply a stepped static load to the deformable sample. The regularities of changing values of the elastic modulus of the ASM depending on the compaction coefficient are shown in Figure 8a, and on the moisture – in Figure 8b.

The method of testing stipulated the soil behavior under normal compaction. In the process of compaction, a more compact packing of particles occurred due to local shears and slipping of smaller particles into the soil pores, which further has strengthened its skeleton. In the compacted state the soil works in the stage of reversible deformations and the shears are practically attenuated. The higher the compaction coefficient, the more compact structure of the soil skeleton is formed in the sample, which means that the load distributes to a bigger number of contact points. Besides the increase the structural strength, it reduces the overall deformability of the material; this has determined the growth of the elastic modulus [20].

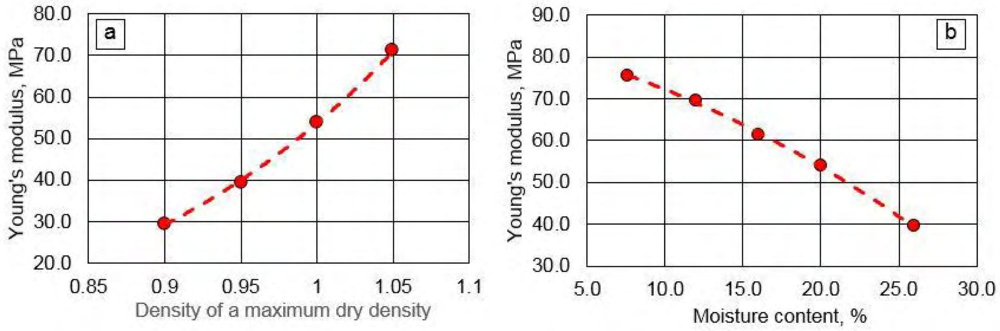

Figure 8. Dependence of the elastic modulus of the ASM on the compaction coefficient (a) and moisture (b)

In contrast to compaction, an increase of soil moisture causes decompression of the skeleton. The higher the moisture, the stronger the negative effect, up to the full moisture capacity at which the effect of particles weighing is created. The direct contacts of the ASM particles decrease, and the existing neutral stress finally decompresses the soil.

It is difficult to compare the results of studies on determining the compression and elastic moduli due to the absence of this method in foreign studies of the ASM. However, there are studies in which the elastic modulus is related to the Californiabearing ratio (CBR) [35]. It is known, that the elastic and deformation moduli can be related by means of the linear dependence [36].

Toth et al. [37] writes that the CBR value of water-saturated samples varies from 6.8 % to 13.5 %, while unsaturated - from 10.8 % to 15.4 %. This indicates a significant decrease in the bearing capacity for the water saturation of ash and slag, which we see in our experiments. Pandian investigated the CBR of waste slag, fly ash and fuel slag with water saturation and without saturation. In his experiments, there is also noted a decrease in the bearing capacity up to two times of waste slag with water saturation, which agrees with our experiments at different moisture content of the ASM [17].

In the framework of the study, we compared the basic deformation parameter - deformation modulus of the ASM with characteristics of natural soils. A comparison showed that the ASM also is not inferior to most natural clay soils in the deformation modulus's value, competing with sandy soils.

The results of our researching show that ASM complies to the medium-formed soils (according to the Russian classification), whereas the results of Martin et al`s experiments display that it was classified as low-compressible (with high stiffness) soil [12].

Tests on triaxial compression devices were carried out on a consolidated and drained scheme, in the "A" type stabilometer at the lateral pressure of 100 kPa. Deformations, chamber pressure and pore pressure were fixed by sensors of the ASIS complex. The vertical pressure stages and the deformation stabilization's time were chosen as for pulverscent sands.

In the frames of stabilometric tests, there was determined a secant modulus of deformation which is necessary indicator for soils modeling using the Hardening Soil model. This indicator is a modulus of soil deformation at half of value of the stress deviator at the moment of destruction [34]. The test results are shown in the Table 4.

Table 4. Results of determining a secant elastic modulus of the ASM

Compaction coefficient	0.90	0.95	1.00
The secant elastic modulus, E_{50}, MPa	11.26	13.23	13.89

Besides the secant modulus of deformation, there was determined the deformation modulus at different value of the vertical pressure (Fig. 9).

In contrast to the method for determining the compression modulus of deformation in the triaxial compression device, the reaction pressure from the lateral surfaces does not increase with a growth of normal pressure, as the soil sample can be expanded. Therefore, with the increase of pressure on the sample, the soil structure is rebuilt, new local shears occur, until there is reached a state of soil's fluidity and its subsequent destruction.

The character of the samples destruction with different compaction also differs. When the compaction coefficient is less than 1.0, the deformation occurs with destruction in the form of a "barrel", and more compact samples are destroyed otherwise - in the form of a shear plane. This indicates a stronger, but brittle structure whose properties are determined, apparently, by the mechanical contacts of the particles [38]. Despite the brittle nature of the destruction, the lateral expansion of the sample to the stage of destruction occurs more intensively. Probably, this is due to the large pore sizes in the structure of the less compacted ASM. These pores are filled at local shears above all, which prevents intensive lateral expansion.

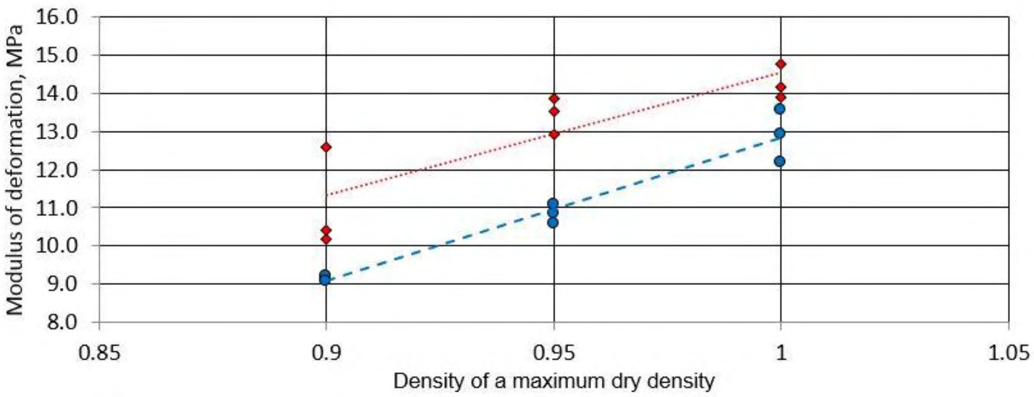

Figure 9. Dependences of the deformation modulus of the ASM on the compaction coefficient at the pressure of: ◆–100 kPa; ●– 200 kPa

The value of the Poisson's ratio for the ASM is determined experimentally and is presented in the Table 5.

Table 5. Results of determining Poisson's ratio

Compaction coefficient	0.90	0.95	1.00
Poisson's ratio	0.094	0.133	0.167

Conclusions

The conducted studies have shown that the ASM is an artificially-produced soil with specific mechanical properties. Thus, the graph of the standard ASM’s compaction shows the absence of clear maxima on the curve, which is typical for sandy soils. At the same time, according to the parameters of mechanical properties and regularities of their variation, the ASM does not refer to non-cohesive soils, as it has been previously thought, but more corresponds to sandy loams or pulverscent sands.

The growth of the ASM skeleton’s density causes an increase of the massif’s strength only until the maximum density of the dry soil is reached and almost does not increase in future. Therefore, the overconsolidation of the ASM for the majority of geotechnical tasks is not advisable.

This artificially-produced soil is resistant to moisture. The shear strength of the ASM is maximal at the moisture close to the optimal, and even at the moisture, corresponding to the maximum moisture capacity, remains at a high level. The deformation parameters of the ASM depend on the density of this soil, and an increase in density by 1 % from MDD gives an increase in the elastic modulus from 2.7 %, and in the deformation modulus from 0.5 MPa to 2.8 MPa, depending on the vertical load. The ASM’s moisture influences the deformation parameters a bit less than the density, with an increase in moisture by 1 % the elastic modulus decreases by an average of 1.9 MPa and the deformation modulus by 0.5 MPa. At the moisture of total saturation, the elastic and deformation moduli have the smallest values.

Comparison of the deformation moduli of natural soils and the ASM shows, that this artificially-produced soil is not inferior on this parameter to natural clay andpulverescent soils and competes with sandy soils.

As a result of the tests it has been found that the ASM after Ekibastuz coal combustion is a ground building material with deformation and strength characteristics that are quite suitable for building a roadbed of motor roads, as well as installing foundations of buildings and structures of any importance class.

Acknowledgement

The research was supported by the Russian Foundation for Basic Research (grant no. 16-48-550508 p_a). Scientific research was carried out from budget resources of the Omsk Region.

References

1. Folgueras M.B., Alonso M., Fernández F.J. Coal and sewage sludge ashes as sources of rare earth elements. *Fuel.* 2017. Vol. 192. Pp. 128-139.
2. Vatin N.I., Petrosov D.V., Kalachev A.I., Lakhtinen P. Use of ashes and ash-and-slad wastes in construction. *Magazine of Civil Engineering.* 2011. No. 4. Pp. 16-21. (rus)
3. Lichman N.V. The use of Norilsk region's sulfur and hes ash for hydraulic engineering and reconstruction. *Magazine of Civil Engineering.* 2011. NO 8. Pp. 29-34. (rus)
4. Haleema A., Luthrab S., Mannana B., Khuranaa S., Kumarc S. Critical factors for the successful usage of fly ash in roads & bridges and embankments: Analyzing Indian perspective. *Resources Policy.* 2016. Vol. 49. Pp. 334-348.
5. Hadbaatar A., Mashkin N.A., Stenina N.G. Study of Ash-Slag Wastes of Electric Power Plants of Mongolia Applied to their Utilization in Road Construction. *Procedia Engineering.* 2016. Vol. 150. Pp. 1558-1562.
6. Sirotyuk V.V., Lunev A.A., Ivanov E.V. Zoloshlakovaya smes' dlya zemlyanogo polotna [Coal ash and slag for road embankments]. *Avtomobil'nye dorogi.* 2016. No. 6. Pp. 72-79. (rus)
7. Ivanov E.V. *Obosnovanie primeneniya zoloshlakovykh smesey dlya stroitel'stva zemlyanogo polotna s uchetom vodno-teplovogo rezhima* [Rationale for the use of ash-and-slag mixtures for construction of subgrade with the water-heat regime]. Omsk, 2015. 165 p. (rus)
8. Fursov V.V., Balyura M.V. Issledovanie morozoustoychivosti zoloshlakovykh otkhodov teplovykh elektrostantsiy dlya tseley stroitel'stva [Research of frost resistance of ashes and slag waste of thermal power stations for construction purposes]. *Vestnik of Tomsk State University of Architecture and Building.* 2013. No. 1. Pp. 242-252. (rus)
9. DiGioia A.M., Nuzzo W.L. Fly Ash as Structural Fill. Journal of Power Division. Vol. 98. Pp. 77-92.
10. Gray D.H., Lin Y.K. Engineering Properties of Compacted Fly Ash. *Journal of the Soil Mechanics and Foundation Engineering Division.* Vol. 98. No. 4. Pp. 361-380.
11. Indraratna B., Nutalaya P. and Koo, K.S. Engineering Behaviour of a Low Carbon Pozzolanic Fly Ash and its Potential as a Construction Fill. *Canadian Geotechnical Journal.* Vol. 28. Pp. 542-555.
12. Martin J.P., Collins R.A., Browning J.S., Biehl F.J. Properties and use of fly ashes for embankments. *Energy.* Vol. 116. Pp. 71-86.
13. Singh S.R., Panda A.P. Utilization of fly ash in geotechnical construction. *Proc. Indian Geotechnical Conf*. Vol. 1. Pp. 547-550.
14. Ossowski R., Gwizdala K. Mechanical properties of a dike formed from a soil-ash composite. *Procedia Engineering.* Vol. 172. Pp. 816-822.
15. Bałachowski L., Sikora Z., Mechancal properties of fly ash - dredged material mixtures on laboratory test. *Studia*

Литература

1. Folgueras M.B., Alonso M., Fernández F.J. Coal and sewage sludge ashes as sources of rare earth elements // Fuel. 2017. Vol. 192. Pp. 128–139.
2. Ватин Н.И., Петросов Д.В., Калачев А.И., Лахтинен П. Применение зол и золошлаковых отходов в строительстве // Инженерно-строительный журнал. 2011. № 4. С. 16–21.
3. Личман Н.В. Применение серы и золы ТЭЦ Норильского региона при строительстве и реконструкции гидротехнических сооружений // Инженерно-строительный журнал. 2011. № 8. С. 29–34.
4. Haleema A., Luthrab S., Mannana B., Khuranaa S., Kumarc S. Critical factors for the successful usage of fly ash in roads & bridges and embankments: Analyzing indian perspective // Resources Policy. 2016. Vol. 49. Pp. 334-348.
5. Hadbaatar A., Mashkin N.A., Stenina N.G. Study of Ash-Slag Wastes of Electric Power Plants of Mongolia Applied to their Utilization in Road Construction // Procedia Engineering. 2016. Vol. 150. Pp. 1558-1562.
6. Сиротюк В.В., Лунёв А.А., Иванов Е.В. Золошлаковая смесь для земляного полотна // Автомобильные дороги. 2016. № 6. С. 72-79.
7. Иванов Е.В. Обоснование применения золошлаковых смесей для строительства земляного полотна с учетом водно-теплового режима: дис. канд. техн. наук. Омск, 2015. 165 с.
8. Фурсов В.В., Балюра М.В. Исследование морозоустойчивости золошлаковых отходов тепловых электростанций для целей строительства // Вестник Томского государственного архитектурно-строительного университета. 2013. № 1. С. 242-252.
9. DiGioia A.M., Nuzzo W.L. Fly Ash as Structural Fill // Journal of Power Division. Vol. 98. Pp. 77-92.
10. Gray D.H., Lin Y.K. Engineering Properties of Compacted Fly Ash // Journal of the Soil Mechanics and Foundation Engineering Division. Vol. 98. № 4. Pp. 361-380.
11. Indraratna B., Nutalaya P. and Koo K.S. Engineering Behaviour of a Low Carbon Pozzolanic Fly Ash and its Potential as a Construction Fill // Canadian Geotechnical journal. Vol. 28. Pp. 542-555.
12. Martin J.P., Collins R.A., Browning J.S., Biehl F.J. Properties and use of fly ashes for embankments // Energy. Vol. 116. Pp. 71-86.
13. Singh S.R., Panda A.P. Utilization of fly ash in geotechnical construction // Proc. Indian Geotechnical Conf. Vol. 1. Pp. 547-550.
14. Ossowski R., Gwizdala K. Mechanical properties of a dike formed from a soil-ash composite // Procedia Engineering. Vol. 172. Pp. 816–822.
15. Bałachowski L., Sikora Z. Mechancal properties of fly ash – dredged material mixtures on laboratory test // Studia Geotechnica et Mechanica. Vol. 35. № 3. Pp. 3-11.

Geotechnica et Mechanica. Vol. 35. No. 3. Pp. 3-11.

16. Sikora Z., Ossowski R. Geotechnical Aspects of Dike Construction Using Soil-Ash Composites. *Proceedia Engineering.* Vol. 57. Pp. 1029-1035.
17. Pandian N.S. Fly ash characterization with reference to geotechnical application. *Journal Indian Institute of Science.* Vol. 84. Pp. 189-216.
18. Kim B., Prezzi M., Salgaro R. Geotechnical Properties of Fly and Bottom Ash Mixtures for Use in Highway Embankments. *Journal of Geotechnical and Geoenvironmental Engineering.* Vol. 131. Issue 7. Pp. 914-924.
19. Pal S.K., Ghosh A. Shear strength behavior of Indian flu ashes. *Indian Geotechnical Conference Geotechnics in Infrastructure Development (GEOTIDE).* Vol. 1. Pp. 18-22.
20. Jakka R.S., Datta M., Ramana G.V. Shear Strength Characteristics of Loose and Compacted Pond Ash. *Journal of Conference: Geotechnical and Geological Engineering.* Vol. 28. Issue 6. Pp. 763-778.
21. Tiwari S.K., Ghiya A. Strength Behavior of Compacted Fly Ash, Bottom Ash and their Combinations. *The Electronic Journal of Geotechnical Engineering.* Vol. 18. Pp. 3085-3106.
22. Melent'ev V.A., Panteleev V.G., Dobkin E.L. *Zoloshlakovye materialy i zolootvaly* [Ashes and Ash Dumps]. Moskow: Energiya, 1978. 295 p. (rus)
23. D'yakonov P.Yu. Utilizatsiya otkhodov teploenergetiki v dorozhnom stroitel'stve [Using waste products of heat-and-power engineering in road building]. *Vestnik MGSU.* 2012. No. 8. Pp. 175-180. (rus)
24. Balyura M.V. *Issledovanie stroitel'nykh svoystv zoly Tomskoy GRES–2* [The study of construction characteristics of the ash Tomsk RPS–2]. Problemy gidrogeologii, inzhenernoy geologii, osnovaniy i fundamentov: sb. nauch. tr. Tomsk: Izd-vo TGU, 1988. Pp. 97-104. (rus)
25. Zabielska-Adamska K. Shear strength parameters of compacted fly ash–HDPE geomembrane interfaces. *Geotextiles and Geomembranes.* Vol. 24. Pp. 91-102.
26. Huang H. W. The use of bottom ash in highway embankments, subgrade, and subbases. *Joint Highway Research Project, Final Report,FHWA/IN/JHRP-90/4.* West Lafayette: Indiana Department of Transportation and Purdue University, 1990. 315 p.
27. Raj P. *Thesis on compaction characteristics and shear parameters of pond ash.* National Institute of Technology, Rourkela, 2010. 58 p.
28. Roberts J.E., DeSouza, J.M. The compressibility of sands. *Proc. American Society for Testing and Materials*. No. 58. Pp. 1269-1277.
29. Lamb D.W. Ash disposal in dams, mounds, structural fills and retaining walls. *Proceedings of the Third International Ash Utilization Symposium.* U.S. Bureau of Mines, Information Circular. No. 8640. Pp. 170-179.
30. Lunev A.A. Sirotyuk V.V., Bezdelov N.S. Sopostavlenie metodov otsenki ustoychivosti vysokoy nasypi iz zoloshlakovoy smesi [Comparison of methods for evaluating of slope stability on high embankment built with the use of bottom ash]. *Vestnik SibADI*. 2016. No. 5. Pp. 106-114. (rus)
31. Golubev A.I., Seleckij A.V. Vybor modeli grunta i ejo parametry v raschetah geotehnicheskih ob'ektov. *Trudy mezhdunarodnoj konferencii po geotehnike "Geotehnicheskie problemy megapolisov* (GEOMOS 2010). Moskow, 2010. Vol. 4. Pp. 1727-1732. (rus)
32. Mel'nikov B.E., Le-Zakharov S.A., Semenov A.S. Sravnitel'nyy analiz rezul'tatov modelirovaniya uprugoplasticheskogo deformirovaniya na osnove kriteriev Mora-Kulona i Drukera-Pragera [Comparative analysis of simulation results of elastic-plastic deformation based on

16. Sikora Z., Ossowski R. Geotechnical Aspects of Dike Construction Using Soil-Ash Composites // Proceedia Engineering. Vol. 57. Pp. 1029-1035.
17. Pandian N.S. Fly ash characterization with reference to geotechnical application. // Journal Indian Institute of Science. Vol. 84. Pp. 189-216.
18. Kim B., Prezzi M., Salgaro R. Geotechnical Properties of Fly and Bottom Ash Mixtures for Use in Highway Embankments // Journal of geotechnical and geoenvironmental engineering. Vol. 131. Issue 7. Pp. 914-924.
19. Pal S.K., Ghosh A. Shear strength behavior of Indian flu ashes // Indian Geotechnical Conference Geotechnics in Infrastructure Development (GEOTIDE). Vol. 1. Pp. 18-22.
20. Jakka R.S., Datta M., Ramana G.V. Shear Strength Characteristics of Loose and Compacted Pond Ash // Journal of Conference: Geotechnical and Geological Engineering. Vol. 28. Issue 6. Pp. 763-778.
21. Tiwari S.K., Ghiya A. Strength Behavior of Compacted Fly Ash, Bottom Ash and their Combinations // The Electronic Journal of Geotechnical Engineering. Vol. 18. Pp. 3085-3106.
22. Пантелеев В.Г., Мелентьев В.А., Добкин Э.Л. и и др. Золошлаковые материалы и золоотвалы. М.: Энергия, 1978. 295 с.
23. Дьяконов П.Ю. Утилизация отходов теплоэнергетики в дорожном строительстве // Вестник МГСУ. 2012. № 8. С. 175-180.
24. Балюра М.В. Исследование строительных свойств золы Томской ГРЭС–2 // Проблемы гидрогеологии, инженерной геологии, оснований и фундаментов: сб. науч. тр. Томск: Изд-во ТГУ, 1988. С. 97–104.
25. Zabielska-Adamska K. Shear strength parameters of compacted fly ash–HDPE geomembrane interfaces // Geotextiles and Geomembranes. Vol. 24. Pp. 91-102.
26. Huang H.W. The use of bottom ash in highway embankments,subgrade, and subbases. Joint Highway Research Project, Final Report,FHWA/IN/JHRP-90/4. - West Lafayette, Indiana: Indiana Department of Transportation and Purdue University, 1990.
27. Raj P. Thesis on compaction characteristics and shear parameters of pond ash. National Institute of Technology, Rourkela, 2010. 58 p.
28. Roberts J. E., DeSouza J. M. The compressibility of sands // Proc. American Society for Testing and Materials. No. 58. Pp. 1269–1277.
29. Lamb D. W. Ash disposal in dams, mounds, structural fills and retaining walls // Proceedings of the Third International Ash Utilization Symposium, U.S. Bureau of Mines, Information Circular. No. 8640. Pp. 170-179.
30. Лунёв А.А. Сиротюк В.В., Безделов Н.С. Сопоставление методов оценки устойчивости высокой насыпи из золошлаковой смеси // Вестник СибАДИ. 2016. № 5. С. 106-114.
31. Голубев А.И., Селецкий А.В. Выбор модели грунта и её параметров в расчётах геотехнических объектов // Геотехнические проблемы мегаполисов (GEOMOS 2010): Труды международной конференции по геотехнике М: РИФ Стройматериалы, 2010. Т. 4. С. 1727-1732.
32. Мельников Б.Е., Захаров С.А., Семёнов А.С. Сравнительный анализ результатов моделирования упругопластического деформирования на основе критериев Мора-Кулона и Друкера-Прагера // XLI Неделя науки СПбГПУ: Материалы международной научно-практической конференции. СПб.: Изд-во СПбПУ, 2012. Ч. 1. С. 91-93.
33. Соколова О.В. Подбор параметров грунтовых моделей в программном комплексе Plaxis 2D // Инженерно-строительный журнал. 2014. № 4. С. 10-16.

the criteria Mohr-Coulomb and Drucker-Prager]. *XLI Nedelya nauki SPbGPU: Materialy mezhdunarodnoy nauchno-prakticheskoy konferentsii.* Saint Petersburg: Izd-vo SPbPU, 2012. Part. 1. Pp. 91-93. (rus)

33. Sokolova O.V. Podbor parametrov gruntovykh modeley v programmnom komplekse Plaxis 2D [The selection of soil models parameters in Plaxis 2D]. *Magazine of Civil Engineering.* 2014. No. 4. Pp. 10-16. (rus)
34. Strokova L.A. Opredelenie parametrov dlya chislennogo modelirovaniya povedeniya gruntov [Determination of parameters for computational modeling of soils]. *Bulletin of Tomsk Polytechnic University*. 2008. Vol. 313. No. 1. Pp. 69-74. (rus)
35. Semenova T.V. Dolgikh G.V., Polugorodnik B.N. Primenenie kaliforniyskogo chisla nesushchey sposobnosti i dinamicheskogo konusnogo penetrometra dlya otsenki kachestva uplotneniya grunta [Using California bearing ratio and dynamic cone penetrometer to assess the quality of compaction of soil]. *Vestnik SibADI.* 2013. No. 1. Pp. 59-66. (rus)
36. Boldyrev G.G. Mel'nikov A.V., Novichkov A.G. Interpretatsiya rezul'tatov laboratornykh ispytaniy s tsel'yu opredeleniya deformatsionnykh kharakteristik gruntov [Interpretation of results of laboratory tests to determine deformation characteristics of soil]. *Inzhenernye izyskaniya.* 2014. No. 5-6. Pp. 98-108. (rus)
37. Toth P.S., Chan H.T., Cragg C.B. Coal ash as structural fill with special reference to Ontario experience. *Canadian Geotechnical Journal.* Vol. 25 Pp. 694–704.
38. Boldyrev G.G. *Metody opredeleniya mekhanicheskikh svoystv gruntov. Sostoyanie voprosa* [Methods for determining mechanical properties of soils. The state of the question]. Penza: Izd-vo PGUAS, 2008. 696 p. (rus)

34. Строкова Л.А. Определение параметров для численного моделирования поведения грунтов // Известия Томского Политехнического университета. 2008. Т.313. № 1. С. 69–74.
35. Семенова Т.В. Долгих Г.В., Полугородник Б.Н. Применение калифорнийского числа несущей способности и динамического конусного пенетрометра для оценки качества уплотнения грунта // Вестник СибАДИ. 2013. № 1.С. 59-66.
36. Болдырев Г.Г. Мельников А.В., Новичков А.Г. Интерпретация результатов лабораторных испытаний с целью определения деформационных характеристик грунтов // Инженерные изыскания. 2014. № 5-6. С. 98-108.
37. Toth P.S., Chan H.T., Cragg C.B. Coal ash as structural fill with special reference to Ontario experience // Canadian Geotechnical Journal. Vol. 25. Pp. 694–704.
38. Болдырев Г.Г. Методы определения механических свойств грунтов. Состояние вопроса. Пенза: Изд-во ПГУАС, 2008. 696 с.

Victor Sirotyuk,
+7(965)9800004; sirvv@yandex.ru

Aleksandr Lunev,
+7(999)4533930; lunev.al.al@gmail.com

Виктор Владимирович Сиротюк,
+7(965)9800004; эл. почта: sirvv@yandex.ru

Александр Александрович Лунёв,
+7(999)4533930;
эл. почта: lunev.al.al@gmail.com

doi: 10.18720/MCE.74.2

Mechanical characteristics of polyethylene

Механические характеристики полиэтилена

L.I. Ogorodov,
O.V. Lustina,
Peter the Great St. Petersburg Polytechnic University, St. Petersburg, Russia

Канд. техн. наук, доцент Л.И. Огородов,
студент О.В. Лустина,
Санкт-Петербургский политехнический университет Петра Великого, г. Санкт-Петербург, Россия

Key words: material resistance; mechanical chracteristics; natural ageing; long-term ageing; polyethilene

Ключевые слова: сопротивление материалов; механические характеристики; естественное старение; длительное старение; полиэтилен

Abstract. An experimental data about the effect of long-term natural aging without load and aging of samples under tensile stress on the mechanical characteristics of low density polyethylene (LDPE) under uniaxial tension are presented. A comparison between the mechanical characteristics of unstabilized and stabilized by a 2 % soot content of polyethylene is made. The influence of long-term impact of ash on the strength of polyethylene is estimated. The dependences for calculating the resource of the impervious elements of structures are given. It is shown that low density polyethylene composites have higher mechanical characteristics than the main component. It is substantiated that polyvinylchloride, manufactured using thirty percent of technological and forty percent of operational PVC waste, has high and stable mechanical characteristics. The influence of long-term aging and the effect of environments have been estimated. It is determined that the glass-filled polyamide and polyamide containing from twenty five to seventy percent of the technological waste has sufficient structural strength.

Аннотация. Представлены экспериментальные данные по влиянию многолетнего естественного старения без нагрузки и старения образцов под растягивающей нагрузкой на механические характеристики полиэтилена низкой плотности (ПЭНП) при одноосном растяжении. Дано сравнение механических характеристик нестабилизированного и стабилизированного двухпроцентным содержанием сажи полиэтилена. Оценено влияние долговременного воздействия золы на прочность полиэтилена. Приведены зависимости для расчета ресурса противофильтрационных элементов конструкций. Показано, что композиционные материалы на основе полиэтилена низкой плотности имеют более высокие механические характеристики, чем основной компонент. Обосновано то, что поливинилхлорид, изготовленный с использованием тридцати процентов технологических и сорока процентов эксплуатационных отходов поливинилхлорида, имеет высокие и стабильные механические характеристики. Оценено влияние многолетнего старения и воздействия сред. Определено, то, что стеклонаполненный полиамид и полиамид, содержащий от двадцати пяти до семидесяти процентов технологических отходов, обладает достаточной конструкционной прочностью.

Introduction

Structure protection against groundwater and surface water (spring waters, precipitation and flood) is a topical branch in hydrotechnical, road, industrial and civil engineering. In the process of sumps, waste collectors, heaps and pool converters operation there is a danger of a leakage of ecologically unsafe substances, which differ from each other in composition and the degree of aggressiveness. Natural and artificial ponds rise the groundwater on adjoining territories, which prevents the economical activity of people. Impervious structures are used for ground and soil structures protection. Different ways of installation of impervious structure elements in soil, foundations, slopes, weirs and dams are known. Laying of the polymer panels on the slopes of the soil structures under the layer of the bulk material, trench and trenchless (vibratory) screen drives are applied. Polymer impervious screens, curtains and membranes are widely spread. Most of the film members were made and are made of low-density polyethylene (LDPE), but other polymer and composite polymer materials are becoming more and more popular.

There is a wide range of research material about designing problems of impervious hydrotechnical structures [1–4], creation and application of new waterproofing materials [5–8], polymer film screen study and construction [9–12]. The names of E.N. Bellendir, A.L. Goldin, Vatin N.I., V.G. Glagovsky, B.M. Davidenko, V.D. Glebov, V.P. Lysenko, A.I. Belyshev, S.P. Paremud, E.S. Argap, S.N. Starshinov and etc. are quiet famous in this field. It is obligatory to check corrosion and durability resistances of polymer and composite materials of impervious structures, used in active and aggressive environment [13]. The questions of application of polymer and composite materials, made with the use of technological and operational waste, in impervious structures are topical today [14–16]. Almost all materials have variable properties in time (ageing), especially polymer and composite polymer materials [17, 18] and others, for example, steels and alloys [19]. The speed of ageing depends on the sensitiveness of the material to the applied factors and their intensity. The changes of the material properties can be reversible and irreversible. The reversible ones are disappearing almost completely after the removal of stimulant exterior factors. The opposite situation takes place in irreversible changes. As we aim to predict the durability of ready-made materials, so we can define ageing as appearance of transformation during storage and exploitation.

The objectives of the present paper are:

1. To estimate the impact of the long-term ageing under load on the mechanical characteristics of the LDPE samples.
2. To compare the results of the experiment with LDPE samples stabilized with 2% soot content under long-term ageing conditions and under influence of CHP ash.
3. To compare the mechanical characteristics of LDPE samples and of LDPE samples stabilized with soot content.
4. To provide the calculation dependences of impervious elements resource considering long-term durability of the material.
5. To provide data about mechanical characteristics of the materials, perspective for applying in impervious structures.

The estimation of the influence of the long-term ageing on mechanical characteristics of low-density polyethylene during storage and under load

The samples and equipment

LDPE samples were made in laboratory complex in All-Union Scientific Research Institute of Hydraulic Engineering named after B.E. Vedeneev. The samples had a shape of a shoulder blade with 25 mm working part length and 3.5 mm width. The thickness was ranged from 0.048…0.064 mm to 0.16…0.23 mm.

Samples of stabilized LDPE had a shape of a shoulder blade with 30 mm working part length, 3.5 mm width and thickness $\delta = 0.58 \dots 0.65$ mm.

LDPE and stabilized LDPE samples were cut in the direction and cross-direction of the film extrusion.

Uniaxial sample tension tests were carried out using FPZ-100/1 and RMI-5 (РМИ-5) installations with different capture displacement speeds (v, mm/min.). Depending on the thickness, the samples were grouped in three, then were tested and results of the experiment were presented as the mean values. The experiments with long-term loaded samples were held on one specimen. The dimensions of these samples were determined before tension test.

The results of tests

Mechanical characteristics ($\sigma_{\rho r}$– proportional limit, σ_ρ и ε_ρ – limit stress and deformation, E_ρ – elastic modulus) of low-density polyethylene (LDPE) under tension (v = 50 mm/min., $\delta = 0.16 \dots 0.23$ mm) are shown in Table 1.

Table 1. Mechanical characteristics of LDPE in original state (the mean values of 3 samples)

Group of samples	**In the direction of the film extrusion**				**In the cross-direction of the film extrusion**			
	σ_{pr}, mPa	σ_{ρ}, mPa	ε_{ρ}, %	E_{ρ}, mPa	σ_{pr}, mPa	σ_{ρ}, mPa	ε_{ρ}, %	E_{ρ}, mPa
1	8.70	15.30	450	73.2	8.44	13.64	470	149.8
2	8.98	16.87	460	154.0	8.39	16.48	540	79.8
3	9.02	16.78	472	110.8	8.73	15.89	512	89.2
4	8.29	15.79	445	105.9	8.36	15.40	558	92.6
5	8.81	16.87	450	109.4	8.68	9.37	295	84.8
Mean	8.76	16.32	455	110.7	8.52	14.16	475	92.2

LDPE samples (in the direction of the film extrusion) have more stable mechanical properties and higher density than samples, made crosswise of the film extrusion.

Limit stress and the value of the elastic modulus are higher in samples cut in the direction of the film extrusion, than in samples cut in the cross-direction of the film extrusion. The influence of the sample thickness in specified range on LDPE mechanical characteristics (Table 1) is insignificant. The results of tension tests (v = 50 mm/min.) of LDPE samples (along of the extrusion) with thicknesses δ = 0.048…0.064 mm confirm this conclusion (Table 2).

Table 2. Mechanical characteristics (in the direction of the extrusion) of LDPE samples

Sample №	**δ, mm**	**σ_{pr}, mPa**	**σ_{ρ}, mPa**	**ε_{ρ}, %**
1	0.052	7.19	14.32	275
2	0.051	8.13	13.93	240
3	0.054	8.59	16.97	360
4	0.064	7.55	16.09	395
5	0.048	8.47	15.40	295
Mean	0.054	7.98	15.34	317

LDPE samples (δ = 0.16…0.23 mm) were loaded by constant tensile load during 189–194 months (~16 years). In the first series of experiments (189 months), initial stresses of ageing under load σ_H were recorded. In the second series of experiments (194 months), beside σ_H, the relative deformation of LDPE samples was recorded in the beginning (ε_H) and in the end (ε_K) of ageing. Tables 3–5 show the results of experiments (σ_{ut} – the durability limit under tension, ε_{nt} – deformations corresponding to the durability limit). Table 6 shows the data of the comparison of obtained results.

Table 3. Mechanical characteristics of LDPE (in the direction of the extrusion) after long-term (189 months) uniaxial compressive loading

Sample №	**σ_H, mPa**	**σ_{pr}, mPa**	**σ_{ρ}, mPa**	**ε_{ρ}, %**	**E_{ρ}, mPa**
1	0.87	2.93	10.55	336	132
2	1.31	5.77	16.16	503	138
3	1.76	5.77	14.01	470	137
4	2.18	5.84	12.59	298	142
5	2.63	5.49	13.86	483	133
Mean	-	5.17	13.43	418	136

Table 4. Mechanical characteristics of LDPE (in the direction of the extrusion) after long-term (194 months) uniaxial tensile loading

Sample №	σ_H, mPa	ε_H, %	ε_K, %	σ_{pr}, mPa	σ_p, mPa	ε_p, %	E_p, mPa	σ_{ut}, mPa	ε_{ut}, %
1	2.63	5.3	6.3	5.50	13.86	480	135	13.86	+
2	5.36	20.8	26.9	5.52	13.63	146	125	13.46	47.0
3	6.25	38.5	59.2	4.71	14.69	78	126	15.25	46.2
4	7.15	51.7	71.2	4.96	17.08	140	122	17.48	41.9
5	8.03	94.5	118.9	5.60	25.21	131	123	25.21	41.8
Mean	-	-	-	5.26	16.89	195	126	17.05	44.2

Table 5. Mechanical characteristics of LDPE (in the cross-direction of the extrusion) after long-term (194 months) uniaxial tensile loading

Sample №	σ_H, mPa	ε_K, %	σ_{pr}, mPa	σ_p, mPa	ε_p, %	E_p, mPa	σ_{ut}, mPa	ε_{ut}, %
1	0.85	2.4	4.96	12.80	707	85	8.41	27.3
2	2.56	5.6	4.54	12.20	572	80	8.65	-
3	4.26	10.0	4.56	10.88	480	72	-	-
4	5.11	24.4	3.75	14.69	540	58	10.31	57.8
5	5.95	21.2	4.04	17.69	487	95	12.69	42.5
6	5.95	30.4	3.96	12.07	224	65	12.24	52.1
Mean	-	-	4.30	13.39	502	81	10.46	44.9

Table 6. Mean values of LDPE mechanical characteristics in original state and after long-term ageing under the load

The sample direction	The sample state	σ_{pr}, mPa	σ_p, mPa	ε_p, %	E_p, mPa
Direction of the extrusion	Original	8.76	16.32	455	111
	Original (thin samples)	7.98	15.34	317	-
	After loading 189 months	5.17	13.43	418	136
	After loading 194 months	5.29	16.89	195	126
	After loading σ_H< 3 mPa	5.22	13.50	428	136
	After loading σ_H> 3 mPa	5.20	17.65	124	124
Cross-direction of the extrusion	Original	8.52	14.16	475	92
	After loading 194 months	4.30	13.39	502	81
	After loading σ_H< 3 mPa	4.75	12.50	640	82
	After loading σ_H> 3 mPa	4.08	13.83	433	80

Let us consider the results of the LDPE stabilized by 2% content of soot tests. Samples of the first series were kept in conditions of heated (without sunlight access) warehouse space during 17 years, and the samples of the second series – in the ash of Magadan CHP during the same time. The samples are oriented in the cross-direction of the extrusion. In each series of the tests, 3 samples were used. Table 7 shows results of the uniaxial tension tests and Table 8 shows their comparisons.

Table 7. Mechanical characteristics of stabilized LDPE samples

Series №	V, mm/min.	I series				II series			
		σ_{pr}, mPa	σ_{nt}, mPa	ε_{nt}, %	E_ρ, mPa	σ_{pr}, mPa	σ_{ut}, mPa	ε_{ut}, %	E_ρ, mPa
1	0.4	2.5	8.7	20.3	140	6.4	9.5	20.0	100
2	2.0	3.0	10.0	20.3	180	7.0	10.7	20.8	120
3	20.0	3.5	11.4	18.0	200	7.7	12.1	19.2	135
4	100.0	4.0	12.4	18.0	240	8.5	13.2	12.5	185

Table 8. Comparison (in %) between the values of the LDPE mechanical characteristics of the second series and the first one

Mechanical characteristics	The deformation speed V (mm/min.)			
	0.4	2.0	20.0	100.0
σ_{pr}	+156.0	+133.0	+120.0	+112.0
σ_{nt}	-9.2	+7.0	+6.1	+6.4
ε_{nt}	+1.5	+2.5	+6.7	-30.6
E_ρ	-28.6	-33.3	-32.5	-22.9

Table 9 shows the results of uniaxial tension tests of LDPE samples (stabilized with 2% soot content) in original state (I) and after ageing (II) during 18 years. The deformation speed was 50 mm/min.

Table 9. Mechanical characteristics of stabilized LDPE in original state and after 18 years of ageing in natural storage conditions

The direction of the sample cutting	σ_ρ, mPa		Change, %	ε_ρ, %		Change, %
	I	II		I	II	
In the direction of the extrusion	14.9	16.8	+ 12.8	476	633	+ 33
In the cross-direction of the extrusion	12.9	11.8	- 8.5	552	575	+ 4.2

Conclusions on the first part of article

1. LDPE samples cut in the direction of the film extrusion in original state have more stable mechanical properties and higher values of limit stresses (on 13 %) and elastic modulus (on 17%), than samples oriented in the cross-direction of the extrusion. That was pointed in papers of other authors.
2. The influence of the sample (film) thicknesses ranged 0.043…0.23 mm on LDPE mechanical characteristics is almost insignificant (considering the dispersion of the results of the experiments), excluding the limit deformations, which are lower in thin films (0.048–0.056 mm) on 30%, than in films with 0.16…0.23 mm thicknesses.
3. Long-term ageing of LDPE samples under load (16–17 years) decreases the proportional limit σ_{pr} on 40 % (in the direction of the extrusion) and the values of the elastic modulus are

changing in different directions, i.e. increasing on 22 % (in the direction of the extrusion) and decreasing on 12 % (in the cross-direction of the extrusion).

4. The ageing of LDPE samples under load with stresses less than 3 mPa decreases the limit stresses σ_{pr} on 17 % (in the direction of the extrusion) and on 12 % (in the cross-direction of the extrusion). With long-term LDPE prestresses higher than 3 mPa the increasing of the tensile limit stresses on 8 % (in the direction of the extrusion) with decreasing the limit deformations more than triple is marked. With the increase of long-term stresses $\sigma_{н}$ the increase of the limit stress $\sigma_{pн}$, the density limit σ_{nt} under subsequent uniaxial tensile loading is marked.
5. The mechanical characteristics of unstabilized and stabilized by 2 % soot content LDPE are insignificantly different. There is an influence on durability limit σ_{ut}, elastic modulus E and proportional limit σ_{pr} of the deformation speed.
6. The influence of the ash from Magadan CHP during 17 years does not change catastrophically the stabilized LDPE mechanical properties. The proportional limit increases more than on 110 % and the elastic modulus decreases on 29 % (average) in comparison with the same characteristics of samples kept in conditions of heated warehouse space during the same time. The limit stresses and deformations were changing insignificantly. The valuable changing of the elastic modulus under stretching has to be considered in calculations of film impervious structures, because the elastic modulus E is a parameter of calculating dependences [2, 9, 11, 12].
7. The natural ageing during 18 years of stabilized LDPE does not lead to significant changes of limit stresses and deformations.

The long-term durability of the film polymer materials and the calculations of the impervious structure resource

Let us consider the durability of the polymer film impervious structures as the limit term of their functioning in structure construction in determined exploitation conditions. The durability of the polymer element is determined by exploitation loads and temperatures, technological influences, ageing of the polymer material and the matrix of composite materials.

The base for predicting the durability (resource) of the polymer structure elements is an experimental data of long-term durability of the used materials. The curves of LDPE long-term durability are represented as correlation dependences $\sigma_i = A - Blg\tau$ (σ_i – the stress intensity, mPa; τ – time, sec.). The experimental data from work [2] was used in static processing. The LDPE membranes with the diameters 6–10 mm and 80–114 mm, thicknesses 0.1 mm and 0.04 mm were tested. The first dependence $\sigma_i = 10.46 - 0.547 lg\tau$ was obtained as a result of the tests of membrane samples made of the film received from manufacturing plant. Considering the results of the short-term uniaxial tension tests, the long-term durability equation was obtained in the following form: $\sigma_i = 12.02 - 1.064\ lg\tau$. The results of static processing of other tests are shown in [9].

For calculating film elements for design scheme of membrane under hydrostatic pressure, the following depending was obtained:

$$\frac{3.8}{S_{\mathrm{adm}}} = \int_D^{\tau} \left[\sqrt[3]{E(\tau)\left(\frac{\alpha_э d_ф}{\delta}\right)^2 q^2(\tau)} \right] \cdot \left[\frac{0.434B}{\xi(A - Blg\xi)^2} \right] d\theta,$$

where: S_{adm} – a safety factor for damages;

$E(\tau)$ – an elastic modulus (mPa) of the material depend on the exploitation time;

$\alpha_э$ – an efficiency factor of pore radius, which value depend on soil fraction [2];

$d_ф$ – a minimal size of the cushion soil fracture;

δ – a film thickness when a homogeneity factor is $k_{ogn} = 1$;

$q(\tau)$ – uniformly distributed load (hydrostatic pressure, mPa) changing in time in general case;

$\xi = (\tau - \theta)$ – time, sec.;

A и B – constants of the correlation equation of the long-term durability (50% probability of destruction).

In another version S_{adm} = 1, but A and B have to be selected with long-term durability curve corresponding to the little probability of material destruction. The influence of technological and exploitation impacts is considered by A and B constants.

When there is a soil settlement (Δ – a vertical settlement, *l* – a horizontal projection of a sagging part)

$$\frac{1}{S_{adm}} = \int_0^{\tau} \left[(l/\delta)q(\tau)\sqrt{(l/2\Delta)^2+1}\right]\left[\frac{0.434B}{\xi(A-Blg\xi)^2}\right]d\theta.$$

In an article [20] the calculated dependences $q - lg\tau$ are compared to the results of the experiments.

Table 10 shows the results of the durability calculations of the film impervious elements by the first suggested dependence.

Table 10. The design durability of LDPE film impervious elements ($d_ф$ = 12 mm)

E, mPa	Durability ($\tau_{расч}$), year					
	Hydrostatic pressure 50 m			Hydrostatic pressure 100 m		
	δ, mm	S_{adm}		δ, mm	S_{adm}	
		1,0	1,25		1,0	1,25
150	1.56	47.6	33.0	6.67	39.4	24.8
100	1.26	47.4	31.3	9.16	58.6	40.7
50	0.91	48.1	31.8	10.00	94.6	74.1
150	0.55	8.9	3.8	2.77	9.1	3.9
100	0.45	9.0	3.9	2.26	9.1	3.9
50	0.37	12.3	5.8	1.60	31.7	18.9
150	0.30	1.7	0.4	1.51	1.7	0.5
100	0.25	1.8	0.5	1.24	1.7	0.5
50	0.17	0.4	0.1	0.87	1.1	0.4

In calculations the values of the film impervious membrane thicknesses (δ) ($\alpha_э = 0{,}55$) were taken from thesis [2]. The probability of the film impervious membrane destruction during designed exploitation period with S_{adm} = 1.25 is not higher than 5 %.

The information about the mechanical characteristics of materials promising for using in impervious structures

The mechanical characteristics of polyethylene of high density and composite material on its base with polyethylene of low density

The main component of composite material is HDPE marked 277 and 276. Another main component is LDPE marked 153.

The compositions (PC-1 and PC-2) include stabilizers; phosphates; benzene OA; antiseptic alkilsulfanat E-30; pigments. The polymer HDPE-276 and PC-2 (obtained by extrusion) are differ from HDPE-277 and PC-1 (obtained by casting); they have greater molar mass and polydispersity (M_n – an average numerical value of the molar mass, M_w– an average weight value of the molar mass, M_w/M_n).

The uniaxial tension tests of plane samples (type 2 Russian State Standard GOST 11262-80) in short-time loading conditions (V=5mm/min.) and cyclic bending tests (f = 5 Hz) are carried out using XP-08 installation in the laboratory of physical and mechanical tests of plastics NGO "Plastpolymer". The fatigue tests in uniaxial tension conditions in the laboratory of material resistance of Peter the Great Saint-Petersburg Polytechnic University (frequency f = 5.7 Hz, asymmetrical cycle factor R = $\sigma_{min}/\sigma_{max}$ = 0.5). The experiments were held under nominal stresses by maintaining determined value of the maximal tensile force by cycle. The longitudinal strain was measured on a base of 20 mm with the help of an optical cathetometer.

Table 11 shows the results of polymer and polymer composite materials tests (σ_{nt} – the destruction limit, σ_y – the yield strength, ε_p – the limit deformation, N_{cp} – an average number of cycles before sample destruction under bending, ε_p^{max}– the limit deformation under cyclic uniaxial tension). The fatigue curves $\sigma_{max} = C - Д lgN$ under tension were obtained by processing the experimental data by the method of the least squares.

Table 11. Molecular characteristics and the results of polyethylene of high density and composite materials experiments

Material	$M_n \cdot 10^{-3}$	$M_w \cdot 10^{-3}$	$\frac{M_w}{M_n}$	σ_{nt}, mPa	σ_y, mPa	ε_p,%	C, mPa	Д,mPa	ε_p^{max},%	N_{cp}
HDPE-277	9	75	8.3	30.2	18.9	88	33.6	4.6	32-57	1370
HDPE-276	11	130	11.8	37.1	29.7	45	40.5	5.4	16-35	9290
PC-1	10	95	7.6	33.0	27.8	128	32.6	3.6	105-262	5797
PC-2	13	125	9.6	40.0	39.6	36	45.7	6.0	29-61	18687

Composite materials PC-1 and PC-2 have higher mechanical characteristics than the polyethylene of high density.

The usage of these composite materials in impervious structures depends on technology abilities of their obtaining on the stacking area.

The mechanical characteristics of PVC sheet fabricated with the use of technological and exploitation waste

The effective way of using all types of industrial and domestic waste, particularly polymeric waste, is their secondary recycling, which allows saving the scarce raw materials with payback costs on producing secondary materials and new composite materials with secondary material components. The prospects of using secondary materials in impervious structures are defined by their relatively low costs.

The modifications of PVS sheet were made by thermal plasticization method [21]. The basis of the new obtained materials containing from 64 % to 78 % of waste was the resin PVC-C635M (Russian State Standard GOST 14332-78). The main compositions are shown in article [21].

The mechanical characteristics of PVC fabricated with the use of technological (30 %) and exploitation (40 %) waste under short-term loadings are shown in paper [21]. From the results of the study it can be concluded, that the obtained modifications of PVC with the use of huge amount of waste have quite high and stable mechanical properties. PVC sheets have an isotropism of mechanical properties in a plane sheet.

In article [22] there are experiments of environment impact (liquid evaporating nitrogen, running water, aqueous solution of 3 % NaCl, machine oil) and natural ageing with and without an environmental impact on mechanical characteristics of the secondary PVC under linear tension. It can be concluded that PVC obtained with the use of 30 % technological and 40 % exploitation PVC waste is resistant to the impact of those environments and to the natural ageing processes.

Short-term loading tests under different deformation speeds [21] allow estimating the range of PVC deformation limits. Relatively small values of these deformations (up to 6 %) allow making tests on the long-term durability with supports and with predetermined values of conditional stresses. During long-term durability tests of one PVC modification was used the batch of identical samples from 4 to 21. Small batch of samples was used, when it was necessary to experimentally confirm really predicted result (including data from [21, 22]). The duration of tests was 10-12 days.

The experimental data was approximated by the least-squared method with the use of correlation equations of long-term durability of the form σ =A-Blg τ, where σ – measured in MPa, τ – the time of destruction, s (time can be dimensionless $\xi = \tau/\tau *$, where $\tau *$– normative time, equal to 1 s). The values of correlation equation of long-term durability factors (A and B) of PVC modifications are shown in Table 12.

Table 12. The values of correlation equation curve of long-term durability factors

PVC modifications	The values of correlation equation curve of long-term durability factors	
	A, MPa	B, MPa
PVC 1	56.66	3.60
PVC 4	55.66	2.66
PVC 5	56.41	3.34
PVC 8	55.31	2.42
PVC 9	58.85	3.32
PVC 10	58.24	2.59
PVC 11	57.37	3.59
PVC 12	56.06	3.01
PVC 13	58.53	3.42
PVC 14	55.88	3.03
PVC 15	61.53	3.79
PVC 16	63.34	3.53
PVC 17	64.36	4.03
PVC 18	62.01	3.69
PVC 19	52.86	3.38

Material modification samples PVC 4, PVC 15, PVC 10 and PVC 16 are made of bilayer blanks (blades). PVC 17, PVC 18 and PVC 19 samples are made of multilayered blades (while making PVC 19 sheets, less durable and with higher waste content PVC layers are used). PVC 11, PVC 12, PVC 13 and PVC 14 samples are made according to the first recipe, PVC 15 and PVC 16 are made according to the second one (in other samples the recipe is not mentioned).

The durability of bilayer PVC 5 material samples is higher, than the one of single-layered PVC 1 (both materials belong to the same batch). The same result appears while comparison between PVC 9 with PVC 10, PVC 15 and PVC 16. The discrepancy between compared PVC long-term durability curves with high stress values is not as significant as with lower stress values.

The long-term durability of PVC modifications, made according to the second recipe, is higher than the one, made according to the first recipe.

The comparison of short-tem [21] and long-term durability of PVC under uniaxial tension allows us to affirm that the high long-term durability of PVC 4, PVC 9, PVC 10 and PVC 16 correlates with the high values of short-term durability limit.

An estimation of environments (nitrogen, tap water, 3 % aqueous NaCl solution, machine oil) preliminary action on PVC modifications long-term durability is made (in [22] the influence of these environments under short-term loading on mechanical characteristics is estimated).

An influence of preliminary action of 3% aqueous NaCl solution during on tap water samples during 150 days and their subsequent one-month storage on their durability is insignificant.

Within the framework of the present work, an experimental estimation of the effect of natural aging on the storage of two-layer PVC 5 samples was conducted in room conditions and exposed to outdoor exposure without sunlight access for two years. The change in the correlation coefficients of the long-term durability can be traced from the data in Table 13.

Table 13. The correlation coefficients values of an equation of the long-term durability curve of PVC 5

The material state	The coefficients on the correlation equality	
	A, MPa	B, MPa
When delivered	56.41	3.34
After storage	57.60	2.84
After exposure	59.69	3.33

The PVC 5 long-term durability both after storage and after exposure during 2 years is increasing in comparison with the material durability in when delivered state.

The PVC 1 samples long-term durability was determined in when delivered state. The other part of PVC 1 batch at the same time was loaded with tensile loads of a predetermined value and maintained in the course of the experiment, which made it possible (about 50 %) to destroy the samples. The samples were then loaded and stored in a heated warehouse for one year. After storage, the samples were loaded again with predetermined loads until failure.

Preloading of PVC 1 samples under tension conditions a year before re-loading under the same conditions as in the case of its long-term durability, does not decreases its long-term durability and moreover, it increases $\sigma = 57.65\text{-}3.33\ lg\tau$. The explanation of this fact can be different, in particular, one can make an assumption about the effect of the workout of the material, its natural aging when stored between the series of tests. The results of the survey also show that the damages that occur during the initial loading process relaxes over time after the intermediate discharge.

PVC obtained using technological (30 %) and operational (up to 40 %) waste is characterized by high stability and long-term durability, including being in condition of preliminary action of explored environments and long-term storage, and also after preloading.

Blade elements of this material in a two-layer design have a higher tensile strength as compared to single-layer elements.

Glass fiber reinforced polyamide with the content of recycling waste for fasteners of impervious structures

In this section, data on the technology of production and the results of the conducted mechanical tests of two batches of primary glass-filled (30 % fiberglass) polyamide PA6-21OKS (OST 6-11-498-79), polyamide containing 20-75 % of recycling waste and secondary polyamide (100% recycled waste) in the state of delivery are presented. The test samples were prepared by injection molding on a thermoplastic automatic machine DE 3327-1. Mixture of primary polyamide PA6-21OKS (in granulated form) and recycled waste (gates, defective products) after crushing on a rotary-type crusher was dried to a humidity of 0.2 % in an air circulation drying cabinet at a temperature of 70-80 ℃ for 24-48 H. The main casting mode: pressure 1100-1300 kgf /cm^2. The temperature in the first zone of the cylinder was 240-250 ℃, in the second – 250–260 ℃, in the third – 260–270 ℃. The cycle time was 20–60 s. (closing of the mold form heated to a temperature of 70–80 ℃, injection of the material, holding under pressure, holding for cooling, opening the mold form, removing the product). After removing the gates, the appearance is monitored in order to detect defects and sample sizes.

The mechanical characteristics of the investigated materials under tension (Russian State Standard GOST 25601-80, σ_{ut} – strength, ε_{ut} – corresponding deformation, E_p – modulus of elasticity) were obtained from the experiments with a displacement speed of machine grippers V = 5 mm/min.

Sample bending tests (Russian State Standard GOST 25604-82) were carried out according to a three-point scheme (L = 60 mm) of loading. The following characteristics were determined: the bending strength σ_{vi}, the maximum deflection $\Delta\omega$, the elastic modulus E_u and the coefficients of variation of the average values of σ_{vi} and E_u (ϑ_σ and ϑ_E, respectively). The resilience values (a_n) and the brittleness indices σ_z were determined in a single shock bending test (Russian State Standard GOST 4647-62).

Tables 14–16 present the average values of mechanical characteristics obtained by testing three to five samples of two batches (I and II) of polyamide.

Table 14. The mechanical characteristics of PA6 – 21 OKS polyamide under tension depending of the recycle waste content

Waste content,%	σ_{ut}, MPa		ε_{ut}		*Ep*, MPa		ϑ_E, %	
	I	II	I	II	I	II	I	II
0	137.2	121.6	0.063	0.059	1750	2060	10.2	3.8
20	133.1	116.7	0.063	0.058	1880	1990	9.3	1.6
30	131.2	114.8	0.058	0.057	1930	2020	8.0	3.1
40	126.8	114.4	0.060	0.058	1930	2000	4.6	3.7
50	126.9	110.3	0.062	0.051	1860	2150	6.2	4.8
75	-	102.9	-	0.048	-	2120	-	5
100	-	98.8	-	0.045	-	2170	-	-

Table 15. The mechanical characteristics of PA6 – 21 OKS polyamide under bending depending of the recycle waste content

Waste content,%	σ_{vi}, MPa		ϑ_σ, %		$\Delta\omega$, mm		E_u, MPa		ϑ_E, %	
	I	II	I	II	I	II	I	II	I	II
0	229.3	192.9	1.2	2.2	1.10	1.12	6500	5700	2.3	8.6
20	216.2	191.1	1.7	2.0	1.23	1.12	5970	6180	4.7	0.7
30	213.4	188.4	2.7	1.9	1.19	1.19	6200	6040	2.2	1.3
40	210.4	186.5	1.3	3.1	1.25	1.19	5880	5990	1.8	0.3
50	209.2	190.7	1.9	2.2	1.27	1.22	5840	6030	4.8	3.4
75	-	189.1	-	4.7	-	1.28	-	5840	-	2.1
100	-	170.9	-	8.2	-	1.61	-	4650	-	7.6

Table 16. The mechanical characteristics of PA6 – 21 OKS polyamide under shock depending of the recycle waste content

Waste content.%	a_p. Н/М		ϑ_v. %		σ_z. Н/м^2		ϑ_σ. %	
	I	II	I	II	I	II	I	II
0	0.390	0.326	2.9	3.0	0.975	0.816	2.9	3.0
20	0.390	0.322	4.2	2.7	0.976	0.804	4.3	2.7
30	0.386	0.311	3.7	3.1	0.966	0.777	3.7	3.1
40	0.386	0.311	1.9	4.4	0.965	0.778	1.9	4.4
50	0.351	0.283	1.4	9.0	0.877	0.708	1.4	9.0
75	-	0.259	-	7.8	-	0.648	-	7.8
100	-	0.244	-	3.5	-	0.611	-	3.5

Based on the data presented in Tables 14-16, it can be concluded that the samples of the first batch of polyamide have higher mechanical characteristics for most of the studied parameters than in the second batch. which can be explained by some differences in the manufacturing technique. The uniform stress state produced by uniaxial stretching of polyamide samples is most dangerous in comparison with the inhomogeneous stress state arising during bending. Modulus of elasticity of polyamide PA6-21OKS with a different content of recycled waste is slightly higher (up to 5 %) than for initial polyamide and practically does not depend on the quantity of recycled wastes used for manufacturing (with the exception of data for secondary polyamide when tested for bending). Reduction of the strength characteristics of polyamide with 40 % of the recycled waste did not exceed 7 % and with a 50 % waste content – 12 % in comparison to the characteristics of the initial polyamide. Some strength characteristics of the secondary polyamide are lower on 25 % than those of the initial polyamide. It should be noted that the values of the coefficient of variation of the average values of the mechanical characteristics of the investigated modifications of PA6-21OKS for all types of tests are almost identical.

Of interest are the results of testing samples of polyamide PA6-21OKS on uniaxial compression. These samples were fabricated by mechanical treatment (rather than injection molding) from second batch samples used in tensile tests. They had the shape of a parallelepiped with dimensions 4x4x10 mm. and were laid in the grippers of plants without lubricants. The values of the mechanical characteristics (resistance. ε_{is} - deformation corresponding to this strength. E_c - modulus of elasticity) during compression of the polyamide are presented in Table 17. The displacement speed of the installation grippers was 5 mm/min.

Table 17. The mechanical characteristics of PA6 – 21 OKS polyamide (the second batch of samples) under compression depending of the recycle waste content

Waste content.%	σ_{is} . MPa	ε_{is}	E_c. MPa
20	100.5	0.102	2340
30	105.4	0.136	2230
40	108.0	0.146	2300
50	104.4	0.146	2330

The limit of proportionality of the polyamide under compression was equal to seventy percent of the strength limit. The modulus of elasticity of a polyamide under compression is on average 13% higher, the strength limit is 8 % smaller and the deformation under uniaxial compression is twice higher than the corresponding characteristics. The decrease in the short-term durability can be explained by the influence of the mechanical processing of the samples.

During the tests on long-term durability (static fatigue) under uniaxial compression of the second batch samples of polyamide PA6-21OKS a constant specified load and temperature (T = 20±2 ℃) were maintained. Taking into account the fact that during loading the change in the cross section of the samples did not exceed 2-3%. the processing of the results of the tests was carried out in conditional stresses. In the static least-squares treatment. the experimental data on the durability of the modification of the polyamide of the second batch were approximated by equations of the form $\sigma = A\text{-}B_{lg}\ \tau$. where σ is the tensile stress. MPa; T - time from Table 18.

Table 18. The results of processing the data of tests for the long-term strength of polyamide PA6-21OKS with a different content of recycled waste

Waste content. %	Number of samples		A long-term durability equation coefficients	
	destroyed	in the batch	A. MPa	B.MPa
0	11	11	126.6	8.0
20	8	8	124.9	8.2
30	9	9	116.4	6.6
40	9	8	114.9	6.2
50	12	9	113.0	5.9
75	8	7	120.4	6.2
100	7	5	106.9	5.2

According to the data in Table 18, it can be assumed that under high stresses and, correspondingly, short loading times, the durability of the polyamide PA6-21OKS with a different content of recycled waste varies more significantly than under low stresses (in the investigated durability range 10^6 s.), where the difference in durability is not confirmed statistically. It should be noted that several samples of polyamide with a recycled waste content of more than 40 % had a lower long-term durability than the samples in the general batch.

Experimental data on cyclic fatigue of a glass-filled polyamide with a 30 %, 40 %, and 50 % recycled waste contents are of interest. Before the tests, the samples were stored in a heated warehouse for 6 months. The loading frequency under uniaxial tension conditions was 5-7 Hz with the asymmetry coefficient of the sinusoidal cycle R = 0.5. During the experiments. the preset value of the conditioned stresses was maintained. By statistical analysis of an experimental data on the method of least squares fatigue curves were obtained: σ_{max} = C-D Lg τ. corresponding to 50 % of the probability of failure. Depending on the percentage of recycled waste in the material 30 %, 40 %, 50 %. the following values are obtained (in MPa): C_1 = 86.6. D_1 = 5.2; C_2 = 77.5. D_2 = 4.6; C_3 = 97.4 and D_3 = 9.0. The fatigue cyclic durability of polyamide PA6 -21OKS modification is below the long-term static durability.

Discussions

Today accelerated ageing is more popular way of long-term durability estimation, than natural one. However, it is impossible to estimate the accuracy of such tests without natural ageing tests. There is some experimental data, which mostly confirms the possibility to forecast the materials' behavior for 15-17 years, but no longer [5, 17]. In case of impervious structures, it is not sufficient, because they may be used for more than 50 years.

Some scientists believes it is impossible to obtain a "good imitation" by accelerated ageing, what is shown with the help of simple kinetic models in general. In any case, with this approach, the problem of the relationship between accelerated and natural aging remains unresolved. The "real approach" uses non-empirical kinetic models taking into account structural changes at all appropriate scales, and also uses the polymer physics to establish a relationship between the polymer structure and the property under consideration. An important characteristic of this approach is that accelerated aging only serves to determine the parameters of the model. [28]

Besides, the most popular test are held on materials under weather conditions with sunlight access. For impervious structures, this kind of test is useless, because the main area of implementation of such structures does not include significant sunlight and weather influences.

Thus, the issue of long-durability prediction methods is not investigated enough and seems appealing and perspective for further researches.

Conclusions

The film of the examined polyethylene of low density (LDPE) in original state has stable mechanical characteristics with some anisotropy related to the direction of the extrusion.

The LDPE long-term ageing (16-17 years) under load in heated warehouse space conditions decreases the proportional limit on 45 % (average). besides the values of the elastic modulus increases on 22 % in the direction of the film extrusion and decreases on 12 % in the cross-direction of the extrusion. The LDPE ageing under load with tensile stresses less than 3 mPa decreases limit stresses under short-term uniaxial tension up to 17 %. The LDPE ageing under load with tensile stresses higher than 3 mPa increases limit stresses under short-term uniaxial tension (in the direction of the extrusion) on 8 % with the deformation decrease more than triple. For samples cut in the cross-direction of the film extrusion, the changes are insignificant.

The mechanical characteristics of unstabilized and stabilized by 2 % soot content LDPE are insignificantly different. Natural ageing during 18 years in heated warehouse space conditions of stabilized LDPE does not lead to significant changes of limit stresses and deformations under uniaxial tension.

The influence of the Magadan CHP ash during 17 years does not change significantly the stabilized LDPE mechanical characteristics. The change of the elastic modulus (the average decrease on 29 %) has to be considered in calculations of film impervious structure elements.

The dependences for the durability (resource) calculations of film impervious LDPE structure elements and calculating resource data are shown.

Composite materials based on the HDPE of two grades and LDPE have higher mechanical characteristics than the main polyethylene component of high density (HDPE). The usage of tested composite materials has perspectives.

The polyvinylchloride fabricated with the use of technological (~30 %) and exploitation (~40 %) waste was tested under long-term and short-term loading conditions by uniaxial tension and under preliminary impact of some environments (liquid evaporating nitrogen. running water. aqueous solution of 3 % NaCl. machine oil) considering the long-term ageing before and after the environmental impact. This sheet PVC has quite high and stable characteristics. Mentioned PVC and polyamide PA6-210CS (ПА6-210КС) with the content of technological waste could be used particularly in impervious structures. In this case, the problem of the waste usage is also solved.

Finally, it is important to emphasize that today the research is continuing: now LDPE samples that have passed through natural ageing for more than 40 years are tested for strength, creep and stress relaxation.

References

1. Goldin A.L., Lysenko V.P., Borisov G.V., Radchenko V.G. Problemy issledovaniy v oblasti sozdaniya negruntovykh protivofiltratsionnykh konstruktsiy podpornykh sooruzheniy [Problems of research in the field of creation of non-ground anti-filtration structures of retaining structures]. *Materialy konferentsiy i soveshchaniy po gidrotekhnik* [Materials of conferences and meetings on hydraulic engineering]. Leningrad: Energoatomizdat. 1990. Pp. 6-13. (rus)
2. Kramer R.W. Embankment dams; impervious elements other than clay cores // *General Report.* Q.61 KhVI Congress I CDLD. San-Francisco. 1988. Vol. 11. Pp. 1191-1253.
3. Justo J.L., Conete P., Manzanares J.L., Del Campo J., De Porcellinis P. The upstream facing of Martin Gonzalo rockfill dam // *KhVI Congress I COLD.* San-Francisco. 1988. Q. 61. R. 45. Pp. 815-837.
4. Balzannikov M.I., Mikhasek A.A. Use of quick setting substances in watertight elements for rock material dams. *Magazine of Civil Engineering.* 2012. No. 3(29). Pp. 48-53. (rus)
5. Lukachev O.N., Teleshev R.I. Protivofiltratsionnyye elementy iz geomembran. Opyt primeneniya v gidrotekhnicheskom stroitelstve [The watertight geomembrane elements. Use experience in the hydraulic engineering]. *Magazine of Civil Engineering.* 2009. No. 6. Pp. 35-43. (rus)
6. Ustyan N.A. Geocontainers in road building and hydraulic engineering construction. *Magazine of Civil Engineering.* 2011. No. 4(22). Pp. 22-25. (rus)
7. Ptukhina I.C., Dalabayev A.C., Turkebayev A.B., Tleukhanov D.C., Bizhanov N.Zh., Dalabayeva A.C. Efficiency of innovative composite materials in construction. *Construction of Unique Buildings and Structures.* 2014. No. 9(24). Pp. 84-96. (rus)
8. Loginova I.I., Artamonova D.A., Stolyarov O.N., Melnikov B.Ye. Effects of structure type on viscoelastic properties of geosynthetics. *Magazine of Civil Engineering.* 2015. No. 4(56). Pp. 11-18. (rus)
9. Glebov V.D. *Polimernyye plenochnyye protivofiltratsionnyye konstruktsii gruntovykh gidrotekhnicheskikh sooruzheniy* [Polymer film anti-filtration structures of soil hydraulic endineering structures]. Abstract of doctors' of technical sciences thesis. Leningrad.1982. 52 p. (rus)
10. Glebov V.D. *Sovremennoye sostoyaniye i problemy razvitiya issledovaniy polimernykh plenochnykh protivofiltratsionnykh konstruktsiy* [Modern conditions and development issues of film anti-filtration structures]. Materialy konferentsiy i soveshchaniy po gidrotekhnike [Materials of conferences and meetings on hydraulic engineering]. Leningrad: Energoatomizdat. 1983. Pp. 92-94. (rus)
11. Belyshev A.N. *Raschet polimernykh ekranov gruntovykh sooruzheniy dlya usloviy stroitelnogo i ekspluatatsionnogo periodov* [Calculation of polymer screens of soil structures for construction and exploitation conditions]. Materialy konferentsiy i soveshchaniy po gidrotekhnike [Materials of conferences and meetings on hydraulic engineering]. Leningrad: Energoatomizdat. 1983. Pp. 98–101. (rus)
12. Lysenko V.P. Osnovnyye napravleniya issledovaniy i vnedreniya polimernykh protivofiltratsionnykh konstruktsiy gidrosooruzheniy [The main directions of research and implementation of polymeric anti-filtration structures of hydraulic structures]. *Materialy konferentsiy i soveshchaniy po gidrotekhnike.* [Materials of conferences and meetings on hydraulic engineering]. Leningrad: Energoatomizdat.1986. Pp. 12–15. (rus)

Литература

1. Гольдин А.Л., Лысенко В.П., Борисов Г.В., Радченко В.Г. Проблемы исследований в области создания негрунтовых противофильтрационных конструкций подпорных сооружений // Материалы конференций и совещаний по гидротехнике: Л.: Энергоатомиздат. 1990. С. 6-13.
2. Kramer R.W. Embankment dams; impervious elements other than clay cores // General Report.Q.61 XVI Congress I CDLD. San-Francisco. 1988. Vol. 11. Pp. 1191-1253.
3. Justo J.L., Conete P., Manzanares J.L., Del Campo J., De Porcellinis P. The upstream facing of Martin Gonzalo rockfill dam // XVI Congress I COLD. San-Francisco. 1988. Q. 61. R. 45. Pp. 815-837.
4. Бальзанников М.И., Михасек А.А. Применение быстротвердеющих веществ для формирования противофильтрационных элементов в плотинах из каменных материалов // Инженерно-строительный журнал. 2012. № 3(29). С. 48-53.
5. Лукачев О.Н., Телешев Р.И. Противофильтрационные элементы из геомембран. Опыт применения в гидротехническом строительстве // Инженерно-строительный журнал. 2009. № 6. С. 35–43.
6. Устян Н.А. Геоконтейнеры в дорожном и гидротехническом строительстве // Инженерно-строительный журнал. 2011. № 4(22). С.22–25.
7. Птухина И.С., Далабаев А.С., Туркебаев А.Б., Тлеуханов Д.С., Бижанов Н.Ж., Далабаева А.С. Эффективность использования инновационных композиционных материалов в строительстве // Строительство уникальных зданий и сооружений. 2014. № 9(24). С. 84–96.
8. Логинова И.И., Артамонова Д.А., Столяров О.Н., Мельников Б.Е. Влияние структуры на вязкоупругие свойства геосинтетических материалов // Инженерно-строительный журнал. 2015. № 4(56). С. 11–18.
9. Глебов В.Д. Полимерные пленочные противофильтрационные конструкции грунтовых гидротехнических сооружений. Автореферат дисс. … докт. техн. наук. Л.: 1982. 52 С.
10. Глебов В.Д. Современное состояние и проблемы развития исследований полимерных пленочных противофильтрационных конструкций // Материалы конференций и совещаний по гидротехнике. Л.: Энергоатомиздат. 1983. С. 92–94.
11. Белышев А.Н. Расчет полимерных экранов грунтовых сооружений для условий строительного и эксплуатационного периодов // Материалы конференций и совещаний по гидротехнике. Л.: Энергоатомиздат, С. 98–101.
12. Лысенко В.П. Основные направления исследований и внедрения полимерных противофильтрационных конструкций гидросооружений // Материалы конференций и совещаний по гидротехнике. Л.: Энергоатомиздат, 1986. С. 12–15.
13. Фролова М.К., Шевченко Е.Н. Об оценке химической стройности противофильтрационного полимерного экрана промышленных гидротехнических сооружений // Материалы конференций и совещаний по гидротехнике. Л.: Энергоатомиздат, 1990. С. 169–171.
14. Портнягин Д.Е., Селиванов Ю.В., Селиванов В.М., Шильцина А.Д. Составы и свойства пеностеклокристаллических материалов из композиций стеклобоя и высококальценированного шлака // Инженерно-строительный журнал. 2011. № 8(26). С. 25-28.

Ogorodov L.I., Lustina O.V. Mechanical characteristics of polyethylene. *Magazine of Civil Engineering*. 2017. No. 6. Pp. 17–32. doi: 10.18720/MCE.74.2.

13. Frolova M.K., Shevchenko Ye.N. Ob otsenke khimicheskoy stroynosti protivofiltratsionnogo polimernogo ekrana promyshlennykh gidrotekhnicheskikh sooruzheniy [About chemical harmony estimation of anti-filtration polymer screen of industrial hydraulic structures]. *Materialy konferentsiy i soveshchaniy po gidrotekhnike.* [Materials of conferences and meetings on hydraulic engineering]. Leningrad: Energoatomizdat. 1990. Pp. 169-171. (rus)
14. Portnyagin D.Ye., Selivanov Yu.V., Selivanov V.M. Shiltsina A.D. Composition and properties of foam glass crystal materials from compound of broken glass and high calcium slag. *Magazine of Civil Engineering.* 2011. No. 8(26). Pp. 25-28. (rus)
15. Burdonov A.G., Barakhtenko V.V., Zelenskaya Ye.V., Suturina Ye.O., Burdonova A.V., Golovnina A.V. Physical and mechanical properties of composite materials of different compositions based on waste products. *Magazine of Civil Engineering.* 2012. No. 9(35). Pp. 14-22. (rus)
16. Barakhtenko V.V. Estimating consumer product characteristics of highly filled polymer-mineral composite material based on polyvinyl chloride and waste TPP. *Magazine of Civil Engineering.* 2014. No. 3(47). Pp. 17-24. (rus)
17. Pavlov N.N. *Stareniye plastmass v yestestvennykh i iskusstvennykh usloviyakh* [Plastic ageing under natural and artificial conditions]. Moskow: Khimiya, 1982. 224 p. (rus)
18. Kirillova E.I., Shulgina E.C. *Stareniye i stabilizatsiya termoplastov* [Ageing and stabilization of termoplasts]. Leningrad: Khimiya, 1988. 240 p. (rus)
19. Yamaleyev K.M., Abramenko L.A. Deformatsionnoye stareniye trubnykh staley v protsesse ekspluatatsii magistralnykh nefteprovodov [Deformation ageing of pipe steels in the operation of the main oil pipelines]. *Problemy prochnosti.* 1989. No. 11. Pp. 125-128. (rus)
20. Egereva L.A. O metodike ispytaniya protivofiltratsionnykh elementov plenochnykh konstruktsiy na dolgovechnost [About the durability test method of anti-filtration film structure elements]. *Materialy konferentsiy i soveshchaniy po gidrotekhnike* [Materials of conferences and meetings on hydraulic engineering]. Leningrad: Energoatomizdat. 1986. Pp. 101-104. (rus)
21. Ogorodov L.I. Mekhanicheskiye kharakteristiki pri kratkovremennom nagruzhenii polivinilkhlorida, izgotovlennogo s ispolzovaniyem tekhnologicheskikh i ekspluatatsionnykh otkhodov [Mechanical characteristics of short-term loaded polyvinyl chloride manufactured by using technological and operational waste]. *Konstruktsii iz kompozitsionnykh materialov.* 1997. No. 3-4. Pp. 61-65. (rus)
22. Ogorodov L.I. Otsenka vliyaniya sred i yestestvennogo stareniya na mekhanicheskiye kharakteristiki polivinilkhlorida, izgotovlennogo s ispolzovaniyem tekhnologicheskikh i ekspluatatsionnykh otkhodov [Estimation of the environment and natural ageing influences on mechanical characteristics of polyvinyl chloride, manufactord by using technological and operational waste]. *Konstruktsii iz kompozitsionnykh materialov.* 1997. No. 3-4. Pp. 66-70. (rus)
23. Ogorodov L.I., Lustina O.V. Mechanical characteristics of low-densily polyethylene and materials, perspective for applying in impervious structures. *Molodoy uchenyi.* 2017. No. 2(136). Pp. 181-185.
24. Panin S.V. *Issledovaniye izmeneniya relyefa poverkhnosti i vlagoperenosa v polimernykh kompozitsionnykh materialakh v protsesse klimaticheskogo stareniya* [Investigation of surface relief changings and moisture transfer in polymer composite materials in the process of climatic ageind]. Diss. na soiskaniye uchenoy stepeni kandidata tekhnicheskikh nauk [thesis for the degree of candidate of technical sciences]: Moskow: FGUP “VIAM” GNTs RF. 2015. 131 p. (rus)
15. Бурдонов А.Г., Барахтенко В.В., Зеленская Е.В., Сутурина Е.О., Бурдонова А.В., Головнина А.В. Физико – механические характеристики композиционных материалов на основе отходов производства с различными рецептурами // Инженерно-строительный журнал. 2012. № 9(35). С. 14-22.
16. Барахтенко В.В. Оценка потребительских изделий из высоконаполненного полимерно – минерального композиционного материала на основе поливинилхлорида и отходов ТЭС // Инженерно-строительный журнал. 2014. № 3(47). С. 17-24.
17. Павлов Н.Н. Старение пластмасс в естественных и искусственных условиях. М.: Химия, 1982. 224с.
18. Кириллова Э.И., Шульгина Э.С. Старение и стабилизация термопластов. Л.: Химия, 1988. 240 с.
19. Ямалеев К.М., Абраменко Л.А. Деформационное старение трубных сталей в процессе эксплуатации магистральных нефтепроводов // Проблемы прочности. 1989. № 11. С. 125-128.
20. Егерева Л.А. О методике испытания противофильтрационных элементов пленочных конструкций на долговечность // Материалы конференций и совещаний по гидротехнике: Л.:. Энергоатомиздат. 1986. С. 101-104.
21. Огородов Л.И. Механические характеристики при кратковременном нагружении поливинилхлорида, изготовленного с использованием технологических и эксплуатационных отходов // Конструкции из композиционных материалов. 1997. № 3-4. С. 61-65.
22. Огородов Л.И. Оценка влияния сред и естественного старения на механические характеристики поливинилхлорида, изготовленного с использованием технологических и эксплуатационных отходов // Конструкции из композиционных материалов. 1997. № 3-4. С. 66-70.
23. Огородов Л.И., Лустина О.В. Mechanical characteristics of low-densily polyethylene and materials, perspective for applying in impervious structures // Молодой ученый. 2017. № 2(136). С. 181-185.
24. Панин С.В. Исследование изменения рельефа поверхности и влагопереноса в полимерных композиционных материалах в процессе климатического старения: диссертация на соискание учёной степени кандидата технических наук: Москва: ФГУП «ВИАМ» ГНЦ РФ. 2015. 131 с.
25. Briassoulis D. The effects of tensile stress and the agrochemical Vapam on the ageing of low density polyethylene (LDPE) agricultural films. Part I. Mechanical behaviour // Polymer Degradation and Stability. 2005. Vol. 88. № 3. Pp. 489–503.
26. Németh A., Marosfalvi J. Effect of climatic ageing on extra long-term fracture mechanical properties of polyethylene // Polymer Degradation and Stability. 2001. Vol. 73. № 2. Pp. 245–249.
27. Turnbull L., Liggat J.J., MacDonald W.A. Ageing of poly (ethylene terephthalate) and poly (ethylene naphthalate) under moderately accelerated conditions // Journal of Applied Polymer Science. 2012. Vol. 124. № 6. Pp. 4517-4529.
28. Verdu J., Colin X., Fayolle B., Audouin L. Methodology of Lifetime Predictionqa in Polymer Aging // Journal of Testing and Evaluation. 2007. Vol. 35. № 3. Pp. 1-8.
29. Oldfield D., Symes T. Long term natural ageing of silicone elastomers // Polymer testing. 1996. Vol. 15. № 2. Pp. 115-128.
30. Jakubowicz I. Effects of artificial and natural ageing on impact-modified poly(vinyl chloride) (PVC) // Polymer testing. 2001. Vol. 20. № 5. Pp. 545-551.
31. Vlastos A.E., Sherif E. Natural ageing of EDPM composite insulators // IEEE Transactions on Power Delivery. 1990.

25. Briassoulis D. The effects of tensile stress and the agrochemical Vapam on the ageing of low density polyethylene (LDPE) agricultural films. Part I. Mechanical behavior. *Polymer Degradation and Stability.* 2005. Vol. 88. No. 3. Pp. 489–503.
26. Németh A., Marosfalvi J. Effect of climatic ageing on extra long-term fracture mechanical properties of polyethylene. *Polymer Degradation and Stability. 2001.* Vol. 73. No. 2. Pp. 245–249.
27. Turnbull L., Liggat J.J., MacDonald W.A. Ageing of poly (ethylene terephthalate) and poly (ethylene naphthalate) under moderately accelerated conditions. *Journal of Applied Polymer Science.* 2012. Vol. 124. No. 6. Pp. 4517–4529.
28. Verdu J., Colin X., Fayolle B., Audouin L. Methodology of lifetime predictionqa in polymer aging. *Journal of Testing and Evaluation.* 2007. Vol. 35. No. 3. Pp. 1-8.
29. Oldfield D., Symes T. Long term natural ageing of silicone elastomers. *Polymer testing.* 1996. Vol. 15. No. 2. Pp. 115-128.
30. Jakubowicz I. Effects of artificial and natural ageing on impact-modified polyvinyl chloride (PVC). *Polymer testing.* 2001. Vol. 20. No. 5. Pp. 545-551.
31. Vlastos A.E., Sherif E. Natural ageing of EDPM composite insulators. *IEEE Transactions on Power Delivery.* 1990. Vol. 5. No. 1. Pp. 406-414.
32. Kiliaris P., Papaspyrides C.D., Pfaendner R. Influence of accelerated aging on clay-reinforced polyamide 6 // *Polymer Degradation and Stability.* 2009. Vol. 94. No. 3. Pp. 389-396.

Vol. 5. № 1. Pp. 406-414.

32. Kiliaris P., Papaspyrides C.D., Pfaendner R. Influence of accelerated aging on clay-reinforced polyamide 6 // Polymer Degradation and Stability. 2009. Vol. 94. № 3. Pp. 389-396.

Leonid Ogorodov,
+7(981)8271355; l.ogorodov@mail.ru

Olga Lustina,
+7(911)2675918; luola94@mail.ru

Леонид Иванович Огородов,
+7(981)8271355; эл. почта: l.ogorodov@mail.ru

Ольга Васильевна Лустина,
+7(911)2675918; эл. почта: luola94@mail.ru

doi: 10.18720/MCE.74.3

Oriented particle boards: effect of the tangential load component

Ориентированные стружечные плиты: влияние касательной составляющей нагрузки

T.A. Gavrilov,
Petersburg State Transport University,
St. Petersburg, Russia
G.N. Kolesnikov,
Petrozavodsk State University, Petrozavodsk,
Russia.

Канд. техн. наук, доцент Т.А. Гаврилов,
Петербургский государственный университет путей сообщения Императора Александра I, г. Санкт-Петербург, Россия
д-р техн. наук, заведующий кафедрой Г.Н. Колесников,
Петрозаводский государственный университет, г. Петрозаводск, Россия

Key words: OSB-plates; inclined plate; tangential load; plate deformation; FE-model as a research tool; construction; civil engineering

Ключевые слова: OSB-пластины; наклонная пластина; тангенциальная нагрузка; деформации плиты; FE-модель как инструмент исследования; строительство; гражданское строительство

Abstract. Object of research: oriented particle boards (OSB) plate under the action of vertical load. As a research tool used standard FE-model of the OSB-plate is used. The functioning of the OSB-plate as an element of the pitched roof structure with a soft tile is considered. In this case, the load on the surface from the snow and the weight of the soft roof has a tangential component distributed over the outer surface of the plate. However the influence of the tangential load on the plate has not been fully studied in well-known literature. The tangential component of the load can cause unevenness in the end joins of the OSB in pitched roofs. The purpose of this study is to identify the causes of unevenness (irregularity) in joints of OSB in structures of inclined roofs and vertical walls, also justify recommendations for addressing these causes. It is obvious that the cost of resources for the implementation of this intention will be justified if the OSB-plates have the prospect of effective use in the construction, including environmental management. For this reason, a brief overview of the OSB evolution is one of the tasks of the presented work. Other actual tasks: modeling the influence of the tangential component of load evenly distributed on one and two surfaces of the OSB-plate, the longitudinal side faces of which were clamped. In each of these two cases of loading, the OSB board can be inclined or vertical. It is shown that the tangential load causes an increase in deflections in the region of one of the end faces of the plate and a decrease in deflections opposite to the edge. This can lead to unevenness at the joints of OSB-plates. In order to exclude the revealed cause of the appearance of unevenness in constructions with OSB, it is suggested that the flexural rigidity of the plates in the area of their ends by stiffeners or carbon fiber strips should be increased.

Аннотация. Объект исследования: ориентированная древесностружечная плита (OSB) под действием вертикальной нагрузки. В качестве инструмента исследования использовалась стандартная FE-модель (конечно-элементная модель) OSB-плиты. Рассмотрено функционирование OSB-плиты как элемента скатной конструкции крыши с мягкой кровлей. В этом случае нагрузка на поверхность от снега и вес мягкой кровли имеет тангенциальную составляющую, распределенную по внешней поверхности пластины. Однако влияние тангенциальной нагрузки на пластину еще не полностью изучено в известной литературе. Тангенциальная составляющая нагрузки может вызвать неравномерность в стыках концов OSB в скатных крышах. Цель этого исследования - выявить причины неравномерности прогибов в стыках OSB в структурах наклонных крыш и вертикальных стен, а также обосновать рекомендации по устранению этих причин. Очевидно, что стоимость ресурсов для реализации этого намерения будет оправдана, если у OSB-пластин есть перспектива эффективного использования в строительстве, в том числе с точки зрения управления окружающей средой. По этой причине краткий обзор эволюции OSB является одной из задач представленной работы. Другие актуальные задачи: моделирование влияния тангенциальной составляющей нагрузки, равномерно распределенной на одной и на двух поверхностях OSB-пластины, продольные боковые грани которой были зажаты. В каждом из этих двух случаев загрузки OSB-плита может быть наклонной или вертикальной. Показано, что тангенциальная нагрузка вызывает увеличение прогибов в области одного из торцов пластины и уменьшение прогибов, противоположных краю. Это может привести к неравномерности в стыках OSB-плит. Чтобы исключить выявленную причину возникновения неровностей в конструкциях с OSB, предлагается увеличить изгибную жесткость пластин в области их концов ребрами жесткости или полосами из углеродного волокна.

Introduction

This article deals with the distribution of displacements and stresses in an inclined plate under the action of a vertical load distributed over one surface plate. The relevance of this work is due to the increasing use of oriented particle boards (OSB) in roof structures [1] and, as analysis of the literature has shown, their inadequate knowledge. The practical significance of the work is justified by the fact that the reliability of the roof depends on the durability and safety of the functioning of the structures, made from OSB.

The focus in this paper is on the mutual movement of inclined plates in the area of their end faces under vertical load. Differences in the deflections of adjacent plates in the area of their end faces at functioning of the OSB-plates, as an element of the pitched roof structure with a soft tile, is considered. These differences in the deflections can lead to uneven wear of the roofing material. For the same reason, local damage to the soft roof in the area of the butt joints of the OSB-plates is possible.

As a tool of represented research, the finite element method (FEM) has been chosen, as well-known analytical solutions to plate bending problems under the action of the tangential surface load [2, 3], making their theoretical contribution, have a limited use in applications [4, 5]. So, the object of the study is the FEM-model of the plate, and the subject of the study is the features of the plate deflection distribution and the stresses in its material under the action of the tangential load distributed over the surface of the OSB-plate. In justifying this choice, the known results were taken into account [5, p. 87], namely, the FEM-model of a plate, based on volumetric finite elements used.

Referring to the general characteristics of the represented work, it should be noted that the research of building structures, in the final analysis, is always aimed at resolving a contradiction between strength, reliability, aesthetical design on one side and - cost-effectiveness on the other. Engineering activities to resolve this contradiction, often at the intersection of sciences, leads to the emergence of new, more advanced building materials, technologies and structures. One of the results of this activity are OSB-plates, the development of production and application of which contributes significantly to the solution of the global problem of rational use of wood as a resource created by nature. Taking into consideration the relevance of the topic of the article, the choice of the object of research and the purpose of the work, we note the following.

Wood as a natural polymer has remained one of the main factors in the development of civilization. History shows, that the sustainable development needs consistent improvement of technologies for the rational use of wood. A necessary element of the modern concept of sustainable development is a continuous improvement process aimed at rational use of resources and minimizing the negative impact on the environment. The implementation of the principles of sustainable development includes organizational, economic, environmental and technological aspects [6]. At the same time, the most important tasks are the reducing the amount of waste and its rational use. The waste is known [7], to be inevitable, so it is important to reduce the amount of waste and to use it rationally. So, contribution to the solution of the multifaceted problems that arise in this connection is introduced by applied research to justify new possibilities for obtaining building materials and improving timber structures. In this paper, we study some features of the functioning of oriented particle boards, known as OSB plates (Oriented Strand Board). Such boards are used in the construction of roofs, walls and other building structures [1, 8].

We can name a number of reasons that motivated the appearance of this work. First of all, it should be noted that the development of production and application of OSB boards contributes to the solution of the environmental and economic problems of sustainable development outlined above. The way to modern production of OSB, according to [6], began with the production of plates from wood residues in the 1920s, when the waste accounted up to 60% of the volume of raw materials in the form of round timber. The first industrial production of plates, known as particleboards, from undirected particles of crushed wood, connected by phenolic binders, was carried out in Bremen, Germany in 1941. By 1954, Canada developed a technology for producing the so-called wafer-boards [9, 10].

As the next stage of the plate evolution, in the mid-1970s, the idea to separate the wood particles into three layers was developed and realized. At the same time, in order to increase the strength characteristics of the plate, a strip-shaped wood particle was used, and in each of the layers the chips were oriented in mutually perpendicular directions. This is already an orthotropic plate. From the point of view of the mechanics of materials, the preferential orientation of the particles in the OSB plates in the direction of the principal stress actions makes it possible to reduce the thickness of the plate by increasing [11].

Thus, modern production of OSB-plate is one of the results of the wood processing technology development. The evolution of OSB-plates is described in more detail in [9–11]. In the context of our work, we note that currently in plate manufacturing, waste accounts approximately 20% of the volume of raw materials in the form of round timber [12]. Plates can be from 6 to 32 mm thick. Areas of plate use: roofing [1], walls, sandwich-type plates, floor structures, beam elements [8, 11]. OSB-plates are positioned as an alternative to plywood. With the decrease in the availability of round timber suitable for the production of plywood, in the 1970s, the development of technologies for the production of structured particle boards became one of the main priorities in the study of wood products [12, 13]. The production of OSB started in the 1980s in the USA and Canada [9, 10, 12].

In Russia, the first production line for OSB appeared in 2012, and since 2016 there have been five plants producing OSB plates [14]. From 2012 to 2016 the production of OSB-plates increased from 3 to 660 thousand cubic meters [14].

Due to the relative novelty of such plates, the features of their functioning have not been fully studied, which also motivated the appearance of this work. Literature review showed that the influence of the tangential component of the vertical load on the surface of the OSB plate when it is used in the roof structure has not been sufficiently studied, both numerically [4, 5, 8, 15] and analytically [2, 3, 17]. The tangential component (Figure 1) of the load on the surface of the sloping plate is determined by the weight of the snow (Figure 2), the soft roof [1] and the wind effect. As the slope of the plate increases, the tangent component increases too. Note that the snow load appears on planes with an inclination angle of even more than 45° (Figure 2).

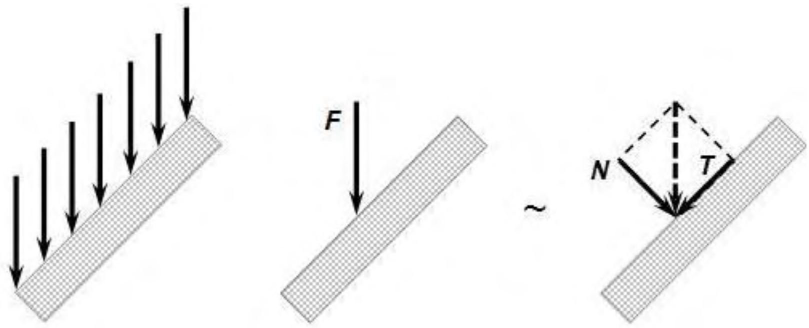

Figure 1. Vertical external force *F* on the plate surface, the normal *N* and tangential *T* components of it

Figure 2. Snow load on the roof

Concerning the choice of the instrument of our research, we note the following. At present, engineering calculations are performed, as a rule, using the finite element method (FEM) [4, 16]. An overview of the FEM-models with reference to the problem of the thick plate bending is given in [5]. Along with numerical methods [11], analytical methods for calculating plates are being developed. The Analysis of publications [15, 17–23] in this area showed that the attention of researchers is focused on the problems of bending under the action of forces normal to the plate surface. However, with a vertical load on the surface of the inclined plate, for example, snow load (Figure 2) and the weight of the soft roof [1], a tangent component appears at each point (Figure 1), which creates a bending moment and a corresponding deformation of a plate with thickness h. As the plate thickness h decreases, the bending moment M decreases linearly (Figure 3).

The following explanation to equivalent transformation in accordance with Figure 3 is required. Let tangential force T be applied at some point of the plate surface. Let two equal in magnitude but oppositely directed forces T_1 and T_2 be applied in a point on the axis. In this case the subsystem of forces T_1 and T_2 is equivalent to zero. Hence, the original system is equivalent to the system of forces T, T_1 and T_2. Equivalence will be retained if all three forces are equal in magnitude: $T = T_1 = T_2$. So, a pair of forces T and T_2 will create a bending moment, and in the median plane along the longitudinal axis will act the force T_1. The magnitude of bending moment is equal $M = T \cdot 0.5h$.

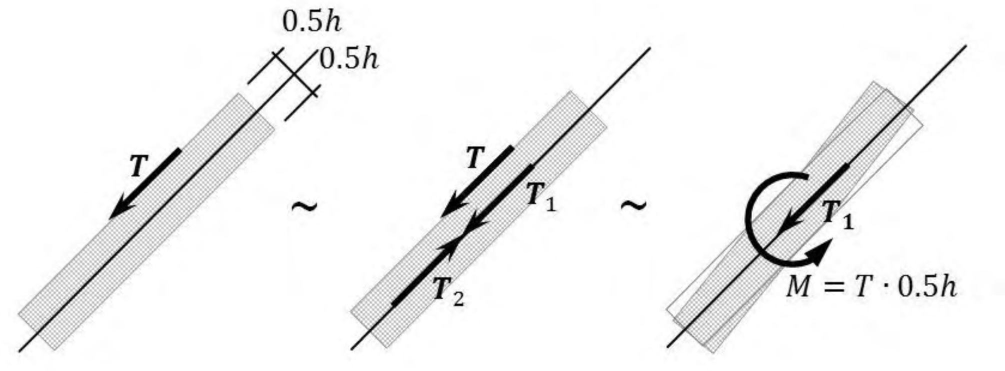

Figure 3. The tangential component of *T* as the cause of the appearance of the bending moment *M*

It is known that a plate, with the thickness more than five times smaller than its width, is called a thin plate. Thin plates usually have a constant thickness. The scheme of a thin plate is represented in the form of its median plane. The reference connections and the load on the thin plate are referred to the middle plane. In the case below, the ratio of the span to the thickness of the plate is ~ 50, which makes it possible to use the model in the form of a thin plate. Then the effect of the tangential load distributed over one of the surfaces of the plate can remain out of sight.

As it has been noted, the effect of the tangential component of the load distributed over the surface of an inclined plate has not been investigated enough for engineering and construction practice. The need to investigate this effect is due to its practical significance and is explained by the fact that in the case of using OSB-plates in the roof skin, the tangential component on the of inclined plates surface can cause unequal deflections of the plates to be joined at their ends. Namely, in the case under consideration (Figure 3) the tangential load on the plate surface causes a decrease in the deflection of the upper end of the plate and an increase in the deflection of the lower end. For this reason, unevenness and, consequently, damage to the soft roof can occur in the area of the butt joints of the OSB-plates.

Methods

In this study we have used the generally accepted methods of mechanical system modeling and finite element analysis of building structures, which reviews can be found in [5, 15, 23]. These methods are used as a tool for applied research of plate deformations and stresses in material, taking into account the tangential component of the load distributed on one of the plate surfaces.

From a methodological point of view, the results presented below can be practically applied after their being adaptated to specific conditions. Experimental and theoretical studies [11, 12] have established that the OSB material can be considered orthotropic. The elastic moduli in the longitudinal and transverse directions of the plates are determined according to the standard procedure EN 310 and according to the standard EN 300 must have values of at least 3500 and 1400 MPa in the longitudinal and lateral directions, respectively [9].

As a research tool, SolidWorks were used. The software generates mesh with one of the two types of elements: linear tetrahedral solid elements or so called parabolic tetrahedral solid elements. A linear tetrahedral element is defined by four nodes in vertexes of tetrahedron. A parabolic tetrahedral element is defined by the same four corner nodes and additionally six mid-side nodes on the edges of a tetrahedron. Therefore for the same mesh density (number of elements), parabolic elements yield better results than linear elements. Parabolic tetrahedral solid element ensures a quadratic interpolation of nodes displacement and is well suited to model irregular meshes. However, parabolic elements require greater computational resources than linear elements. Nevertheless, their advantages are used in various FE-complexes, for example in ANSYS (finite element SOLID 98). In this paper we used linear tetrahedral elements.

Results and Discussion

Let us consider the results of FEM-modeling using the OSB plate with the dimensions 1250 × 625 × 12 mm as an example; The long edges of the plate are fixed to the areas 1250 × 20 mm to two supporting platforms (Figure 4.0); The material of this plate is orthotropic, the moduli of elasticity are 3500 MPa and 1400 MPa, the approximate Poisson's ratio is 0.23.

The influence of tangential external forces distributed over the surface of the plate. We consider an inclined plate, whith a vertical load of 3000 N/m2, uniformly distributed over the plate face. Based on the results of the simulation, the largest resulting displacements occur in the lower and upper end of the plate, respectively, 1.692 mm and 1.551 mm, i.e. the edge effect is evident (Figure 4.3). The difference in deflections creates unevenness at the joint of the plate ends. (Figure 4.2). The reason for the appearance of these differences has been explained above (Figure 3): the tangential load on the surface of the plate causes a decrease in the deflection of the upper end of the plate and an increase in the deflection of its lower end (Figure 4.3 and 4.4).

The greatest stresses (according to Mises) do not exceed 2.6 MPa (Figure 4.5). It is known that the bending strength of OSB boards 11-17 mm thick along the main axis is not less than 20 MPa, and not less than 10 MPa along the minor axis. Criteria for the strength of isotropic and orthotropic materials have been considered in [24–27].

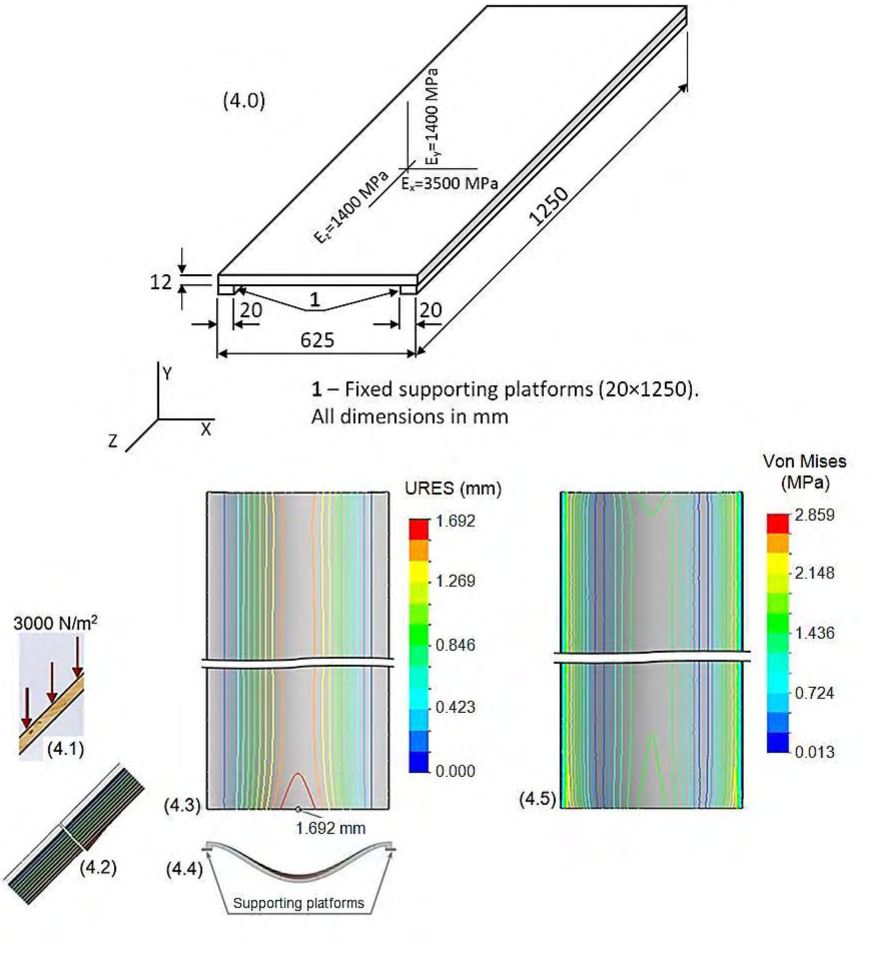

Figure 4. The design scheme of the plate (4.0); the load on the plate (4.1);
the joint of the lower end of the upper plate and the upper end of the lower plate, side view (4.2);
the displacement isolines of points on the plate face (4.3);
the cross-section of the deformed plate (4.4); The stresses von Mises on the upper plate face (4.5)

In the case above, the tangential forces are distributed not only over the outer plate surface, but are transferred to the lower plate surface through the support pads (Figure 4.4). To estimate the effect of these forces, let us consider a model example by repeating the calculation of the same plate under the load in Figure 5. In this case (Figure 5), the bending moment M (Figure 3) of the tangential components of the load is zero.

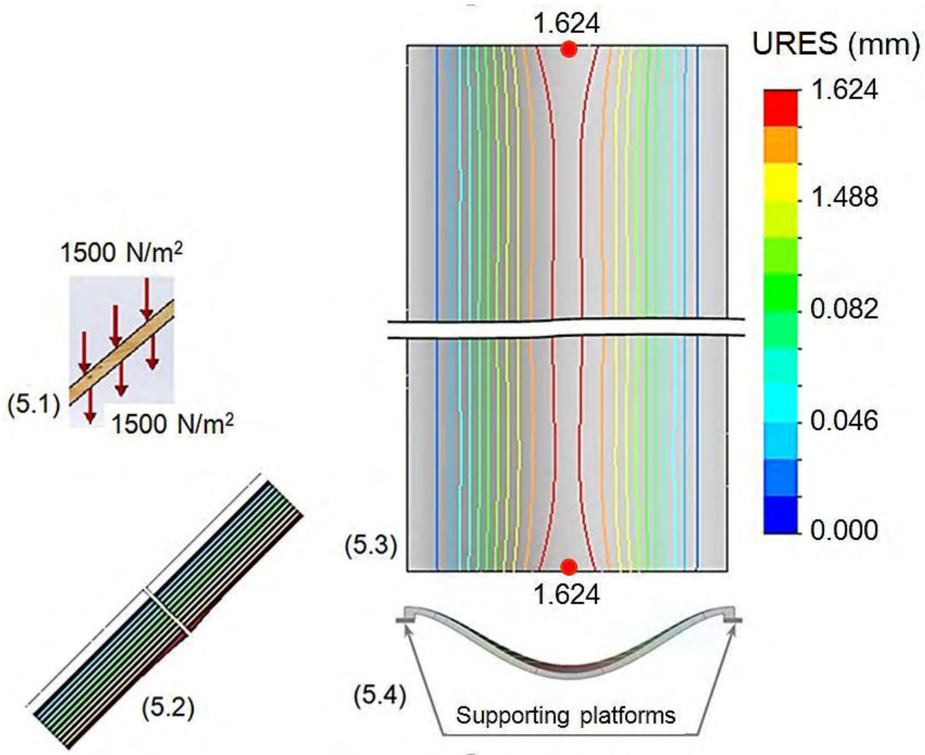

Figure 5. The load on the plate (5.1);
butt joint of the lower end of the upper plate and the upper end of the lower plate, side view (5.2);
the displacement Isolines of the points on the plate face (5.3);
the cross-section of the deformed plate (5.4)

As in the case above (Figure 4), the largest displacements take place at the ends of the plate, i.e. the edge effect is manifested. The deflections of the plate at the ends (~1.62 mm) are almost the same (Figure 5.3), the unevenness in the joint of the plates can be neglected (Figure 5.2). However, in real situations, the load by Figure 4 occurs.

Influence of support conditions. The support conditions (Figures 4.4 and 5.4) of the plate considered above were asymmetric with respect to the middle plane of the plate. Let us consider the same plate, but with the fixed side edges. Namely, all the nodes on the lateral faces with dimensions of 1250 × 12 mm are stationary. For OSB structural element the fixation of side edges can not provided. This "extreme" case, nevertheless the analysis of which will give a more complete idea of the effect of only the tangential load on the plate. Another "extreme" case is a horizontal plate with a vertical load, when the tangential component of the load is zero. It is technically difficult and Impractical to implement the first of these "extreme" cases in practice. But the second case is often encountered in practice. The plate which is placed under the angle 0° < α < 90° refers to the intermediate cases in relation to the above two "extreme" cases.

For the case considered below, if the tangential external forces of 3000 N/m2 intensity are uniformly distributed over only one plate surface, then according to the simulation results we get the following picture of the deformations and stresses according to Mises (Figure 6). The largest displacement is 0.14 mm. Deflections (Figure 6.1) appear as a result of the action of tangential external forces distributed over one surface of the plate. The longitudinal axis of symmetry of the plate is similar to the S-shaped curve (Figure 6.2), which agrees with Figure 3. In the corners of the plate (Figure 6.3), there is a concentration of stresses, the greatest stress is ~ 0.7137 MPa.

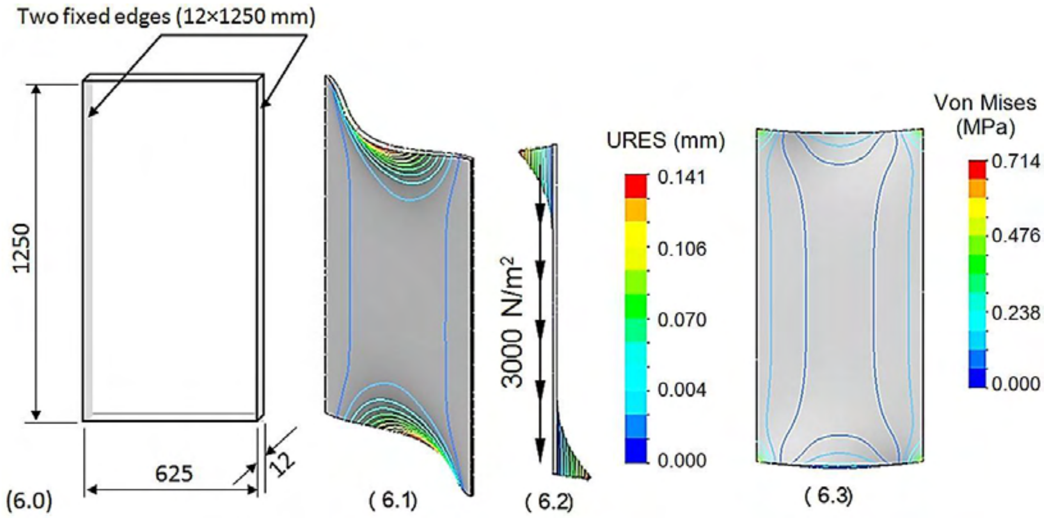

Figure 6. The design scheme of the plate (6.0); the deformed state of the plate (6.1) with pinched lateral vertical faces, the tangential load is evenly distributed only along the left side of the plate (6.2); the stresses von Mises on the right side of the plate (6.3)

At the level of qualitative reasoning it can be seen that in this case the influence of the tangential load distributed over the surface of the plate is analogous to the action of the eccentric longitudinal force on the rod. If the tangential load is symmetrical relatively to the middle surface of the plate (Figure 7.2), then the deformation of the plate bending is zero. However, there will be deformations in the plane of the plate (Figure 7.1). According to the results of modeling under a symmetrical load, flexural deformations are not detected either in the side view (Figure 7.2) or in the view from above (Figure 7.3). This confirms that the bend appears if the tangential load acts on one of the surfaces of the plate.

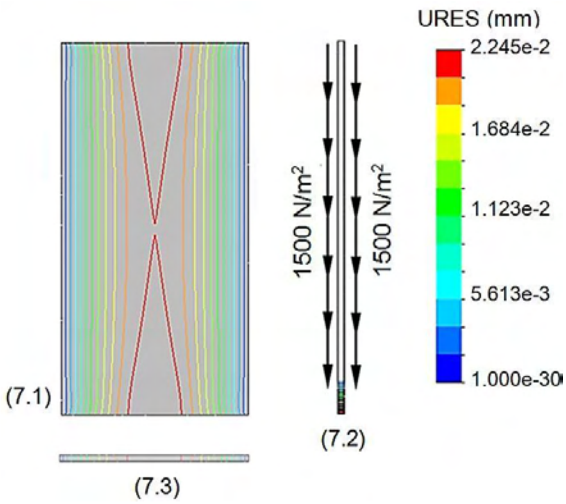

Figure 7. The total deformation of the plate with pinched lateral faces (7.1) under symmetrical loading (7.2) are not accompanied by bending deformations; Longitudinal section of the plate (7.2); The cross-section of the plate (7.3)

Influence of plate thickness on its deflections under surface tangential loading. If we compare the effects of normal and tangential loads on the plate (Figure 1), it can be seen that the influence of the surface tangential load depends on the thickness of the plate. As the thickness of the plate increases, the bending moment increases linearly (Figure 3). However, the deflections of a sufficiently flexible isotropic plate are known to be inversely proportional to the cylindrical rigidity, which is directly proportional to the cube of the plate thickness [22]. Thus, the deflections of the plate with a one-sided tangential load are inversely proportional to the square of the thickness of the plate. This non-strict regularity makes it possible to predict approximately the state of plates under the action of a tangential surface load.

Concerning the practical significance of the presented results, we note the following. The roofing is made from separate plate of certain dimensions. Therefore it is necessary to join the plates to each other.

In this case, the lower end of the upper plate contacts the upper end of the lower plate. The long (lateral) edges of the plates are deadly fixed to the 1250 × 20 mm areas indicated above, so that the butt end of the plates on these platforms is close to the ideal scheme. However, in the middle part of the span of plates the maximum deflection of the lower end is greater than the maximum deflection of the upper end of the plate.

The maximum displacements at the ends of the joined sloping plates (Figure 4.2) differ the more, the greater the slope angles of the plates are, i.e. the tangential load on the face of the plate is greater. As it is noted above, in this design there will be unevenness in the middle part of the span at the plate joints, which may cause damage, for example, to the soft roof [1]. To eliminate the cause of these irregularities, it is necessary to increase the stiffness of the lower end of the upper plate by setting the stiffener. The shape and dimensions of the stiffener should be specified taking into account the peculiarities of the manufacturing technology, packaging, transportation, installation and operating conditions of the plate as an element of the roof structure.

To exclude these irregularities, metal parts to join the OSB-plates in the roof structure can be used. However, the results of the examining of wooden structures with metal joint-elements presented in [25] show that over time, the wood around such a compound begins to deteriorate due to the effects of temperature and humidity. When heated and cooled, the metal parts heat up and cool down much faster than the wood of the plates. At the same time, moisture condenses on the metal part, penetrates into the plate material and gradually destroys it. Reducing the difference in these deflections at the joint of the OSB-plates with stiffeners at the ends will eliminate this disadvantage without the use of metal parts. Flexural stiffness and load-bearing capacity of plates in the area of their ends can be increased by stiffeners, external reinforcement by carbon composite materials and etc. [28–32].

Conclusions

Logic and the results of the work performed lead to the following conclusions.

Based on the results of FEM-modeling of the OSB plate, it is shown that the tangential load distributed over one of the plate surfaces is the cause of plate bending deformations (Figures 4 and 5).

It is established that in the structure of a soft roof, this tangential component of the vertical load causes unevenness at the joints of OSB inclined plates (Figure 6). Based on the results of the simulation, the largest resulting displacements occur in the lower and upper ends of the plate, respectively, 1.551 and 1.692 mm. The differences cannot be attributed to the catastrophic for new structure. But at repeated influences from snow and the dynamic loading wind, these irregularities can lead to defects in the roof over time. These circumstances also indicate the advisability of continuing research in the area.

In a model example of a finite element model of a vertical plate, it is shown that for such a plate the vertical load, evenly distributed over one of the plate surfaces, causes bending with a curvature of the tangential component line in the form of an S-shaped curve with maximal deflection 0.141 mm. For vertical plates the most dangerous may be a dynamic load of wind. Thus, the obtained results contribute to a better understanding of the board functioning. But at this point dynamic load of wind is the direction for future research.

In order to exclude the revealed cause of the unevenness in the structure of the roof with OSB plates, it is suggested to increase the flexural rigidity of the plates at their ends. For this purpose it is recommended to use OSB plates with stiffening ribs or with external reinforcement with the use of carbon composite materials.

References

1. Gordeeva T. E., Bezgina L. N. Ob ispol'zovanii orientirovanno-struzhechnoj plity v sostave krovli iz mjagkoj cherepicy. [About the use of oriented chipboard in the composition of the roof of soft tiles]. *Industrial and Civil Construction.* 2014. No. 3. Pp. 73–76. (rus)
2. Ambarcumjan S.A., Belubekjan M.V. Tonkaja plastina pri dejstvii poverhnostnoj kasatel'noj nagruzki. [Thin plate under the action of a surface tangential load]. *Proceedings of the NAS RA: Technical Sciences.* 1999. No. 3. Pp. 278-283. (rus)
3. Belubekjan M.V., Martirosjan K.L. K zadache izgiba plastinki po forme cilindricheskoj poverhnosti pri nalichii kasatel'nyh nagruzok na licevyh poverhnostjah [To the problem of bending a plate in the shape of a cylindrical surface in the presence of tangential loads on the faces]. *Mechanics. Proceedings of National Academy of Sciences*

Литература

1. Гордеева Т. Е., Безгина Л. Н. Об использовании ориентированно-стружечной плиты в составе кровли из мягкой черепицы // Промышленное и гражданское строительство. 2014. № 3. С. 73-76.
2. Амбарцумян С.А., Белубекян М.В. Тонкая пластина при действии поверхностной касательной нагрузки // Изв. НАН Армении. Сер. техн. наук. 1999. Т. 52. № 3. С. 278-283.
3. Белубекян М.В., Мартиросян К.Л. К задаче изгиба пластинки по форме цилиндрической поверхности при наличии касательных нагрузок на лицевых поверхностях // Mechanics. Proceedings of National Academy of Sciences of Armenia. 2007. Т. 60. № 2. С. 41-46.
4. Золотов А.Б., Акимов П.А., Сидоров В.Н.,

of Armenia. 2007. No. 2. Pp. 41-46. (rus)

4. Zolotov A.B., Akimov P.A., Sidorov V.N., Mozgaleva M.L. *Chislennye i analiticheskie metody rascheta stroitel'nyh konstrukcij* [Numerical and analytical methods for calculating building structures]. Moscow: ASV, 2009. 336 p.(rus)
5. Shirunov G.N., Tugutov Sh.S., Nidzhad A., Sarvilin D.A. Sravnitel'nyj analiz shodimosti ob#emnyh konechno–jelementnyh modelej v zadache izgiba tolstoj izotropnoj plity s zadelannymi bokovymi granjami [A comparative analysis of the convergence of volume finite-element models in the bending problem of a thick isotropic plate with embedded lateral faces]. *Bulletin of Civil Engineers.* 2016. No. 5 (58). Pp. 86–95. (rus)
6. Serditova N.E., Osetrova M.L. Jekologo-jekonomicheskij analiz ustojchivogo lesopol'zovanija i razvitija predprijatij celljulozno-bumazhnoj promyshlennosti [Ecological and economic analysis of sustainable forest management and development of pulp and paper industry enterprises]. *Vestnik of Tver State University.* Series: Geography and Geoecology. 2016. No. 1. Pp. 12–17. (rus)
7. Serditova N.E. Analiz slozhnyh jekologo-jekonomicheskih sistem: termodinamicheskij podhod [Analysis of complex ecological and economic systems: the thermodynamic approach]. *Proceedings of Russian State Hydrometeorological University.* 2008. No. 7. Pp. 138-153. (rus)
8. Popov E.V. *Sovershenstvovanie konstrukcii i tehnologii izgotovlenija derevokompozitnyh plitno-rebristyh izdelij dlja domostroenija* [Perfection of a design and technology of manufacturing wood-composite plate-ribbed products for house-building]. PhD Thesis. Arkhangelsk. 2016. 24 p. (rus)
9. Yashin M. OSB: Istoriya poyavleniya i razvitiya tekhnologii [OSB: History of the emergence and development of technology]. *LesPromInform.* 2006. № 2(33). (rus)
10. Jashin M. OSB: Istorija pojavlenija i razvitija tehnologii. Chast' 2 [OSB: History of the emergence and development of technology. Part 2]. *Lesprominform.* 2006. No. 3(34). (rus).
11. Broun V.I., Ashkenazi E.K., Klar G.V., Tjurikova L.I., Eger' I.V., Ogarkov B.I. Anizotropija drevesnostruzhechnyh plit s orientirovannymi chasticami i metody ee issledovanija [Anisotropy of particle boards with oriented particles and methods of its investigation]. In the book: *Drevesina i drevesnye materialy* [Wood and wood materials]. Krasnoyarsk: 1974. Pp. 138–162. (rus)
12. Zerbe J.I., Cai Z. Harpole G.B. *An evolutionary history of oriented strandboard (OSB).* United States Department of Agriculture, 2015. [Online]. System requirements: AdopeAcrobatReader. URL:https://www.fpl.fs.fed.us/documnts/fplgtr/fpl_gtr236.pdf (date of application: 19.03.2017).
13. Leonovich A.A. *Novyye drevesnoplitnyye materialy* [New wood-based materials]. St. Petersburg. Publisher: Himizdat. 2008. 158 p. (rus)
14. Nikol'skaja, V. Rossijskij rynok OSB orientirovan na rost [The Russian OSB market is oriented to growth]. Lesprominform. 2016. No. 2(116).
15. Carrera E. Theories and finite elements for multilayered, anisotropic, composite plates and shells. *Archives of Computational Methods in Engineering.* 2002. No. 2. Pp. 87–140. (eng)
16. Barashkov V.N., Matveenko A.A. Modelirovanie prostranstvennogo naprjazhenno-deformirovannogo sostojanija balki-stenki [Simulation of the spatial stress-strain state of a beam-wall]. *Vestnik Tomsk State University of Architecture and Building.* 2010. No. 3. Pp. 92–104. (rus)
17. Thai H.T., Choi D.H. Analytical solutions of refined plate theory for bending, buckling and vibration analyses of thick plates. *Applied Mathematical Modelling.* 2013. No. 18. Pp. 8310–8323.
18. Usarov M.K. Buckling of orthotropic plates with

Мозгалева М.Л. Численные и аналитические методы расчета строительных конструкций: монография. М: МГСУ: Изд-во АСВ, 2009. 336 с.

5. Ширунов Г.Н., Тугутов Ш.С., Ниджад А., Сарвилин Д.А. Сравнительный анализ сходимости объемных конечно-элементных моделей в задаче изгиба толстой изотропной плиты с заделанными боковыми гранями // Вестник гражданских инженеров. 2016. № 5(58). С. 86-95.
6. Сердитова Н.Е., Осетрова М.Л. Эколого-экономический анализ устойчивого лесопользования и развития предприятий целлюлозно-бумажной промышленности // Вестник Тверского государственного университета. Серия: География и геоэкология. 2016. № 1. С. 12–17.
7. Сердитова Н.Е. Анализ сложных эколого-экономических систем: термодинамический подход // Ученые записки Российского государственного гидрометеорологического университета. 2008. № 7. С. 138–153.
8. Попов Е.В. Совершенствование конструкции и технологии изготовления деревокомпозитных плитно−ребристых изделий для домостроения. Автореферат канд. техн. наук. Архангельск. 2016. 24 с.
9. Яшин М. OSB: История появления и развития технологии // ЛесПромИнформ. 2006. № 2(33).
10. Яшин М. OSB: История появления и развития технологии. Часть 2 // ЛесПромИнформ. 2006. № 3(34).
11. Анизотропия древесностружечных плит с ориентированными частицами и методы ее исследования / Броун В.И., Ашкенази Е.К., Клар Г.В., Тюрикова Л.И., Егерь И.В., Огарков Б.И. – В кн.: Древесина и древесные материалы. Красноярск, 1974. С. 138-162.
12. Zerbe J.I., Cai Z. Harpole G.B. An evolutionary history of oriented strandboard (OSB). United States Department of Agriculture, 2015. [Электронный ресурс]. Сист.требования: AdopeAcrobatReader. URL:https://www.fpl.fs.fed.us/documnts/fplgtr/fpl_gtr236.pdf (дата обращения: 19.03.2017).
13. Леонович А. А. Новые древесноплитные материалы // Санкт-Петербург. Издательство: Химиздат. 2008. 158 с.
14. Никольская, В. Российский рынок OSB ориентирован на рост // ЛесПромИнформ. 2016. № 2(116).
15. Carrera E. Theories and finite elements for multilayered, anisotropic, composite plates and shells // Archives of Computational Methods in Engineering. 2002. №. 2. Pp. 87–140.
16. Барашков В.Н., Матвеенко А.А. Моделирование пространственного напряженно-деформированного состояния балки-стенки // Вестник Томского государственного архитектурно-строительного университета. 2010. № 3. С. 92–104.
17. Thai H.T., Choi D.H. Analytical solutions of refined plate theory for bending, buckling and vibration analyses of thick plates // Applied Mathematical Modelling. 2013. № 18. Pp. 8310–8323.
18. Усаров М.К. Изгиб ортотропных пластин с учетом бимоментов // Инженерно-строительный журнал. 2015. № 1 (53). С. 80–90.
19. Thai H.T., Nguyen T.K., Vo T.P., Ngo T. A new simple shear deformation plate theory // Composite Structures. 2017. № 1. Pp. 277–285.
20. Zappalorto M. On the stress state in rectilinear anisotropic thick plates with blunt cracks // Fatigue & Fracture of Engineering Materials & Structures. 2017. № 1. Pp. 103-119.
21. Caliri M.F., Ferreira A.J. M., Tita V. A new finite element for thick laminates and sandwich structures using a generalized and unified plate theory // International Journal for Numerical Methods in Engineering. 2017. №. 2. Pp. 290–304. (eng)
22. Тимошенко С.П., Войновский-Кригер С. Пластинки и оболочки // Москва. Издательство URSS. 2009. 640 с.
23. Неклюдова Е.А., Семёнов А.С., Мельников Б.Е.,

bimoments. *Magazine of Civil Engineering.* 2015. No. 1(53). Pp. 80–90. (rus)
19. Thai H.T., Nguyen T.K., Vo T.P., Ngo T. A new simple shear deformation plate theory. *Composite Structures.* 2017. No. 1. Pp. 277–285.
20. Zappalorto M. On the stress state in rectilinear anisotropic thick plates with blunt cracks. *Fatigue & Fracture of Engineering Materials & Structures.* 2017. No. 1. Pp. 103-119.
21. Caliri M.F., Ferreira A.J. M., Tita V. A new finite element for thick laminates and sandwich structures using a generalized and unified plate theory. *International Journal for Numerical Methods in Engineering.* 2017. No. 2. Pp. 290–304.
22. Timoshenko S.P., Voinovsky-Krieger S. *Plastinki i obolochki* [Plates and Shells]. Moscow: Publisher URSS. 2009. 640 p. (rus)
23. Neklyudova Ye.A., Semenov A.S., Melnikov B.Ye., Semenov S.G. Experimental research and finite element analysis of elastic and strength properties of fibreglass composite material. *Magazine of Civil Engineering.* 2014. No. 3(47). Pp. 25–39. (rus)
24. Karpov V.V., Semenov A.A. Kriterii prochnosti dlja tonkostennyh ortotropnyh obolochek. Ch. 1: Analiz osnovnyh kriteriev prochnosti izotropnyh i ortotropnyh materialov [Strength criteria for thin-walled orthotropic shells. Part 1: Analysis of the main criteria for the strength of isotropic and orthotropic materials]. *Bulletin of Civil Engineers.* 2014. No. 6(47). Pp. 43–51. (rus)
25. Lalin V. V., Rybakov V. A. The finite elements for design of building walling made of thin-walled beam. *Magazine of Civil Engineering.* 2011. No. 8. Pp. 69–80. (rus)
26. Karpov V.V., Semenov A.A. Strength criteria for thin-walled orthotropic shells. Part 2: Calculations and analysis. *Bulletin of Civil Engineers.* 2015. No. 1(48). Pp. 60–70. (rus)
27. Chen G., He B. Stress-strain constitutive relation of OSB under axial loading: an experimental investigation. *BioResources.* 2017. No. 3(12). Pp. 6142–6156.
28. Dijachkova A.A., Kuznecov V.D. Raschet usilenija zhelezobetonnyh plit uglerodnymi kompozicionnymi materialami [Calculation of the reinforcement of reinforced concrete slabs by carbon composite materials]. *Magazine of Civil Engineering.* 2009. No. 3. Pp. 25–28. (rus)
29. Beck K., Cloutier A., Salenikovich A., Beauregard R. Comparison of mechanical properties of oriented strand board made from trembling aspen and paper birch. *European Journal of Wood and Wood Products.* 2010. No. 1(68). Pp. 27–33.
30. Yu Z., Fan M. Short-and long-term performance of wood based panel products subjected to various stress modes. *Construction and Building Materials.* 2017. Vol. 156. Pp. 652–660.
31. Salari A., Tabarsa T., Khazaeian A., Saraeian A. Improving some of applied properties of oriented strand board (OSB) made from underutilized low quality paulownia (Paulownia fortunie) wood employing nano-SiO2. *Industrial crops and products.* 2013. Vol. 42. Pp. 1-9.
32. Collins M., Cosgrove T., Mellad A. Characterisation of OSB properties for application in gridshells. *Materials and Structures.* 2017. No. 2(50). P. 131.

Семёнов С.Г. Экспериментальные исследования и анализ методом конечных элементов прочностных и упругих характеристик композитного материала из стеклопластика // Инженерно-строительный журнал. 2014. № 3(47). С. 25–39.
24. Карпов В.В., Семенов А.А. Критерии прочности для тонкостенных ортотропных оболочек. Ч. 1: анализ основных критериев прочности изотропных и ортотропных материалов // Вестник гражданских инженеров. 2014. № 6(47). С. 43–51.
25. Лалин В.В., Рыбаков В.А. Конечные элементы для расчета ограждающих конструкций из тонкостенных профилей // Инженерно-строительный журнал. 2011. № 8. С. 69–80.
26. Карпов В.В., Семенов А.А. Критерии прочности для тонкостенных ортотропных оболочек. Ч. 2: расчеты и анализ // Вестник гражданских инженеров. 2015. № 1(48). С. 60–70.
27. Chen G., He B. Stress-strain constitutive relation of OSB under axial loading: an experimental investigation // BioResources. 2017. № 3(12). Pp. 6142–6156.
28. Дьячкова А.А., Кузнецов В.Д. Расчет усиления железобетонных плит углеродными композиционными материалами // Инженерно-строительный журнал. 2009. № 3. С. 25–28.
29. Beck K., Cloutier A., Salenikovich A., Beauregard R. Comparison of mechanical properties of oriented strand board made from trembling aspen and paper birch // European Journal of Wood and Wood Products. 2010. № 1(68). Pp. 27–33.
30. Yu Z., Fan M. Short-and long-term performance of wood based panel products subjected to various stress modes // Construction and Building Materials. 2017. Vol. 156. Pp. 652–660.
31. Salari A., Tabarsa T., Khazaeian A., Saraeian A. Improving some of applied properties of oriented strand board (OSB) made from underutilized low quality paulownia (Paulownia fortunie) wood employing nano-SiO2 // Industrial Crops and Products. 2013. Vol. 42. Pp. 1–9.
32. Collins M., Cosgrove T., Mellad A. Characterisation of OSB properties for application in gridshells // Materials and Structures. 2017. № 2 (50). P. 131.

Timmo Gavrilov,
+7(911)4249306; gtimmo@mail.ru

Gennady Kolesnikov,
+7(921)4519247; kolesnikovgn@yandex.ru

Тиммо Александрович Гаврилов,
+7(911)4249306; эл. почта: gtimmo@mail.ru

Геннадий Николаевич Колесников,
+7(921)4519247; эл. почта: kolesnikovgn@yandex.ru

Gavrilov T.A., Kolesnikov G.N. Oriented particle boards: effect of the tangential load component. *Magazine of Civil Engineering*. 2017. No. 6. Pp. 33–42. doi: 10.18720/MCE.74.3.

doi: 10.18720/MCE.74.4

Level ice interactions with multi-legged offshore structures

Воздействия ровного ледового поля на многоопорные гидротехнические сооружения

V.A. Politko,
I.G. Kantardgi,
National Research Moscow State Civil Engineering University, Moscow, Russia

Аспирант В.А. Политько,
д-р техн. наук, профессор И.Г. Кантаржи,
Национальный исследовательский Московский государственный строительный университет, г. Москва, Россия

Key words: multi-legged offshore structures; ice actions; numerical model; ANSYS; legs shielding effects

Ключевые слова: многоопорные сооружения; ледовая нагрузка; численная модель; ANSYS; взаимовлияние опор

Abstract. The task of determining the total ice load from drifting level ice floes on 3- and 4-legged structures, widely used in the development of offshore oil & gas fields, was considered in the article. The ANSYS numerical 3D model was used to investigate how the total ice load is influenced by various factors, including the thickness of ice, the leg spacing, the ice drift direction in relation to the structure, the presence of jammed ice between the legs. Based on the results of numerical analysis, a comparison was made between the 3- and 4-legged structures in terms of magnitude of ice load, as well as additional recommendations were done for the procedure of total ice loading calculation in accordance with the Russian national code.

Аннотация. В статье рассмотрены задачи определения суммарной ледовой нагрузки от ровного ледового поля на 3-х и 4-х опорные сооружения, широко применяемые при разработке морских шельфовых месторождений. При помощи численной 3D модели в программе ANSYS было проанализировано влияние на суммарную ледовую нагрузку различных факторов, в том числе толщины льда, расстояния между опорами, угла дрейфа льда относительно сооружения, наличия затора ледовой массы в пространстве между опорами. На основе результатов численного моделирования было проведено сравнение 3-х и 4-х опорного сооружения с точки зрения величины ледовой нагрузки, а также представлены дополнительные рекомендации к расчету суммарной ледовой нагрузки по отечественным строительным нормам.

Introduction

Among the offshore structures there are both single- and multi-leg structures. The quantity, location and distance between them depend on specifics of the structure, its functional purpose and the loading combinations perceived by each leg. Several examples of multi-legged structures are shown on Figure 1.

a) b) c)

Figure 1. Examples of multi-legged offshore structures: a) four-legged offshore oil & gas platform; b) multi-span bridge; c) LNG Jetty

Политько В.А., Кантаржи И.Г. Воздействия ровного ледового поля на многоопорные гидротехнические сооружения // Инженерно-строительный журнал. 2017. № 6(74). С. 43–52.

The task of effective design of multi-legged offshore ice-resistant structures in the waters of northern seas is of ultimate importance now days, and accuracy of determining the ice loads directly affects the material consumption and the final cost of the structure, as well as the operation safety.

The total ice load on a multi-legged structure is determined, as a rule, according to the principle:

Total ice load = number of legs × leg factor × individual leg load.

And according to the Russian Set of Rules SP 38.13330.2012 "Loads and impacts on hydraulic structures" [1], the total load is determined by the formula:

$$F_{total} = n_t K_1 K_2 F_1, \tag{1}$$

where n_t– number of legs; F_1 – ice loading on 1 leg; K_1, K_2 – factors, taking into account non-simultaneous peak loads on individual legs and the shielding effect of adjacent legs accordingly.

After determining the individual ice load per one leg, F_1 (which is a separate task and not considered in detail in this paper), the key issue is consideration of factors that influence the total ice load on a multi-legged structure, namely:

$$F_{total}/F_1 \tag{2}$$

$$\text{or } n_t K_1 K_2 \tag{3}$$

Among the main known factors are the following:

1) mutual influence of legs and leg shielding;

2) non-simultaneous occurrence of load peaks on different legs;

3) probability of ice rubble jamming between the legs.

The influence of the *first* and *second factors* is difficult to track separately. Therefore, their joint influence on the total ice load is usually considered. At the moment, there is a limited number of works presented at various international conferences [2-5], where this theme was highlighted. They all considered 4-legged structures only. The main conclusion of the works was the fact that the ratio F_{total}/F_1 depends on the following main factors:

$$F_{total}/F_1 \sim \alpha;\ L/D \tag{5}$$

where α – is an impact angle of drifting ice in relation to the structure. It was justified that the maximum total ice load on the 4-legged structure takes place when the structure is exposed to the ice drift at the angle of 20-30˚ relative to the horizontal axis of the structure;

L/D - is the ratio of the leg spacing L, m, and the leg diameter D, m. At the same time, different works gave different dependency of F_{total}/F_1 as a function of L/D. In some papers it was said that F_{total}/F_1 is not influenced by L/D variation at L/D>6 [2], in others at L/D>12-20 [3-5].

Another conclusion from the previous works was the fact that, depending on conditions, F_{total}/F_1 for the 4-legged structure may vary in the range of 2-3.5.

Nevertheless, in these works the influence of ice thickness on F_{total}/F_1 was not disclosed, the physics of ice interaction with shielded backside legs depending on α was not fully disclosed, and there was no consistency in certain results. Thus, the need for further research on this issue is evident.

A number of sources [6-8], including the international standard ISO 19906 [8], indicate the need to take into account the *third factor*, the probability of ice jamming in between legs, in the form of an additional coefficient K_{jam} (when L/D <4). At the same time, none of the sources give any specific recommendations on the value of the coefficient. Further studies are needed to justify the coefficient.

Therefore, the main goal of the research was to check the magnitudes of leg factors with the help of numerical modelling and to give certain recommendations for magnitude of the third factor, namely ice jamming factor. The supplementary goal was to check which of the two structures, 3- or 4-legged, perceive less loading from level ice in ice-infested waters.

To achieve these goals the following was done:

1. A 3D numerical model for the level ice was created in ANSYS;

2. Investigation of how F_{total}/F_1 is influenced by the drifting ice impact angle α, the thickness of the ice *h* and the leg spacing L/D;
3. Analysis of physics of ice field – structure interaction process when ice rubble is jammed and consolidated in between the legs. Estimation of the possible increase in ice loading due to this effect;
4. Comparison of 3 and 4- legged structures in terms of ice loading magnitude.

Methods

The study was carried out by numerical simulation in the ANSYS Explicit Dynamics program. In order to study the ice field – structure interaction process, a specially developed numerical 3D model was used, for which the following assumptions had been done:

1) ice was regarded as a solid body;

2) the brittle fracture of ice was considered at relatively high deformation rates. It's assumed that before the brittle failure, the ice behaves in elastic mode under loading. To describe the mechanical behavior of ice under load, the Mohr-Coulomb model was used, in which the strength of ice depended on the lateral pressure, and the compressive strength was an order of magnitude higher than the tensile strength, which corresponds to the actual behavior of ice under load described by many sources [11-13]. Table 1 presents the basic characteristics of the model ice, adopted based on analysis of different Russian and foreign sources [14-17]. The Mohr-Coulomb model had been previously used by other researchers to describe ice behavior [18-21];

3) brittle fracture in dynamics was taken into account by removing individual finite elements (by Element Erosion technique). As a criterion for destruction, the principal normal deformations were assumed;

4) the hydrostatic and hydrodynamic effects of water were not taken into account;

Table 1. Basic physical and mechanical data of the model ice

Density, kg/m3	900
Elastic modulus, MPa	3000
Poisson's ratio	0.3
Angle of internal friction, ˚	30
Cohesion coefficient, MPa	1.0
Maximum principal strain	0.001

Verification of the numerical model was carried out by comparing the simulation results with the results of two experimental studies:

1. Indentation of rectangular horizontal stamp in ice field (full-scale tests in the Sea of Okhotsk, 1998, [9]);

2. Laboratory model tests of ice field interaction with 4-legged structure, 2011, [2].

As verification showed, the numerical model yielded results close to actual conditions. Figure 2 shows that the numerical model accurately reproduces the character of ice load oscillations in time, which was noticed during field trials in the Sea of Okhotsk [9], when the peak load was due to initial contact, and the subsequent load was only 20-80% of the initial load. Figure 3 shows that the nature of the legs penetration through the ice field by numerical modeling and during model tests in the Krylov Research Center [2] actually coincides.

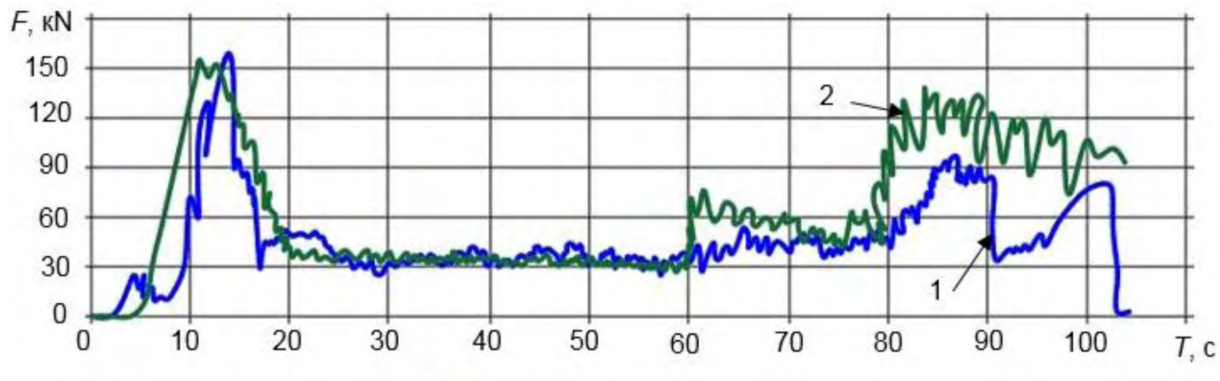

Figure 2. Graph of ice load oscillations during the stamp indentation experiment:
1 – during the field works; 2 – during the numerical modelling [10]

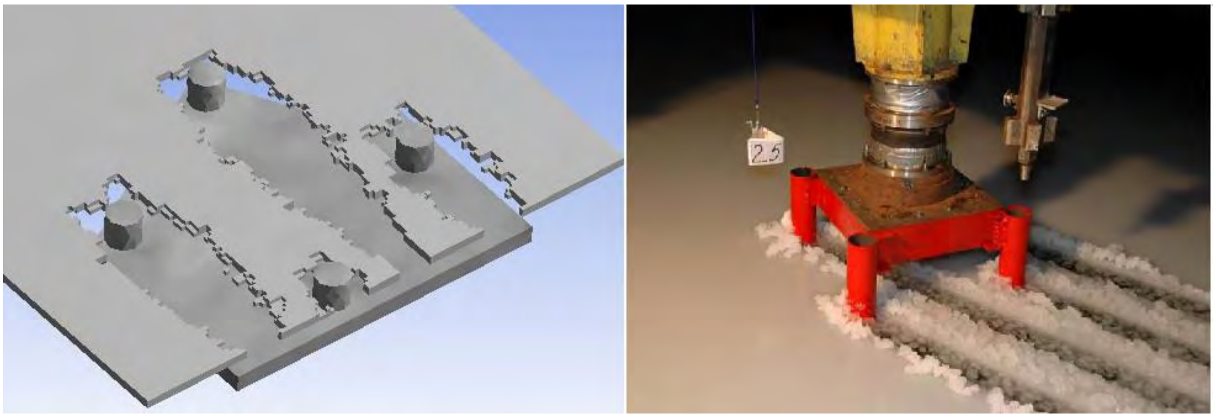

a) **b)**

Figure 3. The picture of 4-legged structure penetration in the ice field when $\alpha = 30°$:
a) during numerical modelling; b) during model tests in the basin

Results and Discussion

In order to investigate the mutual influence of adjacent legs on the total ice load, numerical modeling was carried out for a number of scenarios, namely, for L/D = 3; 4.5; 6; 8 at the drifting ice impact angles α = 0; 15; 22.5; 45˚ for 4-legged structures and at α=0; 15; 30; 60˚ for 3-legged structures. The thickness of ice was taken h = 0.5 m and 1.0 m. The results of numerical modelling are presented in Table 2 and Figures 4, 5 for 4-legged structures, in Table 3 and Figure 7 for 3-legged structures.

Table 2. Results of numerical analysis of mutual influence of legs of the 4-legged structure on the total ice load in the form of F_{total}/F_1.

	0˚	15˚	22.5˚	45˚
h = 0.5 m (D/h = 6)				
L/D = 3	1.9	2.4	2.6	2.6
L/D = 4,5	1.9	2.7	2.9	2.7
L/D = 6	1.9	2.9	3.1	2.7
L/D = 8	1.9	3.0	3.2	2.8
h = 1.0 m (D/h = 3)				
L/D = 3	1.9	2.9	3.1	2.8
L/D = 6	1.9	3.2	3.4	2.8

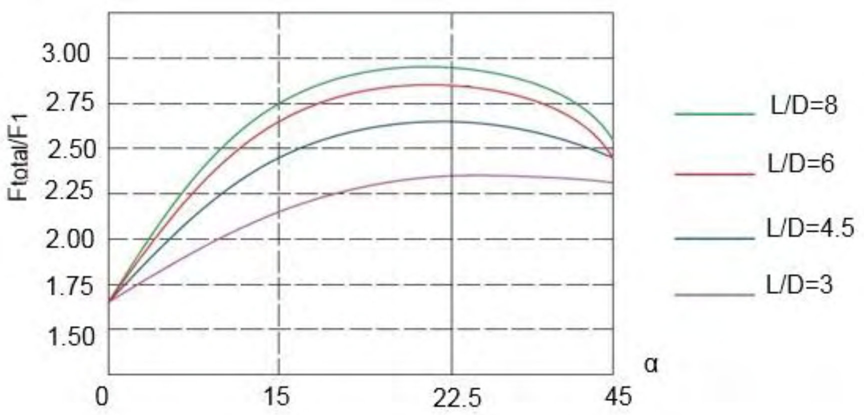

Figure 4. The graph of dependence of F_{total}/F_1 on the leg spacing and ice drift impact angles (for ice thickness h=0,5м) for the 4-legged structure

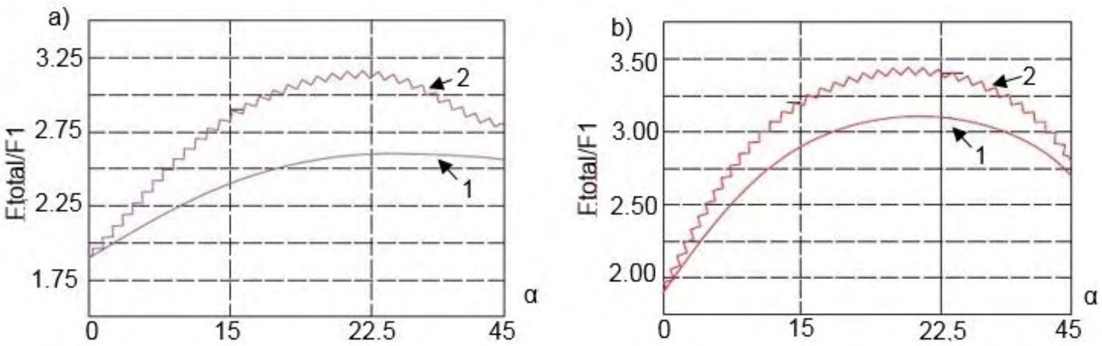

Figure 5. Graph of ice thickness influence on F_{total}/F_1 at:
a) *L/D*=3; b) *L/D*=6; 1–h=0,5m; 2– h=1m

From Table 2 and Figures 4, 5 it can be seen that:

- for the 4-legged structure (when ice thickness h = 0.5 and h = 1.0 m) the ratio F_{total}/F_1 = 1.9-3.4, which, in general, corresponds with the previously declared results by other researchers;
- the peak load was observed when the ice acted on all four legs and when the second row of legs was not in the shadow of the front legs (fully or partially), that is, when the angle of impact was in the range 20-30˚ (Figure 5).
- the ratio F_{total}/F_1 as a function *L/D* did not change significantly for *L/D* = 6 and *L/D* = 8. As a result, it can be assumed that for *L/D*> 8 F_{total}/F_1 will not be influenced by *L/D* increase. This result is higher than 6 from [2], but less than 12-20 from [3-5].
- the thickness of ice, or the ratio *D/h*, has a large influence on F_{total}/F_1, which is clearly showed on Figure 5. This is because, under certain conditions, ice will break down on contact with the second row legs not in compression, but as a result of loss of stability, as depicted in Figure 6a.

Figure 6. Nature of structure legs penetration through the ice field at L/D=6, α=22.5˚:
a) h = 0.5 m; b) h = 1.0 m

Table 3. Results of numerical analysis of mutual influence of legs of the 3-legged structure on the total ice load in the form of F_{total}/F_1.

	0˚	15˚	30˚	60˚
h = 0.5 m (D/h = 7) at D = 3.5 m				
L/D = 3	2.6	2.3	1.9	2.5
L/D = 4.5	2.7	2.4	1.9	2.6
L/D = 6	2.7	2.5	1.9	2.7
L/D = 8	2.8	2.6	1.9	2.7
h = 1.0 m (D/h = 3.5) at D = 3.5 m				
L/D = 3	2.8	2.4	1.9	2.7
L/D = 6	2.9	2.7	1.9	2.9

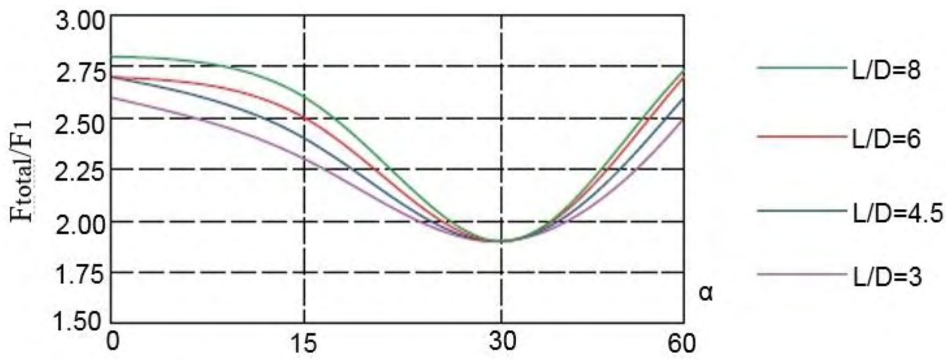

Figure 7. The graph of dependence of F_{total}/F_1 on the leg spacing and ice drift impact angles (for ice thickness h=0,5м) for the 3-legged structure

Analyzing the results for 3-legged structure, shown on Table 3 and Figure 7, it can be concluded that, depending on the ice drift impact angle on the 3-legged structure, the ratio F_{total}/F_1 can vary in the range 1.9-2.9. The smallest load occurs when the third support is completely or partially in the shadow of the front support. Reduction of the total load, as well as in the case with the 4-legged structure, may happen due to increased flexibility of level ice (at h ≤ 0.5 m).

The numerical analysis showed for the 4-legged structure that in some cases the presence of jammed ice mass inevitably leads to an increase in the total ice load, namely, at the drifting ice impact angles close to α = 0 ° and α = 45 °, as shown on Figure 8. It can be seen that the load from the impact of level ice field is transferred to shadow supports through the jammed ice mass. But, in case when there is no jammed ice, these legs remain untouched. The additional load will depend on the strength of the jammed ice mass. But taking into account the reduced strength of jammed ice comparing to level ice, the simulation results give an increase in the total load by 15 % and 10 %, respectively.

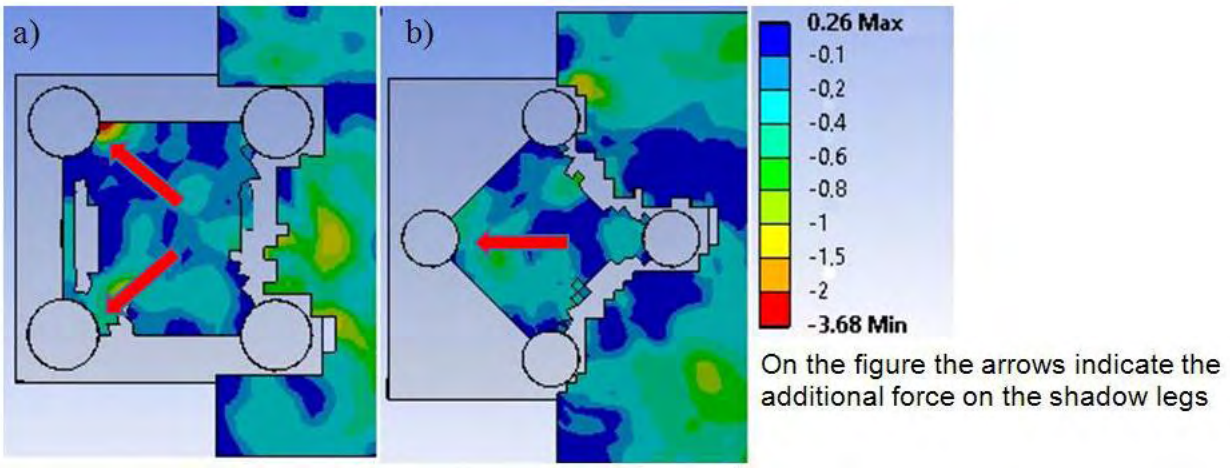

Figure 8. The field of principal normal stresses of drifting level ice and the jammed ice: a)$\alpha = 0°$; b)$\alpha = 45°$.

Politko V.A., Kantardgi I.G. Level ice interactions with multi-legged offshore structures. *Magazine of Civil Engineering*. 2017. No. 6. Pp. 43–52. doi: 10.18720/MCE.74.4.

On Figure 9 there is a picture of ice impacting structure at α = 22.5 °. It can be seen that for three frontal legs, the nature of ice impact does not actually change (as for the case without ice jam). On the 4th backside leg, the ice field acts through the jammed ice mass. Strength and thickness of the ice mass will determine the load on this support. But the numerical simulation showed, that increase in the total load in this case will be not significant. Table 4 presents the values of the total ice load on the 4-legged structure at *L/D* = 3, considering the presence of ice jammed mass and it's absence (for comparison).

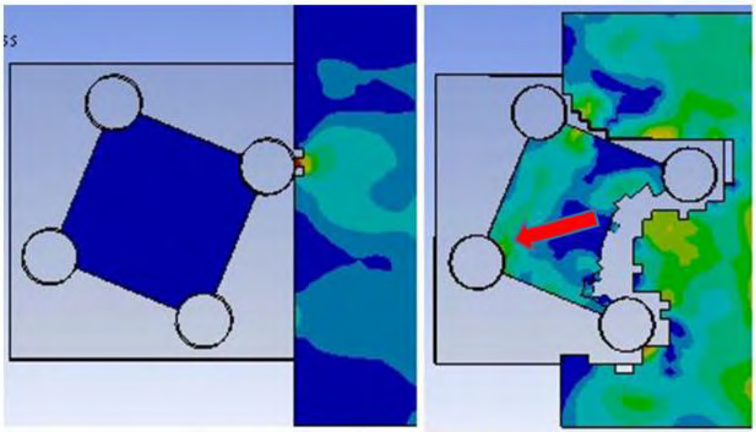

Figure 9. The field of principal normal stresses of drifting level ice and the jammed ice in case of ice field impacting the 4-legged structure at angle $\alpha = 22.5°$

Table 4. Values of the total ice load on 4-legged structure for the jammed ice situation and its absence

	$\alpha = 0°$	$\alpha = 15°$	$\alpha = 22.5°$	$\alpha = 45°$
No jammed ice	2.5 MPa	3.1 MPa	3.4 MPa	3.4 MPa
Jammed ice	2.85 MPa (+ 15 %)	3.25 MPa (+ 5 %)	3.47 MPa (+ 2 %)	3.75 MPa (+ 10 %)

Based on results, it is possible to confirm the validity of introduction of an additional coefficient to account for the effect of ice jam, which is proposed by some sources and standards [6-8], when determining the total ice load on the 4-legged structure at *L/D* < 4. The value of this coefficient should be justified for individual cases, but as numerical study show, the presence of consolidated ice jam can increase the total ice load by no more than 10%. Thus, the coefficient can be taken as K_{jam}=1.1.

For the 3-legged structure the results of the numerical simulation did not show any significant increase in the load. It can be seen on Fig. 10 that the transfer of the compressive forces from the ice field to the backside leg through the ice jam takes place along the length *S*, which is comparable with the diameter of leg - *D*. At the edges of the ice jammed mass, tensile stresses arise which cause a rapid collapse of ice. Thus, the jammed ice factor for 3-legged structures in most cases can be neglected.

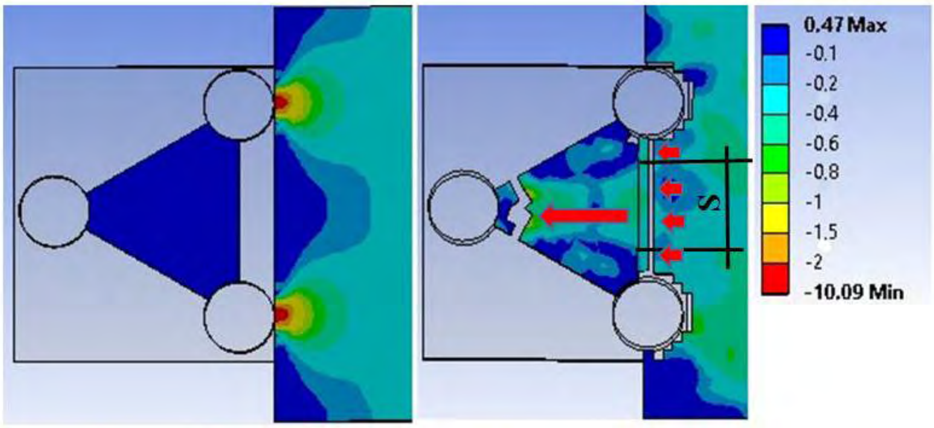

Figure 10. The field of principal normal stresses of drifting level ice and the jammed ice in case of ice field impacting the 3-legged structure at angle $\alpha = 0°$.

As the last point of the current research, the 3- and 4-legged structures are compared in terms of the magnitude of total ice load. Two situations are considered: *L/D* < 4 - when the ice jam present, *L/D* > 4 – no ice jam. The results are applicable for an ice thickness of up to 1 meter, which was considered in the numerical study.

Situation 1. *L/D < 4* (presence of ice jam).

As the numerical study showed for the 4-legged structure (Table 2), the maximum value of ratio F_{total}/F_1 for the case of $\alpha =$ 22.5 and *L/D* < 4 was 3.1. Taking into account the effect of ice jam, $K_{jam} = 1.1$, leg diameter *D*=3m and thickness of ice *h*=1m, the total load is determined as following:

$$F_4 = 3.1F_1 \cdot K_{jam} = 3.1 \cdot p_{ice} \cdot 3 \cdot 1 \cdot 1.1 = 10.23p_{ice}, \quad (6)$$

where p_{ice} – effective pressure of ice (for the study intentionally considered the same for 3- and 4-legged structures).

The total load on the 3-legged structure is determined taking into account the fact that the maximum value of F_{total}/F_1 for the case α = 0˚ and *L/D* < 4 was 2.8 (Table 3), $K_{jam} = 1.0$, diameter of the support *D* = 3.5 m, thickness of ice *h* = 1 m:

$$F_3 = 2.8F_1{}^{/} \cdot K_{jam} = 2.8 \cdot p_{ice} \cdot 3{,}5 \cdot 1 \cdot 1.0 = 9.8p_{ice} \quad (7)$$

As it can be seen from the calculation results, the difference in the ice load is minimal.

Situation 2. *L/D > 4* (no ice jam).

Following the same procedure, as in the first Situation, the total ice loads are determined for the situation when *L/D>4* and ice jam is not present:

$$F_4 = 3.4F_1 = 3.4 \cdot p_{ice} \cdot 3 \cdot 1 = 10.2\, p_{ice} \quad (8)$$

$$F_3 = 2.9F_1{}^{/} = 2.9 \cdot p_{ice} \cdot 3{,}5 \cdot 1 = 10.15\, p_{ice} \quad (9)$$

As it can be seen, the ice load on the 4-legged structure is only slightly higher than the same load on the 3-legged structure. Thus, when choosing one of the two types of structures, other from ice load magnitude criteria will come to the fore, such as the convenience of transportation and construction, the weight of the structure, the layout of the deck, and others. At the current moment the preference is mostly given to 4-legged structures. Though, some researchers, like Vershinin S.A. [14], mentioned that 3-legged structure might be more efficient in ice-infested waters.

Conclusions

1. The results of numerical study showed that mutual influence of adjacent legs on the total ice load is determined by the following factors:

– ice impact angle: for both 3- and 4-legged structures, the biggest ice load is noticed when the second row legs are not shielded by the front legs (fully or partially). For the 4-legged structure this angle is in the range 20-30˚ (as on Figure 6), for the 3-legged structure - when ice initially hits 2 legs (as on Figure 10);

– the leg spacing: as the study showed, F_{total}/F_1 will not be significantly influenced by *L/D* when *L/D* > 8;

– ice thickness *h* (or *D/h* ratio): the thickness of ice implies a significant effect on F_{total}/F_1 and on the total ice load as a result. In case of sufficient flexibility (at *h* ≤ 0.5 m, *D/h* ≥ 6), the ice, acting on the legs of the second row, may break down by loss of stability, rather than in a crushing mode. Thus, based on the numerical simulation results for relative thin ice (*h* ≤ 0.5 m, *D/h* ≥ 6) for the 4-legged structure, the effect of mutual influence of adjacent legs gave the maximum result of F_{total}/F_1 - 3.2; for thicker ice (*h* ≤ 1.0 m, *D/h* ≥ 3) – 3.4. Accordingly, for the 3-legged structure for thin ice (*h* ≤ 0.5 m, *D/h* ≥ 7) - 2.8; for thicker ice (*h* ≤ 1.0 m, *D/h* ≥ 3.5) - 2.9.

2. Regarding the ice jamming effect on the total ice load, the numerical study showed the validity of introducing an additional coefficient accounting for the effect of ice rubble jam in between legs of structure, which is proposed by some sources and standards [6-8], when determining the total ice load on the 4-legged structures at *L/D* < 4. The value of this coefficient should be

justified for each individual case, but as the simulation results showed, the ice jam effect should not increase the total ice load by more than 10 %. Thus, the coefficient can be taken as K_{jam}=1.1.

3. The numerical study showed (when the ice thickness is up to 1 meter) the ice load on the 4-legged structure is only slightly higher than the same load on the 3-legged structure. So, when choosing one of the two types of structures in this case, other criteria, such as the convenience of transportation and construction, the weight of the structure, the layout of the deck, and others will come to the fore.
4. The following provisions should be regarded when estimating total ice loads on 3- and 4-legged structures according to Russian standard [1]:

– since the total ice load depends on various factors, including the ice thickness, leg spacing and drifting ice impact angle, coefficients K_1 and K_2 need to be refined for each individual case by numerical and physical modeling. Nevertheless, the results of the numerical study yielded the values of $n_t K_1 K_2$ close to that, which Russian Set of Rules SP 38.13330.2012 might give, namely 3.4-3.5 for the 4- legged structure. For the 3-legged structure the calculated value of $n_t K_1 K_2$ by Russian Set of Rules SP 38.13330.2012 will yield a result of 2.6-2.7, which is less than the result of the numerical study, which is 2.8-2.9. Therefore, for 3-legged structures, calculations according to the Standard might yield underestimated results, which should be taken into account;

– when there is a possibility of ice rubble jamming and it's consolidation in the space between legs of the structure (as a rule, at *L/D* < 4), it is recommended to introduce an additional coefficient of jammed ice K_{jam}, equal to 1.1 for the 4-legged structures.

References

1. *SP 38.13330.2012 Nagruzki i vozdeistviya na gidrotekhnicheskie sooruzheniya* [Russian Set of Rules SP 38.13330.2012 Loads and impacts on hydraulic structures] (aktualizirovannaya redaktsiya SNiP 2.06.04-82*). Minregion Rossii. Moscow. 2012. 102 p.
2. Karulina M., Shkhinek K., Thomas G. Theoretical and experimental investigations of level ice interaction with four-legged structures. *Proc. 21st Int. Conf. on Port and Ocean Eng. under Arctic cond., POAC 11.* 2011. Pp. 235-246.
3. Huang Y., Shi Q., Song A. Model test study of the shielding effect of multi-pile structures on ice force. *Proc. 18th Int. Conf. on Port and Ocean Eng. under Arctic cond., POAC 05.* 2005. Pp. 47-51.
4. Shkhinek K., Jilenkov A., Blanchet D., Thomas G. Ice loads on a four leg structure. *Proc. 20th Int. Conf. on Port and Ocean Eng. under Arctic cond., POAC 09.* 2009. Pp. 456-469.
5. Barker A., Sayed M. Multi-leg structures in ice – examining global loading uncertainties. *Proc. 22nd Int. Conf. on Port and Ocean Eng. under Arctic cond., POAC 13.* 2013. Pp. 576-584.
6. Palmer A., Wei B., Hien P.L., Thow Y.K. Ice jamming between the legs of multi-leg platforms. *Proc. 23rd Int. Conf. on Port and Ocean Eng. under Arctic cond., POAC 15.* 2015. Pp. 433-442.
7. Palmer A., Croasdale K. *Arctic Offshore Engineering*. World Scientific Publishing Co. Pte. Ltd.. 2013. 420 p.
8. *ISO 19906* Petroleum and natural gas industries – Arctic offshore structures. International Organization of Standardization. 1st edition. 2010. 440 pp.
9. Taylor R., Frederking R., Jordaan I. The nature of high pressure zones in Compressive Ice Failure. *Proc. 19th IAHR international Symposium on Ice.* 2008. 440 p.
10. Polit'ko V.A., Kantarzhi I.G. Chislennoe modelirovanie vozdeistviya ledovykh polei na gidrotekhnicheskie sooruzheniya [Numerical modeling of the effect of ice fields on hydraulic structures]. *Stroitel'stvo – formirovanie sredy zhiznedeyatel'nosti* [Construction - the formation of living environment]. *Proceedings of 20th International*

Литература

1. СП 38.13330.2012 «Нагрузки и воздействия на гидротехнические сооружения» (актуализированная редакция СНиП 2.06.04-82*) / Минрегион России. М.: 2012. 102 с.
2. Karulina M., Shkhinek K., Thomas G. Theoretical and experimental investigations of level ice interaction with four-legged structures // Proc. of 21st Int. Conf. on Port and Ocean Eng. under Arctic cond., POAC 11. 2011. Pp. 235-246.
3. Huang Y., Shi Q., Song A. Model test study of the shielding effect of multi-pile structures on ice force // Proc. of 18th Int. Conf. on Port and Ocean Eng. under Arctic cond., POAC 05. 2005. Pp. 47-51.
4. Shkhinek K., Jilenkov A., Blanchet D., Thomas G. Ice loads on a four leg structure // Proc. of 20th Int. Conf. on Port and Ocean Eng. under Arctic cond., POAC 09. 2009. Pp. 456-469.
5. Barker A., Sayed M. Multi-leg structures in ice – examining global loading uncertainties // Proc. of 22nd Int. Conf. on Port and Ocean Eng. under Arctic cond., POAC 13. 2013. Pp. 576-584.
6. Palmer A., Wei B., Hien P.L., Thow Y.K. Ice jamming between the legs of multi-leg platforms // Proc. of 23rd Int. Conf. on Port and Ocean Eng. under Arctic cond., POAC 15. 2015. Pp. 433-442.
7. Palmer A., Croasdale K. Arctic Offshore Engineering. World Scientific Publishing Co. Pte. Ltd. 2013. 420 p.
8. ISO 19906 “Petroleum and natural gas industries – Arctic offshore structures” / International Organization of Standardization, 1st edition. 2010. 440 p.
9. Taylor R., Frederking R., Jordaan I. The nature of high pressure zones in Compressive Ice Failure // Proc. of 19th IAHR international Symposium on Ice. 2008. Pp. 267-279.
10. Политько В.А., Кантаржи И.Г. Численное моделирование воздействия ледовых полей на гидротехнические сооружения // Строительство – формирование среды жизнедеятельности. Сборник трудов XX Международной межвузовской научно-практической конференции. Москва: МГСУ, 2017. С. 186-196.

University scientific-practical conference. Moscow: MGSU. 2017. Pp. 186-196. (rus)

11. Schulson E.M., Nickolayev O.Y. Failure of columnar saline ice under biaxial compression: failure envelopes and brittle-to-ductile transition. *Journal of Geophysical Research.* 1995. Vol. 100. No. 11. Pp. 383-400.
12. Timco G.W., Frederking R.M.W. Confined compression tests: outlining the failure envelope of columnar sea ice. *Cold Regions Science and Technology*. 1986. No. 12(1). Pp. 13–28.
13. Shkhinek K., Loset S., Karna T. Global ice load dependency on structure width and ice thickness. Proc. 17th Int. Conf. on Port and Ocean Eng. under Arctic cond., POAC 03. 2003. Pp. 367-375.
14. Vershinin S.A., Truskov P.A., Kuzmichev K.V. *Vozdeistvie l'da na sooruzheniya Sakhalinskogo shel'fa* [The impact of ice on the structures of the Sakhalin shelf]. Moscow: Institut Giprostroimost. 2005. 208 p. (rus)
15. Surkov G.A., Zemlyuk S.V., Astaf'ev V.P., Polomoshnov A.M. Fiziko-mekhanicheskie parametry ledyanogo pokrova severnogo shel'fa Sakhalina [Physico-mechanical parameters of the ice cover of the northern shelf of Sakhalin]. *Trudy AANII* [AANII works]. Saint-Petersburg: Gidrometeoizdat. 2001. Vol. 443. Pp. 65-76. (rus)
16. Timco G.W., Weeks W.F. A review of the engineering properties of sea ice. *Cold Regions and Technology.* 2010. No. 60. Pp. 107-129.
17. Jordaan I. Mechanics of ice-structure interaction. *Engineering Fracture Mechanics.* 2001. No. 68. Pp. 47-59.
18. Li Lyan, Shkhinek K.N. Vozdeistvie l'da na otkosnye sooruzheniya [The impact of ice on sloping structures]. Magazine of Civil Engineering. 2014. No. 1. Pp. 24-33. (rus)
19. Loset S., Shkhinek K.N., Gudmestad O., Khoiland K. *Vozdeistvie l'da na morskie i beregovye sooruzheniya* [The impact of ice on marine and coastal structures]. Saint-Petersburg: Lan', 2010. 272 p. (rus)
20. Schreyer H.L., Sulsky D.L., Munday L.B., Coon M.D., Kwok R. Elastic-decohesive constitutive model for sea ice. *Journal of Geophysical Research.* 2006. Vol. 111. Pp. 202-219.
21. Ralston T.D. An analysis of ice sheet indentation. *Proceedings of the 2nd IAHR Symposium on Ice.* Lulee, Sweden.1978. Pp. 13-31.

11. Schulson E.M., Nickolayev O.Y. Failure of columnar saline ice under biaxial compression: failure envelopes and brittle-to-ductile transition // Journal of Geophysical Research. 1995. Vol. 100. № 11. Pp. 383-400.
12. Timco G.W., Frederking R.M.W. Confined compression tests: outlining the failure envelope of columnar sea ice // Cold Regions Science and Technology. 1986. № 12(1). Pp. 13–28.
13. Shkhinek K., Loset S., Karna T. Global ice load dependency on structure width and ice thickness // Proc. of 17th Int. Conf. on Port and Ocean Eng. under Arctic cond., POAC 03. 2003. Pp. 367-375.
14. Вершинин С.А., Трусков П.А., Кузмичев К.В. Воздействие льда на сооружения Сахалинского шельфа. М.: Институт Гипростроймост. 2005 г. 208 с.
15. Сурков Г.А., Землюк С.В., Астафьев В.П., Поломошнов А.М. Физико-механические параметры ледяного покрова северного шельфа Сахалина // Труды ААНИИ. СПб: Гидрометеоиздат, 2001. Т. 443. С. 65-76.
16. Timco G.W., Weeks W.F. A review of the engineering properties of sea ice // Cold Regions and Technology. 2010. № 60. Pp.107-129.
17. Jordaan I. Mechanics of ice-structure interaction // Engineering Fracture Mechanics. 2001. № 68. Pp. 47-59.
18. Ли Лян, Шхинек К.Н. Воздействие льда на откосные сооружения // Инженерно-строительный журнал. 2014. № 1. С. 24-33.
19. Лосет С., Шхинек К.Н., Гудместад О., Хойланд К. Воздействие льда на морские и береговые сооружения. СПб: Лань, 2010. 272 с.
20. Schreyer H.L., Sulsky D.L., Munday L.B., Coon M.D., Kwok R. Elastic-decohesive constitutive model for sea ice // Journal of Geophysical Research. 2006. Vol. 111. Pp. 202-219.
21. Ralston T.D. An analysis of ice sheet indentation // Proceedings of the 2nd IAHR Symposium on Ice. Lulee, Sweden. 1978. Pp. 13-31.

Valentin Politko,
+7(925)8870189; politko@mail.ru

Izmail Kantardgi,
+7(903)5337830; kantardgi@yandex.ru

Валентин Александрович Политько,
+7(925)8870189; эл. почта: politko@mail.ru

Измаил Григорьевич Кантаржи,
+7(903)5337830; эл. почта: kantardgi@yandex.ru

Politko V.A., Kantardgi I.G. Level ice interactions with multi-legged offshore structures. *Magazine of Civil Engineering*. 2017. No. 6. Pp. 43–52. doi: 10.18720/MCE.74.4.

doi: 10.18720/MCE.74.5

Vibroisolating properties of polyurethane elastomeric materials, used in construction

Виброизолирующие свойства полиуретановых эластомеров, применяемых в строительстве

S.N. Yakovlev,
V.L. Mazurin,
Peter the Great St. Petersburg Polytechnic University, St. Petersburg, Russia

Канд. техн. наук, доцент С.Н. Яковлев,
аспирант В.Л. Мазурин,
Санкт-Петербургский политехнический университет Петра Великого, г. Санкт-Петербург, Россия

Key words: polyurethane; vibroisolation of buildings; testing unit; natural frequency; vibroisolation coefficient

Ключевые слова: полиуретан; виброизоляция зданий; испытательный стенд; собственная частота; коэффициент виброизоляции

Abstract. The given study is reasoning the relevancy of replacing the conventional elastomer, that is, rubber, with more advanced polyurethane. The paper presents scientific reasoning for the demand to experimentally study the physical and mechanical properties of polyurethane in cases when it is used as plates for vibroisolation of buildings or industrial equipment and is subjected to considerable load. Due to the regulated rate of motor rotation of the testing unit, it is possible to study the course of vibroisolation in a polyurethane bulk, in relation to the forced frequency, vibration amplitude and static deformation. Based on the considerable amount of test measurements of the vibration amplitude with the piezoelectric accelerometers in various stress modes, an empirical statement has been acquired to determine the natural frequency of the polyurethane-unit system for the polyurethane elastomers of varying hardness depending on the degree of relative compression. The present work offers certain recommendations for determining the ultimate static deformation for the polyurethane plates of varying hardness.

Аннотация. В работе обоснована актуальность замены традиционного эластомера – резины на более совершенный полиуретан. Представлено научное обоснование необходимости экспериментального исследования физико-механических свойств полиуретана, в тех случаях, когда он используется в виде пластин для виброизоляции зданий, промышленного оборудования и находится под действием больших нагрузок. Благодаря регулируемой частоте вращения электродвигателя испытательного стенда возможно изучение процесса виброизоляции в полиуретановом массиве в зависимости от частоты вынужденных колебаний, амплитуды колебаний и величины статической деформации. На основании большого количества экспериментальных замеров величины амплитуды колебаний с помощью пьезоэлектрических акселерометров при различных режимах нагружения, получено эмпирическое выражение для определения частоты собственных колебаний системы агрегат-полиуретан для полиуретановых эластомеров различной твердости в зависимости от величины относительной деформации сжатия. В работе представлены конкретные рекомендации по определению предельной статической нагрузки для полиуретановых пластин различной твердости.

Introduction

From the mid-twentieth century the advanced industrialized countries have substituted rubber with polyurethanes in many engineering applications, as the latter have significant constructional, technological and operational features, even while polyurethanes are 1.5 to 3 times more expensive than rubber.

Polyurethane, as well as rubber, falls within the type of construction materials conventionally called elastomers. Elastomers as construction materials for machine components different from, for instance, metals, are characterized by two features:

- Elasticity – the capacity of significant initial distortion, up to 300 %, different from metals, which have the value of distortion limited by fractions of a percent;

Яковлев С.Н., Мазурин В.Л. Виброизолирующие свойства полиуретановых эластомеров, применяемых в строительстве // Инженерно-строительный журнал. 2017. № 6(74). С. 53–60.

– High internal friction, which can absorb mechanical vibrations, while getting warm and dissipating part of energy as heat into the surrounding environment.

The potential of polyurethanes for the contemporary industry is conditioned by the fact that their properties remarkably complete the application capacities of other elastomers, resins, rubbers etc. Considering their constructional and technological capacities polyurethane is the most universal polymeric material. Polyurethane is characterized by notable physical and mechanical properties, has a significant range of hardness, low wearability, high density, high tear strength, oil-and-petrol resistance, acid resistance, and operational temperature from -35 ^{0}C to +75 ^{0}C [1-6].

Polyurethane elastomers currently have a broad application as a vibroisolating material in contemporary machine and civil engineering to protect the facilities from vibrations created by the movement of subsurface metropolitan trains, railway trains, etc.

Oscillatory damping is based on transforming the kinetic energy of a damped unit into the thermal energy with its following dissipation into the surrounding environment. The transformation of mechanical energy into the thermal one is provided by the internal friction (hysteresis), induced by the viscosity of a polyurethane bulk of the damper [7-12].

The problems of physical and mechanical properties of polyurethane under dynamic loading were studied by many researchers, particularly Sheng Li, Marcos Pacheco, Janusz Datta [13-15]. Under dynamic loading polyurethane, due to the destruction of secondary chemical bonds, undergoes the process of gradual fluxing, with the modulus of elasticity reducing by approximately 15 %. Moreover, under dynamic load polyurethane molecules do not manage to distort at the speed more than 0.4 mm/sec (the given speed is set as a standard for the test determining the compression modulus of elasticity) and the material is also hardening. The phenomenon in question is considered in the papers and the monograph by S.N. Yakovlev [16-18].

Such a wide-spread application of polyurethane elastomers as vibroisolating materials invokes the necessity of an experimental study of physical and mechanical properties of polyurethane and the problems, related to its application in engineering the buildings and constructions, subjected to vibrations.

The aim of the given paper is to provide the empirical equation to determine the natural vibration frequency of the polyurethane-unit system for any value of the relative compression for the polyurethane plates of varying hardness.

To accomplish the desired goal it is necessary to solve the following problems:

1. To design and produce the special testing unit to simulate the loading of polyurethane vibroisolating plates in the frequency range from 10 to 50 Hz.
2. To conduct the tests of polyurethane vibroisolating plates of three degrees of hardness with varying oscillatory amplitude and the value of static deformation.
3. To process the obtained test measurements by means of mathematical statistics and to derive the required equation.

Materials and methods of the study

Polyurethane vibroisolators are used for amplitude loss in the induced cyclical oscillations caused by the stationary underbalanced units. They are also used to dissipate large amounts of energy of the impact force.

Vibroisolators that use the polyurethane elastomers in their design should provide the vibroisolation of buildings, constructions and industrial equipment from the oscillations in the frequency range 20 to 50 Hz, induced by the subsurface metropolitan, trams, large trucks etc. High-frequency oscillations, according to [19, 20] are of low intensity and well-filtered by the ground.

The design parameters of a polyurethane vibroisolator are its hardness and the capacity to decline (dampen) the oscillatory amplitude by means of inner friction of the material (hysteresis losses). The lower is the hardness of a polyurethane vibroisolator, the higher is its deformation and the lower is the natural vibration frequency. Vibroisolation is the better, the higher is the ratio of natural to induced frequencies.

At present the polyurethane elastomers produced by Synair (USA), Getzner Werkstoffe GmbH (Austria), etc are widely spread as a vibroisolating material. The materials are microcellular polyurethane elastomers with mixed vesicular structure, specifically designed to solve the problems of vibroisolation. For the materials in question the following peculiarities are characteristic:

– Not subjective to hydrolysis, as well as to the effects of dilute alkali, acids, dissolvents and oils;

– Carry the long-term repeated load;

– Withstand significant overload;

– During the impact of stationary load the materials do not lose their properties in at least 30 years.

For the study of vibroisolating properties of polyurethane elastomers a special testing unit was designed and produced, allowing the simulation of various kinds of load in a broad range of induced oscillations frequency. The testing unit can simulate the simplest instance of uniaxial harmonic load for a polyurethane vibroisolator.

Polyurethane vibroisolators, while being used, go through an asymmetric load cycle, presented in Figure 1.

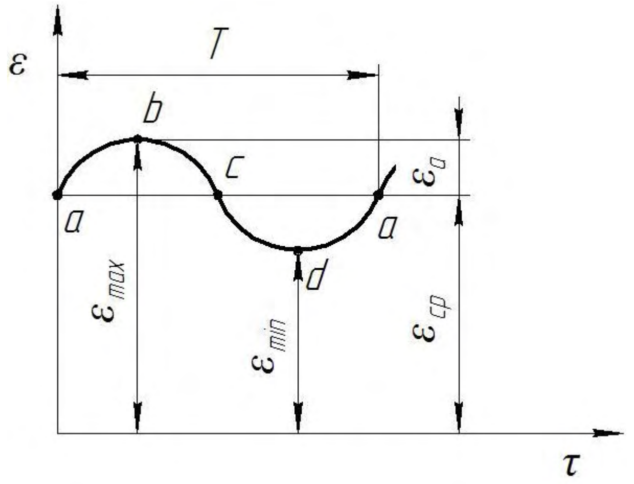

Figure 1. Asymmetric load cycle mode: ε_{cp} - average deformation; ε_a – deformation amplitude; ε_{Max} – maximal deformation; ε_{min} – minimal deformation; *T* - time of oscillation

Semioscillation, shown in Figure 1 in letters *a b c*, corresponds to the compressive deformation, during which the vibroisolator drops as opposed to the average deformation, which in most cases is determined by the weight of a damped unit. Section *c d a* corresponds to the extensional strain of a vibroisolating polyurethane bulk.

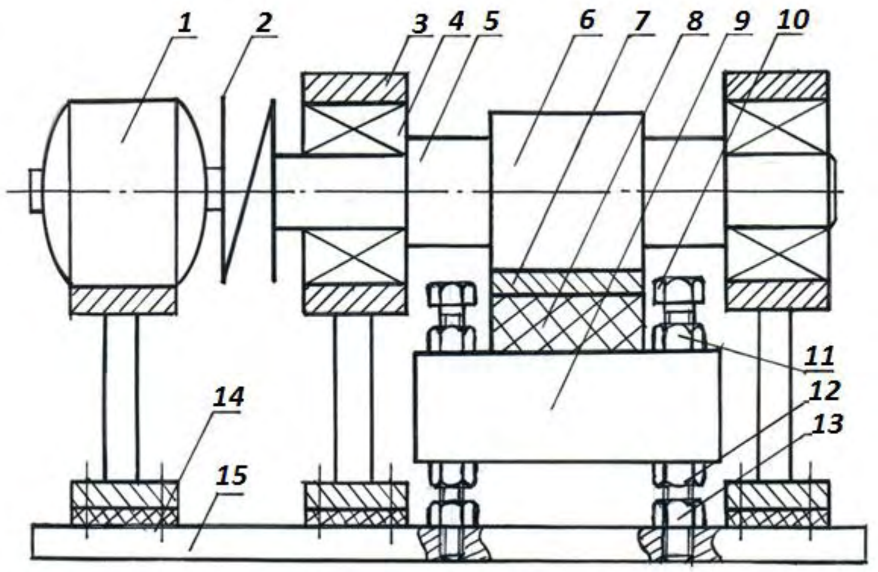

Figure 2. Kinematic diagram of a testing unit: 1 – electric motor; 2 – clutch; 3 – post; 4 – bearing; 5 – shaft; 6 – eccentric; 7 – cushion; 8 – polyurethane; 9 – platform; 10 – lead screw; 11 – lock nut; 12 – lifting nut; 13 – clamping nut; 14 – padding; 15 – base

A kinematic diagram of the testing unit for simulating the dynamic load of polyurethane vibroisolators, being in compression, is shown in Figure 2.

The testing unit consists of an asynchronous motor 5AI71 V2 with the power $P_{mot.}$ = 1.1 KW, the rate of rotation n_{mot} = 3000 rpm and the variable rotation rate; elastic clutch and a camshaft, based on the rolling bearings. The motor and shaft-rolling bearings are set on a platform with the use of vibroisolating paddings 14, to diminish the transference of oscillations.

Due to the variable rotation rate of the motor shaft it is possible to study vibroisolating properties of the polyurethane elastomer in question on the whole range of regularly applied mechanical load frequencies. These frequencies are within the range of 10 to 50 Hz.

To create the stationary load in the polyurethane bulk under consideration, one should unscrew the lock nuts 11 and, rotating the lifting nuts 12, lift the platform 9 to the value of a certain stationary deformation of a polyurethane bulk 8, at which the following sequences of tests would be carried out. After that one should fasten the lock nuts and measure the stationary deformation value of the polyurethane prepared for tests.

Oscillating dynamic load, impacting the polyurethane bulk, is simulated by means of a rotating cam. Taking into consideration the fact that the oscillations follow the harmonic principle

$$U(t) = A\sin(\omega t + \varphi),$$

where A is the oscillatory amplitude or the divergence from zero position, ω is the rotating speed of the shaft, φ is the initial oscillatory phase, the eccentric profile precisely matches the harmonic form of loading of the cam gear with a flat lifter.

The eccentric profile is shown in Figure 3.

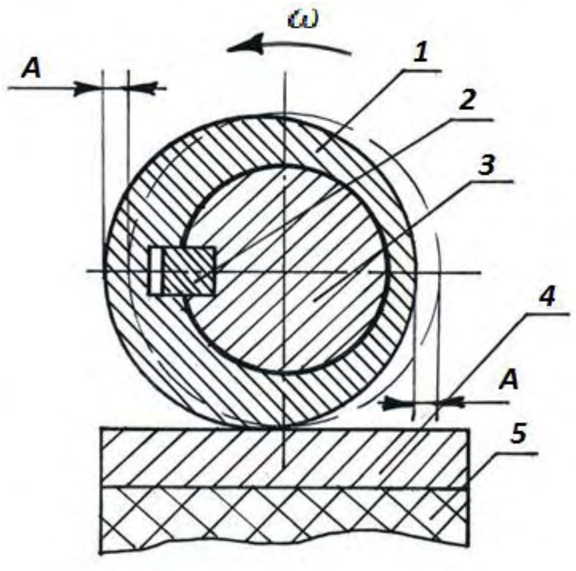

Figure 3. Cam profile, simulating the dynamic load of polyurethane: 1 – eccentric; 2 – connector; 3 – shaft; 4 – cushion; 5 – polyurethane

Eccentricity A of the cam matches the value ε_a – the deformation amplitude.

During the rotation of the cam, the cushion, working as a flat lifter and rigidly connected to the polyurethane bulk (by means of glue), simulates the dynamic load of a vibroisolator.

At the production stage the complex contour of the cam is formed as an envelope for various positions of an abrasive disk with a simple shape. The grinding of the cam surface was carried out on the optical profile grinding machine with the 50-times magnification. For the simpler setting of the coordinates and the following construction of the cam profile, corresponding to the harmonic form of loading of a flat lifter, the polar coordinate system was used.

After the grinding the cams were nitrated to increase the wear-resistance.

For the experimental study three cams were produced with the eccentricity of 0.1; 0.2; 0.3 mm. These values approximately correspond to the amplitudes of the most prevalent mechanical oscillations of the current industrial equipment.

The load frequency of a polyurethane bulk under consideration was split into five fixed frequencies: 10, 20, 30, 40 and 50 Hz, at which the amplitude of forced oscillations of the platform was measured by means of a piezoelectric accelerometer.

Therefore it is possible to examine the process of vibroisolation in a polyurethane bulk of a damper depending on the amplitude of forced oscillations, oscillation amplitude and the value of stationary deformation.

As a drawback of the testing unit should be mentioned the heating of the cushion, transferring the heat from the area of sliding friction of the loading eccentric and the cushion to the polyurethane bulk of the damper.

To diminish the heating and wearing in the frictional contact the cushion was produced of tin bronze and, moreover, a drip-feed lubrication system was organized, with which a container was set above the rotating eccentric, and transmission gear oil dripped from there onto the rotating eccentric and then got into the frictional contact.

For the experimental study of vibroisolating properties of a polyurethane elastomer the samples produced by Synair (USA) were used, with the dimensions 80 × 80 mm and the width 25 mm, the hardness 45 ShA, 55 ShA, 65 ShA.

Research results

The dynamic properties of polyurethane elastomers at the forced oscillations in the stable conditions are described by a differential equation considering the elastic and viscous constants.

The solution to this equation, according to [21], is the assessment of the capacity of a polyurethane elastomer to dampen the oscillations. The efficiency of vibroisolators in dampening the oscillations amplitude is characterized by the vibroisolation coefficient η, which is determined by means of the following equation:

$$\eta = \frac{\sqrt{1+\left(\frac{f_{\text{в}}}{f_{\text{c}}}\right)^2 \frac{4\vartheta^2}{4\pi^2+\vartheta^2}}}{\sqrt{\left[1-\left(\frac{f_{\text{в}}}{f_{\text{c}}}\right)^2\right]^2+\left(\frac{f_{\text{в}}}{f_{\text{c}}}\right)^2 \frac{4\vartheta^2}{4\pi^2+\vartheta^2}}}, \quad (1)$$

where $f_{\text{в}}$ is the frequency of forced oscillations (frequency of the generating force oscillations), Hz;

f_{c} – frequency of the natural oscillations of the polyurethane-unit system, Hz;

ϑ – damping logarithmic decrement for the oscillations of the vibroisolating system.

Oscillatory damping logarithmic decrement $\vartheta = \ln\frac{x_1}{x_2}$ is used to indicate the damping of the oscillations and is determined by the base logarithm of the ratio of two adjacent oscillatory amplitudes.

The lower is the isolation coefficient η, the better is the isolation. The equation (1) for the instance $\frac{f_{\text{в}}}{f_{\text{c}}} = \sqrt{2} = 1.41$ at all values ϑ shows that η = 1, i.e. in the given case there is no vibroisolation.

If we set the oscillatory damping logarithmic decrement ϑ close to zero, i.e. consider the inner friction in a polyurethane bulk negligible, we get the following:

$$\eta = \frac{1}{\left[1-\left(\frac{f_{\text{в}}}{f_{\text{c}}}\right)^2\right]}\ , \quad (2)$$

At $\frac{f_{\text{в}}}{f_{\text{c}}} < \sqrt{2}$ the value of $\eta > 1$, and in that case not only there is no vibroisolation, but, on the contrary, the amplitude of the common driving energy is increased. At $\frac{f_{\text{в}}}{f_{\text{c}}} > \sqrt{2}$ the value of $\eta < 1$ and the vibroisolation takes place. Examining the equation (1), it is possible to draw the conclusion that for a good isolation it is necessary to provide the natural frequency of the system being much less than the frequency of forced oscillations.

In case $f_В = f_С$, while solving the equation (2) theoretically, it results in η = ∞, which matches the resonance phenomenon.

The assumption, underlying the equation (2), also largely holds for the metal spring vibroisolators without a considerable inner friction and providing vibroisolation by means of shaping metal in a certain way.

For polyurethane elastomers used in vibroisolating equipment, the value of ϑ, dependent on hysteresis losses, stays within the range 0.4 to 0.8. Thus a polyurethane vibroisolator provides a finite value of the vibroisolation coefficient η with the resonance as well.

While the increase of η at the resonance is not connected to the increase of the energy costs, in some instances the use of polyurethane vibroisolators is acceptable even in the vicinity of a resonating area, however, such a work, due to the inner friction in polyurethane, involves a significant heating of the polyurethane bulk and may cause the destruction of the material.

On the basis of a considerable number of experimental measurements of oscillatory amplitude of the platform for various loading modes a ratio was obtained for the isolation coefficient of polyurethane elastomers in relation to the correlation of the frequencies of forced oscillations and the natural frequency of polyurethane-unit system for elastomers of varying hardness.

The obtained correlations are presented in Figure 4.

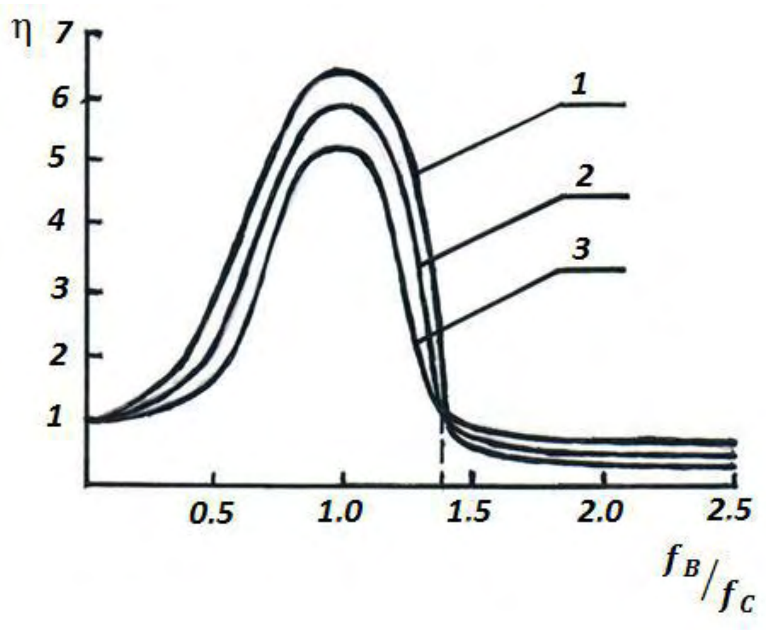

Figure 4. The correlation of vibroisolation coefficient of polyurethane to the frequency ratio $\frac{f_В}{f_С}$: 1 – 45 ShA; 2 – 55 ShA; 3 – 65 ShA.

Picture 4 shows that the less the value of ϑ is, the higher is the value of η in the resonating area. However, at the same time η is diminishing with the increase of the ratio $\frac{f_В}{f_С}$. While the oscillatory damping logarithmic decrement ϑ depends on hysteresis losses in polyurethane, they in their turn being determined by $\sin\varphi$ (phase angle between the force and deformation), the relation $\frac{4\vartheta^2}{(4\pi^2+\vartheta^2)}$ in equation (1) can be substituted with $\sin\varphi^2$, which is easy to determine by means of experiment, using the record of natural oscillations of the testing unit lever, being in rotational oscillatory motion around a stationary axis.

The given system is considered a single degree of freedom system, where a polyurethane bulk with a certain stationary deformation is used as a damping element. The lever oscillations are recorded by means of a Geiger recorder.

Table 1 presents the values of oscillatory damping logarithmic decrement ϑ, obtained by means of experiment in the area of the regularly applied working stationary deformations for polyurethane elastomers in three degrees of hardness.

Table 1. Oscillatory damping logarithmic decrement for the polyurethanes of various degrees of hardness with varying values of a relative stationary deformation

Relative deformation, ε	Polyurethane hardness, ShA		
	45	50	55
0.10	0.48	0.53	0.58
0.15	0.50	0.55	0.60
0.20	0.52	0.57	0.62
0.25	0.54	0.59	0.64

As has been mentioned above, to provide the efficient vibroisolation, the frequency of natural oscillations of the polyurethane-unit system f_c should be less than $f_в$, the frequency of forced oscillations.

Following the results of a considerable number of experiments, an empirical correlation was obtained for the determination of the natural oscillations frequency for the polyurethane-unit system:

$$f_c = 18 + 0.1\varepsilon + 0.2(\mathrm{ShA} - 45), \quad (3)$$

where ε is the value of relative deformation; ShA – the hardness of polyurethane according to Shore.

The proposed empirical correlation for the determination of the natural oscillation frequency of the polyurethane-unit system holds for the range of the values of relative stress deformation of polyurethane vibroisolating plates, prevalently used in practice.

Conclusions

According to the results of a wide experimental study of the vibroisolating polyurethane plates produced by Syniar (USA), it is possible to draw the following conclusions and to give certain recommendations for their application in engineering of various buildings and constructions:

1. With the known drop δ of a polyurethane vibroisolator, under the set stationary load, the natural frequency of the vibroisolator-unit system is determined; it would be the lower, the higher is the drop of δ. The drop of δ would be the more considerable, the lower is the elasticity mode of the polyurethane elastomer and the lower is the form coefficient (determined by the standard geometrical properties) of a vibroisolator.
2. The use of polyurethane vibroisolators with the height of more than 30 mm is not recommended, as it may cause the lateral displacement of a damped unit.
3. The vibroisolation coefficient, calculated according to the formula (1) and the experimental measurements of the oscillatory amplitudes by means of the piezoelectric accelerometer show the divergence in 6 to 8 %, which is considered a satisfactory value in engineering calculations. In practice the vibroisolational coefficient η has the value η = 0.2…0.7.
4. Considering the elastic posts made of vibroisolating polyurethane elastomer, used in engineering of buildings and constructions, the following values may be recommended as a limiting dead load: [p] = 0.15 MPa for polyurethane with the hardness 45 ShA, [p] = 0.20 MPa for polyurethane with the hardness 50 ShA, [p] = 0.25 MPa for polyurethane with the hardness 55 ShA.

References

1. Valero M.F. Preparation and properties of polyurethanes based on castor oil chemically modified with yucca starch glycoside. *Journal of Elastomers and Plastics.* 2009. No. 41. Pp. 223-244.
2. Maity M. Polyblend systems of polyurethane rubber and silicone rubber in the presence of silane grafting agent. *Journal of Elastomers and Plastics*. 2001. No. 33. Pp. 211-224.
3. Kahraman H., Haberstroh E. Einfluss von aktiven Fullstoffen in Elastomeren auf den anisotropen Mullins-Effekt. Anisotroper Mullins-Effekt. *Gummi. Fasern. Kunststoffe*. 2014. No. 5. Pp. 296-298.

Литература

1. Valero M.F. Preparation and properties of polyurethanes based on castor oil chemically modified with yucca starch glycoside // Journal of Elastomers and Plastics. 2009. № 41. Pp. 223-244.
2. Maity M. Polyblend systems of polyurethane rubber and silicone rubber in the presence of silane grafting agent // Journal of Elastomers and Plastics. 2001. № 33. Pp. 211-224.
3. Kahraman H., Haberstroh E. Einfluss von aktiven Fullstoffen in Elastomeren auf den anisotropen Mullins-Effekt. Anisotroper Mullins-Effekt // Gummi. Fasern. Kunststoffe. 2014. № 5. Pp. 296-298.

4. Gonella L.B. New reclaiming process of thermoset polyurethane foam and blending with polyamide-12 and thermoplastic polyurethane. *Journal of Elastomers and Plastics*. 2009. No. 41. Pp. 303-322.
5. Neise E., Zepp C. Optische Deformationsanalyse von Fahrzeugreifen. Dynamische Reifenanalyse. *Gummi. Fasern. Kunststoffe.* 2013. No. 1. Pp. 23-30.
6. Yokoyama N. Properties of polyurethane containing new phenolic additives. *Journal of Elastomers and Plastics*. 2007. No.39. Pp. 347-369.
7. Khatua B.B. Elastomeris blends of polyurethane and polychloroprene elastomers (culfur cure) with reference to the interchain crosslinking reaction. *Journal of Elastomers and Plastics.* 2000. No. 32. Pp. 231-247.
8. Janusz D. Influence of glycols on the glycolysis process and the structure and properties of polyurethane elastomers. *Journal of Elastomers and Plastics.* 2011. No. 43. Pp. 529-541.
9. Zhang H., Chen Y., Zhang Y., Sun X., Ye H., Li W. Synthesis and characterization of polyurethane elastomers. *Journal of Elastomers and Plastics.* 2008. No. 40. Pp. 161-177.
10. Raympel I. *Shassi avtomobilya. Amortizatory, shiny i kolesa* [The chassi of the car. Shock abcorbers, tires and wheels]. Moscow: Mashinostroyeniye, 2006. 320 p. (rus)
11. Frolov K.V. *Vibratsiya - drug ili vrag* [Vibration - friend or foe]. Moscow: Nauka, 2004. 144 p. (rus)
12. Jayasree T.K. Effect of fillers on mechanical properties of dinamically crosslinked styrene butadiene rubber. *Journal of Elastomers and Plastics.* 2008. No. 40. Pp. 127-146.
13. Li S., Li B. Effect of elastomer on flame retardancy, thermal degradation, and mechanical properties of intumescent flame-retardant polyethylene. *Journal of Elastomers and Plastics.* 2011. No. 43. Pp. 257-273.
14. Pacheco M.F.M., Bianchi O, Fiorio R., Zattera A.J., Zeni M., Giovanela M., Crespo J.S. Thermal, chemical, and morphological characterization of microcellular polyurethane elastomers. *Journal of Elastomers and Plastics.* 2009. No. 41. Pp. 323-338.
15. Janusz D. Synthesis and investigation of glycolysates and obtained polyurethane elastomers. *Journal of Elastomers and Plastics.* 2010. No. 42. Pp. 117-127.
16. Yakovlev S.N. Self-oscillation of an elastic polyurethane coating in polishing. *Russian Engineering Research*. 2014. No. 5. Pp. 295-298.
17. Yakovlev S.N. Dynamic hardening of structural polyurethanes. *Russian Engineering Research.* 2016. No. 4. Pp. 255-257.
18. Yakovlev S.N. Proyektirovaniye i osnovy tekhnologii detaley mashin iz poliuretana [Design and the fundamentals of the technology of machine parts from polyurethane]. Saint-Petersburg: Renome, 2013. 176 p.
19. Kagan A.A. Raschetnyye kharakteristiki gruntov [Estimated soil characteristics]. Moscow: Stroyizdat, 1985. 248 p.
20. Barshteyn F.M. Dinamicheskiy raschet zdaniy i sooruzheniy [Dynamic calculation of buildings and structures.]. Moscow: Stroyizdat, 1984. 303 p.
21. Lepetov V.A., Yurtsev L.N. Raschety i proyektirovaniye rezinovykh izdeliy [Calculation and design of rubber products]. Leningrad: Khimiya, 1977. 408 p.

4. Gonella L.B. New reclaiming process of thermoset polyurethane foam and blending with polyamide-12 and thermoplastic polyurethane // Journal of Elastomers and Plastics. 2009. № 41. Pp. 303-322.
5. Neise E., Zepp C. Optische Deformationsanalyse von Fahrzeugreifen. Dynamische Reifenanalyse // Gummi. Fasern. Kunststoffe. 2013. № 1. Pp. 23-30.
6. Yokoyama N. Properties of polyurethane containing new phenolic additives // Journal of Elastomers and Plastics. 2007. № 39. Pp. 347-369.
7. Khatua B.B. Elastomeris blends of polyurethane and polychloroprene elastomers (culfur cure) with reference to the interchain crosslinking reaction //Journal of Elastomers and Plastics. 2000. № 32. Pp. 231-247.
8. Janusz D. Influence of glycols on the glycolysis process and the structure and properties of polyurethane elastomers // Journal of Elastomers and Plastics. 2011. № 43. Pp. 529-541.
9. Zhang H., Chen Y., Zhang Y., Sun X., Ye H., Li W. Synthesis and characterization of polyurethane elastomers // Journal of Elastomers and Plastics. 2008. № 40. Pp. 161-177.
10. Раймпель Й. Шасси автомобиля. Амортизаторы, шины и колеса. М.: Машиностроение, 2006. 320 с.
11. Фролов К.В. Вибрация – друг или враг. М.: Наука, 2004. 144 с.
12. Jayasree T.K. Effect of fillers on mechanical properties of dinamically crosslinked styrene butadiene rubber // Journal of Elastomers and Plastics. 2008. № 40. Pp. 127-146.
13. Li S., Li B. Effect of elastomer on flame retardancy, thermal degradation, and mechanical properties of intumescent flame-retardant polyethylene // Journal of Elastomers and Plastics. 2011. № 43. Pp. 257-273.
14. Pacheco M.F.M., Bianchi O, Fiorio R., Zattera A.J., Zeni M., Giovanela M., Crespo J.S. Thermal, chemical, and morphological characterization of microcellular polyurethane elastomers // Journal of Elastomers and Plastics. 2009. № 41. Pp. 323-338.
15. Janusz D. Synthesis and investigation of glycolysates and obtained polyurethane elastomers // Journal of Elastomers and Plastics. 2010. № 42. Pp. 117-127.
16. Yakovlev S.N. Self-oscillation of an elastic polyurethane coating in polishing // Russian Engineering Research. 2014. № 5. Pp. 295-298.
17. Yakovlev S.N. Dynamic hardening of structural polyurethanes // Russian Engineering Research. 2016. № 4. Pp. 255-257.
18. Яковлев С.Н. Проектирвоание и основы технологии деталей машин из полиуританa. СПб: Реноме, 2013. 176 с.
19. Каган А.А. Расчетные характеристики грунтов. М.: Стройиздат, 1985. 248 с.
20. Барштейн Ф.М. Динамический расчет зданий и сооружений. М.: Стройиздат, 1984. 303 с.
21. Лепетов В.А., Юрцев Л.Н. Расчет и проектирование резиновых изделий. Л.: Химия, 1977. 408 с.

Stanislav Yakovlev,
+7(921)9081535; stannik59@mail.ru

Valerii Mazurin,
+7(911)1837341; valmazurin@rambler.ru

Станислав Николаевич Яковлев,
+7(921)9081535; эл. почта: stannik59@mail.ru

Валерий Леонидович Мазурин,
+7(911)1837341;
эл. почта: valmazurin@rambler.ru

Yakovlev S.N., Mazurin V.L. Vibroisolating properties of polyurethane elastomeric materials, used in construction. *Magazine of Civil Engineering*. 2017. No. 6. Pp. 53–60. doi: 10.18720/MCE.74.5.

doi: 10.18720/MCE.74.6

Reasons of delays in construction projects

Причины отставаний строительных проектов

Yu.B. Kalugin,
Military Institute of rail transport troops and military communications, Petrodvorets, St. Petersburg, Russia

Д-р техн. наук, профессор Ю.Б. Калугин,
Военный институт железнодорожных войск и военных сообщений, Петродворец, г.Санкт-Петербург, Россия

Key words: civil engineering; construction management; project scheduling; critical path method

Ключевые слова: управление инвестиционно-строительными проектами; расписание проекта; метод критического пути

Abstract. Usually, the actual duration of construction projects significantly exceeds the scheduled duration. Reasons for this phenomenon are presented. Firstly, numerous stochastic factors impact on the works. The second reason is insufficiently reliability of traditional scheduling methods. Finally, the third reason is quasi-activities that were not included in the schedule. This paper discloses the essence quasi-activities, their impact on the completion times. The approach is identified additional dummy arcs, causing implicit activities. The general applicability of the method is demonstrated. A comparison was drawn between the proposed method and traditional techniques. The mean duration of the simple chain of activities is underestimated by 15-20%.It is confirmed that the traditional method of calculating the time to complete a project is almost always shorter. Implementation of this method will allow for the determination of a more precise duration for the performance of complex works at the planning stage. The suggested methodology can be recommended for use by construction project managers.

Аннотация. Как правило, фактическая продолжительность строительства значительно превышает запланированные сроки. Представлены причины этого явления. Во-первых - это влияние на работы множества случайных факторов. Второй причиной является недостаточная достоверность и надежность традиционных методов планирования. Наконец, третья причина-это квази-работы, которые не были включены в календарный график. В статье раскрыта сущность квази-работ, их влияние на сроки строительства. Подход выявил неявные дополнительные ресурсно-объектные связи, вызванные квази-работами, находящимися вне поля графика. Изложенный подход проиллюстрирован расчетами. Проведено сравнение между предложенным и традиционным методами. Установлено, что средняя продолжительность ряда последовательных работ, рассчитанная традиционным методом, занижена в среднем на 15-20%. Реализация метода позволит определять более точные сроки завершения строительного проекта на стадии планирования. Предложенная методология может быть рекомендована для использования руководителями строительных проектов.

Introduction

The analysis of the current state of the theory and practice of scheduling illustrates the lack of realistic scheduling.

Therefore, the actual duration of various construction projects significantly exceeds the planned ones [1-8].

The reason for the significant difference between planned and actual construction durations is, primarily, the impact of the works due to numerous stochastic factors [9, 10]. So, for average and strong levels of impact of destabilizing factors on technological processes, their mean productivity is reduced in 1.5-2.5 times from the norm [10]. It is established that process productivity is subject to the normal law of distribution. The duration of the activities is described by a Beta distribution or inverse to normal law [11]. In these circumstances, duration of activities can be evaluated using probabilistic estimation [12-16].

The second reason is insufficiently reliable traditional PERT (Program Evaluation and Review Technique) method. The PERT method is generally intended for the calculation of schedules that have certain structures set by unambiguous technological processes. The activity time spans are assumed to follow a general Beta distribution [17-21].

The traditional PERT method uses only the activity time means to calculate the critical path, reducing the stochastic model to a deterministic model. In PERT, three-time estimates are required for each activity. The time estimates represent a pessimistic time, an optimistic time, and a most likely time for the duration of the activity.

The method assumes that the sum of the mean completion times of activities on the critical path is normally distributed. This allows the calculation of the probability of completing the project within a given time period. A single critical path is thus calculated and relied upon, where in reality, there may be numerous possible critical paths that exist. For a large network plan, the probability that any given path could be the critical path may be very small. PERT method yields results which are biased high. The construction project manager is thus grossly misled into thinking his chances are very good when in reality they are very poor. If the network has multiple parallel paths with relatively equal means, PERT calculations will be considerably biased [22]). As a result, the time to complete a project calculated by the traditional PERT method is almost always too short [23]).

A universal method developed for the calculation of networks schedule with multiple critical paths. This method was used for the calculation of a more realistic time span for the construction of a road [24]. A comparison was drawn between the proposed method and traditional techniques. The mean duration of the technological process calculated by a universal method is 30 % more than for a known critical path method. It is confirmed that the traditional method of calculating the time to complete a project is almost always shorter.

Similar results have also been observed when using the technique of crashing PERT [25]). Completion times with the PERT method are much shorter than completion times calculated with the Monte Carlo method [19, 26, 27].

The third reason for delays in construction projects is quasi-activities that were not included in the schedule [28].

The aim of the present paper is to reveal the essence quasi-activities, their impact on the completion times.

Objectives of the study are:

1. Show essence of the resource-object relations, that constitute the inner nature of schedules;
2. Reveal impact of quasi-activities on the completion times;
3. Calculate the completion times of the chain of activities.

Methods

Assume, that sequential works of crews F, G, H on the 5-th object (chain of activities) is presented in Figure 1.

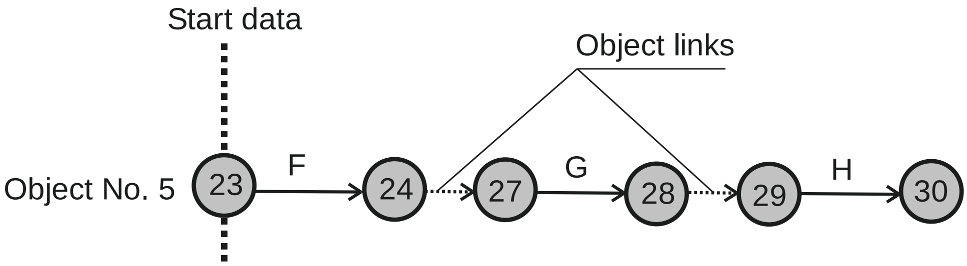

Figure 1. Fragment of chain activities

It is obvious that for deterministic values the length of the chain (23-24-27-28-29-30) is the sum of the durations of individual activities.

For stochastic estimates, the parameters of the event 30 are determined by the composition of the laws of duration of work of each crew. So, for the normal distributions, the mathematical expectation of the length of the chain (23-24-27-28-29-30) will be the sum of the activity time means.

However, the actual time the events of 30 always exceed the planned.

The sequential chain (Fig. 1) does not reflect fully the essence of the resource-object relations that constitute the inner nature of schedules.

So, the crews G and H to the planned date of the beginning of their work usually always busy at the previous objects (work areas), which causes additional resource links.

This allows us to convert the initial model (Fig 2).

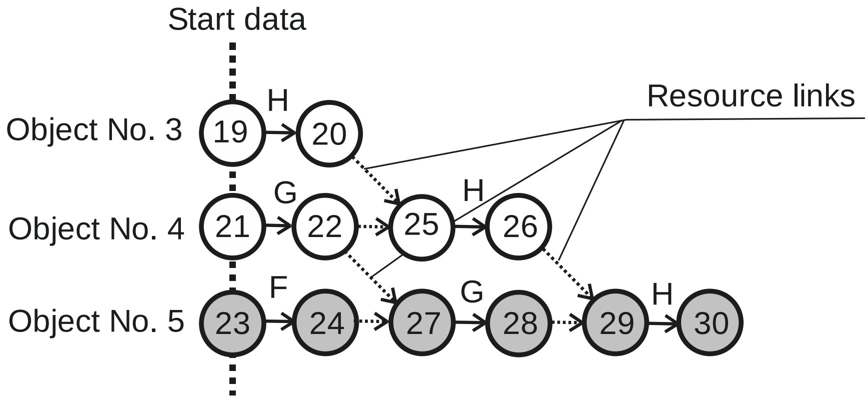

Figure 2. Model of the chain of activities, taking into account implicit resource links

This scheme is lawful to use only in the case where the scheduling date coincides with the start date. Otherwise, the model chain of activities of is converted into the following (Fig. 3).

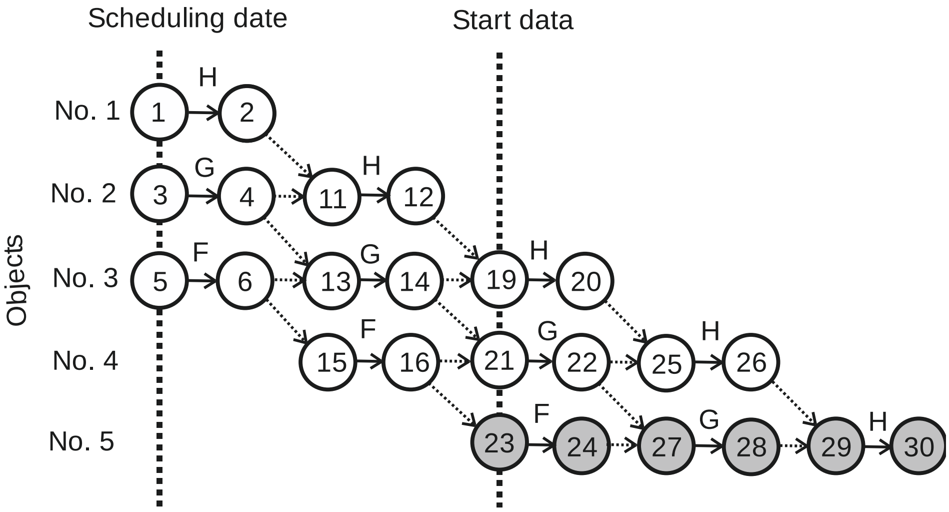

Figure 3. Model of the chain of activities, taking into account to the scheduling date and an implicit of the resource links

It is obvious that increase in an interval between start date and date of planning, leads to increase in resource and object links for works G and H.

In addition, in this case there are additional (implicit) object links caused by the necessity of preparing the fifth object for the crew F.

This, in turn, causes the need to consider possible links with the previous crews (E and D) on objects 4 and 5 (Fig. 4).

This scheme is the model of the initial chain (F, G, H) (model quasi-activities).

Quasi-activities are works of crews outside of the schedule and causing an implicit resource and object links to the events of the schedule.

The presented model of quasi-activities on the structure is equivalent to model of a flow of works with multiple critical paths and can be calculated in a similar way.

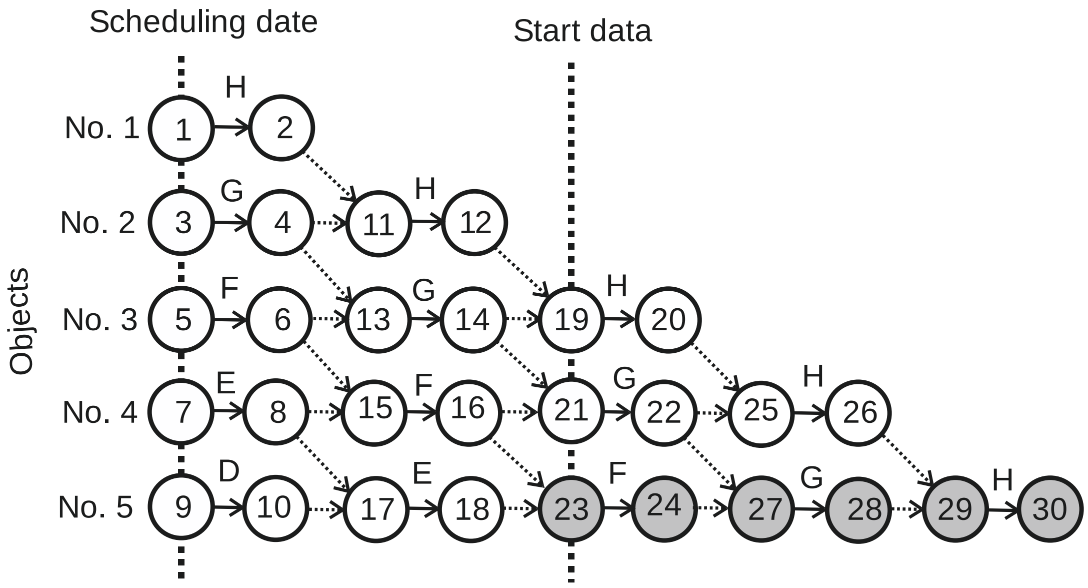

Figure 4. The converted model of initial chain (model of quasi-activities)

Results and Discussion

Model of the chain of activities (Fig. 4) was realized by means of the universal method and Monte-Carlo method under the following data.

The duration of work of each crew follows a general Beta distribution with the parameters: $\alpha = 1, \beta = 2, A = 5, B = 15.$ The mean duration is 8.33.

The flow of works with equal durations is presented in Figure 5.

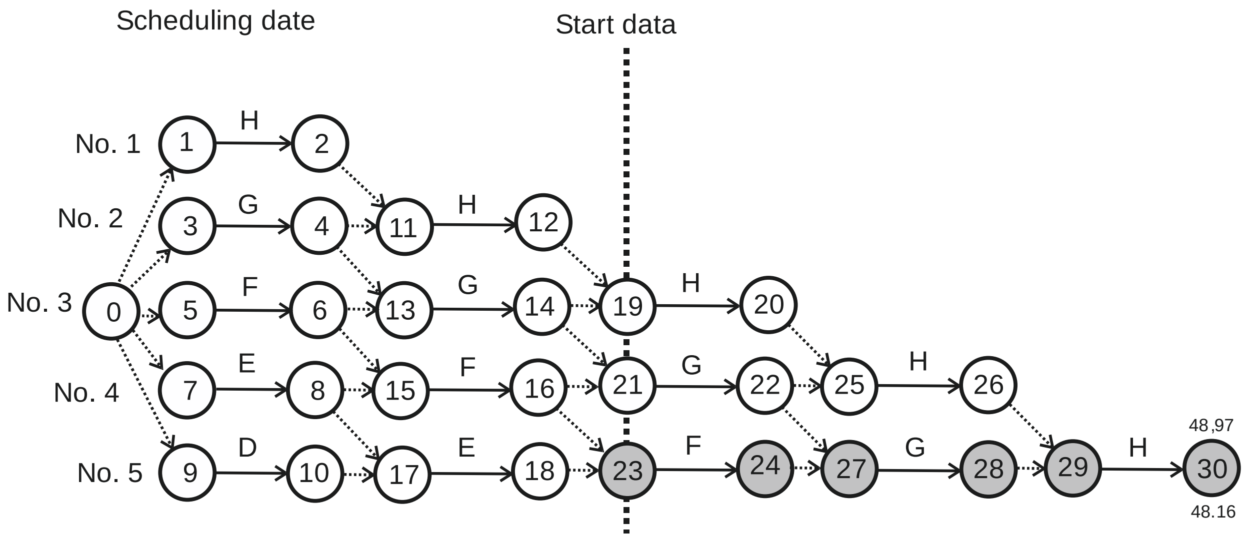

Figure 5. Network of a flow of works

The stochastic parameters of the events network of a flow of works were calculated by the universal method (Table 1).

Table 1. Stochastic parameters of events

# an of event	20 equiprobable values time, shift																				P(t)=0.25	P(t)=0.5	P(t)=0.75
1	0.00	0.00	0.00	0.00	0.00	0.00	0.00	0.00	0.00	0.00	0.00	0.00	0.00	0.00	0.00	0.00	0.00	0.00	0.00	0.00	0.00	0.00	0.00
2	5.13	5.38	5.65	5.92	6.20	6.49	6.78	7.09	7.42	7.75	8.11	8.48	8.88	9.30	9.76	10.26	10.82	11.46	12.26	13.42	6.34	8.33	10.01
3	0.00	0.00	0.00	0.00	0.00	0.00	0.00	0.00	0.00	0.00	0.00	0.00	0.00	0.00	0.00	0.00	0.00	0.00	0.00	0.00	0.00	0.00	0.00
4	5.13	5.38	5.65	5.92	6.20	6.49	6.78	7.09	7.42	7.75	8.11	8.48	8.88	9.30	9.76	10.26	10.82	11.46	12.26	13.42	6.34	8.33	10.01
5	0.00	0.00	0.00	0.00	0.00	0.00	0.00	0.00	0.00	0.00	0.00	0.00	0.00	0.00	0.00	0.00	0.00	0.00	0.00	0.00	0.00	0.00	0.00
6	5.13	5.38	5.65	5.92	6.20	6.49	6.78	7.09	7.42	7.75	8.11	8.48	8.88	9.30	9.76	10.26	10.82	11.46	12.26	13.42	6.34	8.33	10.01
7	0.00	0.00	0.00	0.00	0.00	0.00	0.00	0.00	0.00	0.00	0.00	0.00	0.00	0.00	0.00	0.00	0.00	0.00	0.00	0.00	0.00	0.00	0.00
8	5.13	5.38	5.65	5.92	6.20	6.49	6.78	7.09	7.42	7.75	8.11	8.48	8.88	9.30	9.76	10.26	10.82	11.46	12.26	13.42	6.34	8.33	10.01
9	0.00	0.00	0.00	0.00	0.00	0.00	0.00	0.00	0.00	0.00	0.00	0.00	0.00	0.00	0.00	0.00	0.00	0.00	0.00	0.00	0.00	0.00	0.00
10	5.13	5.38	5.65	5.92	6.20	6.49	6.78	7.09	7.42	7.75	8.11	8.48	8.88	9.30	9.76	10.26	10.82	11.46	12.26	13.42	6.34	8.33	10.01
11	5.79	6.47	6.95	7.35	7.74	8.11	8.46	8.80	9.11	9.39	9.76	10.13	10.37	10.82	11.17	11.46	12.10	12.26	13.36	13.42	7.92	9.65	11.32
12	12.18	13.43	14.20	14.82	15.37	15.86	16.34	16.76	17.22	17.63	18.06	18.50	18.93	19.38	19.87	20.44	21.07	21.85	22.88	24.77	15.61	17.98	20.15
13	5.79	6.47	6.95	7.35	7.74	8.11	8.46	8.80	9.11	9.39	9.76	10.13	10.37	10.82	11.17	11.46	12.10	12.26	13.36	13.42	7.92	9.65	11.32
14	12.18	13.43	14.20	14.82	15.37	15.86	16.34	16.76	17.22	17.63	18.06	18.50	18.93	19.38	19.87	20.44	21.07	21.85	22.88	24.77	15.61	17.98	20.15
15	5.79	6.47	6.95	7.35	7.74	8.11	8.46	8.80	9.11	9.39	9.76	10.13	10.37	10.82	11.17	11.46	12.10	12.26	13.36	13.42	7.92	9.65	11.32
16	12.18	13.43	14.20	14.82	15.37	15.86	16.34	16.76	17.22	17.63	18.06	18.50	18.93	19.38	19.87	20.44	21.07	21.85	22.88	24.77	15.61	17.98	20.15

# an of event	20 equiprobable values time, shift																				P(t)=0.25	P(t)=0.5	P(t)=0.75
17	5.79	6.47	6.95	7.35	7.74	8.11	8.46	8.80	9.11	9.39	9.76	10.13	10.37	10.82	11.17	11.46	12.10	12.26	13.36	13.42	7.92	9.65	11.32
18	12.18	13.43	14.20	14.82	15.37	15.86	16.34	16.76	17.22	17.63	18.06	18.50	18.93	19.38	19.87	20.44	21.07	21.85	22.88	24.77	15.61	17.98	20.15
19	14.43	15.83	16.57	17.12	17.61	18.06	18.48	18.85	19.18	19.48	19.87	20.29	20.56	21.07	21.50	21.85	22.67	22.88	24.67	24.77	17.84	19.79	21.68
20	21.30	23.00	23.94	24.64	25.25	25.79	26.31	26.79	27.26	27.77	28.19	28.69	29.21	29.78	30.30	30.89	31.57	32.41	33.52	35.70	25.52	28.12	30.59
21	14.43	15.83	16.57	17.12	17.61	18.06	18.48	18.85	19.18	19.48	19.87	20.29	20.56	21.07	21.50	21.85	22.67	22.88	24.67	24.77	17.84	19.79	21.68
22	21.30	23.00	23.94	24.64	25.25	25.79	26.31	26.79	27.26	27.77	28.19	28.69	29.21	29.78	30.30	30.89	31.57	32.41	33.52	35.70	25.52	28.12	30.59
23	14.43	15.83	16.57	17.12	17.61	18.06	18.48	18.85	19.18	19.48	19.87	20.29	20.56	21.07	21.50	21.85	22.67	22.88	24.67	24.77	17.84	19.79	21.68
24	21.30	23.00	23.94	24.64	25.25	25.79	26.31	26.79	27.26	27.77	28.19	28.69	29.21	29.78	30.30	30.89	31.57	32.41	33.52	35.70	25.52	28.12	30.59
25	24.17	25.76	26.58	27.17	27.74	28.19	28.66	29.11	29.52	29.88	30.30	30.74	31.03	31.57	32.03	32.41	33.30	33.52	35.60	35.70	27.97	30.15	32.22
26	31.15	32.99	34.00	34.78	35.44	36.03	36.57	37.11	37.59	38.10	38.61	39.09	39.63	40.23	40.84	41.47	42.16	43.03	44.21	46.50	35.74	38.48	41.15
27	24.17	25.76	26.58	27.17	27.74	28.19	28.66	29.11	29.52	29.88	30.30	30.74	31.03	31.57	32.03	32.41	33.30	33.52	35.60	35.70	27.97	30.15	32.22
28	31.15	32.99	34.00	34.78	35.44	36.03	36.57	37.11	37.59	38.10	38.61	39.09	39.63	40.23	40.84	41.47	42.16	43.03	44.21	46.50	35.74	38.48	41.15
29	34.27	35.99	36.86	37.50	38.07	38.61	39.06	39.52	39.96	40.35	40.84	41.31	41.60	42.16	42.64	43.03	43.98	44.21	46.39	46.50	38.34	40.64	42.83
30	41.32	43.26	44.32	45.13	45.82	46.45	47.01	47.56	48.08	48.58	49.13	49.62	50.17	50.78	51.44	52.09	52.79	53.69	54.90	57.25	46.14	48.97	51.76

When modeling Monte Carlo's method has carried out 10000 realizations. The mean duration of completion times for the 30th event was equal to 48.16 shifts.

The distributions of completion times for the 30th event are presented in Figure 6.

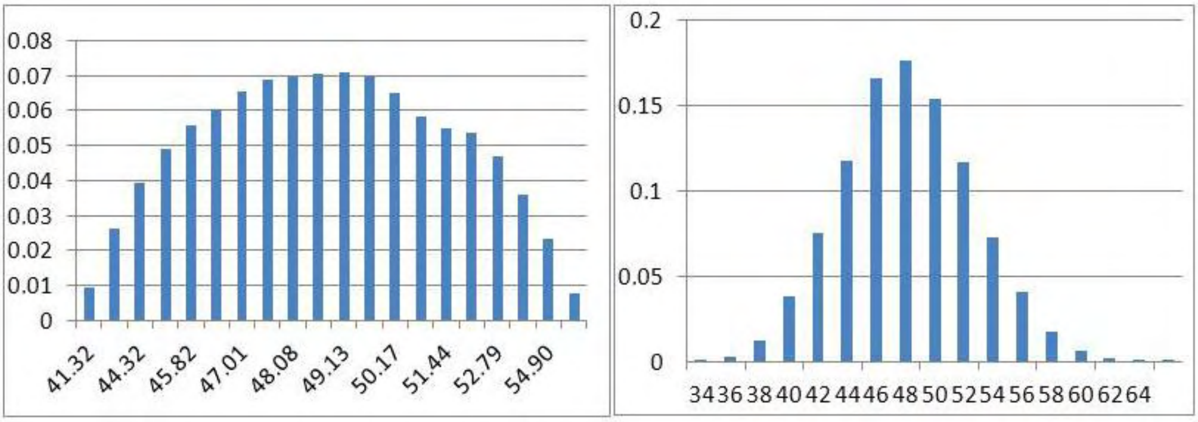

a) Universal method **b) Monte Carlo's method**

Figure 6. Distributions of completion times (for the 30th event)

Comparison of the two distributions shows their proximity.

Somewhat compressed laterally, the histogram of the density distribution for a universal method is due to rounding of extreme values at each calculation step. In addition, the interval values on the axis X are different.

The length of the chain (9-10-17-18-23-24-27-28-29-30) is the sum of the mean durations. It is 41.65 shifts.

The length of the chain 23-24-27-28-29 (Fig. 1) is 16.66 shifts. The mean duration of completion times was equal to 19.79 shifts (Table 1).

Thus the mean duration of completion times of the chain of activities is underestimated by 15-20%.

Similar results have also been observed when using the other techniques. Completion times with the traditional method are perceptibly shorter than completion times calculated with the Monte Carlo method and universal method [19, 23, 24, 28].

Conclusions

1. The actual duration of various construction projects significantly exceeds the scheduled durations. Firstly, numerous stochastic factors impact on the works. The second reason is insufficiently reliability of traditional scheduling methods. Finally, the third reason is quasi-activities that were not included in the schedule. As a result, the traditional method of calculating the time to complete a project is almost always too short.

2. The essence of the impact of quasi-activities on the completion times presented.

The crews to the planned date of the beginning of their work usually always busy at the previous objects (work areas), which causes additional resource links. In addition, in this case, there are additional (implicit) object links caused by the necessity of preparing the objects for the crews. Quasi-activities are works of crews outside of the schedule and causing an implicit resource and object links to the events of the schedule.

The presented model of the chain of activities is equivalent to the model of a flow of works with multiple critical paths and was calculated in a similar way.

3. The model of a flow of works with the Beta distribution of duration was calculated by the universal method and Monte Carlo's method (10000 realizations). Comparison of the two distributions of completion times shows their proximity.

The calculation showed that the mean duration of completion times of the chain of activities is underestimated by 15-20 %. With a probability of 0.75, the completion times will exceed the scheduled durations on 24 %.

4. These results show the efficacy of the offered method to calculate more realistic of completion times. Implementation of this method will allow for the determination of a more precise duration for the performance of complex works at the planning stage. The suggested method can be recommended for

use by construction project managers in order to prevent a potential failure of project completion deadlines.

References

1. Afanasyev V., Afanasyev A. *Potochnaya organizatsiya rabot v stroitelstve* [Flowing organization works in construction]. Saint-Petersburg: SPbGASU. 2000.169 p. (rus)
2. Bolotin S., Birjukov A. Time Management in Drafting Probability Schedules for Construction Work. *World Applied Sciences Journal.* 2013. Vol. 23. No.13. Pp. 1-4.
3. Bovteev S.V., Kanyukova S.V. Development of methodology for time management of construction projects *Magazine of Civil Engineering*. 2016. No. 2. Pp. 102-112.
4. Sadi A., Sadiq A. Causes of delay in large construction projects. *Journal Project Management.* 2006. No. 24(4). Pp. 349-357.
5. Simankina T., Sergeenkova O. Resource optimization of construction on a basis of the frontal and rhythmical stream. *Applied Mechanics and Materials.* 2015. Vols. 725-726. Pp. 984-989.
6. Simankina T.S. *Sovershenstvovaniye kalendarnogo planirovaniya resursosberegayushchikh potokov s uchetom additivnosti intensivnosti truda ispolniteley: diss. na soisk. uchen. step. k. t. n.: Spets. 05.23.08.* [Improvement of scheduling of resource-saving streams taking into account additivity of intensity of work of performers. Cand. Tech. sci. diss.] Saint-Petersburg: 2007. 156 p. (rus)
7. Kurochka P.I. *Razrabotka modeley i mekhanizmov organizatsionno-tekhnologicheskogo proyektirovaniya stroitelnogo proizvodstva: diss. na soisk. uchen. step. d. t. n.: Spets. 05.23.08.* [Development of models and mechanisms of organizational and technological design of construction production. Doc. Tech. sci. diss.] Voronezh: 2004. 324 p. (rus)
8. Trauner T., Manginelli W., Lowe J., Nagata M., Furniss B. Construction delays: understanding them clearly and delay analysis in construction analyzing them correctly. London, UK: Elsevier Inc. 2009. 288 p.
9. Romanovich M.A. *Povysheniye organizatsionno-tekhnologicheskoy nadezhnosti monolitnogo domostroyeniya na osnove modelirovaniya parametrov kalendarnogo plana: diss. na soisk. uchen. step. k. t. n.: Spets. 05.23.08.* [Increase in organizational and technological reliability of monolithic housing construction on the basis of modeling of parameters of the planned schedule. Cand. Tech. sci. diss] Saint-Petersburg: 2015. 194 p. (rus)
10. Kalugin Ju.B. Modelirovanie vozdeistviya destabiliziruyushchikh faktorov na tekhnologicheskii kompleks [Modeling of destabilizing factors of the technological complex]. *News of Higher Educational Institutions. Construction.* 2013. No. 7. Pp. 93–102. (rus)
11. Kalugin Ju.B. Osobennosti i sushchnost rascheta veroyatnostnykh vremennykh parametrov otdelnoy raboty (tekhnologicheskogo protsessa) [Features and essence of calculation of probabilistic temporary for work (technological process]. *News of Higher Educational Institutions. Construction.* 2013. No. 8. Pp. 104–109. (rus)
12. Golenko-Ginzburg D.I. *Stokhasticheskie setevye modeli planirovaniya i upravleniya razrabotkami* [Stochastic models of network planning and management development]. Voronezh: Science Book. 2010. 284 p. (rus)
13. Golenko-Ginzburg D. On the Distribution of Activity Time in PERT. *Journal of the Operational Research Society.* 1988. Vol. 39. No. 8. Pp. 767-771.
14. Maltsev Y. *Ekonomiko-matematicheskie metody proektirovaniya transportnykh sooruzhenii* [Economic-mathematical methods of design of transport objects]. Moscow: Academia. 2010. 320 p. (rus)
15. Miller R. *Schedule, Cost and Profit Control with PERT*.

Литература

1. Афанасьев В.А., Афанасьев А.В. Поточная организация работ в строительстве. СПб:СПбГАСУ. 169 с.
2. Bolotin S., Birjukov A. Time management in drafting probability schedules for construction work // World Applied Sciences Journal. 2013. Vol. 23. № 13. Pp. 1-4.
3. Бовтеев С.В., Канюкова С.В. Развитие методики контроля сроков инвестиционно-строительного проекта // Инженерно-строительный журнал. 2016. № 2(62). С. 102-112.
4. Sadi A., Sadiq A. Causes of delay in large construction projects // Journal Project Management. 2006. № 24(4). Pp. 349-357.
5. Simankina T., Sergeenkova O. Resource optimization of construction on a basis of the frontal and rhythmical stream // Applied Mechanics and Materials. 2015. Vols. 725-726. Pp. 984-989.
6. Симанкина Т.С. Совершенствование календарного планирования ресурсосберегающих потоков с учетом аддитивности интенсивности труда исполнителей: дисс. на соиск. учен. степ. к. т. н.: Спец. 05.23.08. СПб: 2007. 156 с.
7. Курочка П.И. Разработка моделей и механизмов организационно-технологического проектирования строительного производства: дисс. на соиск. учен. степ. д. т. н.: Спец. 05.23.08. Воронеж: 2004. 324 с.
8. Trauner T., Manginelli W., Lowe J., Nagata M., Furniss B. Construction Delays: Understanding them Clearly and Delay Analysis in Construction Analyzing them Correctly. London, UK: Elsevier Inc. 2009. 288 p.
9. Романович М.А. Повышение организационно-технологической надежности монолитного домостроения на основе моделирования параметров календарного плана: дисс. на соиск. учен. степ. к. т. н.: Спец. 05.23.08. СПб: 2015. 194 с.
10. Калугин Ю.Б. Моделирование воздействия дестабилизирующих факторов на технологический комплекс // Известия вузов. Строительство. 2013. № 7. С. 93-102.
11. Калугин Ю.Б. Особенности и сущность расчета вероятностных временных параметров отдельной работы (технологического процесса) // Известия вузов. Строительство. 2013. № 8. С. 104-109.
12. Голенко-Гинзбург Д.И. Стохастические сетевые модели планирования и управления разработками. Воронеж: Научная книга. 2010. 284 с.
13. Golenko-Ginzburg D. On the Distribution of Activity Time in PERT // Journal of the Operational Research Society. 1988. Vol. 39. № 8. Pp. 767-771.
14. Мальцев Ю.А. Экономико-математические методы проектирования транспортных сооружений. М.: Академия. 2010. 320 с.
15. Miller R. Schedule, Cost and Profit Control with PERT. McGraw-Hill. 1963. 58 p.
16. Руководство по разработке и применению вероятностных сетевых моделей в строительстве. М.: ЦНИПИАСС. 1979. 56 с.
17. A Guide to the Project Management Body of Knowledge. Project Management Institute. 2008. 506 p.
18. Birrell G. Construction planning beyond the critical path // J. Constr. Div. ASCE. 1980. Vol. 106(3). Pp. 389–407.
19. Голенко Д.И. Статистические методы сетевого планирования и управления. М.: Наука. 1968. 400 с.
20. Mubarak S. Construction Project Scheduling and Control. Second Edition. New Jersey. Hoboken: John Wiley & Sons, Inc. 2010. 479 p.

McGraw-Hill. 1963. 58 p.

16. *Rukovodstvo po razrabotke i primeneniyu veroyatnostnykh setevykh modelei v stroitel'stve* [Guidelines for the development and application of probabilistic network models in construction]. Moscow: TsNIPIASS. 1979. 56 p. (rus)
17. *A Guide to the Project Management Body of Knowledge.* Project Management Institute. 2008. 506 p.
18. Birrell G. Construction planning beyond the critical path. *J. Constr. Div. ASCE.* 1980. No. 106(3). Pp. 389–407.
19. Golenko D.I. *Statisticheskie metody setevogo planirovaniya i upravleniya* [Statistical methods of network planning and management]. Moscow: Science. 1968. 400 p. (rus)
20. Mubarak S. *Construction Project Scheduling and Control.* Second Edition. New Jersey. Hoboken: John Wiley & Sons, Inc. 2010. 479 p.
21. Oleinikova S.A. Kriticheskii analiz metoda PERT resheniya zadachi upravleniya proektami so sluchainoi dlitel'nost'yu vypolneniya rabot [Critical analysis of the PERT method for solving the problem of project management with random duration of the work]. *Control Systems and Information Technology.* 2013. Vol. 51. No 1. Pp. 20-24. (rus)
22. Klingel A. Bias in PERT completion times calculations for a real network. *Management Science.* 1966. Vol. 13(4). Pp. 476-489.
23. Schonberger R. Why projects are always late: a rationale based on manual simulation of a PERT/CPM network. *Interfaces.* 1981. Vol. 11(5). Pp. 66-70.
24. Kalugin Ju.B. Universal method for calculation of reliable completion times. *Magazine of Civil Engineering*. 2016. No. 7, Pp. 70-80.
25. Haga W., O'Keefe T. Crashing PERT Networks: A Simulation Approach. *Proc. of the 4th International conference of the Academy of Business and Administrative Sciences Conference.* Quebec City, Canada. 2001.
26. Burt J., Garman M. Conditional Monte Carlo: A simulation technique for stochastic network analysis. *Management Science*. 1971. No. 18(3). Pp. 207-217.
27. Van Slyke R. Monte Carlo methods and the PERT problem. *Operations Research.* 1963. Vol. 13. Pp. 141-143.
28. Kalugin Ju.B. Prognozirovanie srokov realizatsii proekta s pomoshchyu modeli kvaziparallelnykh rabot [Predicting the timing of the project with the help of a model quasi-parallel processes]. *News of Higher Educational Institutions. Construction.* 2011. No. 3. Pp. 45–51. (rus)

21. Олейникова С.А. Критический анализ метода PERT решения задачи управления проектами со случайной длительностью выполнения работ// Системы управления и информационные технологии. 2013. Т. 51. № 1. С. 20-24.
22. Klingel A. Bias in PERT completion times calculations for a real network // Management Science. 1966. Vol. 13(4). Pp. 476-489.
23. Schonberger R. Why projects are always late: a rationale based on manual simulation of a PERT/CPM network // Interfaces. 1981. Vol. 11(5). Pp. 66-70.
24. Калугин Ю.Б. Универсальный метод вычисления достоверных сроков реализации проекта. // Инженерно-строительный журнал. 2016. № 7. С. 70-80.
25. Haga W., O'Keefe T. Crashing PERT Networks: A Simulation Approach // Proc. of the 4th International conference of the Academy of Business and Administrative Sciences Conference. Quebec City, Canada, 2001.
26. Burt, J., Garman M. Conditional Monte Carlo: A simulation technique for stochastic network analysis // Management Science. 1971. № 18(3). Pp. 207-217.
27. Van Slyke R. Monte Carlo methods and the PERT problem // Operations Research. 1963. Vol. 13. Pp. 141-143.
28. Калугин Ю.Б. Прогнозирование сроков реализации проекта с помощью модели квазипараллельных работ// Известия вузов. Строительство. 2011. № 3. С. 45-51.

Yuri Kalugin,
+7(905)2162825; yuri_kalugin@inbox.ru

Юрий Борисович Калугин,
+7(905)2162825;
эл. почта: yuri_kalugin@inbox.ru

Калугин Ю.Б. Причины отставаний строительных проектов // Инженерно-строительный журнал. 2017. № 6(74). С. 61–69.

doi: 10.18720/MCE.74.7

Results of technical inspection monitoring of the operation object

Результаты мониторинга технического обследования объекта эксплуатации

N.V. Braila,
K.L. Khazieva,
A.A. Staritcyna,
Peter the Great St. Petersburg Polytechnic University, St. Petersburg, Russia

Канд. техн. наук, доцент Н.В. Брайла,
студент Л.Ф. Хазиева,
студент А.А. Старицына,
Санкт-Петербургский политехнический университет Петра Великого, г. Санкт-Петербург, Россия

Key words: physical deterioration; technical inspection; results monitoring; service conditions; actual age (taking into account service conditions); chronological age

Ключевые слова: физический износ; техническое обследование; контроль результатов; условия эксплуатации; действительный возраст (с учетом условий эксплуатации); хронологический возраст

Abstract. The article proposes analysis tool of the engineering survey series results. Analysis is based on a study of the physical depreciation accumulation by capital construction objects and deterioration models presented in it for various classes of structural schemes. The main provisions and user activity sequence with a brief explanation of the possible obtained results were clarified through steps. The proposed tool will allow timely detection of factors that cause the accelerated dynamics of deterioration (exceeding the normative one), reduce the risk of an accident, increase the expenses of element/object servicing, and also accurately predict the future costs of repair and construction activities. One of the advantages of this tool is a low capital intensity in the prosses of implementing and further using of tool by the real estate company. However, in the long term, the effect of the application will be expressed in the timely detection of errors in the conduct of buildings and structures surveys. Its result will be minimizing the deviation of the estimated (planned) costs of repair and construction work from the actual.

Аннотация. В статье предлагается инструмент анализа результатов серии обследований, основанный на исследовании о накоплении физического износа объектами капитального строительства и представленных в нем моделях износа по различным классам конструктивных схем. Пошагово разъяснены основные положения и последовательность действий пользователей с кратким разъяснением возможных полученных результатов. Предложенный инструмент позволит своевременно обнаруживать факторы, вызывающие ускоренную динамику износа (превышающую нормативную), снизить риск аварии и увеличение затрат на обслуживание элемента/ объекта, а также максимально точно спрогнозировать будущие затраты на проведение ремонтно-строительных мероприятий. Одним из преимуществ предложения является низкая капиталоемкость при внедрении и дальнейшем использовании инструмента эксплуатирующей недвижимость компанией. Вместе с тем в долгосрочной перспективе эффект от применения будет выражаться в своевременном выявлении ошибок при проведении обследований зданий и конструкций, результатом чего станет минимизация отклонения расчетных (планируемых) затрат на проведение ремонтно-строительных работ от фактических.

Introduction

The problem of dilapidated and dangerous housing remains topical in Russia not for the first decade. In the 1990s during the period of market economy development the condition of housing stock had been deteriorated: building operation had come down just to the exploitation, there were almost no maintenance of the normative state. A large number of researches of domestic scientists confirms the relevance of the problem [1–5].

As far as social and economic situation was stabilized and institute of housing and public utility services was developed situation began to change for the better. First of all standard technical documentation was actualized and it keeps updating, building inspection and repair works are carried out. Some buildings still are not regularly repaired and there are still some violations of repair technology, but scales have considerably decreased.

It is noted that specific weight of dilapidated and dangerous housing in the total area of all housing stock gradually decreases. From 2007 to the beginning of 2014 the amount of dilapidated and dangerous housing stock in absolute terms remains almost at the same level that is caused by the following factors:

- high intensity of new construction;
- continuous allocation of financing for major repairs and refurbishment works;
- regional measures, for example, there is a program in St. Petersburg for renovation of the first mass series of housing (Khrushchev-era housing).

The main indicators of housing stock development in Russian Federation are given in Table 1. Data for the table was taken from the official sites of the government statistics [6, 7], in case of absence of information data was completed by other source (in the table it is marked as "*") [8].

Table 1. Dilapidated and dangerous housing stock of Russian Federation (at the end of year) volume of construction and major repairs

	Dilapidated housing stock, mln m^2	**Dangerous housing stock, mln m^2**	**New construction, mln m^2**	**Major repair and reconstruction, mln m^2**	**Cost of major repair, mln m^2**
1990	28.9	3.3	49.30*	n/a	n/a
1995	32.8	4.9	41.00*	n/a	n/a
2000	56.1	9.5	36.4	n/a	n/a
2005	83.4	11.2	54.8	n/a	n/a
2006	83.2	12.7	50.60*	n/a	n/a
2007	84	15.1	61.20*	n/a	n/a
2008	83.2	16.5	64.10*	0.2	120.57
2009	80.1	19.4	59.90*	0.28	137.47
2010	78.9	20.5	70.3	0.63	107.82
2011	78.4	20.5	77.2	0.1	76.11
2012	77.7	22.2	82	0.16	128.95
2013	70.1	23.8	70.50*	0.04	80.23
2014	69.5	23.8	87.1	0.08	67.9
2015	н/д	н/д	83.8	0.06	71.29

Due to the current economic crisis stagnation or even regress of the outlined positive tendency in housing and public utility branch is expected. So it is known that in St. Petersburg some quarters of "Khrushchev-era housing" are supposed to be excluded from the program for renovation in the nearest future. However, dramatic recession will not happen again.

Responsible owner or operating company are always interested in increase of useful lifetime of the building and improvement or maintenance its operational properties at the necessary level. Along the planning of repair and construction works (RCW) the problem of forecasting of works volume and required capital investments is especially complicated.

Practice shows that qualitatively conducted technical inspection of the building, which authentically reflects the current situation, promotes timely repair and construction works and also provides an optimum finance and time expenditure.

Market monitoring showed that there is a big price difference in services of technical inspection. Companies which offer price much lower than average market price, raise big doubts. High-quality inspection requires special equipment, so, its cost has to be put in cost of technical inspection. A lot of companies give low quality reports, work of such companies is oriented to the "flow".

The problem of competence of technical inspections exists and is discussed at the field-specific events (conferences, seminars, etc.) by the practicing experts and scientific community, for example, [9-11], and also is considered in the researches and works by authors [22-27].

Literature review showed that at the present time a lot of researches on methods of scheduling of (RCW) and problems of inspection of separately taken structural elements or the whole building (construction) are conducted [12-18], it is separately possible to allocate works of P. Christoua, K. Alatorella, J. Bhandari and M. Cassar [28-31]. However there are almost no works analyzing consequences of an incorrect technical evaluation and possible methods of tracking correlation between results of technical inspection and previously conducted inspections and also their coordination with accidents and repairs during the period between inspections.

The conscientious owner or operating company conducts inspection of technical condition of an object with a certain frequency. According to All-Union state standard 31937-2011 “Buildings and constructions. Rules of inspection and monitoring of technical condition” for the structures working in normal conditions the first technical inspection after placing facility in operation is conducted not later than in 2 years, further at least once in 10 years.

Thus, during operation of the capital building the whole series of planned and unplanned technical inspections will be carried out. The comparative analysis of two and more consistently executed technical inspections of an object can be very interesting from the point of view of monitoring of technical condition in the course of time and possibility of forecasting accidents with help of indirect signs.

Methods and Results

The instrument for analysis of results of series of inspections can allow the following:

- identify possible mistakes of each technical inspection. As it was mentioned competently executed technical inspection allows predict future costs of repairs;

- timely find factors which cause accelerated dynamics of depreciation. Accelerated physical deterioration of construction conceals in itself two dangers: growth of risk of an accident and increase of maintenance costs. Both of them contradict the main postulates of effective operation;

In the Figure 1 the flowchart of control of results of technical inspection of the operated object is submitted.

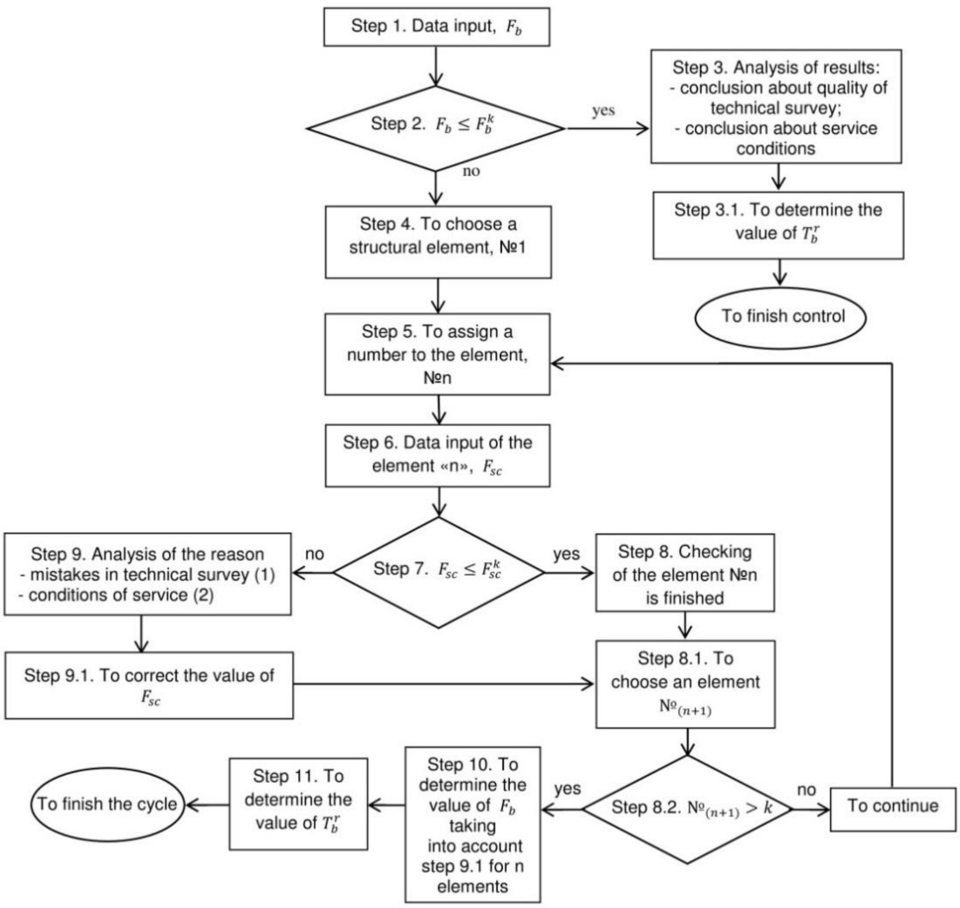

Figure 1. The flowchart of control of results of technical inspection of the operated object

Fb – physical deterioration of the surveyed object;

Fbk – control value of physical deterioration, is identified strictly by the actual age of the surveyed object;

Tbr – actual age of the surveyed object, considers service conditions (during analysis of results of the first technical survey it is accepted as equal to chronological, for the subsequent - as the sum of actual age defined at the previous inspection and the number of years between inspections);

Fsc – physical deterioration of the structural element №n;

k – total quantity of the elements;

Fsck – control value of physical deterioration of the element, is identified by the actual age of the surveyed object or the element, for example, if he was replaced.

Discussion

Let us consider features and restrictive conditions of application of a technique:

1. On the step 2 it is necessary to compare physical deterioration F_b, of the building determined during technical inspection and control value F_b^k, determined by one of possible techniques. The analysis of different techniques of calculation of physical deterioration by its valid and standard service life is carried out in work [19]. Most of the described dependencies take into consideration the lifetime of the building. However it is known that building materials and, respectively, structural elements even with similar standard service life can have schedules of a physical deterioration which are different in type of curvature, as the main applied building materials have dissimilar characteristics of plasticity, susceptibility to fatigue failures, elasticity, fragility, ability to work for compression or bend etc. Besides most of developments consider certain normal service conditions without taking into account, for example, climatic conditions and other features of external "aggressors".

Thus, using of these dependences can give very accurate calculation of physical deterioration depending on service life for one objects and essential mistake for others.

There is also more modern research [20] based on processing of representative selection of 1 880 147 buildings in different technical condition and of different years of construction. The advantage of this research is that there is represented how physical deterioration of buildings of different construction design depends on time, that is more convenient for the final consumer. Restriction – the subject of research were buildings of Moscow region, so, for example, for northern latitudes using of these dependences can be referred to controversial issues.

Nevertheless, the research confirms previously set judgment, fig.3 shows that for each type of design its own curve of accumulation of physical deterioration is determined. Interpretations of constructive schemes CS-1 – CS-13 are given in Table 2.

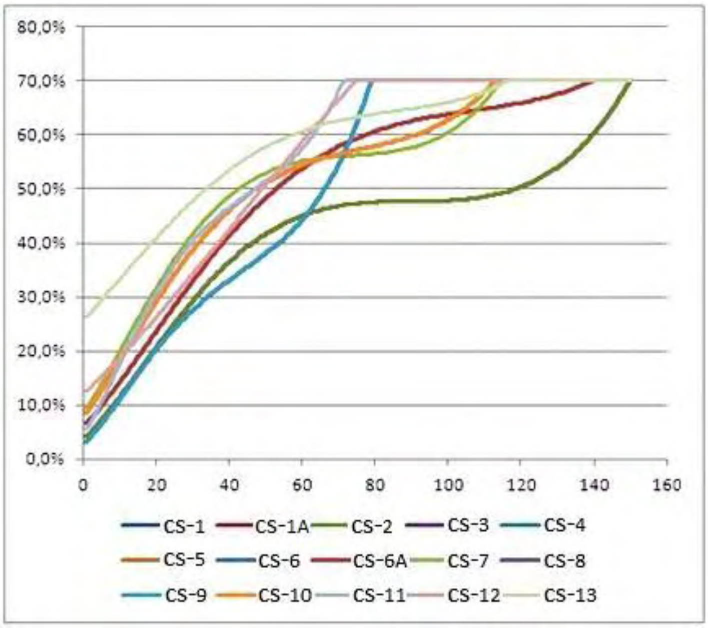

Figure 2. Graphic display of models of physical deterioration depending on classes of the constructive systems "CO-INVEST"

Table 2. Description of constructive systems

Class of the constructive scheme	Basic material
CS-1	Enclosing structures – brick; bearing structures – reinforced concrete, steel
CS-1A	Enclosing structures – small cellular and layered wall blocks; bearing structures – reinforced concrete, steel
CS-2	Enclosing structures – brick; bearing structures – wood
CS-3	Enclosing structures – reinforced concrete; bearing structures – reinforced concrete in frameless systems
CS-4	Enclosing structures – reinforced concrete; bearing – reinforced concrete in frame systems
CS-5	Enclosing structures – reinforced concrete; bearing structures – steel
CS-6	Enclosing structures – thin metal sheet and effective heat-insulating materials; bearing structures – reinforced concrete, steel
CS-6A	Enclosing structures – glass; bearing structures – reinforced concrete or steel frame
CS-7	Enclosing structures– wood; bearing structures – wood and other construction material
CS-8	With primary application of nonmetallic materials and concrete
CS-9	With primary application of cast reinforced concrete
CS-10	With primary application of prefabricated concrete
CS-11	With primary application of constructional steel
CS-12	With primary application of steel pipes
CS-13	With primary application of wood
CS-14	With primary application of cables and leads
CS-15	Site improvements (planting)

Let us give an example of definition of control value of physical deterioration F_b^k using as example building of CS-7 (enclosing structures – wood; bearing - wood and other construction material), which actual age on date of survey is 50 years (Figure 3).

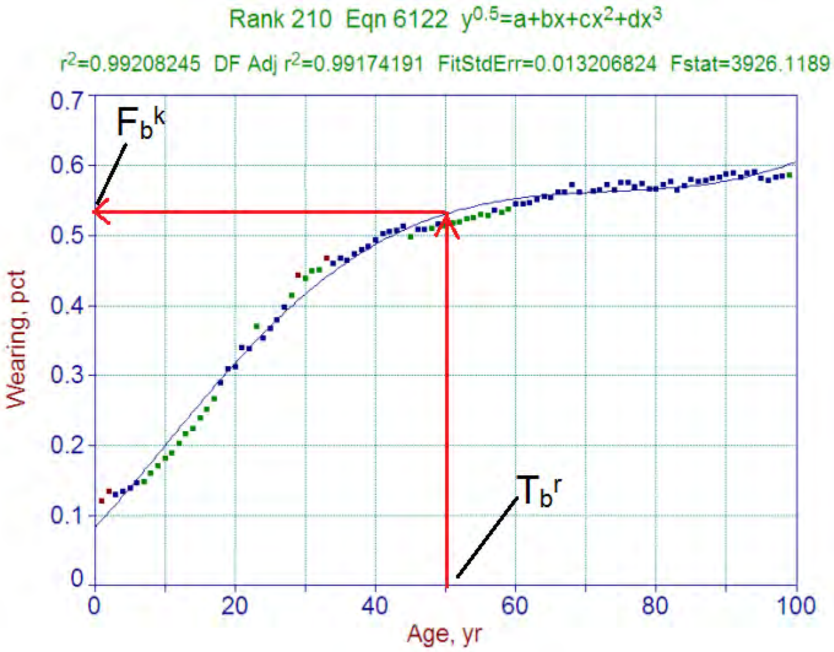

Figure 3. Graphic method of definition of control value by the form and characteristics of the model of physical deterioration for CS-7

Conclusions on the step 2 are very important, also for the analysis of results of the subsequent technical surveys:

a) if physical deterioration after survey is equal to its control value ($F_b=F_b^k$), then it means that service conditions are normal: object is operated in accordance with requirements of the project and standard technical documentation, repair and operational events are held on-time; actual age of the object (T_b^r), taking into account service conditions, is equal to the chronological age (T_b^t).

b) if physical deterioration after survey is less than its control value ($F_b<F_b^k$), then service conditions are characterized as good. Accordingly actual age is less than chronological ($T_b^r<T_b^t$) and it can be determined by a solution of inverse problem which idea is presented in the Figure 3.

2. By the same way control values for structural elements can be determined, for example, by VSN 53-86 (r) [21]. In this normative document there are submitted schedules of physical deterioration of layered constructions with service life of 60-125 years and 10-50. However now there is a great variety of building constructions and new materials for which such dependences are not found out yet.

3. A key step of the flowchart is the step 9. Exactly here, in case if physical deterioration considerably exceeds control value, it is necessary to carry out careful analysis of the reasons.

As a result there has to be received an answer to the question: if it was mistake in determining of physical deterioration during technical inspection or not. In this case it should be corrected. Also it is possible that the jump of physical deterioration became consequence of inadequate service conditions, then it is required to eliminate the cause immediately and take preventative actions against repetitions.

4. Step 10 assumes recalculation of physical deterioration of the surveyed object (F_b) taking into account the executed corrections of physical deterioration of structural elements (F_{sc}) by the following formula [21]:

$$F_b = \sum_{i=1}^{i=k} F_{sci} \times l_i \quad (1)$$

where F_{sci} - physical deterioration of the separate construction, element or system, %;

l_i – coefficient, which corresponds to the part of recovery cost of the separate construction, element or system in the total recovery cost of the building.

Conclusions

One of advantages of the method is possibility of monitoring of dynamics of change of technical condition of an object by results of the general inspection based on the analysis and testing payment using the data of visual survey. Cost of this work is not high as special tools and equipment are not required. It will allow the operating company to order this service and in interstandard terms (more often than once in 10 years).

Thus, in spite of the fact that costs for application of the technique are not big, its application will allow to find mistakes during inspections or inadequate service conditions, that finally will be reflected in the maximum approximation of calculation of the planned and actual costs of carrying out repair and construction works.

References

1. Dmitriyeva T.N., Khanzhov I.S., Bolshakova S.M. Podkhody k resheniyu problem vetkhogo i avariynogo zhilya [Approaches to the solution of problems of the shabby and hazardous dwelling]. *Ekonomika i menedzhment innovatsionnykh tekhnologiy.* 2014. No. 8. Pp. 47-55. (rus)
2. Novikova G.Yu. , Achkasova A.P. Problema avariynogo i vetkhogo zhilya v Rossii [Problem of hazardous and shabby dwelling in Russia]. *Razvitiye ekonomiki regiona: vzglyad v budushcheye : materialy II gorod. nauch.prakt. konf.* Volgograd: Volgogr. gos. arkhitektur.stroit. unt, 2013. Pp. 177-179. (rus)
3. Sheina S.G. Metodika razrabotki tselevykh programm po likvidatsii vetkhogo i avariynogo zhilya munitsipalnogo obrazovaniya [Technique of development of target programs for elimination of the shabby and hazardous dwelling of municipal unit] // Vestnik grazhdanskikh inzhenerov. 2008. No. 2. Pp. 87–91. (rus)

Литература

1. Дмитриева Т.Н., Ханьжов И.С., Большакова С.М. Подходы к решению проблем ветхого и аварийного жилья // Экономика и менеджмент инновационных технологий. 2014. № 8 С. 47-55.
2. Новикова Г.Ю., Ачкасова А.П. Проблема аварийного и ветхого жилья в России // Развитие экономики региона: взгляд в будущее: материалы II город. научно-практической конф. Волгоград: Волгогр. гос. архитектур. строит. унт, 2013. С. 177-179.
3. Шеина С.Г. Методика разработки целевых программ по ликвидации ветхого и аварийного жилья муниципального образования // Вестник гражданских инженеров. 2008. № 2. С. 87–91.
4. Ибрагимова З.Ф., Япарова-Абдулхаликова Г.И. О некоторых проблемах в сфере ветхого и аварийного жилья // Вестник УГАЭС. Наука, образование, экономика. Серия: Экономика. 2015. № 1(11). С. 69-73.
5. Прокопович В.П., Иваницкая Л.В. Прогнозирование

4. Ibragimova Z.F., Yaparova-Abdulkhalikova G.I. O nekotorykh problemakh v sfere vetkhogo i avariynogo zhilya [About some problems in the sphere of the shabby and hazardous dwelling]. *Vestnik UGAES. Nauka, obrazovaniye, ekonomika. Seriya: Ekonomika.* 2015. No. 1(11). Pp. 69-73. (rus)
5. Prokopovich V.P., Ivanitskaya L.V. Prognozirovaniye sostoyaniya zhilogo fonda s tselyu obosnovaniya yezhegodnykh ekonomicheskikh resursov, trebuyemykh dlya pereseleniya grazhdan iz avariynogo i vetkhogo zhilya [Forecasting of a condition of housing stock for the purpose of justification of the annual economic resources demanded for resettlement of citizens from hazardous and shabby dwelling]. *Vestnik Rossiyskoy akademii yestestvennykh nauk.* 2014. No. 3. Pp. 79-85. (rus)
6. *Federalnaya sluzhba gosudarstvennoy statistiki* [Russian Federal State Statistics Service]. [Online] URL: http://www.gks.ru/.
7. *Yedinaya mezhvedomstvennaya informatsionno-statisticheskaya sistema (YeMISS)* [Single interdepartmental information and statistical system] [Online]. URL: www.fedstat.ru
8. *HOMA Chemical Engineering.* [Online] URL: http://homa.ru/company/novosti/rynok-stroitelnykh-i-otdelochnykh-materialov-2015-2016-gg/
9. Patrikeyev A.V., Salatov Ye.K. Osnovy metodiki dinamicheskogo monitoringa deformatsionnykh kharakteristik zdaniy i sooruzheniy [Bases of a technique of dynamic monitoring of deformation characteristics of buildings and constructions]. *Vestnik MGSU.* 2013. No. 1. Pp. 133-138. (rus)
10. Patrikeyev A.V., Salatov Ye.K., Spiridonov V.P. Dinamicheskiy monitoring zdaniy i sooruzheniy kak odin iz kriteriyev obespecheniya bezopasnoy ekspluatatsii [Dynamic monitoring of buildings and constructions as one of criteria of ensuring safe operation]. *Tekhnologicheskiye problemy prochnosti: materialy XVIII Mezhdunar. seminara.* Podolsk. 2011. Pp. 78-81. (rus)
11. Sudar O.Yu., Ulybin A.V., Kukushkina G.A. Calculation of cost of works on inspection of buildings and constructions for labor costs. *Construction of Unique Buildings and Structures.* 2016. No. 5(44). Pp. 58-71. (rus)
12. Ulybin A.V., Vatin N.I. Quality of visual inspection of buildings and constructions and technique of his performance. *Construction of Unique Buildings and Structures.* 2014. No. 10(25). Pp. 134-146. (rus)
13. Zolina T.V. Poryadok provedeniya obsledovaniy zdaniya s tselyu posleduyushchey otsenki yego ostatochnogo resursa [Order of carrying out inspections of the building for the purpose of the subsequent assessment of his residual resource]. *Vestnik MGSU.* 2014. No. 11. Pp. 98-108. (rus)
14. Brayla N.V., Khaziyeva L.F. Vliyaniye kachestva obsledovaniya obyekta nedvizhimosti na planirovaniye remontno-stroitelnykh rabot [Influence of quality of inspection of a real estate object on planning of repair construction works]. *Materialy Mezhdunarodnoy nauchno-prakticheskoy konferentsii Komsomolsk-na-Amure.* 2015. (rus)
15. Poduvaltsev V.V., Mogilyuk Zh.G., Khlystunov M.S. Dostovernost rezultatov dinamicheskikh obsledovaniy zdaniy i sooruzheniy [Reliability of results of dynamic inspections of buildings and constructions]. *Izmiritelnaya tekhnika.* 2013. No. 8. Pp. 9-11.
16. Ilchenko D.P., Simankina T.L., Romanovich M.A. Korrektirovka kalendarnogo plana remontno-stroitelnykh rabot na osnove metoda zameshcheniya planovykh rabot [Updating of the planned schedule of repair construction works on the basis of a method of replacement of planned works]. *Vestnik grazhdanskikh inzhenerov.* 2013. No. 2(37). Pp. 125-130. (rus)
17. Rogonskiy V.A., Kostrits A.I., Sheryakov V.F. *Ekspluatatsionnaya nadezhnost zdaniy i sooruzheniy.* Saint-Peterburg: OAO «Izdatelstvo «Stroyizdat SPb».

состояния жилого фонда с целью обоснования ежегодных экономических ресурсов, требуемых для переселения граждан из аварийного и ветхого жилья / В. П. Прокопович, // Вестник Российской академии естественных наук. 2014. № 3. С. 79-85.
6. Федеральная служба государственной статистики: [Электронный ресурс] URL: http://www.gks.ru/.
7. Единая межведомственная информационно-статистическая система (ЕМИСС) [Электронный ресурс] URL: www.fedstat.ru
8. HOMA Chemical Engineering: [Электронный ресурс] URL: http://homa.ru/company/novosti/rynok-stroitelnykh-i-otdelochnykh-materialov-2015-2016-gg/
9. Патрикеев А.В., Салатов Е.К. Основы методики динамического мониторинга деформационных характеристик зданий и сооружений // Вестник МГСУ, 2013. № 1. С. 133-138.
10. Патрикеев А.В., Салатов Е.К., Спиридонов В.П. Динамический мониторинг зданий и сооружений как один из критериев обеспечения безопасной эксплуатации // Технологические проблемы прочности: материалы XVIII Междунар. семинара. Подольск, 2011. С. 78-81.
11. Сударь О.Ю., Улыбин А.В., Кукушкина Г.А. Расчёт стоимости работ по обследованию зданий и сооружений по трудозатратам // Строительство уникальных зданий и сооружений. 2016. № 5(44). С. 58-71.
12. Улыбин А.В., Ватин Н.И. «Качество визуального обследования зданий и сооружений и методика его выполнения» // Строительство уникальных зданий и сооружений. 2014. № 10(25). С. 134-146.
13. Золина Т.В. Порядок проведения обследований здания с целью последующей оценки его остаточного ресурса // Вестник МГСУ. 2014. № 11. С. 98–108.
14. Брайла Н.В., Хазиева Л.Ф. Влияние качества обследования объекта недвижимости на планирование ремонтно-строительных работ // Материалы Международной научно-практической конференции Комсомольск-на-Амуре. 2015.
15. Подувальцев В.В., Могилюк Ж.Г., Хлыстунов М.С. Достоверность результатов динамических обследований зданий и сооружений // Измирительная техника. 2013. № 8. С. 9-11.
16. Ильченко Д.П., Симанкина Т.Л., Романович М.А. «Корректировка календарного плана ремонтно-строительных работ на основе метода замещения плановых работ»// Вестник гражданских инженеров. 2013. № 2(37). С. 125-130.
17. Рогонский В.А., Костриц А.И., Шеряков В.Ф. [и др.] Эксплуатационная надежность зданий и сооружений. С.-Петербург: ОАО «Издательство «Стройиздат СПб». 2004. 172 с.
18. Симанкина Т.Л., Попова О.Н. Квалиметрическая экспертиза при оценке состояния застройки урбанизированной территории // Строительство уникальных зданий и сооружений. 2013. № 7(12). С. 71-78.
19. Брайла Н.В. Календарное планирование ремонтно-строительных работ на основе совершенствования методики определения физического износа объектов: Дисс.канд.техн. наук. СПб, 2012. 174 с.
20. Корсаков Р.О. Величина физического износа объектов капитального строительства на основании данных учета МОБТИ [Электронный ресурс]. Систем. требования: AdobeAcrobatReader. URL: http://avg.ru/docs/2015-10-28-model-fizicheskogo-iznosa-oks-2015.pdf. (дата обращения: 23.05.2017).
21. ВСН 53-86(р) Правила оценки физического износа жилых зданий.
22. Sheils E., O'Connor A., Breysse D., Schoefs F., Yotte S. Development of a two-stage inspection process for the assessment of deteriorating infrastructure // Reliability Engineering & System Safety. 2010. Vol. 95. Issue 3.

2004. 172 p.

18. Simankina T.L., Popova O.N. Qualimetrical examination at assessment of a condition of building of the urbanized territory. *Construction of Unique Buildings and Structures*. 2013. No. 7(12). Pp. 71-78. (rus)
19. Brayla N.V. Kalendarnoye planirovaniye remontno-stroitelnykh rabot na osnove sovershenstvovaniya metodiki opredeleniya fizicheskogo iznosa obyektov. [Scheduling of repair and construction works on the basis of improving the methodology for determining the physical wear and tear of objects: PhD Thesis]. Saint-Petersburg, 2012. 174 p. (rus)
20. Korsakov R.O. *Velichina fizicheskogo iznosa obyektov kapitalnogo stroitelstva na osnovanii dannykh ucheta MOBTI* [The amount of physical depreciation of capital construction objects on the basis of the MOTI data]. [Электронный ресурс]. System requirements: AdobeAcrobatReader. URL: http://avg.ru/docs/2015-10-28-model-fizicheskogo-iznosa-oks-2015.pdf. (date of application: 23.05.2017). (rus)
21. VSN 53-86(r) Pravila otsenki fizicheskogo iznosa zhilykh zdaniy [Rules for assessing the physical wear and tear of residential buildings]. (rus)
22. Sheils E., O'Connor A., Breysse D., Schoefs F., Yotte S. Development of a two-stage inspection process for the assessment of deteriorating infrastructure. *Reliability Engineering & System Safety*. 2010. Vol. 95. Issue 3. Pp. 182-194.
23. Roger M. Groves, comprehensive composite materials ii, reference module. *Materials Science and Materials Engineering.* 2018. Vol. 3. Pp. 300–311.
24. Balaras C.A., Droutsa K., Dascalaki E., Kontoyiannidis S. Deterioration of European apartment buildings. *Energy and Buildings.* 2005. Vol. 37. Issue 5. Pp. 515-527.
25. Wang L., Chu J., Mao W. A condition-based replacement and spare provisioning policy for deteriorating systems with uncertain deterioration to failure. *European Journal of Operational Research.* 2009. Vol. 194. Issue 1. Pp. 184-205.
26. Ezrin M. *Failure Related to Service Conditions, Plastics Failure Guide (Second Edition).* 2013. Pp. 279–320.
27. Balaras C.A., Argiriou A.A., Infrared thermography for building diagnostics. *Energy and Buildings*. 2002. Vol. 34. Issue 2. Pp. 171-183.
28. Kylilia A., Fokaidesa P., Christoua P., Kalogiroub S.A. Infrared thermography (IRT) applications for building diagnostics: A review. *Applied Energy.* 2014. Vol. 134. Pp. 531-549.
29. Alatorella K., Vprabhu P. A review of human error in aviation maintenance and inspection. *International Journal of Industrial Ergonomics.* 2000. Vol. 26. No. 2. Pp. 133-161.
30. Bhandari J., Khan F., Abbassia R., Garaniyaa V., Ojedaa R. Modelling of pitting corrosion in marine and offshore steel structures – A technical review. *Journal of Loss Prevention in the Process Industries*. 2015. Vol. 37. Pp. 39-62.
31. Cassar M. Preventive conservation and building maintenance. *Museum Management and Curatorship*. 1994. Vol. 13. Issue 1. Pp. 39-47.

Pp. 182-194.

23. Roger M. Groves, comprehensive composite materials ii, reference module // Materials Science and Materials Engineering. 2018. Vol. 3. Pp. 300–311.
24. Balaras C.A., Droutsa K., Dascalaki E., Kontoyiannidis S. Deterioration of European apartment buildings // Energy and Buildings. 2005. Vol. 37. Issue 5. Pp. 515-527.
25. Wang L., Chu J., Mao W. A condition-based replacement and spare provisioning policy for deteriorating systems with uncertain deterioration to failure // European Journal of Operational Research. 2009. Vol. 194. Issue 1. Pp. 184-205.
26. Ezrin M. Failure Related to Service Conditions. Plastics Failure Guide (Second Edition). 2013. Pp. 279–320
27. Balaras C.A., Argiriou A.A. Infrared thermography for building diagnostics // Energy and Buildings. 2002. Vol. 34. Issue 2. Pp. 171-183.
28. Kylilia A., Fokaidesa P., Christoua P., Kalogiroub S.A. Infrared thermography (IRT) applications for building diagnostics: A review // Applied Energy. 2014. Vol. 134. Pp. 531-549.
29. Alatorella K., Vprabhu P. A review of human error in aviation maintenance and inspection // International Journal of Industrial Ergonomics. 2000. Vol. 26. Issue 2. Pp. 133-161.
30. Bhandari J., Khan F., Abbassia R., Garaniyaa V., Ojedaa R. Modelling of pitting corrosion in marine and offshore steel structures – A technical review // Journal of Loss Prevention in the Process Industries. 2015. Vol. 37. Pp. 39-62.
31. Cassar M. Preventive conservation and building maintenance // Museum Management and Curatorship. 1994. Vol. 13. Issue 1. Pp. 39-47.

Natalya Braila,
+7(921)3926512; nashi-n-v@mail.ru

Lina Khazieva,
+79043373419; lina_hazieva@mail.ru

Anastasiia Staritcyna,
+7(911)0050215; a.staritsyna@mail.ru

Наталья Васильевна Брайла,
+7(921)3926512; эл. почта: nashi-n-v@mail.ru

Лина Фахимовна Хазиева,
+79043373419; эл. почта: lina_hazieva@mail.ru

Анастасия Андреевна Старицына,
+7(911)0050215; эл. почта: a.staritsyna@mail.ru

Braila N.V., Khazieva K.L., Staritcyna A.A. Results of technical inspection monitoring of the operation object. *Magazine of Civil Engineering*. 2017. No. 6. Pp. 70–77. doi: 10.18720/MCE.74.7.

doi: 10.18720/MCE.74.8

Modeling of indentation and slip of wedge punch

Моделирование внедрения и сдвига штампа клиновидной формы

A.S. Semenov,
S.G. Semenov,
B.E. Melnikov,
Peter the Great St. Petersburg Polytechnic University, St. Petersburg, Russia
V.S. Tikhonov,
Weatherford, Moscow Russia

Канд. физ.-мат. наук, доцент А.С. Семенов,
инженер С.Г. Семенов,
д-р техн. наук, проф. Б.Е. Мельников,
Санкт-Петербургский политехнический университет Петра Великого, г. Санкт-Петербург, Россия
канд. техн. наук, заведующий сектором В.С. Тихонов,
Weatherford, Москва, Россия

Key words: modeling; experiment; elasticity; plasticity; slip; drillpipe; indentation; punch; contact; finite element method

Ключевые слова: моделирование; эксперимент, упругость; пластичность; клиновый захват; бурильная труба; внедрение; штамп; контакт; метод конечных элементов

Abstract. To determine the load-carrying capacity of the drillpipe slip, it is necessary to calculate the drag force on the surface between the pipe and the slip. To improve such capacity, the grip surface is provided with teeth that can indent into the pipe body. As a result, the friction force on the contact surface is supplemented with the drag force generated by plastic shear strain of the pipe body. The paper presents an analytic dependence of the indentation force of an ideal (untruncated) and non-ideal (truncated) wedge punch that models tooth operation on the indentation depth and friction factor on the punch lateral face both for shallow (with prevailing elastic strain of the gripped body) and deep indentation (with prevailing plastic strain). Multiple computational experiments were performed to identify parameters of the proposed formula. Such computations were complemented with determination of the punch drag force dependence on the indentation depth during punch shearing. The developed model was verified by experimental studies of punch indentation and slip as well as indentation and drag force measurements. The obtained results proved the high level of accuracy of the analytical indentation force model. The outcome of drag force determination experiments was further used to calculate the slip load-carrying capacity.

Аннотация. При определении несущей способности клинового захвата бурильных труб возникает проблема расчета силы контактного сопротивления на поверхности раздела захвата и удерживаемой им конструкции. Для повышения надежности поверхность захватывающего устройства снабжается зубцами, которые могут внедряться в тело конструкции. В результате наряду с силой трения на контактной поверхности будет дополнительно действовать сила сопротивления, вызванная пластической деформацией тела при сдвиге. В статье предложена аналитическая зависимость для силы внедрения штампа идеальной (неусеченной) и неидеальной (усеченной) клиновидной формы, моделирующего работу зубца, в зависимости от глубины внедрения и коэффициента трения на боковой поверхности штампа как при неглубоком (с преимущественно упругим деформированием захватываемого тела), так и при глубоком внедрении (с преимущественно пластическим деформированием). Для идентификации параметров предложенной формулы были выполнены многовариантные вычислительные эксперименты. Расчет дополнялся определением зависимости силы сопротивления штампа при сдвиге от глубины внедрения. С целью верификации разработанной модели были проведены экспериментальные исследования процессов внедрения и сдвига штампа с измерением сил внедрения и сопротивления. Полученные результаты подтвердили высокую точность аналитической модели для силы внедрения. Результаты эксперимента с определением силы сопротивления были в дальнейшем использованы для расчета удерживающей силы клинового захвата.

Семенов А.С., Семенов С.Г., Мельников Б.Е., Тихонов В.С. Моделирование внедрения и сдвига штампа клиновидной формы // Инженерно-строительный журнал. 2017. № 6(74). С. 78–101.

Introduction

Slips, slip elevators, spiders, etc. have been widely used as oilfield service tools to hold drillstrings, drill collars and casings acting as a wedge [1] (Fig. 1). A pipe in a slip with a conical bearing surface is subjected to compound loads comprised of axial tensile, compression and bending stresses. To increase the holding force, the bearing surface of the gripping device is provided with teeth that can indent into the pipe body. This generates additional drag force on the contact surface resulting from plastic strain of the pipe surface as it shears relative to the slip that supplements the friction force.

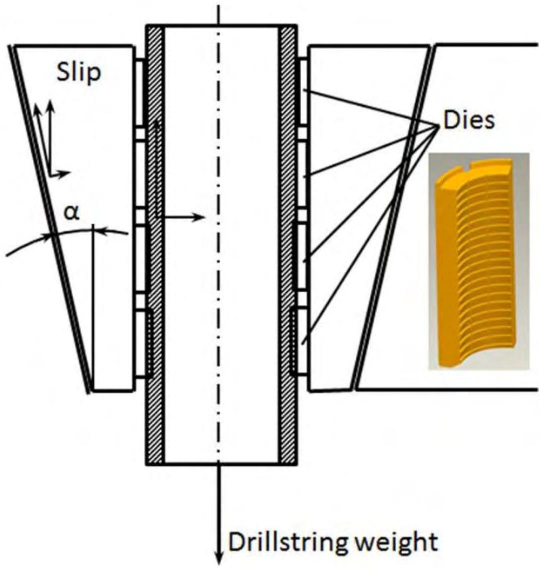

Figure 1. Slip scheme

The Reinhold-Spiri equation [2] accounting for the maximum breaking stress limit being equivalent (von Mises) stress is used in drilling mechanics to determine the holding force. Pipe failures in slips during deepwater drilling in the 1990s and full-scale experiments demonstrated that in some cases the Reinhold-Spiri equation could provide a non-conservative estimation [3]. This results from pipe strength reduction as its surface is damaged by teeth.

An accurate model of contact interaction of the pipe contact surface with the gripping device equipped with teeth of various forms is required for better understanding of causes of pipe breaking in a slip. Such model is based on a single tooth model where such tooth can be considered as a wedge punch: ideal (untruncated) or non-ideal (truncated).

Finite element (FE) modeling of the indentation and scratch processes of a wedge-shaped indenter are considered in [4-8], while experimental investigations are discussed in [9-11, 6, 5]. However, a universal analytical description, which takes into account the wedge geometry, process staging and friction, which oriented to practice, was not proposed.

The purpose of this study is to develop a unified universal model of deep and shallow indentation and shift of an ideal and non-ideal wedge-shape punch, taking into account the dependence of force on the depth of the indented tooth, its geometry and friction on the lateral surface. To achieve the goal, analytical and experimental studies along with numerical simulations are carried out.

The analytic dependences for the indentation force from the depth of wedge teeth indentation into the pipe body are developed for the most common shapes of teeth used in oilfield service tools. In case of shallow (elastic) truncated wedge indentation, it is offered to use known solutions of the linear elastic problem of rectangular shaped punch pressure on half space. The dependence of indentation force on indentation depth and friction factor on the lateral wedge face in case of deep (plastic) indentation is more complex. Parameters of such dependence were identified by multiple FE method computations, where the wedge drag force dependence on the indentation depth during its shearing was additionally calculated. The calculations used both the simplest rigid ideally plastic models [12-14] and elastic-plastic models with nonlinear hardening [15-17].

The developed model is verified by multiple experimental studies of indentation and shift with indentation, breakout and drag force measurements. The obtained results proved the high level of accuracy of the proposed models and can be used to calculate the force of pipe holding in a slip.

Experimental Data

The experimental setup used for wedge punch (single slip tooth) indentation and shear testing was comprised of Instron 8801 multipurpose test system with additional accessories (Fig. 2) to create force normal to the main force generated by the test system. Instron 8801 is a servohydraulic testing system with a maximum load capacity of 100kN and stroke of ~ 80mm. The force measurement accuracy is ±0.5 % of indicated load (load cell capacity 1:100), crosshead position measurement accuracy is ±1 µm. Accessories (Fig. 2) include tooth holder 1, lower table 2 with above installed U-shaped frame 3. Pipe segment 4 is installed on lower table 2 on special mandrel 5. The mandrel is installed on roller guides 6 to reduce the measurement error. Besides, movement in the perpendicular plane is limited by four adjustable rollers 7 to exclude any movement normal to the applied shear force. Shear force (marked with a blue arrow in Fig. 2) is generated by jack 8 actuated by a manual pump, force is measured with load cell 9 with an accuracy of ±200 N. Shear is measured with LVDT transducer 10 with an accuracy of ±1 µm fixed on frame 3.

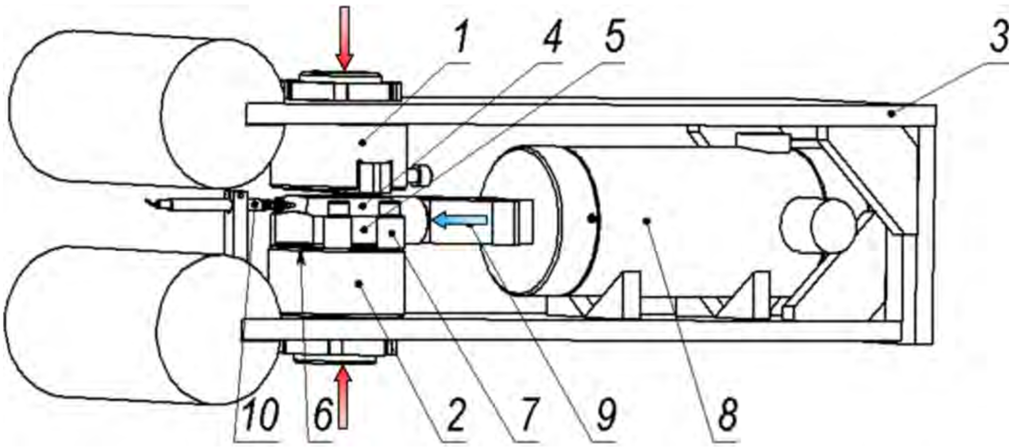

Figure 2. Single tooth test setup

The test program was as follows:

– The tooth was indented to a set depth with the multipurpose test system with simultaneous recording of the indentation diagram using the developed software;

– While the constant indentation depth was maintained, the pipe segment was sheared in relation to the tooth using the jack driven by a manual pump with simultaneous recording of the indentation force and shear force vs. shear diagram using the developed software.

Figure 3 presents the results of single tooth indentation into the pipe segment for as-received and ground surfaces and three depths (~150 µm, ~350 µm and ~750 µm). The diagrams were plotted by averaging of three tests with further correction for the system compliance. Based on the above diagrams, the indentation curves for corroded surfaces feature a sufficiently large statistical variability while ground surface curves practically do not demonstrate such variability.

It was established that indentation depth during testing should be measured excluding as many compliant elements as possible. Optimally, noncontact measurement methods should be used that measure the distance between the tooth and the pipe segment.

Figure 4 presents shear curves for various depths and surface conditions. Such curves demonstrate sensitivity both to the indentation depth and surface condition. The appearance of specimens after the shear tests is shown in Figure 5.

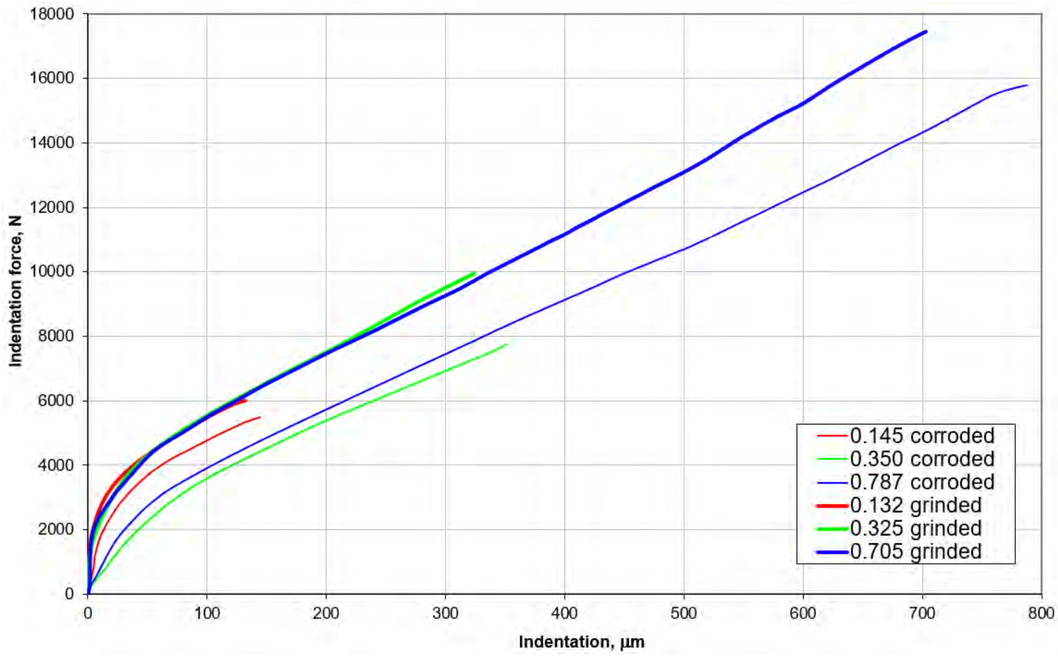

Figure 3. Sample experimental indentation curves

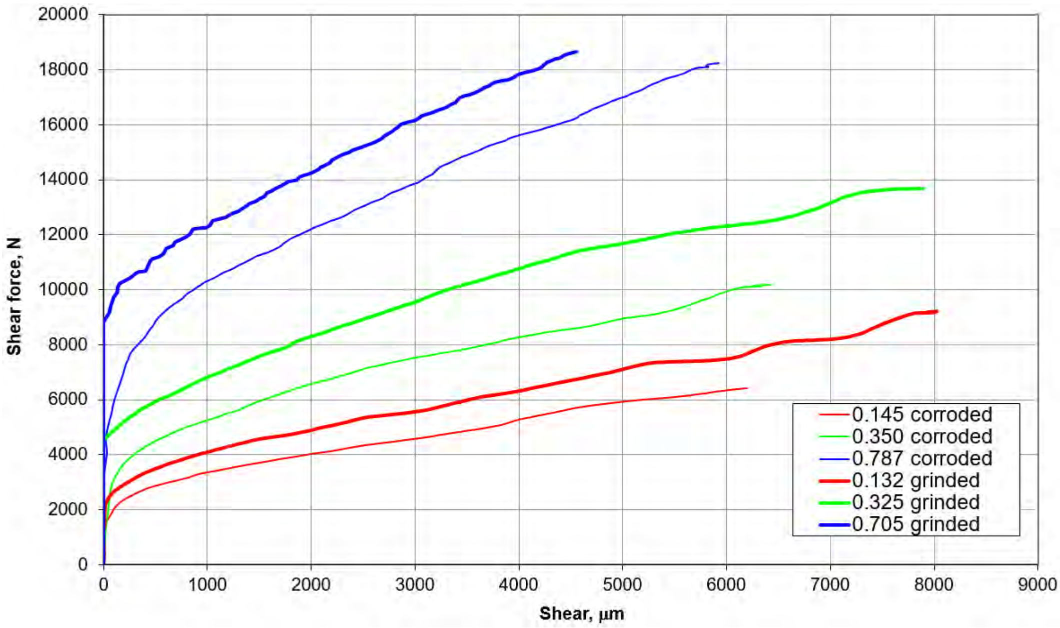

Figure 4. Sample experimental shear curves


a) b) c)

Figure 5. Appearance of specimens after indentation with further shear tests.
Initial indentation depth: a) 150μm, b) 350μm, c) 750μm

An interpolation surface (Fig. 6) was plotted for ground specimens based on the test results, which represented shear force dependence on the indentation depth and shear.

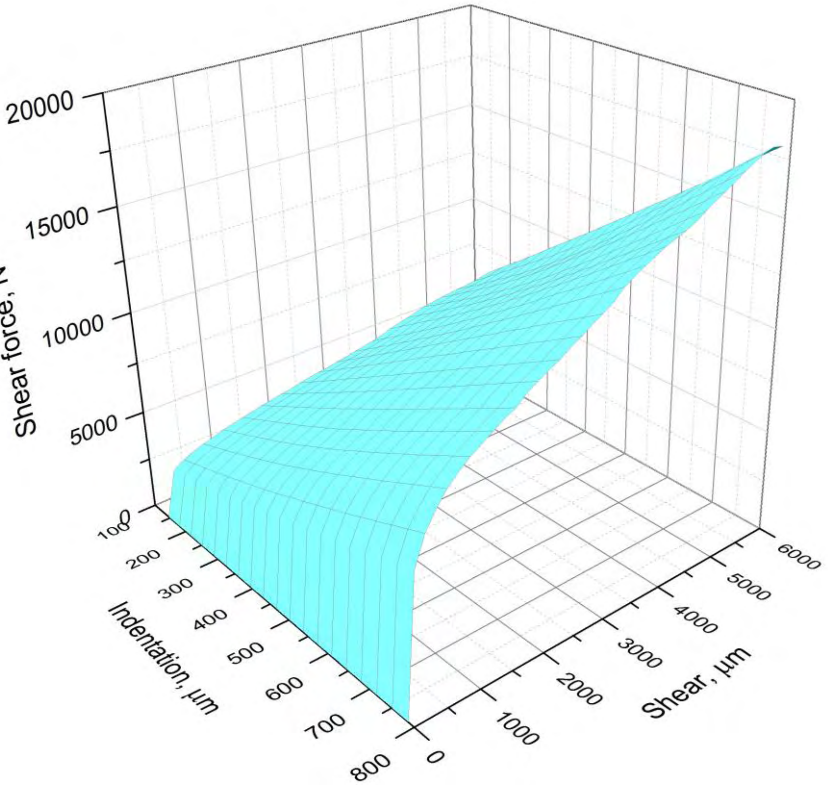

Figure 6. Interpolation surface of shear force dependence on indentation and shear

The resulting dent profiles were measured at the indentation depth of 150μm (ground surface) (Fig. 7). Depth was measured with MIG measuring head in the grooved section (accuracy ±1μm) and a dial gauge in the “crest” section (accuracy ±10μm). Positioning in the shear direction was ensured by the lathe carriage with an accuracy of ±50μm.

A section with newly formed smooth surface (about 2mm in the shear direction) and a ruptured section can be distinguished on all the tested specimens. The correct description of the ruptured section requires utilization of fracture mechanics methods [18, 19].

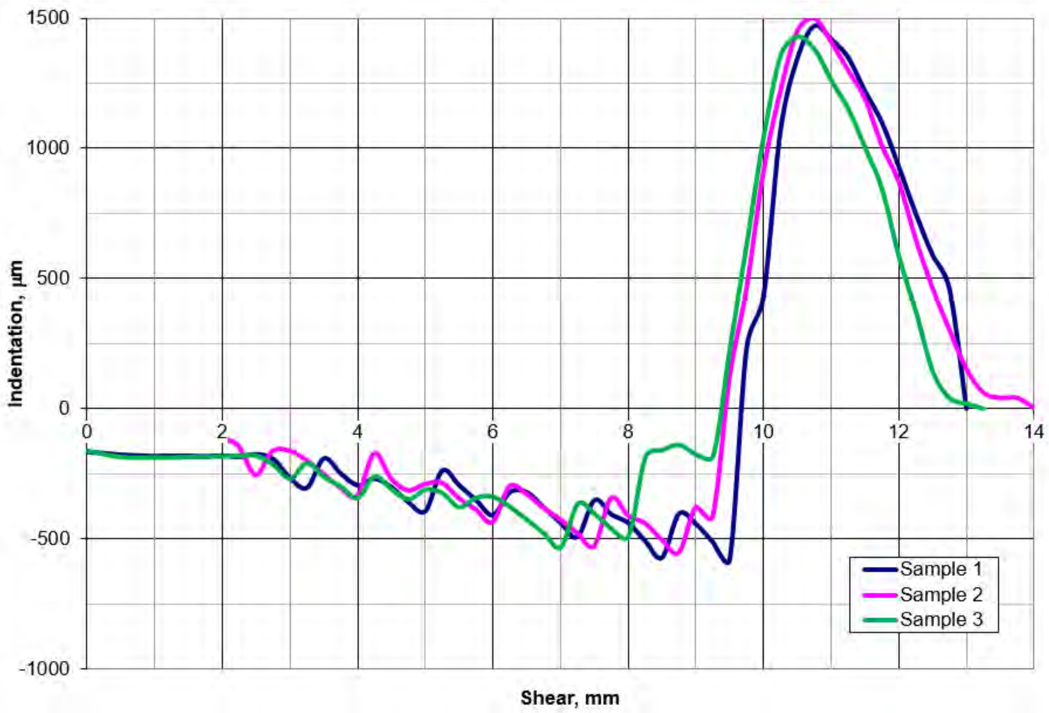

Figure 7. Dent profiles for the initial indentation depth of 150μm

Approximation of indentation curves of ideal (untruncated) and non-ideal (truncated) wedge punch

Mathematical formulation of indentation model

The representative experimental indentation curve (plotted by averaging of multiple tests) of a symmetric wedge punch with a rectangular flat base (Fig. 8) takes the form of a monotonic increasing dependence of force on indentation depth $F = F(h)$, tending to an oblique asymptote not passing through the origin of coordinates.

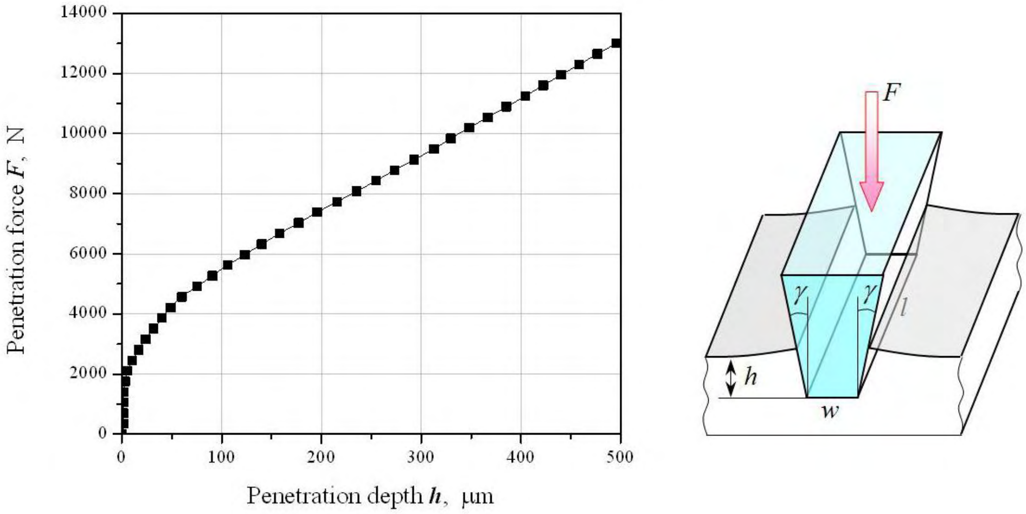

Figure 8. Representative experimental indentation curve (left) of a wedge punch with a rectangular flat base (right) (w=381μm, l=4.826μm, γ=30º)

To approximate indentation curves of ideal and non-ideal (flat base) wedge punches $F = F(h)$, this paper proposes to use the following equation:

$$F = \left(k_p h + F_0\right)\left(1 - e^{-\frac{k_e}{F_0}h}\right), \tag{1}$$

which at $h \to \infty$ asymptotically tends to the straight line:

$$F = k_p h + F_0, \tag{2}$$

and at $h \to 0$ to the straight line:

$$F = k_e h. \tag{3}$$

Equation (1) uses three parameters: k_e, k_p, F_0, which characterize the initial and final slopes of the indentation curve and the height of asymptote intersection with Y-axis (Fig. 9):

$$\begin{aligned} k_e &= \left.\frac{dF}{dh}\right|_{h \to 0} \\ k_p &= \left.\frac{dF}{dh}\right|_{h \to \infty} \\ F_0 &= \left[F(h) - k_p h\right]_{h \to \infty} \end{aligned} \tag{4}$$

The validity of equalities (4) can be easily verified using equation for the derivative of *F*(*h*) function (1):

$$\frac{dF}{dh} = k_p\left(1 - e^{-\frac{k_e}{F_0}h}\right) + \left(k_p h + F_0\right)\frac{k_e}{F_0} e^{-\frac{k_e}{F_0}h}. \tag{5}$$

The choice of the exponent function used to describe the nonlinear indentation curve segment is proved by the calculation data, which does not preclude searching of any alternatives.

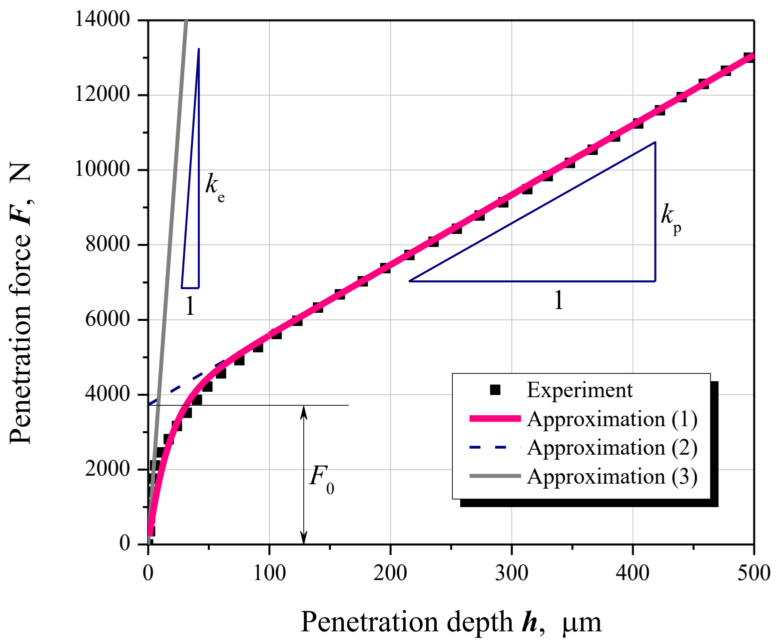

Figure 9. Approximation (1) of the indentation curve of a wedge punch with a rectangular flat base and geometric interpretation of its parameters

To analyze processes of indentation of *non-ideal* (truncated) wedges to considerable depths $h > w/7$, where *w* is the truncated wedge base width, linear approximation (2) can be used instead of (1), which differs from (1) by less than 0.1% for typical values of used wedge parameters. When indentation processes of *ideal* ($w = 0$) wedges are analyzed, there is no pressure contribution in the area perpendicular to the action of force ($F_0 = 0$) and it would be reasonable to use the simplified equation

$$F = k_p h. \tag{6}$$

Approximation in the form of Eq. (1) using three parameters k_e, k_p, F_0 can be justified by the ability to estimate the latter based on the known analytical solutions of contact problems in the context of the theory of elasticity (for k_e) and theory of plasticity (for k_p, F_0). It should be noted that, in the general case, parameters k_e, k_p, F_0 admit dependence on the wedge geometry and mechanical properties of the indenting and indented material. Analytical solutions help define the above dependences concretely.

Elastic and plastic analytic solutions

At the *initial* stage ($h \to 0$) of indentation of a wedge punch with a flat base, solution of the *linear elastic problem* of punch pressure with a rectangular base on half space [20, 21] can be used:

$$F = \frac{E}{1 - \nu^2}\frac{\sqrt{wl}}{m}h, \tag{7}$$

where E is Young's modulus, v is Poisson's ratio, w is the truncated wedge base width, l is the truncated wedge base length, m is the parameter determined as the ratio of the base sides (if $l/w=10$ $m=0.71$, Fig. 10). Eq. (7) was derived by generalization of the solution of the Boussinesq problem on the action of a normal concentrated force on the surface of elastic half-space. It should be noted that solution (7) was derived based on the assumptions of infinitesimal mechanics, where small strains are assumed and the difference between the actual and reference configurations are neglected. In this case, the form of the wedge side face is not crucial, only the truncated wedge base sizes are essential. The solution is true for very weak indentation forces only and, therefore, for shallow penetration depths ($h \to 0$), when the plastic zone and contact on the side wedge faces may be neglected. When solution (7) was derived, it was assumed that contact pressure was evenly distributed, there was no friction and *h* was assumed as the average displacement value under the punch. Such conditions are not crucial as the difference from the solution for the rigid punch (constant displacements and variable contact pressures) is about 8% [20].

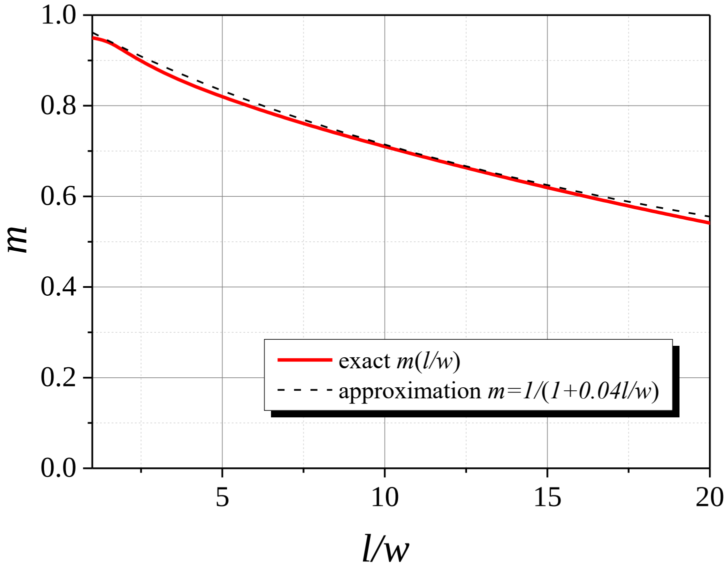

Figure 10. Parameter *m* in Eq. (7) vs. base side ratio l/w. The simplest approximation of this dependence within the range up to *l/w*<20 is $m = 1/(1+0.04l/w)$

Comparison of Eqs. (7) and (3), get an estimate of the initial indentation curve section slope:

$$k_e = \frac{E}{1-v^2}\frac{\sqrt{wl}}{m} \approx \frac{E}{1-v^2}\sqrt{wl}\left(1+\frac{l}{25w}\right). \tag{8}$$

For the considered case with $E = 210$ GPa, $v = 0.3$, $w = 381$ μm, $l = 4826$ μm, $m = 0.67$:

$$k_e = 467 \text{ N/μm}. \tag{9}$$

At the stage of *deep* ($h \to \infty$) indentation of an ideal wedge punch, the solution of the *rigid ideally plastic problem* can be used accounting for geometric similarity of transient plastic flow at plane strain. For the indentation case without friction in [12], the following equation is proposed for the resulting vertical load on the wedge during indentation:

$$F = \frac{4\sigma_Y}{\sqrt{3}} l \frac{(1+\theta)\sin\gamma}{\cos\gamma - \sin(\gamma-\theta)} h. \tag{10}$$

where σ_Y is the yield stress, γ is the wedge half-angle, θ is the angle implicitly defined by the equality $\cos\theta = [\cos\gamma - \sin(\gamma-\theta)][\cos(\gamma-\theta)+\sin\gamma]$ (Fig. 11).

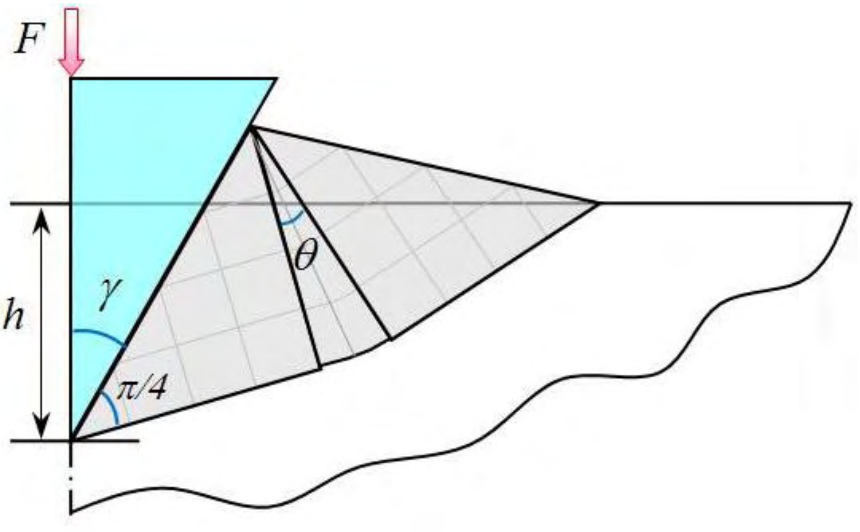

Figure 11. Rigid wedge indentation in half plane. The plastic zone is highlighted in grey

Correlation of Eq. (10) with (6) results in the equation for the final penetration curve section slope:

$$k_p = \frac{4\sigma_Y}{\sqrt{3}} l \frac{(1+\theta)\sin\gamma}{\cos\gamma - \sin(\gamma-\theta)}. \tag{11}$$

The equation for an ideal wedge with $\sigma_Y = 660$ MPa, $l = 4826$ μm, $\gamma = 30°$:

$$k_p = 7.41 \text{ N/μm}. \tag{12}$$

Analytic solutions similar to (10) can be derived for the case of wedge indentation with taking into consideration the friction [13, 14, 10]. Curves corresponding to elastic solution (7) and a series of rigid ideal plastic solutions for various friction coefficients μ are shown in Figure 12.

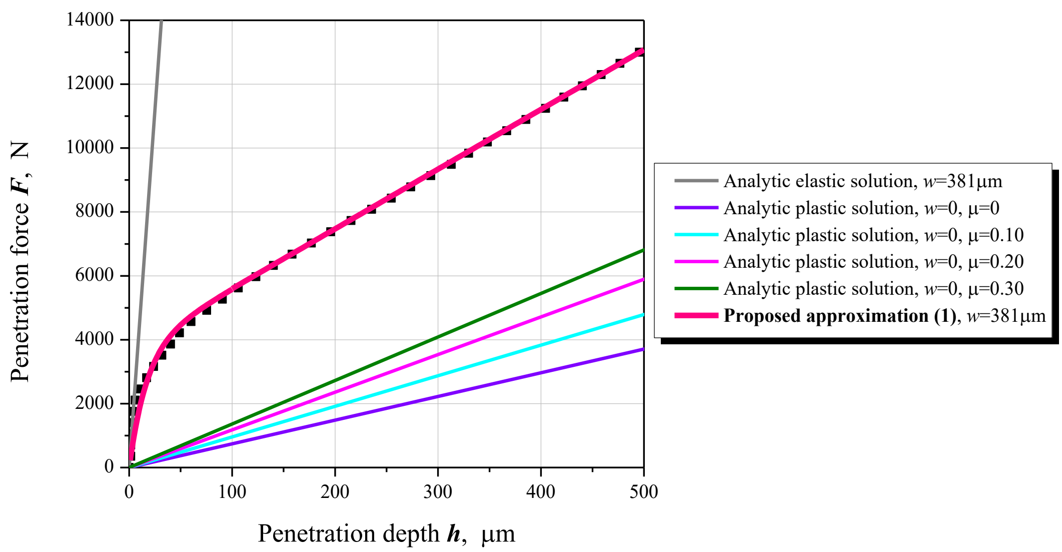

Figure 12. Linear approximations of indentation curve based on analytic elastic and plastic solutions with various values of friction coefficient μ

There are two causes of mismatch of curves plotted based on the ideal plastic solution with the experimental curve shown in Figure 8. First, different geometry: truncated wedge in the experimental studies and ideal (untruncated) wedge in the analytic solution. Truncation additionally contributes to the resulting pressure force acting on the wedge base area, which raises the indentation curve. This is proved by experimental results [22] and FE computations (Fig. 13). The quoted results require consideration of $F_0(w)$ in model (1). Second, real material hardening that is not considered in the analytic solution obtained based on the ideal plastic model. Comparison of analytic indentation curves for an ideally plastic material with FE solutions (Fig. 14) that consider hardening shows slope increase by 20-30 % due to hardening.

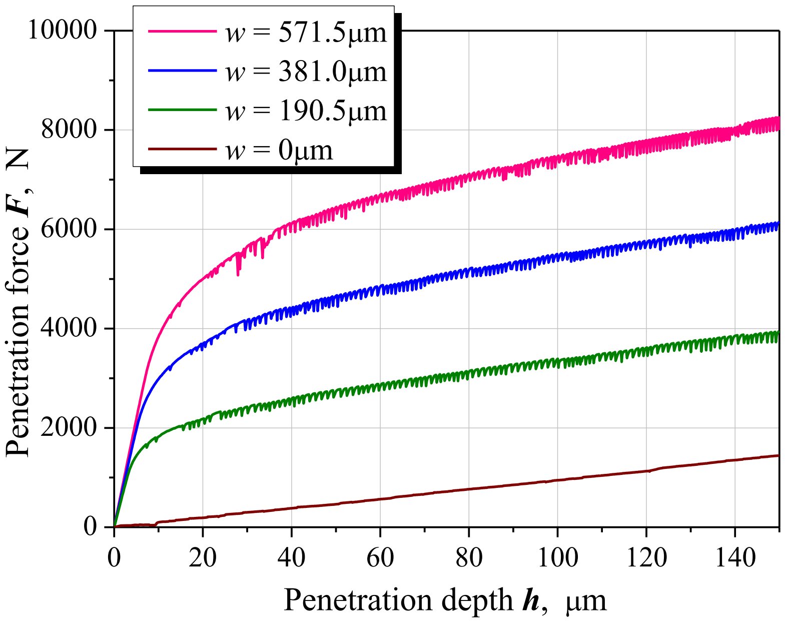

Figure 13. Indentation curves of truncated wedge punches with various base dimensions *w* plotted based on FE computations (μ = 0)

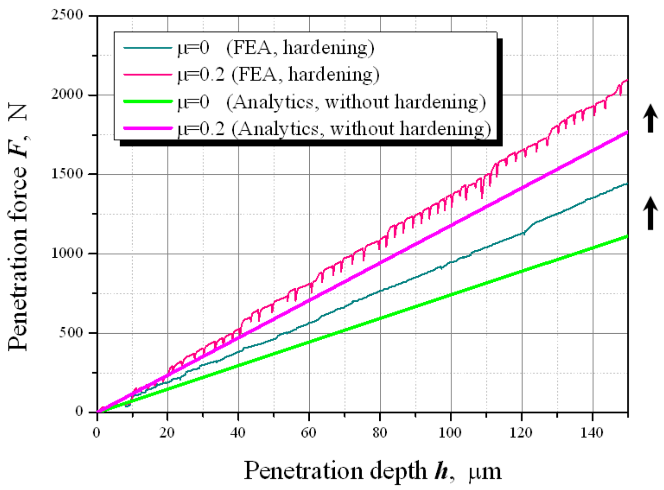

Figure 14. Effect of hardening on the slope of wedge punch indentation curves (*w* = 0)

The analytic solutions of simplified elastic and plastic indentation problems provided above enable to determine the linear character of indentation force dependence on its depth for the studied idealized loading cases and wedge geometry and get explicit dependences of respective slopes of indentation curves on such parameters as E, ν, σ_Y, μ, l, etc. In the general case of truncated wedges and hardening of the indented material, FE computations are required to identify the parameters k_p, F_0 of model (1) that characterize the process of indentation at various developed plastic strains. The parameter k_e that characterizes the initial stage of indentation can be completely determined by Eq. (8).

Identification of k_p and F_0 for a truncated wedge

Assume that the parameters k_p, F_0 depend on the truncated wedge base width w and friction coefficient μ. To identify the specified dependences, multiple computational experiments were performed for four values of w =0 μm; 190.5 μm (50 % of the standard value); 381 μm (100%); 571.5 μm (200%) and three values of μ=0; 0.2; 0.4. The results of computations are shown in Figure 15.

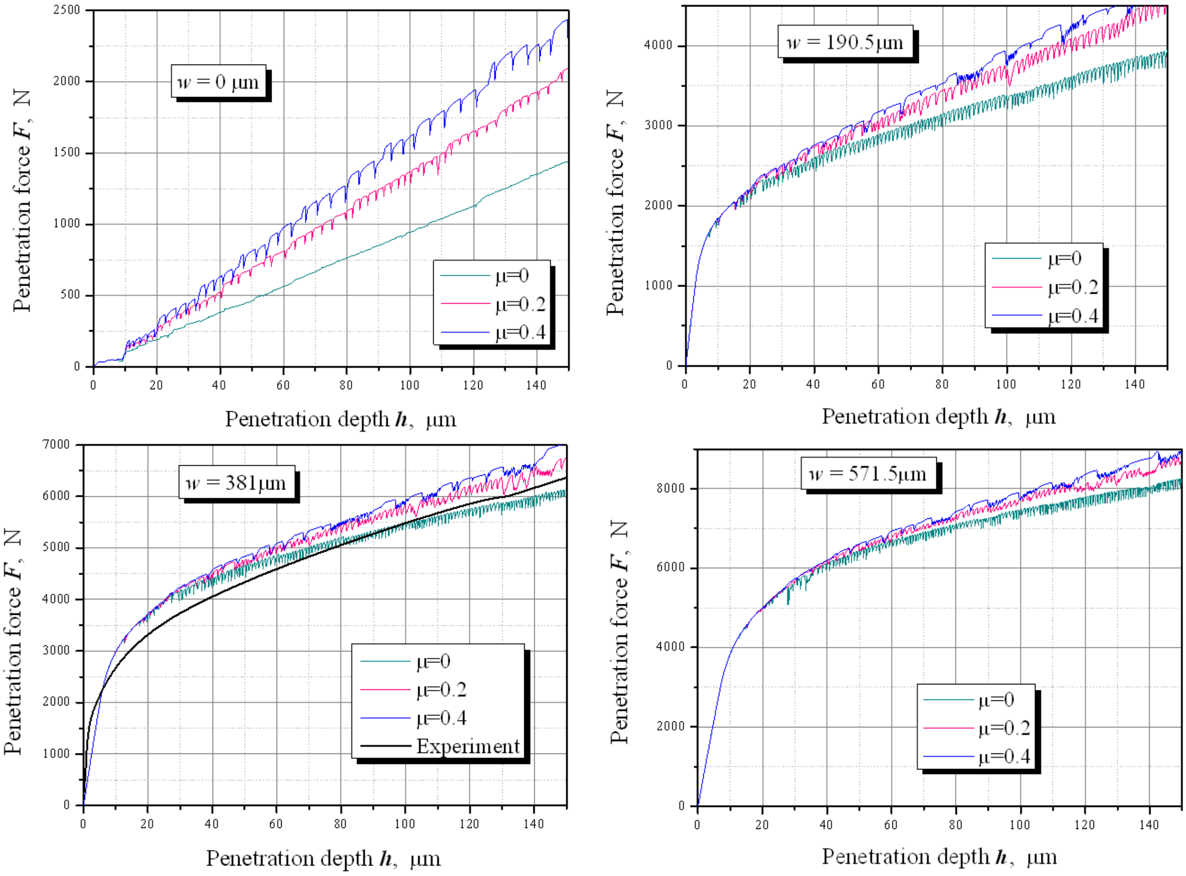

Figure 15. Indentation curves of a wedge punch with various base dimensions w and values of friction coefficient μ plotted based on FE computation results

The model of an elastic-plastic body with nonlinear hardening (see for details [15-17, 23, 24]) was used for FE computations. The experimental stress-strain curve is shown in Figure 16. It is plain that its ideally plastic approximation is crude enough. Computations were made by multiplicative decomposition of the strain gradient into elastic and plastic parts. Dissipation along the contact line due to the Coulomb friction was considered along with volume plastic dissipation.

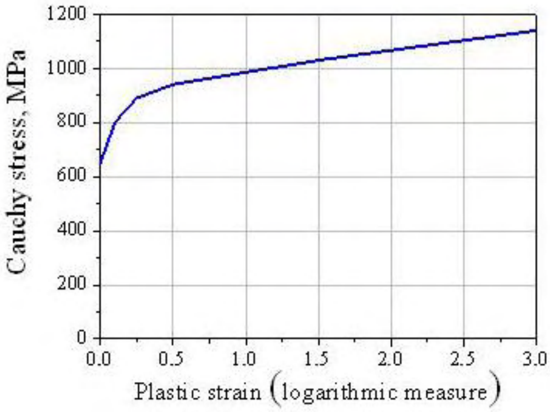

Figure 16. Stress-strain curve used in FE computations

An indentation in computational experiments was modelled by rigid indenters with various wedge base width values. Computations were made under assumption of the plane strain conditions. The results of computations are provided in Figure 17.

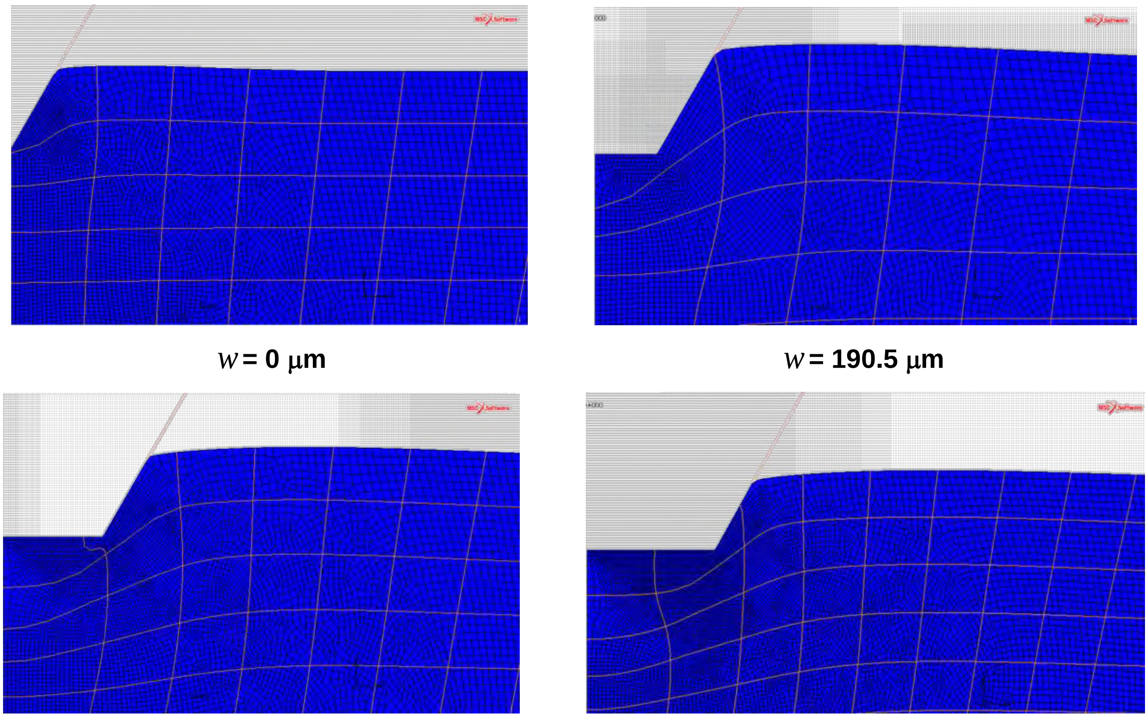

w = 0 μm

w = 190.5 μm

w = 381 μm

w = 571.5 μm

Figure 17. Deformed states after indentation of wedge punches with various base dimensions *w*

The slopes of asymptote k_p and the heights of asymptote intersection with Y-axis determined based on the calculated indentation curves presented in Fig. 9 are provided in Tables 1 and 2.

Table 1. Slopes of asymptote k_p [N/μm] vs. wedge base width w and friction coefficient μ

	μ = 0	μ = 0.2	μ = 0.4
w = 0 μm	9.66	13.9	16.4
w = 190.5 μm	12.3	16.7	18.7
w = 381.0 μm	15.6	19.3	21.4
w = 571.5 μm	18.1	21.8	23.5

Table 2. Heights of asymptote intersection with Y-axis F_0 [N] vs. wedge base width w and friction coefficient

	μ = 0	μ = 0.2	μ = 0.4
w = 0 μm	0	0	0
w = 190.5 μm	2095	2029	2013
w = 381.0 μm	3835	3787	3748
w = 571.5 μm	5548	5481	5469

The graphic presentation of the parameters k_p and F_0 is shown in Figure 18.

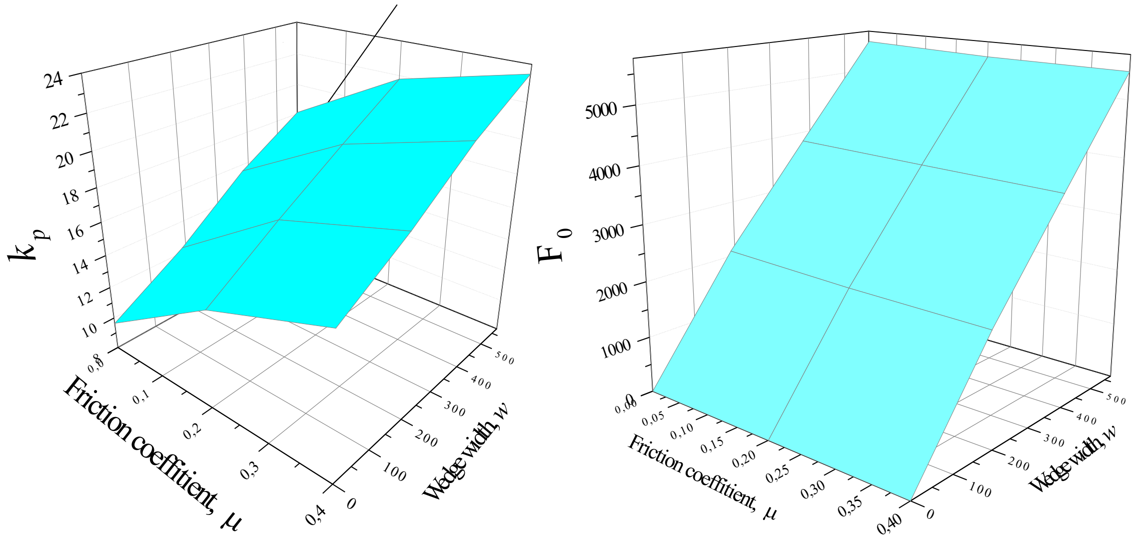

Figure 18. Dependences of $k_p(w,\mu)$ **and** $F_0(w,\mu)$

Constants of bilinear, biquadratic and mixed approximation of $k_p(w,\mu)$ and $F_0(w,\mu)$ were determined using the least square method.

For *bilinear* approximation

$$k_p = A + Bw + C\mu \tag{13}$$

the constants take the following values

$$\begin{aligned} A &= 10.2915 \quad \text{N/µm} \\ B &= 0.01381 \quad \text{N/µm}^2 \\ C &= 15.2125 \quad \text{N/µm} \end{aligned} \tag{14}$$

The root mean square (RMS) error in this case is χ=0.358.

For *biquadratic* approximation

$$k_p = A + Bw + C\mu + Dw^2 + Q\mu^2 + Pw\mu \tag{15}$$

the constants take the following values

$$\begin{aligned} A &= 9.56917 \quad \text{N/µm} \\ B &= 0.01586 \quad \text{N/µm}^2 \\ C &= 26.62 \quad \text{N/µm} \\ D &= -1.4696 \cdot 10^{-6} \ \text{N/µm}^3 \\ Q &= -24.1875 \quad \text{N/µm} \\ P &= -0.00606 \quad \text{N/µm}^2 \end{aligned} \tag{16}$$

The RMS error in this case is χ=0.0267.

For *mixed* approximation

$$k_p = A + Bw + C\mu + D\mu^2 \tag{17}$$

the constants take the following values

$$\begin{aligned} &A = 9.969 \quad \text{N}/\mu\text{m} \\ &B = 0.01381 \quad \text{N}/\mu\text{m}^2 \\ &C = 24.89 \quad \text{N}/\mu\text{m} \\ &D = \text{-}24.19 \quad \text{N}/\mu\text{m} \end{aligned} \tag{18}$$

The RMS error in this case is χ=0.0810.

The dependence $F_0(w,\mu)$ (Fig. 12) demonstrates almost total absence of μ effect on F_0, and the dependence $F_0(w)$ is close to linear, therefore, assume that

$$F_0 = G + Hw, \tag{19}$$

where the best values of constants are as follows

$$\begin{aligned} &G = 95 \quad \text{N} \\ &H = 9.6 \quad \text{N}/\mu\text{m} \end{aligned}. \tag{20}$$

It should be noted that constant *G* is small as compared to the observed levels of *F* (thousands and tens of thousands Newton) and it may be neglected.

The constants from (14), (16), (18), (20) fit the case of l = 4826 μm and should be changed proportionally to the changes in the wedge base length *l*.

Visual analysis of functions $k_p(w,\mu)$ (Fig. 12) demonstrates that dependence $k_p(w)$ is very close to linear, while $k_p(\mu)$ is nonlinear. Therefore mixed approximation (17) will be further considered as the principal one. Usage of approximations (17) and (19) is equivalent to development of an indentation model based on two hypotheses:

Linear dependence of slope k_p and shear in Y direction F_0 on the base width *w*;

Quadratic dependence of slope k_p and independence of F_0 from the friction coefficient μ.

Thus, based on (17) and (19), approximation (1) can be presented as

$$F(h;\ w,\mu) = \left[\left(A + Bw + C\mu + D\mu^2\right)h + G + Hw\ \right]\left(1 - e^{-\frac{k_e}{G+Hw}h}\right). \tag{21}$$

Comparison of approximation (21) with results of FE computations demonstrated (Fig. 19) good accuracy in a wide range of the parameters w and μ.

Dependences $F(h,\mu)$ at four different values of w and $F(h,w)$ and three values of μ demonstrate (Fig. 20) that w has a dominant impact on the indentation force of the two considered parameters w and μ. If the friction coefficient μ has a fixed value, approximation (21) will be simplified:

$$F(h;\ w) = \left[\left(A' + Bw\right)h + G + Hw\ \right]\left(1 - e^{-\frac{k_e}{G+Hw}h}\right). \tag{22}$$

If the base width value w is fixed, approximation (21) takes the following form:

$$F(h;\ \mu) = \left[\left(A'' + C\mu + D\mu^2\right)h + G'\ \right]\left(1 - e^{-Q'h}\right). \tag{23}$$

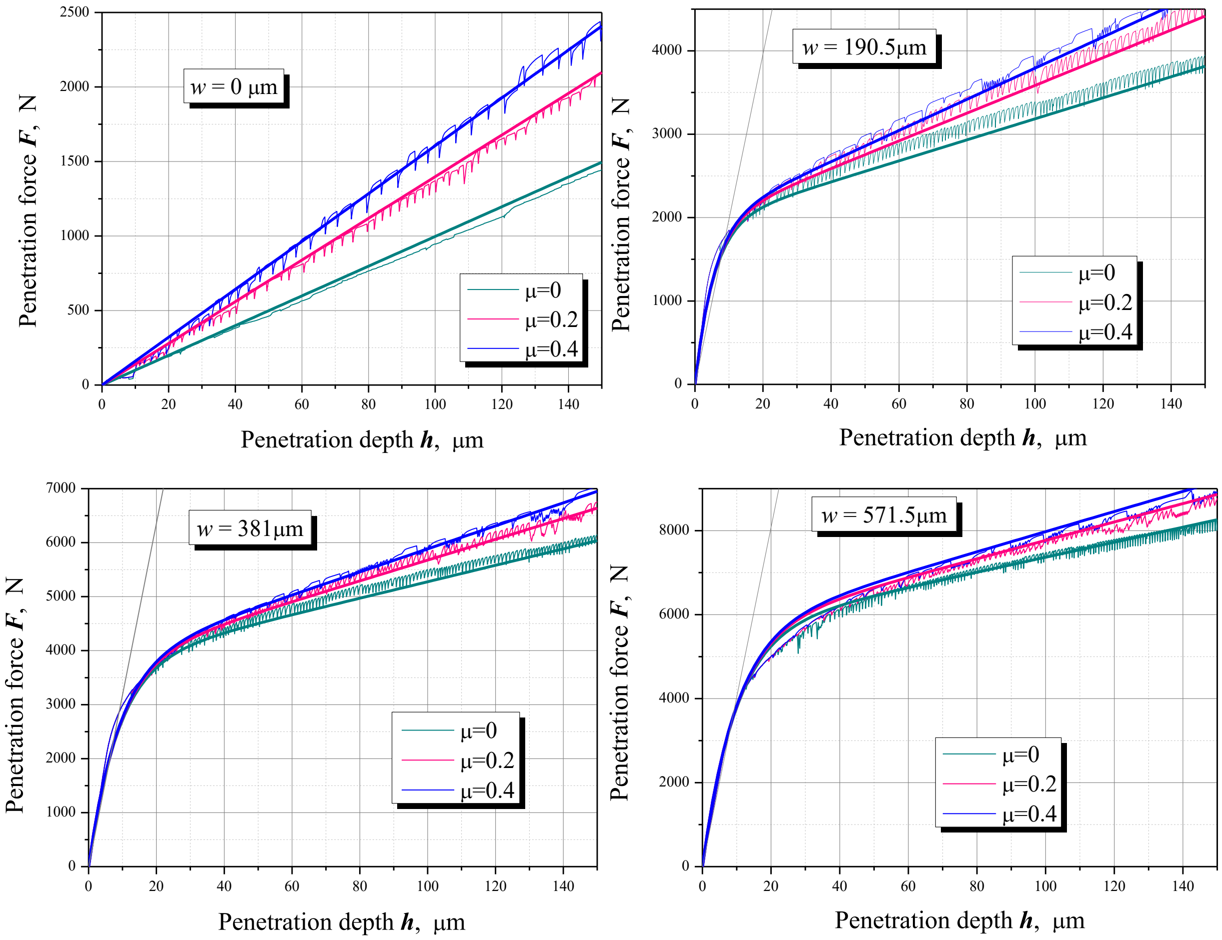

Figure 19. Comparison of calculated wedge punch indentation curves with approximation (21) (thick lines) at various base dimensions w and friction coefficients

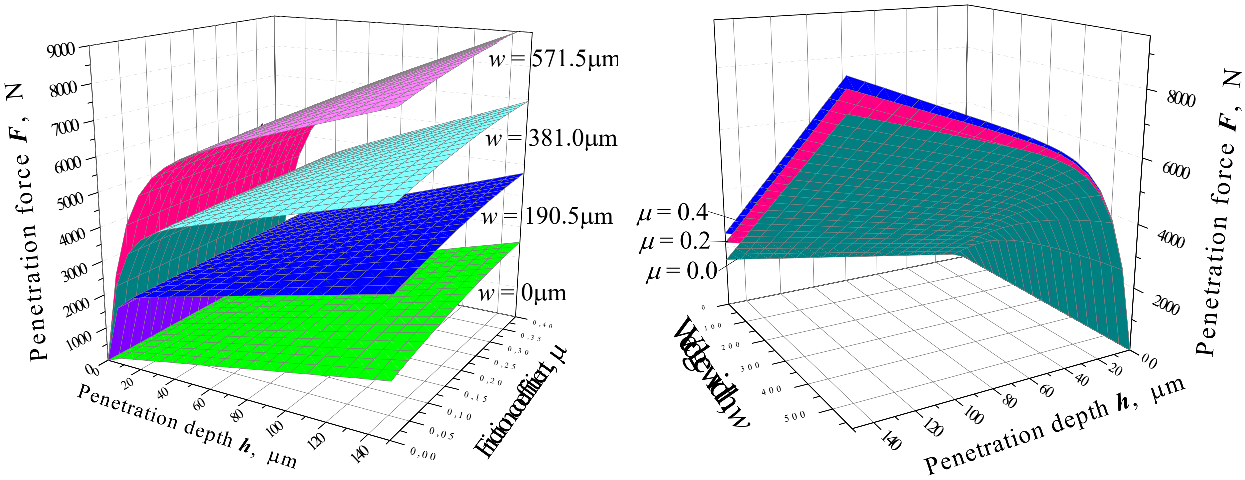

Figure 20. Parametric analysis of approximation (21)

The size of the area of the nonlinear (transition) indentation curve section at the deviation from the linear approximation of $\delta = 1$ %, neglecting G and assuming that k_e is constant, can be roughly estimated based on the relationship

$$h_{\delta=1\%} \approx -\frac{H \ln 0.01}{k_e} w \approx w/10\,. \tag{24}$$

If the deviation from the linear approximation δ=0.1%:

$$h_{\delta=0.1\%} \approx -\frac{H \ln 0.001}{k_e} w \approx w/7 . \tag{25}$$

For a more accurate estimate, the following equation should be used

$$h_\delta = -\frac{1-v^2}{E} m \frac{(Hw+G)\ln\delta}{\sqrt{wl}} . \tag{26}$$

For the set of parameters $E = 210$ GPa, $v = 0.3$, $w = 381$ μm, $l = 4826$ μm, $m = 0.67$, obtain $h_{\delta=1\%} = 37$ μm and $h_{\delta=0.1\%} = 55$ μm.

To determine the coefficients of Eq. (21), both experimental and FE results can be used.

Subject to the plane strain state condition (w << l), it is possible to consider the dependence on l explicitly and use the following approximation instead of (17) to calculate k_p

$$k_p = \left(\overline{A} + \overline{B}w + \overline{C}\mu + \overline{D}\mu^2\right) l , \tag{27}$$

where the constants are obtained by dividing the values of constants from (18) by l = 4826 μm:

$$\begin{aligned} \overline{A} &= 0.207 && \text{N/μm}^2 \\ \overline{B} &= 0.00000286 && \text{N/μm}^3 \\ \overline{C} &= 0.00516 && \text{N/μm}^2 \\ \overline{D} &= \text{-}0.00501 && \text{N/μm}^2 \end{aligned} \tag{28}$$

Eq. (19) can be modified for F_0 in a similar way

$$F_0 = \left(\overline{G} + \overline{H}w\right) l , \tag{29}$$

where the constants take the following values

$$\begin{aligned} \overline{G} &= 0.0197 && \text{N/μm} \\ \overline{H} &= 0.00199 && \text{N/μm}^2 \end{aligned} \tag{30}$$

Based on the obtained results (27) and (29) and the explicit equation of k_e in terms of w and l (8), if 1/20 < w/l << 1, the following formula should be used instead of (21):

$$F(h;\ w,l,\mu) = \left[\left(\overline{A} + \overline{B}w + \overline{C}\mu + \overline{D}\mu^2\right) h + \overline{G} + \overline{H}w\ \right] l \left(1 - e^{-\frac{E}{1-v^2}\sqrt{wl}\left(1+\frac{l}{25w}\right)\frac{h}{\overline{G}+\overline{H}w}}\right). \tag{31}$$

Identification of parameter k_p for untruncated (ideal) wedges

Symmetric untruncated wedges (Fig. 21a) can be considered as a special case of symmetric truncated wedges at $w = 0$ (see Fig. 2). Unsymmetric untruncated wedges (Fig. 21b) should be considered separately. However, based on the experimental and FE computations data, both cases allow for linear approximation (6)

$$F = k_p h . \tag{6}$$

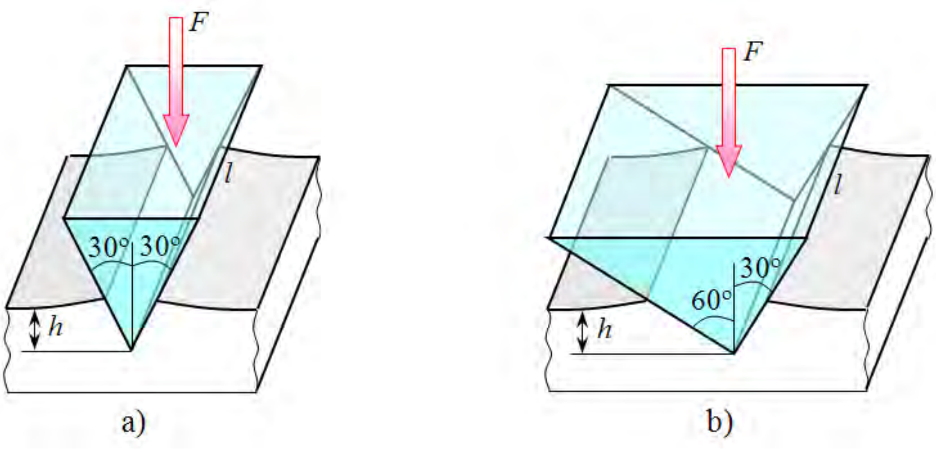

Figure 21. Symmetric (a) and unsymmetric (b) untruncated (ideal) wedges

It is assumed that the parameter k_p depends on the friction coefficient μ. Computational experiments were performed to identify the above dependence for three values of μ = 0; 0.2; 0.4. The results of FE computations are provided in Figure 22.

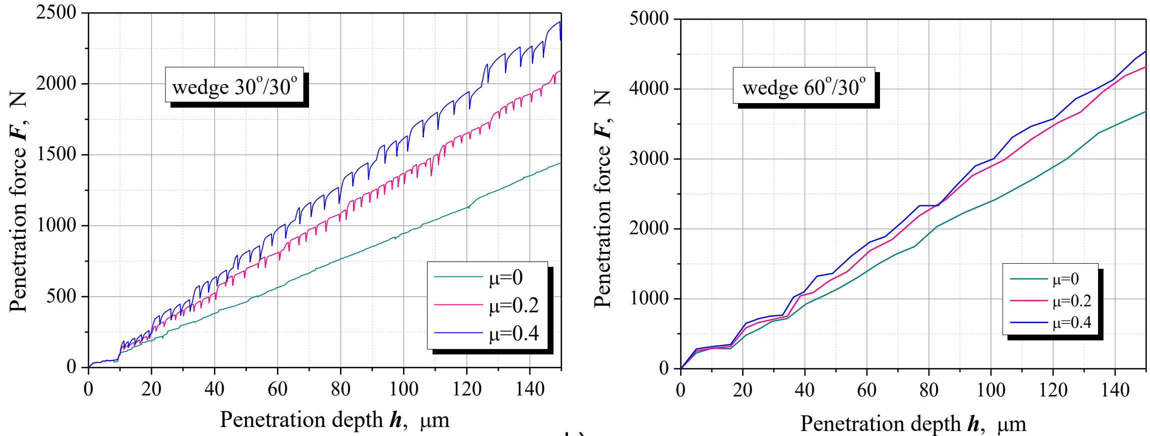

a) b)

Figure 22. Indentation curves of symmetric (a) and unsymmetric (b) untruncated wedge punches at various friction coefficients μ, obtained using FE method

The model of an elastic-plastic body with nonlinear hardening was used for the indented material in FE computations. The strain diagram obtained from experiments and used for computations is shown in Fig. 16. A rigid indenter was used for indentation. Computations were based on the plane strain state hypothesis. Computation results are shown in Figure 23.

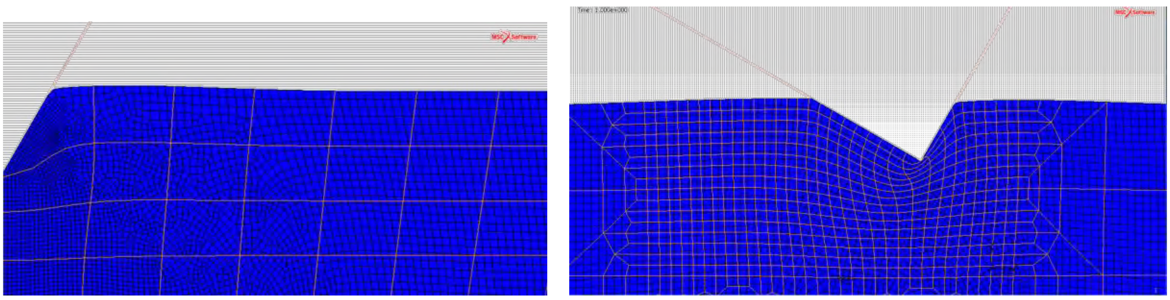

a) **b)**

Figure 23. Strain state during indentation of a symmetric (a) and unsymmetric (b) untruncated wedge punches

The asymptote k_p slope values determined by the predicted indentation curves shown in Figure 22 are provided in Table 3.

Table 3. Asymptote k_p [N/μm] slope values vs. friction coefficient μ.

	$\mu = 0$	$\mu = 0.2$	$\mu = 0.4$
Symmetric wedge 30º/30º	9.55	13.7	16.1
Unsymmetric wedge 60º/30º	24.2	28.6	29.9

The graphic representation of the parameter k_p vs. μ is shown in Fig. 24. Dependences for symmetric and unsymmetric wedges are practically similar. The only significant difference is the height of the intersection point with Y-axis.

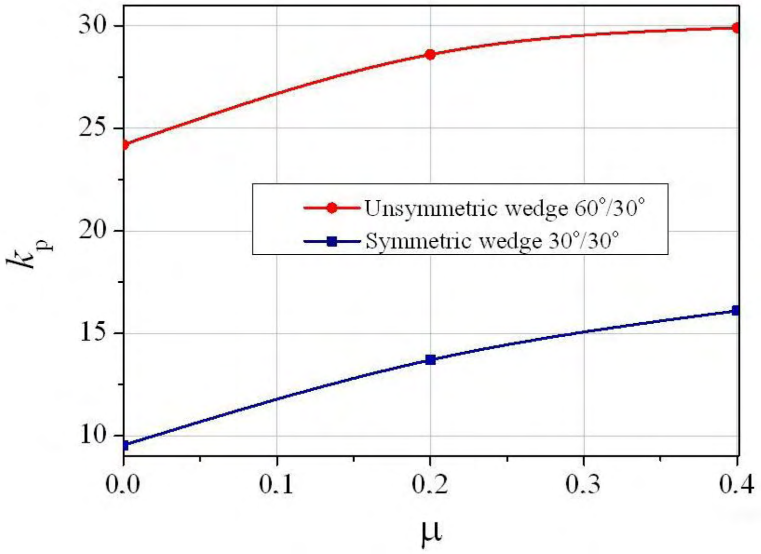

Figure 24. Dependence $k_p(\mu)$

The quadratic approximation constants $k_p(\mu)$ were determined using the least square method:

$$k_p = A + C\mu + D\mu^2 \tag{32}$$

the constant values for a symmetric wedge are:

$$\begin{aligned} A_{30/30} &= 9.55 \quad \text{N/μm} \\ C_{30/30} &= 25.13 \quad \text{N/μm} \\ D_{30/30} &= \text{-}21.88 \quad \text{N/μm} \end{aligned} \tag{33}$$

the constant values for an unsymmetric wedge are:

$$\begin{aligned} A_{60/30} &= 24.20 \quad \text{N/μm} \\ C_{60/30} &= 29.75 \quad \text{N/μm} \\ D_{60/30} &= \text{-}38.75 \quad \text{N/μm} \end{aligned} \tag{34}$$

The above constants are valid for l = 4826 μm and should be changed proportionately to the changes in the wedge base length l.

Some difference of the constant values (33) as compared to (18) (also describing the untruncated wedge behavior at w = 0) is due to the fact that the constants (18) were obtained from a wider calculations database that accounts for w variations and therefore provides a less correct prediction for the case under consideration.

Based on (32), approximation (6) can be rewritten as

$$F(h;\ \mu) = \left(A + C\mu + D\mu^2\right)h \tag{35}$$

It is obvious that Eq. (35) can be considered as a special case of function (21).

Comparison of approximation (35) with FE computation data showed (Fig. 25) good accuracy in a wide range of parameter μ variation.

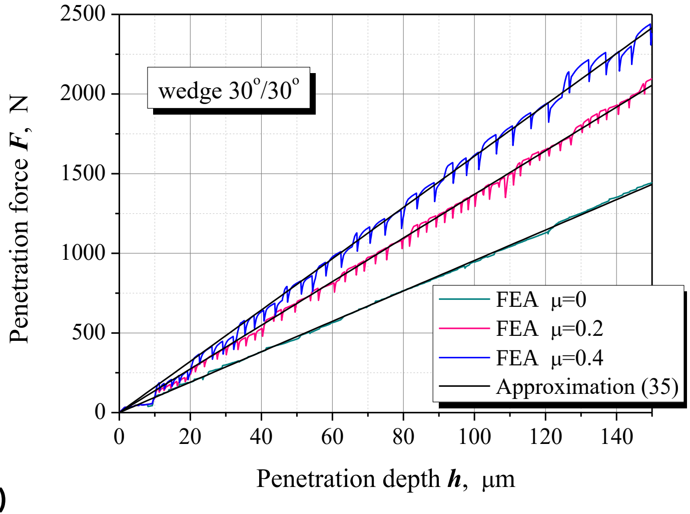

a)

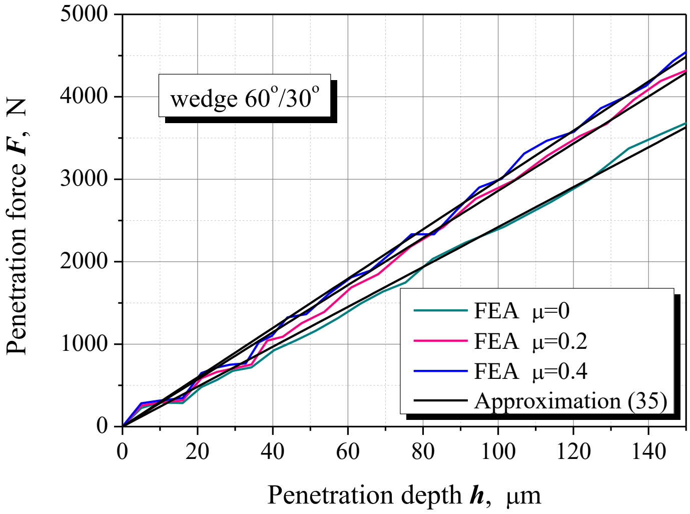

b)

Figure 25. Comparison of predicted indentation curves of symmetric (a) and unsymmetric (b) untruncated wedge punches with approximation (35) at various friction coefficients μ.

Subject to the plane strain state condition (*w*<<*l*), it is possible to consider the dependence on the wedge length *l* explicitly and use the following approximation instead of (23) to calculate k_p

$$k_p = \left(\bar{A} + \bar{C}\mu + \bar{D}\mu^2\right)l\,, \tag{36}$$

where the constants are obtained by dividing the values of constants from (33) and (34) by l = 4826 µm. For a symmetric wedge, such constants are as follows:

$$\begin{aligned} \bar{A}_{30/30} &= 0.00198 \quad \mathrm{N}/\mu\mathrm{m}^2 \\ \bar{C}_{30/30} &= 0.00521 \quad \mathrm{N}/\mu\mathrm{m}^2 \\ \bar{D}_{30/30} &= \text{-}0.00453 \quad \mathrm{N}/\mu\mathrm{m}^2 \end{aligned} \tag{37}$$

and for an unsymmetric wedge, such constants are as follows:

$$\begin{aligned} \overline{A}_{60/30} &= 0.00501 \quad \text{N/}\mu\text{m}^2 \\ \overline{C}_{60/30} &= 0.00616 \quad \text{N/}\mu\text{m}^2 \\ \overline{D}_{60/30} &= \text{-}0.00803 \quad \text{N/}\mu\text{m}^2 \end{aligned} \qquad (38)$$

If approximation (32) is substituted by (36), the following equation that comprises explicit dependence on the wedge length l can be considered instead of (35):

$$F(h;\ l,\mu) = \left(\overline{A} + \overline{C}\mu + \overline{D}\mu^2\right)hl\,. \qquad (39)$$

It should be noted that both experimental and FE computation data can be used to determine constants of Eqs. (35) and (39). Approximation (39) is valid only if $w << l$ and its factors can be obtained using 2D FE analysis.

Results of FE modeling of slip of indented tooth

Obtaining of universal analytical estimations to describe the transient indented tooth slip process is an independent and quite difficult problem. Such problem is confined below to consideration of 3D FE modeling of the single tooth slip and experimental data. In future they can be useful for development of an analytical tooth breakaway force model.

Figures 26 and 27 show the results of FE computations of single tooth indentation to a depth of 150 µm with its further slip. The problem was solved for the symmetric case.

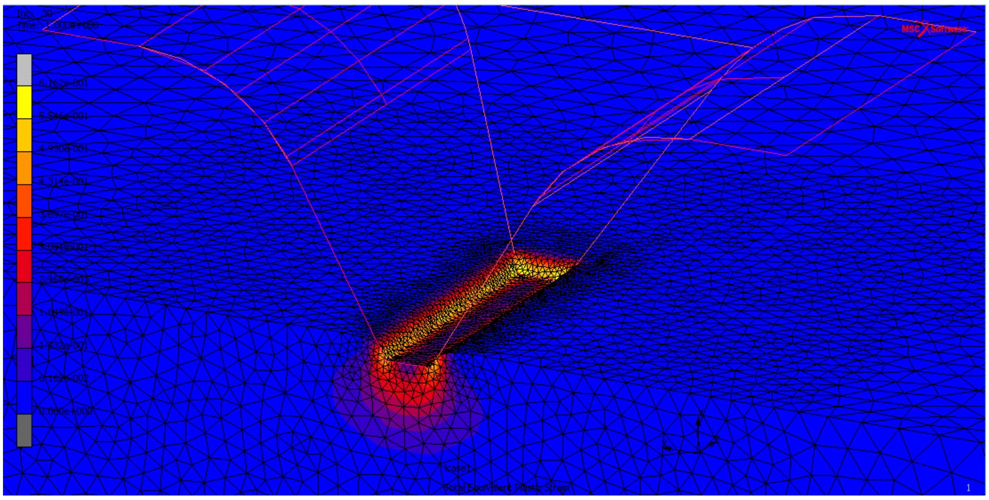

Figure 26. Plastic strain intensity field distribution during tooth indentation

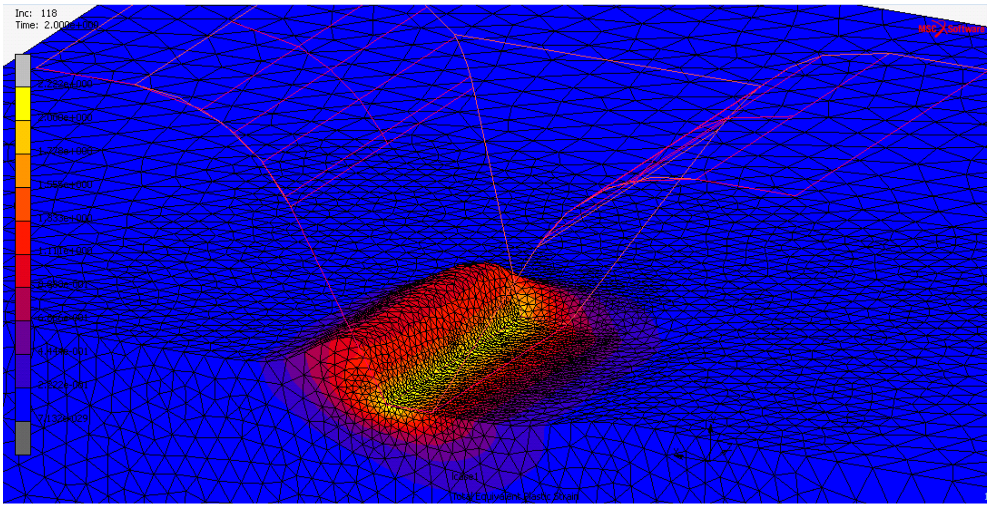

Figure 27. Plastic strain intensity field distribution during indented tooth slip

According to the figures, the material is subjected to a considerable plastic strain when a bed is formed in front of the slipping wedge even at shallow indentation depths. The effect of the side edge and 3D strain is shown in Figure 27. It results in a smaller bed formed in front of the tooth near the side edge, besides an additional lateral face is formed where tribological phenomena are also taking place.

Figure 28 shows tooth slip diagrams drawn based on 2D and 3D FE solutions. The tooth was assumed to be a rigid body. Oscillations on the assumption slip diagrams are attributable to inhomogeneity of the dynamic process of slipping during shear. It should be noted that similar oscillations are also present on the experimental diagrams (see Fig. 4). Figure 28 shows a smooth monotone approximation derived by averaging of several tests results. The comparison of the solutions in 2D and 3D statements enables to assess the effect of side edges and 3D strain state close to such edges. Such effect does not exceed 10 %.

The solution of this boundary value problem accounting for the nonlinearities of three types (plasticity, finite strains, and contact with friction) requires effective computation methods [24], detailed spatial discretization and a considerable amount of time increments for convergence of iterative procedures. The geometrically nonlinear problems were solved using FE software MSC.Marc [25]. The Lagrange updated formulation was used. The model of elastic-plastic body with nonlinear hardening was used for the indented material in FE computations (Fig. 16). Computations included multiplicative decomposition of the strain gradient into the elastic and plastic parts.

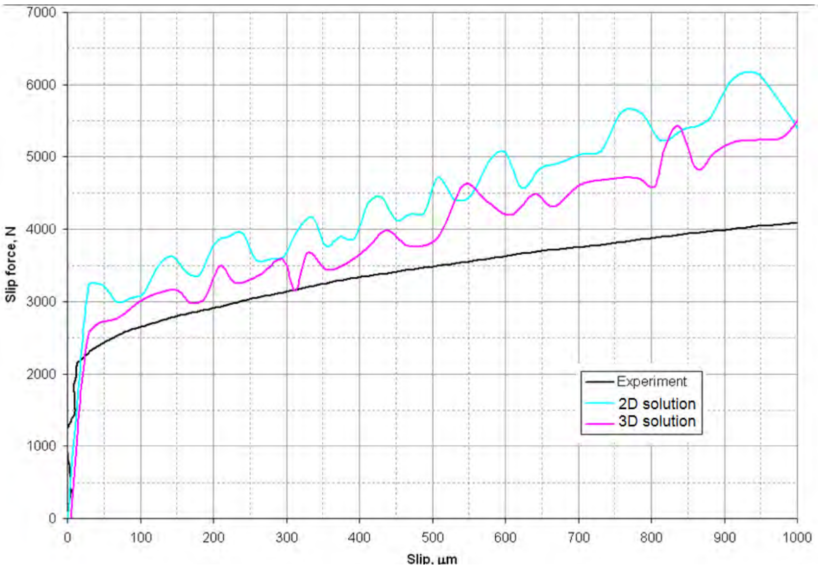

Figure 28. Single tooth shear diagrams

The comparison of the computational and experimental shear diagrams demonstrated satisfactory accuracy (less than 15 % for the shear of up to 500 µm), therefore the computational diagrams may be used as the basis for assessment of the punch indentation force and punch breakaway drag force during its shearing as a function of indentation depth. A limitation of such approach is the need to perform new FE computations for each new punch size, configuration and each material grade. This requires development of universal analytical models to describe the slip process similar to those proposed above (see e.g. (35), (40), (41)) to describe the indentation process.

Discussion

The results of analytical [12-14, 20, 21, etc.] and experimental [9-11, 6, 5, etc.] studies of the processes of teeth indentation in to the elastic [20, 21, etc.] and plastic [12-14, etc.] continuum are widely presented in the literature. However, there is no unified model of deep and shallow indentation processes of an ideal and non-ideal wedge-shaped punch, taking into account the dependence of force on the depth of the indented die, its geometry, plastic hardening of material and lateral friction, which is oriented to the determining the load bearing capacity of gripping devices for drillpipes. In this paper, an attempt is made to construct a similar unified model based on the unification and generalization of known analytical solutions, as well as identification of model parameters based on multivariant finite element computations and its experimental verification.

The proposed analytic dependence of the indentation force of an ideal and non-ideal wedge-shaped tooth with symmetrically sloped sides (30°) and unsymmetrically sloped sides (30°/60°) modeling tooth operation as a function of indentation depth and friction coefficient on the punch lateral face both for shallow and deep indentation is determined *in general case* by the expression:

$$F(h;\ w,\mu) = \left[\left(A + Bw + C\mu + D\mu^2\right)h + G + Hw\ \right]\left(1 - e^{-\frac{k_e}{G+Hw}h}\right). \tag{21}$$

Simplified version of (21) in the form of the linear approximation (6) can be used to analyze the process of indentation of *ideal (untruncated)* symmetric and unsymmetric wedges, which in expanded form (35) allows for the following representation:

$$F(h;\ \mu) = \left(A + C\mu + D\mu^2\right)h, \tag{35}$$

which constants are determined according to (33) for a symmetric wedge and according to (34) for an unsymmetric wedge. An analogous (linear in respect to h) dependence is considered in [13].

Linear approximation (2) can be used to describe the process of *non-ideal (truncated)* wedge indentation to *considerable depths* ($h > w/7$, where *h* is the indentation depth, *w* is the truncated wedge base width), which in expended form (obtained for special case (21) at high h/w values) can be rewritten as:

$$F(h;\ w,\mu) = \left(A + Bw + C\mu + D\mu^2\right)h + G + Hw, \tag{40}$$

where the constants for a symmetric wedge are determined according to (18)-(20).

Nonlinear approximation (1) should be used to analyze the process of truncated wedge indentation to *shallow depths* ($h < w/7$), which in expended form (obtained for special case (31) at low h/w) can be rewritten as:

$$F(h;\ w,\mu) = \left[\left(A + Bw + C\mu + D\mu^2\right)h + G + Hw\ \right]\left(1 - e^{-\frac{Q\sqrt{w}}{G+Hw}h}\right), \tag{41}$$

where $Q = 23.9\ \mathrm{N/\mu m^{3/2}}$ and the remaining constants A, B, C, D, G, H are the same as the above factors for considerable indentation depths (18)-(20).

The form of introduced approximations is based on the analysis of experimental indentation curves and analytic solutions of the boundary value elasticity and plasticity problems. The constants of the introduced approximations were obtained by the least square method based on the results of multiple FE computations and agree with the available experimental data. The ranges of the valid argument variations, for which the approximation is kept interpolational are:

$$0\ \mu\mathrm{m} \le h \le 150\ \mu\mathrm{m},$$
$$0\ \mu\mathrm{m} \le w \le 571.5\ \mu\mathrm{m},$$
$$0 \le \mu \le 0.4.$$

The wedge base length *l* and the wedge half-angle γ were assumed fixed *l* = 4826 μm*,* γ = 30º to determine the approximation factors. Subject to the condition $w << l$, it is possible to use the approximation that explicitly provides for the dependence on *l*, as (39) for untruncated and (31) for truncated wedges. Cases with $\gamma \ne 30^\circ$ require further study, which can be performed in a similar way, if necessary, based on multiple computational experiments.

Conclusion

A simplified analytical model was proposed to determine the indentation force of an ideal (untruncated) and non-ideal (truncated) wedge punch with symmetrically sloped sides (30º) and unsymmetrically sloped sides (30º/60º) modeling tooth operation as a function of indentation depth and friction coefficient on the punch lateral face both for shallow (mostly typical of elastic strain) and deep (mostly typical of plastic strain) indentation. The developed models closely agree with the FE analysis and experimental data.

The FE modeling of single tooth indentation and slip was performed with using 2D and 3D models. The comparison of the computational slip diagrams with the experimental data demonstrated satisfactory accuracy, therefore such computational diagrams may be used as a basis for assessment of punch indentation, breakaway and drag forces during its shearing as a function of the indentation depth.

The obtained results can be used to develop a holding force model for a multi-tooth slip.

Acknowledgement

The research was carried out on the contract of Weatherford and supported also by the Russian Foundation for Basic Research (grant no. 16-08-00845).

References

1. Saroian A.E. *Teoriia i praktika raboty buril'noi kolonny.* [Theory and practice of drill string operation] M.: Nedra, 1990. 263 p. (rus)
2. Spiri W.H., Reinhold W.B. Why does drill pipe fail in the slip area? *World Oil*. 1959. October. Pp. 100-115.
3. Paslay P., Pattillo P.D., Pattillo D. II, Sathuvalli U.B.R., Payne M.L. A re-examination of Drillpipe/Slip Mechanics. *Proceedings of the IADC/SPE Drilling Conference, Miami, Florida.* 2006. Paper IADC/SPE 99074. Pp. 1-8.
4. Jayadevan K.R., Narasimhan R. Finite element simulation of wedge indentation. *Computers & Structures.* 1995. No. 5(57). Pp. 915-927.
5. Mitsomwang P., Natpukkana P., Borrisutthekul R., Nagasawa S. Effects of blade tip geometry on cutting characteristics of lead alloy sheet subjected to wedge indentation. *Key Engineering Materials.* 2017. Vol. 719. Pp. 137-141.
6. Kim W., Kawai K., Koyama H. Metal flow in wedge indentation of V- and W-shaped tools. *Journal of Materials Processing Technology.* 2007. No. 1(189). Pp. 392-400.
7. Voyiadjis G.Z., Buckner N.E. Indentation of a half-space with a rigid indentor. *Int. J. Numer. Methods Engrg.* 1983. No. 10(19). Pp. 1555-1578.
8. Bucaille J.L., Felder E., Hochstetter G. Mechanical analysis of the scratch test on elastic and perfectly plastic materials with the three-dimensional finite element modeling. *Wear*. 2001. No. 5(249). Pp. 422-432.
9. Dugdale D.S. Wedge indentation experiments with cold-worked metals. *Journal of the Mechanics and Physics of Solids.* 1953. No. 1(2). Pp. 14-26.
10. Grunzweig J., Longman I.M., Petch N.J. Calculations and measurements on wedge-indentation. *J. Mechanics and Physics of Solids.* 1954. No. 2(2). Pp. 81–86.
11. Kailas S.V., Biswas S.K. Material response to two-dimensional scratching by wedges. *Wear.* 1993. Vol. 162. Pp. 110-118.
12. Hill R., Lee E.H., Tupper S.J. The theory of wedge indentation of ductile materials. P*roc. of the Royal Society of London. Series A, Mathematical and Physical Sciences.* 1947. No. 1013(188). Pp. 273-289.
13. Sokolovskii V.V. *Teoriia plastichnosti* [Theory of plasticity]. 1969. Moscow: «Vysshaya shkola». 608 p. (rus)
14. Nepershin R.I. Vnedrenie konechnogo klina v ideal'noplasticheskoe poluprostranstvo [Indention of a finite wedge into an ideally plastic half-space]. *Izvestiia Rossiiskoi Akademii Nauk. Mekhanika tverdogo tela.* 2003. No. 4. Pp. 176-183. (rus)
15. Melnikov B.E., Semenov A.S. Creation and application of hierarchical sequence of material models for numerical analysis of elasto-plastic structures. *Zeitschrift für Angewandte Mathematik und Mechanik.* 1996. No. S2(76). Pp. 615-616.
16. Semenov A., Melnikov B. Interactive rheological modeling in elasto-visco-plastic finite element analysis. *Procedia*

Литература

1. Сароян А.Е. Теория и практика работы бурильной колонны. М.: Недра, 1990. 263 с.
2. Spiri W.H., Reinhold W.B. Why does drill pipe fail in the slip area? // World Oil. 1959, October. Pp. 100-115.
3. Paslay P., Pattillo P.D., Pattillo D., Sathuvalli U.B.R., Payne M.L. A re-examination of Drillpipe/Slip Mechanics // Proceedings of the IADC/SPE Drilling Conference, Miami, Florida. 2006. Paper IADC/SPE 99074. Pp. 1-8.
4. Jayadevan K.R., Narasimhan R. Finite element simulation of wedge indentation // Computers & Structures. 1995. № 5(57). Pp. 915-927.
5. Mitsomwang P., Natpukkana P., Borrisutthekul R., Nagasawa S. Effects of blade tip geometry on cutting characteristics of lead alloy sheet subjected to wedge indentation // Key Engineering Materials. 2017. Vol. 719. Pp. 137-141.
6. Kim W., Kawai K., Koyama H. Metal flow in wedge indentation of V- and W-shaped tools // Journal of Materials Processing Technology. 2007. № 1(189). Pp. 392-400.
7. Voyiadjis G.Z., Buckner N.E. Indentation of a half-space with a rigid indentor // Internat. J. Numer. Methods Engrg. 1983. № 10(19). Pp. 1555-1578.
8. Bucaille J.L., Felder E., Hochstetter G. Mechanical analysis of the scratch test on elastic and perfectly plastic materials with the three-dimensional finite element modeling // Wear. 2001. № 5(249). Pp. 422-432.
9. Dugdale D.S. Wedge indentation experiments with cold-worked metals // Journal of the Mechanics and Physics of Solids. 1953. № 1(2). Pp. 14-26.
10. Grunzweig J., Longman I.M., Petch N.J. Calculations and measurements on wedge-indentation // J. Mechanics and Physics of Solids. 1954. № 2(2). Pp. 81–86.
11. Kailas S.V., Biswas S.K. Material response to two-dimensional scratching by wedges // Wear. 1993. Vol. 162. Pp. 110-118.
12. Hill R., Lee E.H., Tupper S.J. The theory of wedge indentation of ductile materials // Proc. of the Royal Society of London. Series A, Mathematical and Physical Sciences, 1947. № 1013(188). Pp. 273-289.
13. Соколовский. В.В. Теория пластичности. М.: «Высш. школа», 1969. 608 с.
14. Непершин Р.И. Внедрение конечного клина в идеальнопластическое полупространство // Известия Российской Академии Наук. Механика твердого тела. 2003. № 4. С. 176-183.
15. Melnikov B.E., Semenov A.S. Creation and application of hierarchical sequence of material models for numerical analysis of elasto-plastic structures // Zeitschrift für Angewandte Mathematik und Mechanik. 1996. № S2(76). Pp. 615-616.
16. Semenov A., Melnikov B. Interactive rheological modeling in elasto-visco-plastic finite element analysis // Procedia Engineering. 2016. Vol. 165. Pp. 1748-1756.
17. Semenov A.S., Melnikov B.E., Gorokhov M.Y. About the

Engineering. 2016. Vol. 165. Pp. 1748-1756.

17. Semenov A.S., Melnikov B.E., Gorokhov M.Y. About the causes of cyclical instability at computations of large elasto-plastic strains. *Proc. SPIE.* 2005. Vol. 5831. Pp. 167-173.
18. Pavlov P.A., Ainabekov A.I., Raimberdiev T.P., Mel'nikov B.E. *Dlitel'naia prochnost' stalei v usloviiakh slozhnogo i termomekhanicheskogo nagruzheniia.* Almaty: Fylym. 1996. 247 p. (rus)
19. Melnikov B.E., Semenov A.S. Fatigue damage accumulation under the complex varying loading. *Applied Mechanics and Materials.* 2014. Vol. 617. Pp. 187-192.
20. Timoshenko S.P., Goodier J.N. *Theory of Elasticity, 3 Ed.* McGraw-Hill, New York. 1970. 519 p.
21. Schleicher F. Die Verteilung der Bodenpressungen unter starren Gründungskorpern" (Distribution of Soil Pressures Under Rigid Foundation Bodies). *Der Bauingenieur.* 1933. Vol. 14. Pp. 242-245.
22. Johnson W., Mahtab F.U., Willams A. Further experiments concerning geometrically similar indentations. *Int. J. Mech. Sci.* 1966. No. 1(8). Pp. 49-59.
23. Kitaeva D.A., Pazylov S.T., Rudaev Ya.I. Temperature-strain rate deformation conditions of aluminum alloys, *Journal of Applied Mechanics and Technical Physics.* 2016. No. 2(57). Pp. 352-358.
24. Semenov A.S. *Vychislitel'nye metody v teorii plastichnosti* [Computational methods in theory of plasticity]. St.-Petersburg: Izd-vo SPbGPU. 2008. 211 p. (rus)
25. [Online] URL: http://www.mscsoftware.com/product/marc (date of application: 07.11.2017)

causes of cyclical instability at computations of large elasto-plastic strains // Proc. SPIE. 2005. Vol. 5831. Pp. 167-173.

18. Павлов П.А., Айнабеков А.И., Раимбердиев Т.П., Мельников Б.Е. Длительная прочность сталей в условиях сложного и термомеханического нагружения. Алматы: Гылым. 1996. 247 с.
19. Melnikov B.E., Semenov A.S. Fatigue damage accumulation under the complex varying loading // Applied Mechanics and Materials. 2014. Vol. 617. Pp. 187-192.
20. Тимошенко С.П., Гудьер Дж. Теория упругости. М.:Наука, 1975. 576 с.
21. Schleicher F. Die Verteilung der Bodenpressungen unter starren Gründungskorpern (Distribution of Soil Pressures Under Rigid Foundation Bodies) // Der Bauingenieur. 1933. Vol. 14. Pp. 242-245.
22. Johnson W., Mahtab F.U., Willams A. Further experiments concerning geometrically similar indentations // Int. J. Mech. Sci. 1966. № 1(8). Pp. 49-59.
23. Kitaeva D.A., Pazylov S.T., Rudaev Ya.I. Temperature-strain rate deformation conditions of aluminum alloys // Journal of Applied Mechanics and Technical Physics. № 57(2). 2016. Pp. 352-358.
24. Семенов А.С. Вычислительные методы в теории пластичности. СПб.: Изд-во СПбГПУ, 2008. 211 с.
25. [Электронный ресурс] URL: http://www.mscsoftware.com/product/marc (дата обращения:07.11.2017)

Artem Semenov,
+7(905)2721188;
Semenov.Artem@googlemail.com

Sergey Semenov,
+7(921)9834456; ssgrus@gmail.com

Boris Melnikov,
+7(812)5526303; melnikovboris@mail.ru

Vadim Tikhonov,
+7(910)4936512;
Vadim.Tikhonov@eu.weatherford.com

Артем Семенович Семенов,
+7(905)2721188;
эл. почта: Semenov.Artem@googlemail.com

Сергей Георгиевич Семенов,
+7(921)9834456;
эл. почта: ssgrus@gmail.com

Борис Евгеньевич Мельников,
+7(812)5526303;
эл. почта: melnikovboris@mail.ru

Вадим Семенович Тихонов,
+7(910)4936512; эл. почта:
Vadim.Tikhonov@eu.weatherford.com

doi: 10.18720/MCE.74.9

Ground moisture phase transitions: Accounting in BHE'S design

Фазовые переходы влаги в грунте: Учет при проектировании грунтовых теплообменников

G.P. Vasilyev,
V.F. Gornov,
N.V. Peskov,
Mik.P. Popov,
M.V. Kolesova,
V.A. Yurchenko,
JSC "INSOLAR-INVEST", Moscow, Russia

Д-р техн. наук, научный руководитель Г.П. Васильев,
директор проектного отделения В.Ф. Горнов,
д-р физ.-мат. наук, ст. науч. сотр. Н.В. Песков,
канд. техн. наук, ст. науч. сотр. М.И. Попов,
ведущий инженер-эколог М.В. Колесова,
науч. сотрудник В.А. Юрченко,
ОАО "ИНСОЛАР-ИНВЕСТ", г. Москва, Россия

Key words: ground source heat pump; phase transition; ground moisture; borehole heat exchanger; thermal conductivity; energy efficiency; thermal conditions

Ключевые слова: геотермальная теплонасосная система теплоснабжения; фазовый переход; поровая влага; термоскважина; теплопроводность; энергетическая эффективность; тепловой режим

Abstract. The results of numerical and experimental studies devoted to the evaluation of the effect of phase transitions of pore moisture in the soil mass surrounding the borehole heat exchangers (BHE) on the thermal conductivity of the adjacent soil and on the temperature of the coolant circulating through the heat exchanger are presented. A mathematical model is presented that allows one to describe the spatial non-stationary thermal regime of a soil massif with BHEs, taking into account the processes associated with phase transitions of moisture in the pore space of the soil. This mathematical model is based on the method of accounting the latent heat of phase transitions of pore moisture in the ground by the use of such a parameter as the "equivalent" thermal conductivity. The essence of the method is to take into account the heat of phase transitions of pore moisture in the ground by introducing a new "equivalent" thermal conductivity of the soil, consisting of the direct thermal conductivity of the soil and an additive that is responsible for the freezing / thawing of pore moisture. The methods, equipment and results of experimental studies on the «equivalent» thermal conductivity of soil accounting the phase transition of pore moisture during freezing and thawing performed in laboratory on the test bench simulating borehole heat exchangers working conditions are described. The results of the simulation illustrate the need to take into account the phase transitions of the ground moisture in the ground during the design of BHEs. The effect caused by pore moisture condensation during the operation of BHEs and the associated intensification of the processes of heat exchange was experimentally observed.

Аннотация. В статье приведены результаты численных и экспериментальных исследований, посвящённых оценке влияния фазовых переходов поровой влаги в грунтовом массиве, окружающем термоскважины, на теплопроводность прилегающего грунта и на температуру теплоносителя, циркулирующего через теплообменник. Представлена математическая модель, позволяющая описать пространственный нестационарный тепловой режим грунтового массива с термоскважинами с учётом процессов, связанных с фазовыми превращениями влаги в поровом пространстве грунта. Данная математическая модель основывается на методе учёта скрытой теплоты фазовых переходов поровой влаги в грунте за счёт использования такого параметра, как «эквивалентная» теплопроводность. Суть метода состоит в том, чтобы учесть теплоту фазовых переходов поровой влаги в грунте с помощью введения новой «эквивалентной» теплопроводности грунта, состоящей из непосредственно теплопроводности грунта и добавки, учитывающей замерзание/оттаивание поровой влаги.

Васильев Г.П., Горнов В.Ф., Песков Н.В., Попов М.И., Колесова М.В., Юрченко В.А. Фазовые переходы влаги в грунте. Учет при проектировании грунтовых теплообменников // Инженерно-строительный журнал. 2017. № 6(74). С. 102–117.

Описаны методы, оборудование и результаты экспериментальных исследований по оценке «эквивалентной» теплопроводности грунта, учитывающей фазовый переход поровой влаги при замораживании и оттаивании грунта, выполненные в лабораторных условиях на экспериментальном стенде, моделирующем эксплуатационные режимы термоскважин. Результатами моделирования проиллюстрирована необходимость учёта фазовых переходов поровой влаги в грунте при проектировании ГТСТ. Экспериментально обнаружен эффект, вызываемый конденсацией при эксплуатации ГТСТ водяного пара, содержащегося в поровом пространстве грунта, и связанная с этим интенсификация процессов теплообмена между термоскважиной и грунтом.

Introduction

Currently, the use of geothermal heat pumps (GSHP) is quite a popular solution for providing heating, hot water supply and conditioning in buildings of various purposes due to their energy efficiency and environmental friendliness [1–3]. These systems are actively used including in regions with a cold climate [4–7].

One of the most important parts of such systems are the borehole heat exchangers (BHE) which are used for extraction/rejection heat from the ground and in most cases determine the whole systems efficiency.

The two most commonly used modifications of BHEs are coaxial and U-shaped.

Coaxial BHEs represent a large diameter pipe, inside which a smaller diameter pipe is located so that the coolant supplied through the inside pipe is then introduced into the annular channel, raising there and exchanging heat with the surrounding ground through the wall of the larger (outside) tube. Coaxial BHEs can be made of both metal and polyethylene, where the inner tube is usually made of polyethylene as a material with a lower thermal conductivity in order to minimize the thermal interference of descending and ascending flows of coolant (thermal short circuit effect).U-shaped models are mainly made of plastic tubes and used in two modifications - with one or two U-shaped loops within a single borehole.

BHEs functioning in cold regions have to meet some additional challenges. The heating period in most of Russia’s territory is noticeably longer and the ambient temperatures are much lower than, for example in Europe, all this leads to a significant decrease in ground temperatures during the operation of the GSHP, which in turn leads to a decrease in their efficiency.

There are several ways to cope with this effect: increasing borehole space [8, 9], modifying borehole layout [10], improving thermal properties [11], but the most common way is to increase the length or the number of the ground heat exchangers [12].

At present, many works are being devoted to the search for ways to improve the efficiency of ground heat exchangers, and part of them are aimed at studying the thermal conductivity: the effect of both the thermal conductivity of the materials used in the heat exchanger [13–15] and the thermal conductivity of the soil surrounding BHEs [16, 17].

The long-term operation of GSHP in the climatic conditions of most Russia's territory causes freezing and thawing of the soil surrounding the borehole heat exchanger [18, 19]. Accounting for these processes within mathematical models of such complicated multi-component pore structures as soil is an extremely difficult task [20].

In a precise approach, in the design of borehole heat exchangers not only ground moisture phase transition mechanisms and heat and mass transfer processes, but also chemical and mineralogical composition of soil, mechanical structure of hard particles material, the degree of dispersion in the medium, shape and size of both particles and pores, the ratio of different water phases and their distribution across the soil, and lots of other physical and chemical parameters of soil massif should be accounted for. A detailed account of these factors with the help of a modern mathematical apparatus, as demonstrated by the study of existing heat transfer models of the soil-BHE system [21–24], is practically impossible. But on the other hand we have to make a years-long forecast of how BHE will interact with ground during GSHP operation in order to guarantee system’s reliability.

To make a quite accurate forecast and at the same time to simplify calculations, for the practical purposes in the GSHP design it is possible to describe all these multiple factors using the model of «equivalent» thermal conductivity developed by A.F.Chudnovsky [21] by the standard conductivity equation with "equivalent" heat and mass transfer parameters. In this case, the soil is considered as a

Vasilyev G.P., Gornov V.F., Peskov N.V., Popov M.P., Kolesova M.V., Yurchenko V.A. Ground moisture phase transitions: Accounting in BHE’S design. *Magazine of Civil Engineering*. 2017. No. 6. Pp. 102–117. doi: 10.18720/MCE.74.9.

quasihomogeneous body, to which the usual heat conduction equation is applicable, and its thermal characteristics can vary both in time and in coordinates.

Special mention should be made of the need to take into account the influence of pore moisture and it's migration has on the thermal processes occurring during the operation of the GSHP. In the capillary-porous system, which is a soil massif, the presence of moisture in the pore space has a significant effect on the process of heat distribution. So, for example, if there is a temperature gradient in the ground massif, the water vapor molecules move to a zone having a lower temperature. But at the same time, under the action of gravitational forces, a directed flow of moisture in the liquid phase appears which can partially compensate for heat fluxes carried by vapor moisture and, consequently, reduce the influence of migration processes of moisture on the thermal performance of BHE. Correct accounting of such influence for today is associated with considerable difficulties.

This research is devoted to developing of simple and accurate enough for practical purposes method of considering ground moisture freezing and thawing around the BHE during its operation. The objectives of research are to propose and adequate mathematical model, using an "effective" heat and mass transfer characteristics of soil to account for ground moisture phase transitions, and to evaluate «effective» thermal conductivity of soil in both heat rejection and heat extraction modes.

In this research, the problem of developing a mathematical model allowing one to describe in simple form the heat transfer process in a two-phase medium with an unknown position of the phase boundary (Stefan's problem) was solved, as well as the problems of estimating the effect of phase transitions of the ground moisture in the soil on its "equivalent" heat conductivity and on the overall efficiency of the geothermal heat pump system.

Research methods

Numerical study

The non-stationary process of heat transfer, including taking into account the humidity of the medium, is considered in [25–27].

The mathematical model represented here is based on a simplified description of the spatial non-stationary thermal regime of the cylindrical soil massif in which the BHEs are located.

The heat conduction equation for this case in cylindrical coordinates is as follows [28]:

$$c\rho\frac{\partial t}{\partial \tau}=\lambda_g\left(\frac{\partial^2 t}{\partial r^2}+\frac{1}{r}\frac{\partial t}{\partial r}+\frac{\partial^2 t}{\partial z^2}\right), \tag{1}$$

where τ – is time, hours;

r – radius of the cylinder under consideration, m;

z – vertical coordinate, m;

T(r,z,τ) - deviation of soil temperature from natural values, °C;

c – specific heat of the soil, J/(kg×°C);

ρ – soil density, kg/m^3;

λ_g – thermal conductivity of the soil, J/(h×m×°C);

It is important to note that equation (1) does not take into account the latent heat of phase transitions; therefore, it is applicable only if the ground temperature remains positive during the operation of the heat pump. In actual fact, during the operation of the GSHP the temperature of the soil near the borehole heat exchangers can drop below zero. In this case, the moisture contained in the soil will freeze, releasing the latent heat of the phase transition of water from the liquid state to the solid state. After heat collection is terminated (e.g. in summer) the frozen moisture will thaw, i.e. there will be a reverse phase transition that absorbs additional heat energy from the soil.

Thus, instead of equation (1) the Stefan problem should be solved – the problem concerning the heat transfer in a biphasic system with the unknown position of the phase boundary. The solution for the Stefan problem in this case may be obtained only numerically, besides because of the problem's nonlinear nature, these methods i=ought to be iterative. Moreover, solving the Stefan problem for a considerably long period (years) requires a lot of CPU time. And for the significant cost of computational resources used for obtaining an accurate solution in the design of GSHP as a rule are not justified. Therefore, at the design stage, it is advisable to use more cost-effective methods of taking into account the latent heat of phase transitions for the determination of soil temperature, one of which was developed by the authors of this paper and is presented below.

The essence of the method is to account for the heat of phase transition of ground moisture in the soil by introducing a new "equivalent" ground thermal conductivity λ_{eq} consisting of ground thermal conductivity itself and additives, taking into account the freezing / thawing of ground moisture.

During the freezing of the soil, the volumetric heat of the phase transition can be determined by the following equation [29]:

$$L_v = m\sigma\rho \tag{2}$$

where L_v – volumetric heat of phase transition, W·h/m^3;

m – volumetric humidity of soil, (m^3 of moisture/m^3 of ground);

σ – phase transition heat of a unit of weight of water, equals 93 W·h/kg [29];

ρ – density of the solidification agent (ice), kg/m^3.

Consider the problem of freezing an unlimited body of soil with a cylindrical cavity (borehole heat exchanger tube), the design scheme of which is shown in

Figure 1, where the following notation is used:

R_k – boundary of soil freezing, m;
q_{st} – heat flow density (per 1 linear meter of cylinder) from the unfrozen soil, W/m;
t_p – temperature at the surface of the cylindrical cavity, °C;
t_0 – freezing temperature of water in the pores of the body of soil, t_0 = 0 °C;
t_r – the temperature of the soil infinitely distanced from the cylindrical cavity (borehole heat exchanger), °C;
R_0 – radius of the cylindrical cavity (the borehole heat exchanger), m.

The design scheme in fact illustrates the operating conditions of a borehole heat exchanger with radius R_0. Indeed, after a time τ (h) when the soil contacting with the heat exchanger tube reaches the temperature tp (°C), lower than t_0 = 0 °C, a region of frozen soil of radius R_k appears.

The heat balance equation for the soil freezing around the heat exchanger with radius r = R_k in the absence of heat input from the unfrozen soil (($t_r \approx$ or slightly greater than t_0) is as follows.

$$q_t = q_{st} + q_{ft}, \tag{3}$$

where q_t – specific (per 1 meter of the tube) thermal flow to the heat exchanger tube, W/m;
q_{st} – specific heat flow from the unfrozen soil, W/m;
q_{ft} – specific heat flow, caused by the release of latent heat of ground moisture phase transition in the freezing soil, W/m.

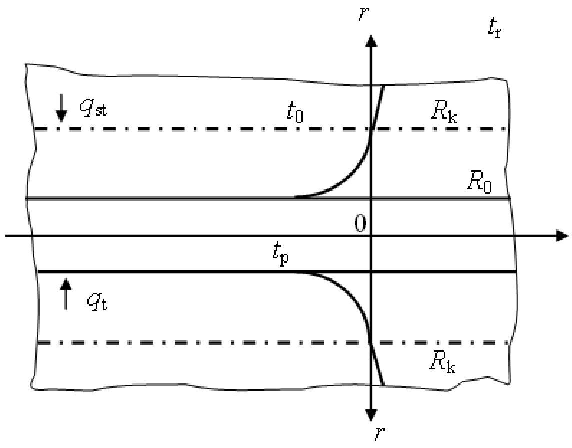

Figure 1. Design scheme for freezing an unlimited body of soil with a cylindrical cavity

Vasilyev G.P., Gornov V.F., Peskov N.V., Popov M.P., Kolesova M.V., Yurchenko V.A. Ground moisture phase transitions: Accounting in BHE'S design. *Magazine of Civil Engineering*. 2017. No. 6. Pp. 102–117. doi: 10.18720/MCE.74.9.

Assume that all heat flows are conditionally constant and averaged over time. Then to determine them the following expressions can be used:

$$q_t = \frac{2\pi\lambda_{экв}}{\ln\left(R_k / R_0\right)}\left(t_0 - t_p\right), \tag{4}$$

$$q_{st} = \frac{2\pi\lambda_g}{\ln\left(R_k / R_0\right)}\left(t_0 - t_p\right); \tag{5}$$

$$q_{ft} = \pi\left(R_k^2 - R_0^2\right)\frac{L_v}{\tau}; \tag{6}$$

where: λ_g – thermal conductivity of the frozen soil, W/(m·°C);

$\lambda_{экв}$ - "equivalent" thermal conductivity of the soil, accounting for the release of the latent heat of ground moisture phase transition, W/(m·°C);

τ - time needed for freezing of soil within the radius R_k, h.

Thus by introducing $\lambda_{экв}$ we substituted the problem of thermal conditions in a cylinder of frozen soil around the heat exchanger tube with radius R_k and thermal conductivity λ_g by a quasi-stationary problem (4) with similar temperature distribution, same boundary conditions (boundary temperatures are respectively t_0 and t_p), but with another "equivalent" thermal conductivity $\lambda_{экв}$, which accounts for pore moisture phase transitions.

An "equivalent" problem is the problem of the stationary thermal regime of an unlimited soil massif with a cylindrical cavity whose temperature field coincides with the temperature field of the main problem (with the region of the frozen ground of the Stefan problem), presented in Figure 1, but there is no latent heat released. Obviously, it is possible to achieve an approximately similar temperature distribution in both cases only by introducing new thermal conductivity of the soil to the second problem - $\lambda_{экв}$, that is in fact an "equivalent" thermal conductivity of the soil, that ensures that temperature distributions coincide, or at least are very similar to one another.

To determine q_{st} we use the same quasi-stationary problem (5), with the same boundary conditions, but with the actual thermal conductivity of the soil, W/(m·°C).

To determine q_{ft} (6) lets average the amount of thermal energy released during the freezing of the hollow cylinder with an inner radius R_0 and outer radius R_k over time τ.

The other way to determine q_{ft} is to, as in expressions (4) and (5), use the same quasi-stationary problem (remember, that the heat flow from the unfrozen soil equals "0") with thermal conductivity λ_{ft}, that ensures thermal impact on the heat exchanger equivalent to (6). In this case, q_{ft} can be expressed as follows

$$q_{ft} = \frac{2\pi\lambda_{ft}}{\ln\left(R_k / R_0\right)}\left(t_0 - t_p\right). \tag{7}$$

Thus by introducing expressions (4), (5) and (7) into equation (3), we may present the heat balance equation in a new form:

$$\frac{2\pi\lambda_{экв}}{\ln\left(R_k / R_0\right)}\left(t_0 - t_p\right) = \frac{2\pi\lambda_g}{\ln\left(R_k / R_0\right)}\left(t_0 - t_p\right) + \frac{2\pi\lambda_{ft}}{\ln\left(R_k / R_0\right)}\left(t_0 - t_p\right). \tag{8}$$

Dividing both parts of the equation (8) by $\frac{2\pi}{\ln(R_k/R_0)}(t_0-t_p)$, produces a new expression for $\lambda_{экв}$

$$\lambda_{экв} = \lambda_g + \lambda_{ft}. \tag{9}$$

Finally, the “equivalent” thermal conductivity of ground, accounting for the latent heat of pore moisture phase transitions, equals to the actual ground thermal conductivity, increased by the "virtual" part λ_{ft}, which can be determined from the equality of expressions (6) and (7):

$$\frac{2\pi\lambda_{ft}}{\ln(R_k/R_0)}(t_0-t_p) = \pi(R_k^2-R_0^2)\frac{L_v}{\tau}. \tag{10}$$

Solving the equation (10) for λ_{ft}, obtain the required expression

$$\lambda_{ft} = \frac{L_v(R_k^2-R_0^2)}{2\tau(t_0-t_p)}\ln(R_k/R_0). \tag{11}$$

Thus, all the unknowns needed to calculate the “equivalent” thermal conductivity of the soil $\lambda_{экв}$, except for R_k have been determined.

To determine R_k consider the same quasi-stationary problem (the case when $q_{st} = 0$) and write down the heat balance equation at the boundary of soil freezing]

$$-\lambda_g \frac{t_0-t_p}{R_k\ln(R_k/R_0)} = L_v\frac{dR_k}{d\tau}. \tag{12}$$

The solution for this equation looks as follows:

$$\eta_k^2(2\ln\eta_k-1)+1 = 4\Pi. \tag{13}$$

where:

$$\eta_k = \frac{R_k}{R_0};\quad \Pi = \frac{\lambda_g\tau(t_0-t_p)}{L_vR_0^2}. \tag{14}$$

The equation (13) may be solved numerically, using, for example, the Newton's method. The obtained value of R_k is used for calculating λ_{ft} from (11).

Experimental study

Experimental study of estimation of “equivalent” thermal conductivity of the ground, accounting for the phase transition of the ground moisture during the thawing and freezing of the soil, has been performed in the laboratory on the test bench simulating borehole heat exchangers working conditions. The scheme of the test bench is shown on Figure 2, and its photograph on Figure 3.

The test bench consisted of two models of borehole heat exchangers - metal tubes with the outer diameter of 33.5 mm, inner diameter of 27.1 mm and wall thickness of 3.2 mm. Metal-plastic pipes 15 mm in diameter were placed inside metal pipes, and the ends of the metal tubes were plugged. Heat-carrying medium was pumped into the borehole model through the inner pipes, and flowed out through the annulus. Water solution of ethylene glycol was used as heat-carrying medium. Models of boreholes were placed inside plastic finned tubes with internal diameter of 314 mm. The space between borehole model and the plastic tube is filled with soil. Borehole model No. 1 is placed in loam and borehole model No. 2 is placed in sand. The soil properties are shown in the Table 1 [30]. The length of each model is 2 m. The borehole models are parallel connected to the hydraulic circuit along with the refrigeration unit and the electric heater. Either the electric heater or the refrigeration unit are turned on depending on experiment's purpose - simulating of summer or winter conditions. The refrigeration unit was placed into isolated chamber to avoid the influence of heat from its condensers on thermal conditions of the laboratory facilities and boreholes under study.

To measure the soil temperature, the soil temperature sensors of the TP101 series were used with the measurement error ± (0.15 ºC + 0.002 | T |), and the coolant temperature was measured by submersible Pt1000 sensors with a measurement error of 0.3ºC + 0.002 | T |, where T - current measured temperature.

The flow rate of the heat carrier was determined from the readings of the water meter with a measurement error of ± 2 %.

The measurements were carried out with a periodicity of 5 minutes.

The thermal load Nt, W, supplied to the BHE, was determined as

$$Nt = Cp * \Delta T * G,$$

where Cp - is the specific heat of the coolant, J / (kg * °C);

ΔT - temperature difference at the inlet and outlet of the BHE;

G - coolant flow, kg / s.

Table 1. Thermal and physical properties pf the soil [30]

	Soil type	Density, kg/m^3	Heat capacity when thawed, J / (kg * K)	Heat capacity when frozen, J / (kg * K)	Thermal conductivity when thawed, W / (m * K)	Thermal conductivity when frozen, W / (m * K)
Borehole 1	Clay loam	2000	2.26	2.10	1.16	1.27
Borehole 2	Sand	1800	2.42	2.04	1.97	2.20

Three series of experiments were conducted.

<u>The purpose of the first series of experiments</u> was to determine the «equivalent» thermal conductivity of the soil at heat extraction regime.

The procedure for conducting experiments in this series was as follows. The flow rate of the heating medium through Borehole 2 was overlapped in order to ensure that all cooling power was directed to Borehole 1. The refrigeration machine was switched on and ground temperatures were recorded. At the same time, the room temperature was maintained at +18 °C. The soil around the Borehole was frozen. The soil was humidified, and then kept at almost stationary humidity conditions. The electric power meter was measured using an electric meter, after which the «equivalent» thermal conductivity of the soil was determined.

<u>The purpose of the second series of the experiments</u> was to determine the «equivalent» thermal conductivity of the soil at heat rejection regime.

The procedure for conducting experiments in this series was as follows. The water heater was turned on, equal coolant flow rates for both boreholes were set, and the parameters of the soil temperature and humidity were recorded. At the same time, the room temperature was maintained at 20 °C. After the heater was turned off, the soil was moistened, brought to the stationary humidity regime, after which the heater was switched on again. By electric meter, the electric power consumption was measured, and then the «equivalent» thermal conductivity of the soil was determined.

<u>The purpose of the third series of the experiments</u> was to evaluate the impact of cyclical loads and heat-accumulating properties of the soil on its “equivalent” thermal conductivity.

The experiments of this series included three periods: the first period - heat extraction - the chiller was switched on, the second period - the heat rejection - the electric heater was turned on, and the chiller was switched off, and the third period - heat extraction - the electric heater was switched off and the chiller was switched on again. At the same time, the temperature of the indoor air in the laboratory room was maintained at a constant level. The electric meter measured the consumed electric power, the specific heat exchange was determined for 1 m of the length of the boreholes, and then the “equivalent” thermal conductivities of the soil were determined for each period.

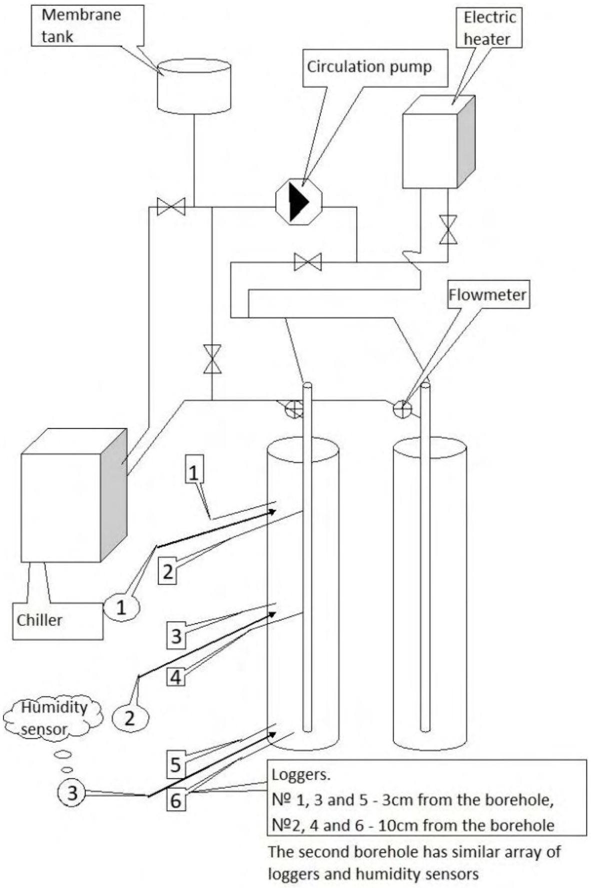

Figure 2. Test bench schematics

Figure 3. Photo of borehole models

Results and discussion

Numerical study

Numerical studies were carried out using the mathematical model described above. To implement it, a computer program was created.

Calculations were carried out using the example of a hypothetical cottage with a heated area of 200 square meters, equipped with GSHP with a single vertical borehole of 0.16 m in diameter and 70 m in depth. Climatic conditions were taken for the city of Moscow. Ground considered was a loam with a volume weight of 2000 kg / m^3 with a thermal conductivity of 1.16 W / (m * ºC). The natural undisturbed temperature of the ground is 8 ºC. GSHP provides only the heating, without domestic hot water. The beginning of the countdown is the beginning of the heating season - October 1. The time horizon for modeling is the first 60 months of system's operation.

When performing calculations, the influence of the process of pore moisture freezing was evaluated. Two options were calculated - without taking into account the freezing and with its account. As the evaluation criterion, the temperatures of the coolant and the ground at the entrance to the borehole were assumed (the minimum temperature, after the heat pump evaporator).

Figure 4 shows the graphs of the temperature change of the heat carrier of borehole during operation, calculated without taking into account and taking into account the freezing of pore moisture.

Figure 5 shows graphs of the change in the freezing radius of the soil around the borehole during its operation, as well as the "equivalent" thermal conductivity of the soil, determined according to the methodology described in paragraph 2.1. of this article.

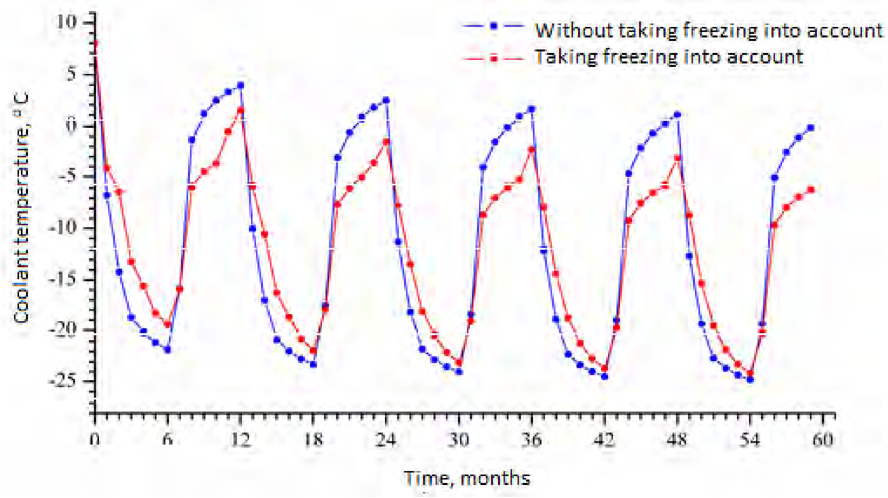

Figure 4 Temperature of the coolant in a borehole heat exchanger, calculated with and without taking into account freezing of ground moisture in the body of soil

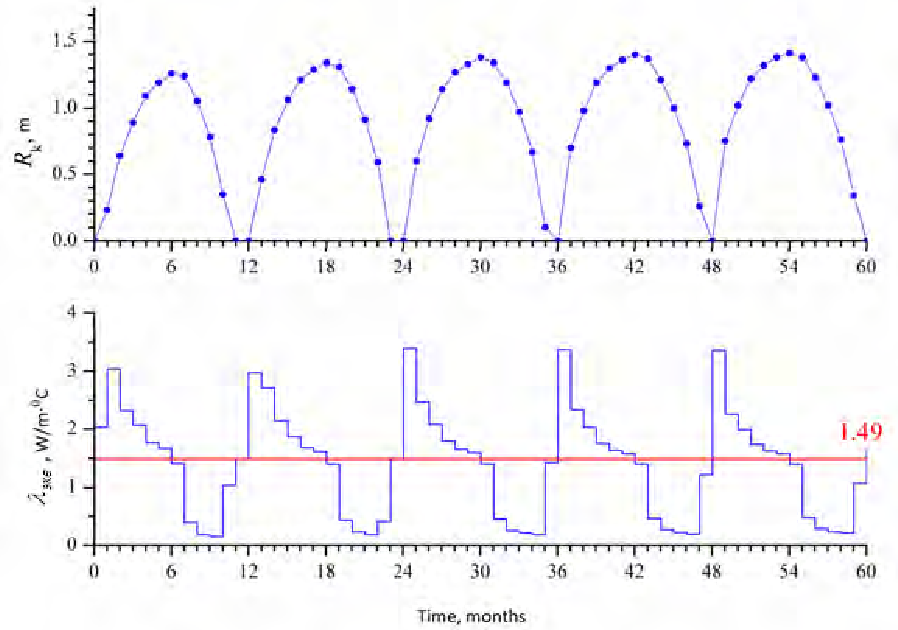

Figure 5. Radius of frozen soil around the borehole heat exchanger and «equivalent» thermal conductivity of the soil

As can be seen from the graphs presented in Figure 4, that taking into account the freezing of pore moisture the coolant temperature by the end of the heating period (the minimum points in the graph of Figure 4) is higher by 3 °C in the first year of operation than in the calculation without taking the freezing into account, but in following years this temperature difference decreases.

The maximum temperature of the coolant in the case of freezing is below the analogous temperature for the case when phase transitions of pore moisture are not taken into account.

The upper graph in Fig. 5 shows that in the operating conditions under consideration, an ice formed around the borehole during its work, has enough time to defrost in first two years, but on the third and subsequent periods complete melting of ice does not occur.

The «equivalent» thermal conductivity of the soil (the lower graph in Fig. 5.), taking into account the latent heat of freezing of the pore moisture, varies from 1.16 to 3.0 W / (m * ° C) during the heating period, and the average for the first five heating periods “equivalent” thermal conductivity is 1.49 W / (m * °C).

Experimental study

The results of all three series of experiments are shown in table 2. The data in Table 2 are obtained by averaging the corresponding parameters during the test period (indicated in the second column). Average for a period of specific heat extraction from 1 m of the BHE was calculated by dividing the average heat load per BHE by its length.

Table 2. The results of the three series of experiments

№	TEST PERIODS	Average heat extraction from 1 meter of BHE during the period q_{st}, W/m	Average coolant temperature, ° C	Average soil temperature 50 mm away from the BHE, °C	Average soil temperature 100 mm away from the BHE, °C	Average “equivalent” thermal conductivity of the soil Rk=50, W/(m°C)	Average “equivalent” thermal conductivity of the soil Rk=100, W/(m°C)
First series (heat extraction)							
BHE №1 (clay loam)	No. 1 (77 h)	291	-13.9	-3.3	0.3	6.81	6.98
Second series (heat rejection)							
BHE №1 (clay loam)	No. 1 (89.9 h)	33.00	42.1	31.0	24.5	0.73	0.64
	No. 2 (40.7 h)	68.00	55.2	39.3	28.1	1.05	0.85
	No. 3 (21.4 h)	72.00	53.7	45.3	35.6	2.11	1.35
	No. 4 (75.2 h)	96.00	53.7	37.0	30.1	1.42	1.38
BHE №2 (sand)	No. 1 (89.9 h)	33.00	42.1	28.8	25.0	0.61	0.65
	No. 2 (40.7 h)	68.0	55.2	35.6	29.8	0.86	0.91
	No. 3 (21.4 h)	72.0	53.7	40.7	35.7	1.37	1.36
	No. 4 (75.2 h)	96.00	53.7	37.0	30.1	1.42	1.38
Third series (cyclic loads)							
BHE №1 (clay loam)	No. 1 (96.2 h) cooling	171.93	-2.59	7.10	9.29	4.37	4.90
	No. 2 (119.5 h) heating	58.74	50.84	29.32	26.91	0.49	0.60
	No. 3 (141.0 h) cooling	188.09	-1.58	8.81	10.77	4.46	5.16

It should be mentioned that during the first series borehole 2 was shut off, and all the cooling capacity was directed to borehole 1, yet no stationary regime was achieved. This fact is apparently due to the influence of the latent heat of pore moisture freezing on thermal balance of borehole. Experimentally obtained values of “equivalent” thermal conductivity of the soil of 6.8-7.0 W/m°C, are 5.3 to 5.5 times higher than the value of the thermal conductivity of loam in the frozen state, equal to 1.27 W/(m*°C) (Table 1). The results of the first series of experiments in a graphical form are shown in Figure 6.

The purpose of the second series of the experiments was to determine the thermal conductivity of the soil in heat rejection mode. This series included 4 periods; soil in the borehole heat exchangers' models during all the periods was thawed and heated. The water heater was turned on; coolant flow rates for both boreholes were equalized, while temperature of soil and coolant was logged. Before the beginning of the third period, 2 liters of water were poured into the borehole 1, and 4 liters - into the borehole 2. Then before the fourth period, 8 more liters were poured into the borehole 1, and 11 more - into the borehole 2. We note the fact that coolant temperature in the borehole heat exchangers during periods 2, 3 and 4 was almost constant, while soil temperature and specific heat rejection underwent quite regular changes in accordance with the increasing humidity of the soil: specific heat rejection per 1 meter increased, while the difference between soil and coolant temperatures decreased. The results of the second series of experiments are shown in Figures 7 and 8.

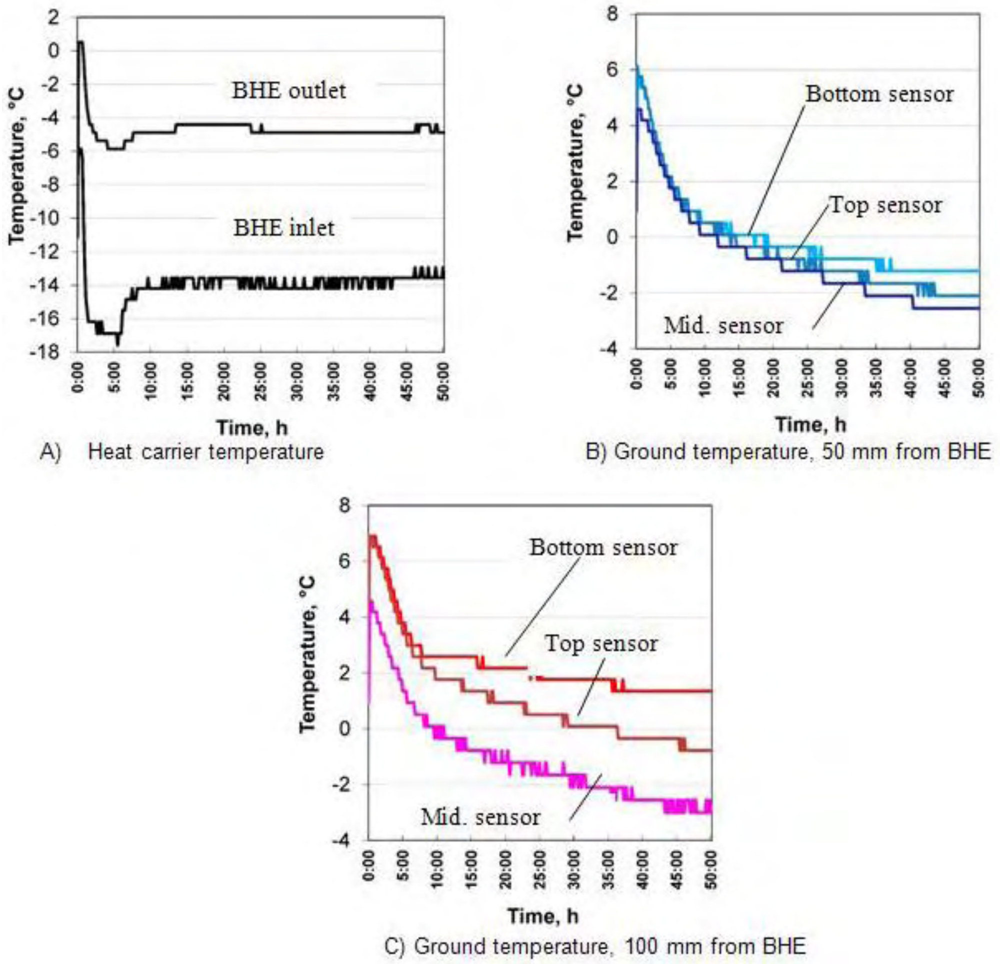

Figure 6. First series results

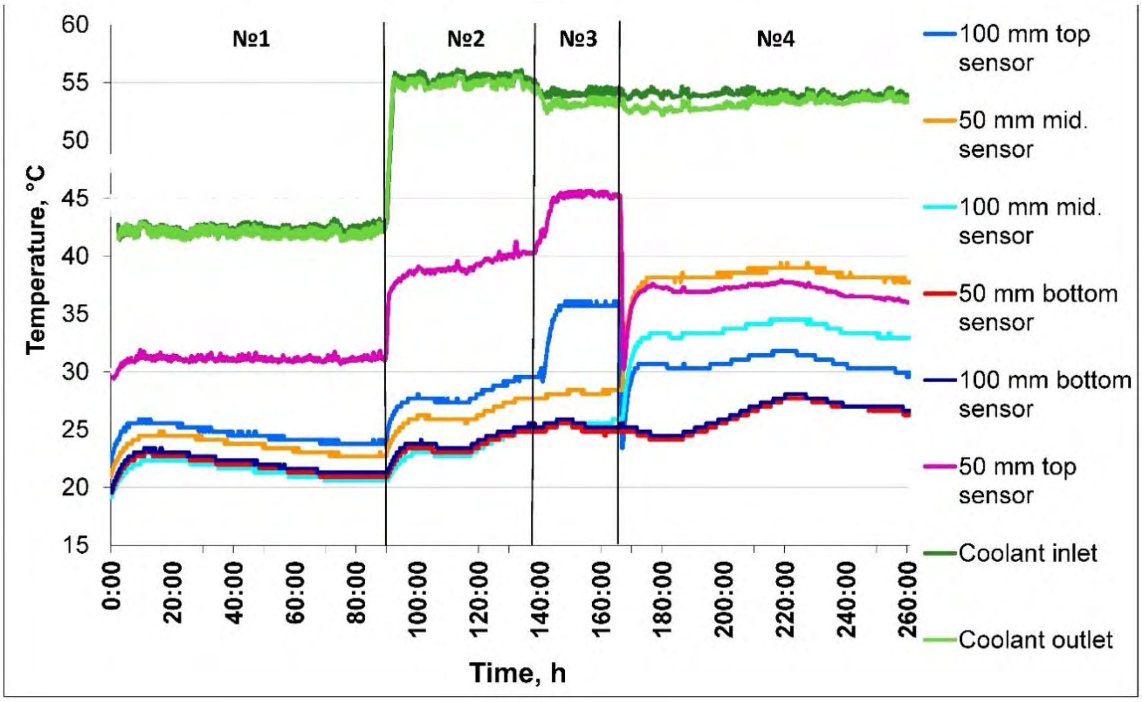

Figure 7. Second series results, BHE No. 1

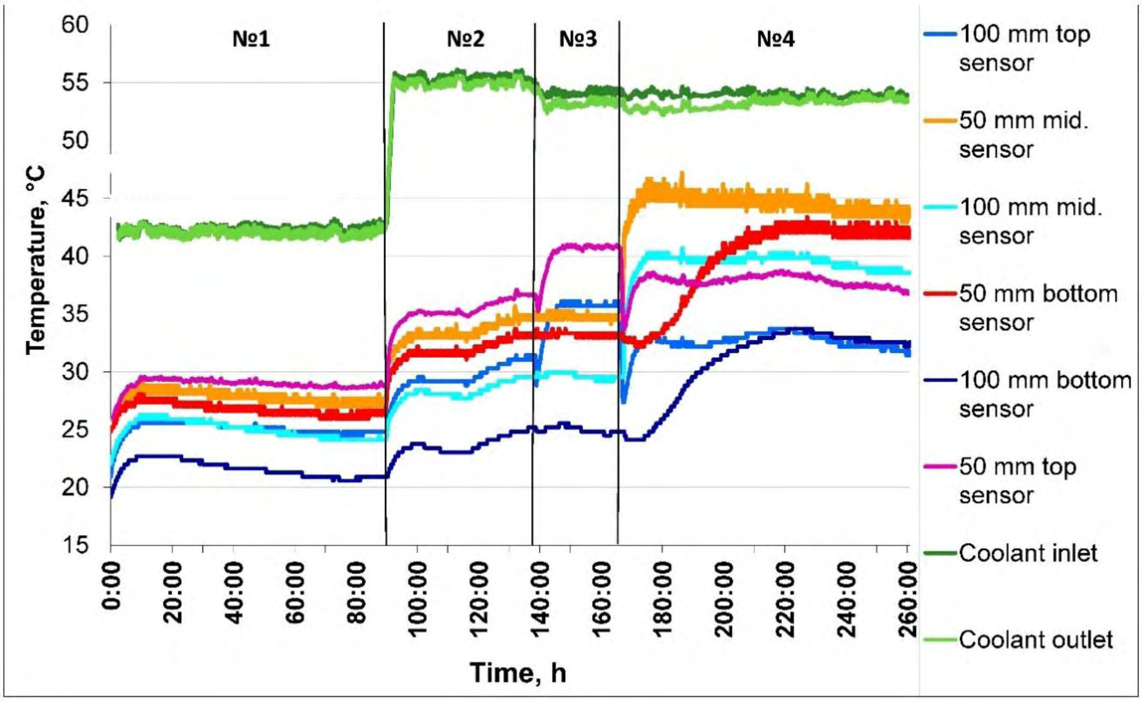

Figure 8. Second series results, BHE No. 2

During the third series of experiments, the impact of cyclic loads (annual cycle) and heat accumulating properties of the ground on its "equivalent" thermal conductivity was studied. The experiments included three periods: the first period - heat extraction - the chiller was switched on; the second period – heat rejection - the electric heater was switched on, and the chiller was switched off; and the third period - heat extraction - the electric heater was switched off and the chiller was turned back on. The results of the third series of experiments presented in Table 2 illustrate the independence of the specific heat gains from 1 meter of the borehole heat exchanger from the cyclicity of the heat load. The results of the third series of experiments are presented in Figures 9 and 10.

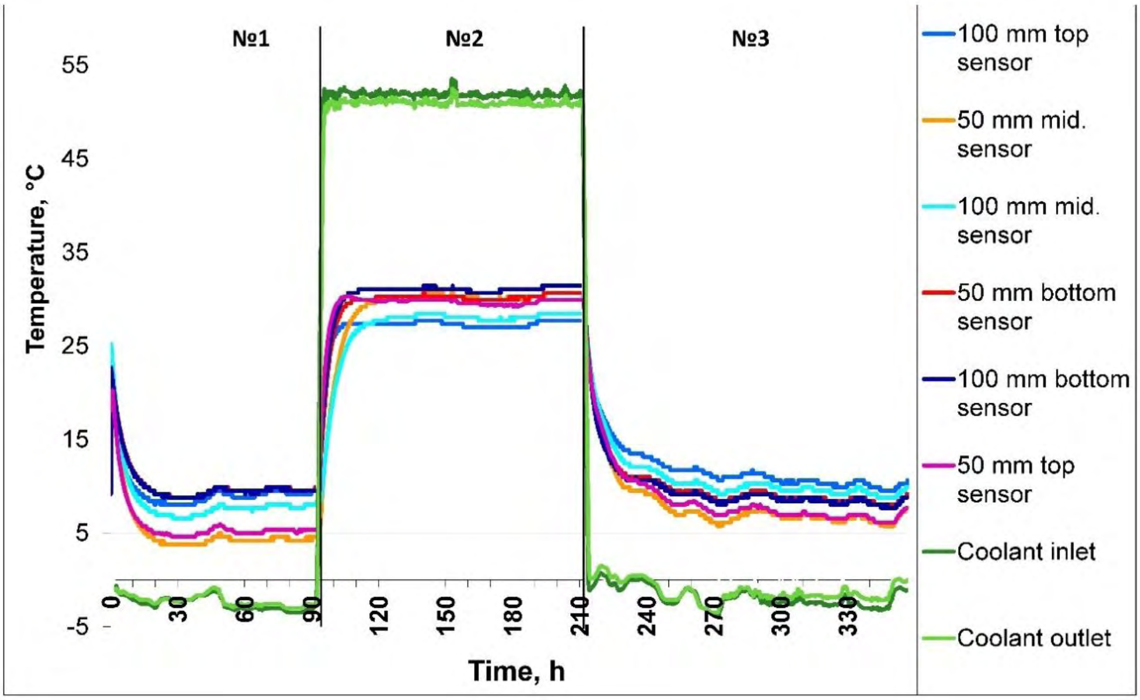

Figure 9. Third series results BHE, No. 1

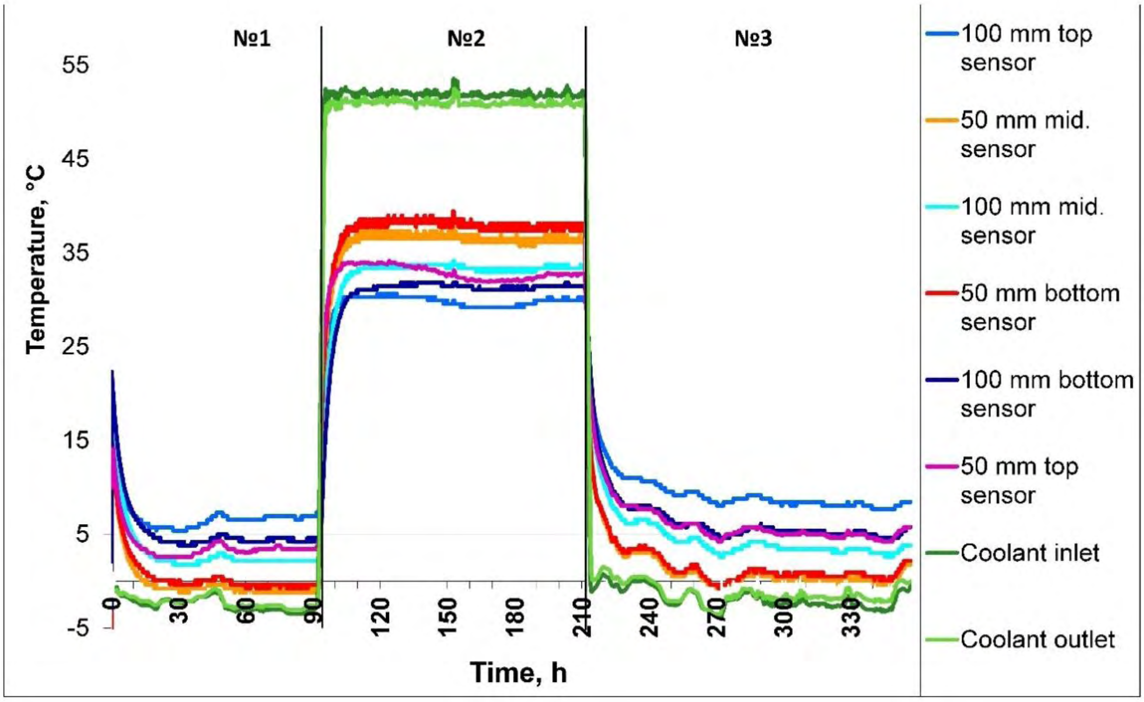

Figure 10. Third series results, BHE No. 2

The calculation results showed that accounting for phase transitions of pore moisture in the soil has a significant effect on the temperature of the coolant circulating through the ground heat exchanger. These changes relate to both minimum and maximum temperatures of the coolant in the annual cycle, and taking into account the phase transitions of the pore moisture, the coolant temperature minimums are higher than in the calculation that does not take into account the phase transitions, while the maximums, on the contrary, are lower. The same thermal behavior was demonstrated in [31], where the similar problem of incorporating phase change effects into a final element method software for ground properties simulation was investigated. This observation can be offered the following explanation. At a time when heat is removed from the ground and associated processes of pore moisture freezing are taking place, the latent heat of the phase transition is released during crystallization, which changes the heat balance and leads to higher temperatures of the coolant. At a time when heat from the ground is not consumed and its natural recovery occurs, the frozen ground thaws due to the influx of heat from the external environment. Calculations that take phase transitions into account show that in this case the temperature of the coolant is lower than in calculations without considering the phase transitions. The heat of the phase transition is taken into account in this case with a negative sign, and some of the heat coming from the environment is used to compensate for the latent heat of melting, so not all heat can be transferred to the heat carrier, which leads to lower temperatures.

The general trend of reducing the temperature of the coolant during consecutive heating periods is maintained for both variants of calculation. The temperature of the ground does not have time to return to its initial value over the summer period, and the longer the heat recovery period, i.e. heating period, so, accordingly, less time remains for the restoration of soil, and the stronger this trend will be.

It should be noted that the calculations, taking into account the phase transitions, on average give lower values of the coolant temperature (Fig. 4). The result will be a lower COP of the geothermal heat pump system.

Under given conditions, the ice that formed during the heating period around the boreholes is completely melted only after the first two seasons of operation (Fig. 5).

“Equivalent” thermal conductivity of the soil, taking into account the latent heat of freezing of pore moisture, during the heating period changes significantly and can increase by 2-3 times in comparison with the intrinsic thermal conductivity of the soil.

An important result of the experimental studies, according to the authors, is the fact that the values of the ground “equivalent” thermal conductivity in periods 1 and 3 of the third series of experiments (Table 2) differ from the analogous values obtained in the first series for the heat extraction mode. The fact is that in the third series of experiments the soil was in a thawed state. Despite the small negative temperatures of the coolant during periods 1 and 3, the soil temperatures throughout the third series of experiments were positive and freezing of moisture in the ground did not occur. In this case, one would expect that the thermal conductivity of the soil in periods 1, 2 and 3 will be close, since in all regimes the ground is in a thawed state, but in reality we obtained a different picture: the «equivalent» thermal conductivity of the soil in periods 1 and 3 is 8-10 times higher than the thermal conductivity of soil in regime 2. The authors assume that we are dealing with a little-studied effect caused by the condensation of water vapor contained in the pore space of the soil and the related intensification of the heat exchange processes between BHEs and the ground. As it turned out, the influence of this effect on the intensity of heat exchange in the soil can be commensurate and even exceed the effect of freezing / thawing of pore moisture. This effect deserves attention and further study, as it can fundamentally change our current understanding of the BHEs performance.

Conclusions

A new method of accounting of pore moisture phase transitions in the ground during BHE operation is proposed together with mathematical model. The essence of the method is to introduce a new "equivalent" thermal conductivity of the soil, consisting of the direct thermal conductivity of the soil and an additive that is responsible for the freezing / thawing of pore moisture.

The model proposed helps to solve the Stefan problem of heat transfer in a biphasic system with the unknown position of the phase boundary for BHE operational parameters forecast while designing GSHP system simple enough for engineering calculation.

Numerical simulation results show, that accounting for phase transitions leads to lower amplitude of temperature variation of the coolant in the annual cycle while keeping the general trend of reducing the temperature of the coolant during consecutive heating periods. The important thing is that accounting for the phase transitions on average gives lower values of the coolant temperature which will result in lower design COP of GSHP.

"Equivalent" thermal conductivity of the soil, accounting the latent heat of freezing of pore moisture, during the heating period changes by 2–3 times in comparison with the intrinsic thermal conductivity of the soil. If not frozen, ground’s "equivalent" thermal conductivity appears to be 8 to 10 times higher in heat extraction mode than in hear rejection. The author’s assumption is that the effect is caused by the condensation of water vapor contained in the pore space of the soil. Authors suppose that effect is worth for further study.

Acknowledgement

The Research was conducted by JSC "INSOLAR-INVEST" with the financial support of the Ministry of Education and Science of Russia. Unique identifier of the project RFMEFI57915X0115.

Reference

1. Spitler J.D. Ground-source heat pump system re-search—Past, present and future. *HVAC & R Res.* 2005. No. 11. Pp. 165–167.
2. Nagano K. The progress of GSHP in Japan. *IEA Heat Pump Centre Newsletter.* 2015. Vol. 33. Pp. 21–25.
3. Gorshkov A.S., Rakova X.M., Musorina T.A., Tseytin D.N. Building project with low consumption of thermal energy for heating. *Construction of Unique Buildings and Structures.* 2015. No. 4(31). Pp. 232-247. (rus)
4. *European Heat Pump Statistics.* The European Heat Pump Association. Outlook 2011.
5. Zhang Y., Ma Q., Li B., Fan X., Fu Zh. Application of an air source heat pump (ASHP) for heating in Harbin, the coldest provincial capital of China. *Energy and Buildings*. 2017. No. 138. Pp. 96–103.
6. Lund J.W., Boyd T.L. Direct utilization of geothermal energy. Worldwide review 2015. *Geothermics.* 2016. No. 60. Pp. 66–93.
7. Antics M., Bertani R., Sanner B. Summary of EGC 2013 country update reports on geo-thermal energy in Europe. *European Geothermal Conference.* Pisa (Italy), 2013. Pp. 1-18.

Литература

1. Spitler J.D. Ground-source heat pump system research — Past, present and future. // HVAC & R Res. 2005. № 11. Pp. 165–167.
2. Nagano K. The progress of GSHP in Japan // IEA Heat Pump Centre Newsletter. 2015. Vol. 33. Pp. 21–25.
3. Горшков А.С., Ракова К.М., Мусорина Т.А., Цейтин Д.Н. Проект здания с низким потреблением тепловой энергии на отопление // Строительство уникальных зданий и сооружений. 2015. № 4(31). С. 232-247.
4. European Heat Pump Statistics. The European Heat Pump Association. Outlook 2011.
5. Zhang Y., Ma Q., Li B., Fan X., Fu Zh. Application of an air source heat pump (ASHP) for heating in Harbin, the coldest provincial capital of China. // Energy and Buildings. 2017. № 138. Pp. 96–103.
6. Lund J.W., Boyd T.L. Direct utilization of geo-thermal energy. Worldwide review 2015. // Geothermics. 2016. № 60. Pp. 66–93.
7. Antics M., Bertani R., Sanner B. Summary of EGC 2013 country update reports on geo-thermal energy in Europe // European Geothermal Conference. Pisa, Italy, 2013. Pp. 1-18.

Vasilyev G.P., Gornov V.F., Peskov N.V., Popov M.P., Kolesova M.V., Yurchenko V.A. Ground moisture phase transitions: Accounting in BHE’S design. *Magazine of Civil Engineering.* 2017. No. 6. Pp. 102–117. doi: 10.18720/MCE.74.9.

8. Qian H., Wang Y. Modeling the interactions between the performance of ground source heat pumps and soil temperature variations. *Energy for Sustainable Development*. 2014. No. 23. Pp. 115–211.
9. Gornov V.F., Peskov N.V., Vasilyev G.P., Kolesova M.V. Assessment of impact of borehole heat exchanger design on heat extraction/rejection efficiency. *MATEC Web of Conferences.* 2016. No. 75. No. 09009. Pp. 1-5.
10. Zhou J., Wang Q.J., Zhang G.Q. Heat transfer analysis of vertical underground heat exchanger under different layout forms of pipe-groups. *Fluid Mach.* 2012. No. 40(9). Pp. 56–61.
11. Chiasson A.D., Rees S.J., Spitler J.D. *A preliminary assessment of the effects of groundwater flow on closed-loop ground source heat pump systems.* Stillwater, Oklahoma State Univ. 2000.
12. Ji W.J., You T., Bai S.W., et al. Effects of buried pipe design parameters on performance of ground-source heat pump systems in cold zone. *HV&AC*. 2015. No. 45(3). Pp. 113–118.
13. Sáez Blázquez C., Farfán Martín A., Martín Nieto I., Carrasco García P., Sánchez Pérez L.S., González-Aguilera D. Efficiency Analysis of the Main Components of a Vertical Closed-Loop System in a Borehole Heat Exchanger. *Energies.* 2017. No. 10. P. 201.
14. Erol S., François B. Efficiency of various grouting materials for borehole heat exchangers. *Applied Thermal Engineering.* 2014. No. 70. Pp. 788-799.
15. Focaccia S., Tinti F. An innovative Borehole Heat Exchanger configuration with improved heat transfer. *Geothermics.* 2013. No. 48. Pp. 93–100.
16. Platts A.B., Cameron D.A., Ward J. Improving the performance of Ground Coupled Heat Exchangers in unsaturated soils. *Energy and Buildings*. 2015. No. 104. Pp. 323–335.
17. Sáez Blázquez C., Farfán Martín A., Martín Nieto I., González-Aguilera D. Measuring of thermal conductivities of soils and rocks to be used in the calculation of a geothermal installation. *Energies.* 2017. No. 10(6). P. 795.
18. Vasiliev G.P. Geotermal'nye teplonasosnye sistemy otopleniya [Ground source heat pumps heating systems]. *Thermal engineering.* 2004. No. 6. Pp. 33–41. (rus)
19. Vasiliev G.P. Rezul'taty naturnyh issledovanij teplovogo rezhima ehksperimental'nogo ehnergoehffektivnogo doma [Results of field tests of thermal conditions of an experimental energy efficient building]. *Building materials, equipment, technologies of the XXI century.* 2002. No. 6. Pp. 3–5. (rus)
20. Gupta S.C. *The classical Stefan problem: basic concepts, modeling and analysis.* The Classical Stefan Problem 2nd Edition. Elsevier. 2003. 385p.
21. Chudnovsky A.F. *Teplofizicheskie harakteristiki dispersnyh materialov* [Thermophysical characteristics of dispersed materials]. M.: Fizmatgiz, 1962. 456 p. (rus)
22. Yang H., Cui P., Fang Z. Vertical borehole ground coupled heat pumps: A review of models and systems. *Applied Energy.* 2010. No. 87. Pp. 16–27.
23. Lamarche L., Kajl S., Beauchamp B. A review of methods to evaluate borehole thermal resistances in geothermal heat pump systems. *Geothermics.* 2010. No. 39. Pp. 187–200.
24. Carslaw H.S., Jaeger J.C. *Conduction of heat in solids*. Oxford, UK: Claremore Press. 1946.
25. Vatin N., Gorshkov A., Rymkevich P., Nemova D., Tarasova D. Nonstationary thermal conduction through the building envelope. *Applied Mechanics and Materials.* 2014. Vol. 670-671. Pp. 356-369.
26. Gorshkov A., Rymkevich P. A diagram method of describing the process of non-stationary heat transfer. *Magazine of*

8. Qian H, Wang Y. Modeling the interactions between the performance of ground source heat pumps and soil temperature variations // Energy for Sustainable Development. 2014. № 23. Pp. 115–21.
9. Gornov V.F., Peskov N.V., Vasilyev G.P., Kolesova M.V. Assessment of impact of borehole heat exchanger design on heat extraction/rejection efficiency // MATEC Web of Conferences. 2016. № 75. No. 09009. Pp. 1-5.
10. Zhou J, Wang QJ, Zhang GQ. Heat transfer analysis of vertical underground heat exchanger under different layout forms of pipe-groups // Fluid Mach. 2012. № 40(9). Pp. 56–61
11. Chiasson A.D., Rees S.J., Spitler J.D. A preliminary assessment of the effects of groundwater flow on closed-loop ground source heat pump systems. Stillwater, Oklahoma State Univ. 2000.
12. Ji W.J., You T., Bai S.W., et al. Effects of buried pipe design parameters on performance of ground-source heat pump systems in cold zone // HV&AC. 2015. № 45(3). Pp. 113–118
13. Sáez Blázquez C., Farfán Martín A., Martín Nieto I., Carrasco García P., Sánchez Pérez L.S., González-Aguilera D. Efficiency analysis of the main components of a vertical closed-loop system in a borehole heat exchanger // Energies. 2017. № 10. Pp. 201.
14. Erol S., François B. Efficiency of various grouting materials for borehole heat exchangers // Applied Thermal Engineering. 2014. № 70. Pp. 788-799.
15. Focaccia S., Tinti F. An innovative Borehole Heat Exchanger configuration with improved heat transfer // Geothermics. 2013. № 48. Pp. 93–100.
16. Platts A.B., Cameron D.A., Ward J. Improving the performance of Ground Coupled HeatExchangers in unsaturated soils // Energy and Buildings. 2015. № 104. Pp. 323–335.
17. Sáez Blázquez C., Farfán Martín A., Martín Nieto I., González-Aguilera D. Measuring of thermal conductivities of soils and rocks to be used in the calculation of a geothermal installation // Energies. 2017. № 10(6). Pp. 795.
18. Васильев Г.П. Геотермальные теплонасосные системы отопления // Теплоэнергетика. 2004. № 6. С. 33-41.
19. Васильев Г.П. Результаты натурных исследований теплового режима экспериментального энергоэффективного дома // Строительные материалы, оборудование, технологии XXI века. 2002. № 6. С. 3-5.
20. Gupta S.C. The classical Stefan problem: basic con-cepts, modeling and analysis. The Classical Stefan Problem 2nd Edition. Elsevier. 2003. 385p.
21. Чудновский А.Ф. Теплофизические характеристики дисперсных материалов. М.: Физмат изд., 1962. 456 с.
22. Yang H., Cui P., Fang Z. Vertical borehole ground cou-pled heat pumps: A review of models and systems // Applied Energy. 2010. № 87. Pp. 16–27.
23. Lamarche L., Kajl S., Beauchamp B. A review of meth-ods to evaluate borehole thermal resistances in geothermal heat pump systems // Geothermics. 2010. № 39. Pp. 187–200.
24. Carslaw H.S., Jaeger J.C. Conduction of heat in solids. Oxford, UK: Claremore Press, 1946.
25. Vatin N., Gorshkov A., Rymkevich P., Nemova D., Tarasova D. Nonstationary thermal conduction through the building envelope // Applied Mechanics and Materials. 2014. Vol. 670-671. Pp. 356-369.
26. Горшков А.С., Рымкевич П.П. Диаграммный метод описания процесса нестационарной теплопередачи // Инженерно-строительный журнал. 2015. № 8(60). С. 68-82.
27. Горшков А.С., Рымкевич П.П., Ватин Н.И. Моделирование процессов нестационарного переноса

Civil Engineering. 2015. No. 8(60). Pp. 68-82.

27. Gorshkov A., Rymkevich P., Vatin N. Simulation of non-stationary heat transfer processes in autoclaved aerated concrete-walls. *Magazine of Civil Engineering.* 2014. No. 8(52). Pp. 38-48.
28. E.R.G. Eckert. *Heat and mass transfer.* 1959.
29. Pekhovich A.I., Zhidkikh V.M. Raschety teplovogo rezhima tverdyh tel [Calculations of the thermal regime of solids]. *Ehnergiya.* 1976. Pp. 117. (rus)
30. *Russian Building Norms and Rules SNiP 2.02.04-88.* Basements and foundations on permafrost soils. (rus)
31. Anbergen H., Rühaak W., Frank J., Müller L., Sass I. Numerical Simulation of Freezing-Thawing-Cycles in the Grout of Borehole Heat Exchangers. *Proceedings World Geothermal Congress.* Melbourne, Australia, 2015.

тепла в стеновых конструкциях из газобетонных блоков // Инженерно-строительный журнал. 2014. № 8(52). С. 38-48.

28. E.R.G. Eckert. Heat and mass transfer. 1959.
29. Пехович А.И., Жидких В.М. Расчеты теплового режима твердых тел. Энергия. 1976. С. 117.
30. СНиП 2.02.04-88 Основания и фундаменты на вечномерзлых грунтах.
31. Anbergen H., Rühaak W., Frank J., Müller L., Sass I. Numerical Simulation of Freezing-Thawing-Cycles in the Grout of Borehole Heat Exchangers // Proceedings World Geothermal Congress. Melbourne, Australia, 2015.

Gregory Vasilyev,
+7(499)1440667; gpvassiliev@mail.ru

Victor Gornov,
+7(499)1440667; insolar-invest@yandex.ru

Nikolay Peskov,
+7(499)1440667; peskovnick@gmail.com

Mikhail Popov,
+7(926)6097760; m.popov78@gmail.com

Marina Kolesova,
+7(499)1440667; eco-insolar@mail.ru

Victoria Yurchenko,
+7(499)1440667; vikayurch@gmail.com

Григорий Петрович Васильев,
+7(499)1440667; эл. почта: gpvassiliev@mail.ru

Виктор Федорович Горнов,
+7(499)1440667;
эл. почта: insolar-invest@yandex.ru

Николай Владимирович Песков,
+7(499)1440667;
эл. почта: peskovnick@gmail.com

Михаил Иванович Попов,
+7(926)6097760;
эл. почта: m.popov78@gmail.com

Марина Владимировна Колесова,
+7(499)1440667; эл. почта: eco-insolar@mail.ru

Виктория Александровна Юрченко,
+7(499)1440667;
эл. почта: vikayurch@gmail.com

Vasilyev G.P., Gornov V.F., Peskov N.V., Popov M.P., Kolesova M.V., Yurchenko V.A. Ground moisture phase transitions: Accounting in BHE’S design. *Magazine of Civil Engineering.* 2017. No. 6. Pp. 102–117. doi: 10.18720/MCE.74.9.

doi: 10.18720/MCE.74.10

The forming cyclic loads on the offshore structures during ice field edge fracture

Формирование циклических нагрузок на шельфовые сооружения при разрушении льда

V.G. Tsuprik,
Far Eastern Federal University, Vladivostok, Russia

Канд. техн. наук, профессор В.Г. Цуприк,
Дальневосточный Федеральный Университет, г. Владивосток, Россия

Key words: offshore structures; sea ice; cyclic load; vibration; destruction of ice

Ключевые слова: шельфовые сооружения; морской лед; циклические нагрузки; вибрация конструкций; разрушение льда

Abstract. The non-stationary process of ice breaking at the contact of the edge of a drifting ice field (IF) and the sea ice-resistant platform (IRP) can lead to dangerous vibrations and potentially dangerous dynamic loads on this offshore structure. Extreme resonant oscillations of the platform base can cause not only violations of the regular functioning of the object, but also significantly reduce the reliability of the structure and its durability, causing fatigue fracture in the structure of the IRP or its equipment, also such process can change the bearing capacity of the soil under the platform foundation. Dynamic ice destruction is a complex process, and the development of models of this phenomenon requires a well defined methodology and research procedure. The dynamic reaction of the structure on impact of the ice field depends on a combination of many factors: the size and flexibility of the impacted leg of the platform; the ice loading velocity, temperature and physical-mechanical parameters of ice, and others. The object of this research is the physical processes involved in the real system "IF-IRP” - the energy transfer from the moving ice fields to the control volume of ice in the contact area, accumulates the elastic energy received to its critical level in this volume and causes its destruction with a certain frequency. The most important property of the object of study, i.e. the subject of the research, is the mechanism of ice fracture in the zone of interaction of two basic elements of the system: the ice field and IRP. The aim of the study is to identify and describe the regularities of formation of cyclic ice loads on the structureand describe the process, taking into account the phenomenological features of sea ice fracture as a mechanism for converting the kinetic energy of the ice field into the elastic energy spent on to deviations leg of the platform and the energy spent on destructing the ice.

Аннотация. Нестационарный процесс разрушения льда на контакте кромки дрейфующего ледового поля (ЛП) и морского ледостойкого основания (МЛО) может привести к опасным вибрациям и потенциально опасным динамическим нагрузкам на шельфовые сооружения. Такие явления значительно снижают надежность сооружения и его долговечность, потому что вызывают усталостные разрушения в элементах конструкции и изменения несущей способности грунта под фундаментом платформы. Учитывая актуальность проблемы, данная статья посвящена процессу функционирования системы «дрейфующее ледовое поле − морское ледостойкое основание». Целью исследования является выявление и описание причины и закономерностей формирования циклической ледовой нагрузки на сооружение, описывающих процесс с учетом феноменологических особенностей разрушения морского льда. Метод исследования, примененный в данной работе - изучение результатов полномасштабных и лабораторных экспериментов, а также теоретических научно-исследовательских работ, связанных с процессами взаимодействия ЛП-МЛО, включая и работы автора. Объектом исследования является механизм преобразования кинетической энергии ледового поля в энергию упругих отклонений сооружения и энергию, затраченную на разрушения льда. Показано, что периодичность циклов разрушения льда регулируется достижением предельного значения удельной энергии разрушения льда в его сжатом объеме на контакте с сооружением. Рекомендуется эту характеристику применять в качестве критерия разрушения льда и продолжить исследовать ее стабильность и воспроизводимость в экспериментах для определения ее параметров.

Цуприк В.Г. Формирование циклических нагрузок на шельфовые сооружения при разрушении льда // Инженерно-строительный журнал. 2017. № 6(74). С. 118-139.

Introduction

Significant attention from the researchers in the field of investigation of ice formation interaction with shelf structures during the development of the problem was directed upon the analysis of calculation methods for the maximum ice load. So, periodical updating of standards and norms for the procedures for defining the parameters of the ice load calculation formula was obtained as a result of such investigations. Several years ago, such update was made for the Russian Code SP 38.13330.2012 [1] and the International Normative Document ISO/DIS 19906 [2]. The Russian norms provide no recommendations for the calculation of the dynamic impact of ice; the international norms provide the directions to consider this case.

The process of ice load formation began to be seriously investigated after the discovery of significant and hazardous vibrations for structures and personnel, including dangerous oscillations for drilling equipment located on operating platforms within the Cook Inlet, lighthouses in the Gulf of Bothnia, drilling platforms at Caspian, Asov Sea and Bohai Gulf, and ice-resistant platform structures within the Sakhalin region.

The first experimental works for the investigation of the vibration of marine structures were made in natural conditions for the real marine drilling platform in the Cook Inlet. The first scientists investigating this problem were Peyton [3] and Blenkarn [4].

In this period, the records on saw-tooth ice load upon supports of railway/road bridges [5, 6] and water dams [7] were obtained and also investigations were actively conducted on the vibration of the lighthouses within the Gulf of Bothnia [8, 9]. The reason for beginning these investigations was due to the fact that in this area in 1966, drifting ice fields budged and destroyed the lighthouse Tainio (Finland) [10]. The caisson of the lighthouse was set at a depth on 14 m on to sand bottom and overturned due to contact with a rocky ledge. In 1969, the Nygran Lighthouse was destroyed due to drifting ice fields (Sweden) [10]. The 2.5meter diameter lighthouse tower was damaged at 1-meter deep under the sea level; however, there was no displacement of the foundation. In 1974, the Kemi Lighthouse (Finland) was fractured at the upper section due to strong vibration [11]. In 1977-79 the reinforced concrete foundation of a drilling platform that has a shape of a polyhedron with 8 m diameter was damaged on the Azov Sea shelf [12]. There are many other cases of marine lighthouse foundation destruction in shallow waters. Serious damages exhibited by steel truss-type drilling platforms under the influence of single year ice fields within the Bohai Gulf and the destruction of one of such platforms disposited here have forced scientists in China and engineers from other countries to begin investigating this problem carefully. Specific analysis of the dynamic influence of ice fields acting upon the truss type platforms has shown that as a result of the tensile fatigue that occurs as a cyclical ice load, steel struts and bracings on platforms were destroyed. These events provided the conditions for increasing the values of oscillation and flexible deviation of the platform, therefore personnel were not able to operate subject to such conditions [13, 14, 15].

It shall be noted that the dynamic interaction of ice and marine structures is usual not only for flexible structures with small transversal supports. In winter 1985-1986, the Molikpaq Platform, with a 54 000-ton caisson and a 111-m^2 foundation, located within the Beaufort Sea, was influenced by 1 x 2 km drifting multi-year ice field [15, 16]. In compliance with the analysis, it was defined [17] that as a result of a 0.5 - 3 Hz vibration caused by 30 minutes of ice destruction at a contact zone, the platform was put into critical condition close to shear stability loss over the foundation soil surface. Pore pressure in sandy soil core foundation increased and this led to its liquefaction. In this regard, the bearing capacity of the foundation under the caisson reached its critical minimum value. At the time such results were unexpected for specialists. So, it can be supposed that there is a serious probability of shear of reinforced concrete caissons of lighthouses' foundations located within the Gulf of Bothnia subject to the same conditions as the Molikpaq Platform. The destruction of tower structures can occur due to fatigue as a result of a long-term cycle load, the same as the destruction of steel elements of lattice structures of drilling platforms within the Bohai Gulf. In recent years, the problem of the influence of cyclical loads on the strength of foundations has been present in oil platforms in the Sakhalin Shelf. [18].

The investigation of formation and development of vibration caused by ice impact shall be continue because the inevitable transition to deep waters on the one hand, and the necessity to increase the dimensions (and weight) of the underwater section of structure (in order to eliminate wave impact on the drilling equipment) on the other hand. This will lead to the flexibility of the structure as a whole (subject to provision of required strength of the structure) which will increase the negative impact of cyclic loads on the overall structural strength, and this requires that designers use materials with higher fatigue strength, ensuring its service life. In the last years, designers of marine wind generators have been faced with this problem when developing foundations for Baltic Sea areas [19,20].

However, as it was noted by some authors at the end of the last century and at the beginning of the new century [21,22,23], no details of structure and ice interaction process providing the vibration were developed up to the designing practice application level. Modern scientists have noted that no basic mechanism for the process is clear up to the present time, so the investigation shall be continued [24, 25, 26].

Thus, cyclical action of ice is an important factor in determining the reliability and durability of the IRS and the relevance of this problem remains topical due to two reasons. Firstly, due to the prospects of development of industrial shelf areas. Secondly, due to the absence of normative documents to ensure solutions provide safety and a longer service life of designed structures shelf ice-covered seas.

Given the relevance of the problem, presently it is necessary to achieve a deeper understanding of all the physical phenomena that jointly provide the vibration process of the structure during its interaction with an ice field. The aim of the study is to identify and describe the reasons and regularities for the formation of the cyclic ice loads on the structure, and to describe the process taking into account the phenomenological fracture characteristics of sea ice. Given that the load of ice on the structure reaches its maximum value at the moment of rupture of the ice , search the solution of the task about the frequency of occurrence of the peaks of the contact forces, which cause periodic oscillation of structure should be by studies and analyzed of the mechanism of destruction of ice. So any idea about the formation of ice loads shall be based on a mathematical description of the process of destruction of the edge of the ice field, taking into account the phenomenological characteristics of ice. In this regard, the main objective of this research should be the task of studying the mechanism of destruction of ice, as the environment, which exerts a forcical pressure on marine structures.

Research methods of interoperability issues ice fields and structures on the shelf

On the basis of the aforementioned aims and objectives of the work, the method of research applied in this work is to study the results of full scale and laboratory experiments and also the results of the theoretical scientific-research works related with the processes of the IF-IRP interaction, including the works of the author. The object of study is the mechanism of the conversion of the kinetic energy of the ice floes into elastic energy deviations of structures and the energy spent on the destruction of ice.

The phenomenon of vibration of marine structures during their interaction with a moving ice field, as was shown in the introduction to this work, in the first time was fixed while conducting experiments with full-scale platform in Cook Bay [3.4]. The aim of the first full-scale experiments held by Payton [3] in 1966-68, was to obtain the maximum pressure of ice on the support platform. Here during the study of the force action of ice moving at speeds from 0.5 to 2.1 m/s on cylindrical legs of the platform, 91 cm in diameter, H.R. Peyton found a strong vibration of the structure, which was caused by the destruction of ice. And during the process of interaction of the edge of the Ice field with the platform leg surface, the ice destructed from compression in the contact zone and the ice load on the leg was a "serrated" line with different frequency peaks depending on several factors. Peyton has defined that due to an increase of the ice field velocity, the frequency of ice destruction increased, but the ice load value range decreased.

The phenomenon of the vibration of structures caused by the movement of ice fields showed that it is necessary to take into account the fatigue in the calculations of structural elements, and to very carefully research the factors influencing the forming of vibrations and its development.

Experimental methods of researches regularities of occurrence oscillations of platforms

Blenkarn [4] also has performed investigations within the Cook Inlet in Alaska. Comparing the frequency of self-oscillation of the structure and the ice destruction frequency, he proposed that the "ice field - structure" system can provide the resonance of ice destruction frequency and self-oscillation frequency of the structure.

Thus, the findings were obtained, which give reason to assume the possibility of the emergence of platform resonant oscillations with the fluctuations of the force causing the edge ice field fracture. The nature of these phenomena requires special investigation due to a hazardous decrease of reliability and service life of expensive structures. These experiments can be considered as an accelerator for the development of investigations in the field of cyclic contact destruction of ice.

Given, that very difficult to control the structure and texture of ice in field measurements of ice forces on real constructions, the cutting process of the ice cover by supports have been extensively investigated on models of supports, these impactting on the full-scale ice cover. Simultaneously, the technology of model ice preparation was developed; ice basins were constructed; and technical means for registration of the quickly processes were developed subject tofor application in these areas.

The researche of fracture mechanisms of the edge of natural ice cover during its interaction with the structure models

This type of experimental works was developed by a group of scientists from the beginning of 60th; however, such works are continued in the present time. Natural ice provides the possibility for elimination of serious problems related to physical-mechanical ice modeling, becourse the results can be directly applied for analysis. For several years, starting in 1969, experiments with natural ice performed by J. Schwartz [27], and K.P. Croasdale and others [28–30] was made. During the interaction If-IRS provided the entry multiprocess processes destroying the edge of the ice field, occurring in the contact zone of the front surface of the model. These authors note that in addition to the initial radial vertical cracks and horizontal cracks in the array of ice plates, ice on the contact surfaces are completely crushed. Also, before the support appeared limited volume of highly compressed ice. The ice inside this volume has a lot of cracks, which are directed randomly.Also, before front surface of support occurs forming wedge-shaped volumes of ice, which are extruding by the surface of the support during moving ice field and are sliding in the direction of the upper and lower surfaces of the ice field.

These phenomena were completely approved by Tryde [31], Hirayama and others [32], Vershinin and others [33], Kivisild and Iyer [34], Nevel and others [35], Michel and Toussaint [36], Khrapaty and Tsuprik [37], Kry [38], Taylor [39], Ojima and others [40], Saeki and others [41, 42], Yamashita and others [43], Bekker [44], Karulin [45] and a lot of other scientists. For these experiments subject to detailed investigation of local ice pressure acting upon support and analysis of ice-structure interaction and vibration of structure, special strain gage panels were used, for example, by Sodhi and others [46]. The typical schemes of ice fields edges destruction due its interaction with a cylinder support is shown in Figure 1.

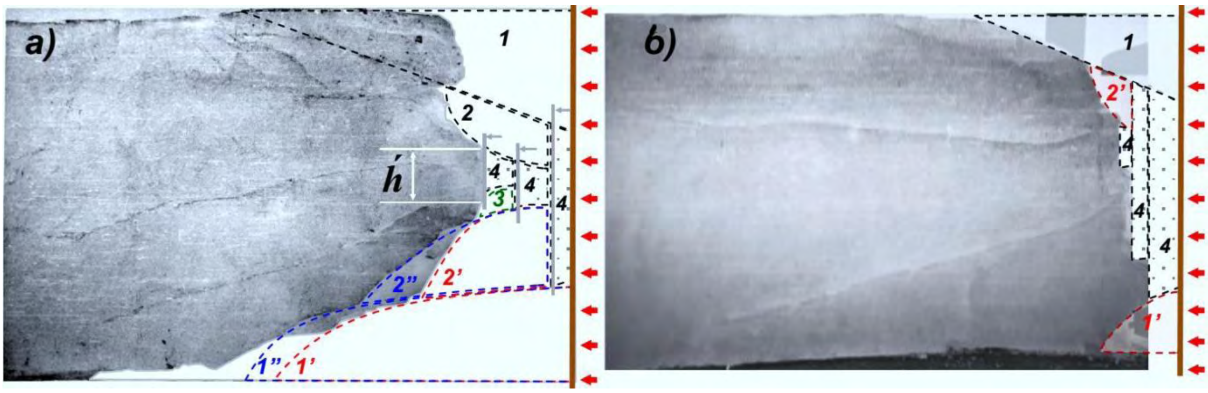

Figure 1. Photo of the natural ice fracture (experiment by the author 1978; Japan Sea) after dynamic introduction a cylindrical model of supportin ice edge:
a) decrease of effective thickness h´ by spalls (1, 2, 3) the sides of the ice plate and crushing of the middle section wedge (4) with model speed V= 3.2 m/sec;
b) – also with model speed V= 2.5 m/sec.

From analysis of the pictures of destruction it can be approved that the mechanism of ice destruction has the most complex character. The part of ice field movement energy at a contact zone of edge ice field and structure support surface is used for ice destruction, i.e. for horizontal and vertical cracks development, shear cracks, crushing of ice and displacement of products of ice fracture out of the contact zone. Energytransferried into the structure provides the deflection from equilibrium and creates the local forces onto its structural elements. The sizes, number and orientation of long vertical/horizontal cracks and shear cracks define the volume of compressed area in front of the support at the middle section of the field inclusive of its depth and height ***h´***. However, these parameters directly depend on the ice strength σ_i, ice field velocity V_{if} and ice thickness ***h***. But moreover, due to close contact in front of the support, the limited volume of strongly compressed ice (prism area) has appeared in front of the support. Ice within this area is crushing [50].

Tsuprik V.G. The forming cyclic loads on the offshore structures during ice field edge fracture. *Magazine of Civil Engineering*. 2017. No. 6. Pp. 118–139. doi: 10.18720/MCE.74.10.

Laboratory investigation of the cyclical destruction of ice in the interaction process with the structure models

The high price of full-scale measurement of ice forces upon real structures, natural ice and model supports subject to the impossibility of operational updating of the structure and ice field interaction conditions, provides the wide application of laboratory investigations. The first experiments for investigation of ice cover and hydrotechnical structure support surface interaction performed for laboratory model ice were developed by Afanasyev and others [51] at the ice basin of AANII. Two types of ice destruction in front of the support were revealed as a result of these experiments: destruction due to penetration and ice field stability loss. Contact force due to ice penetration is usually greater than in the case of ice field stability loss, so the calculating issue shall be referred to as ice penetration by the support. Besides, it shall be considered that contact pressure is decreased due to an increase of support width; ice destruction type shall be defined by its stability and ice velocity. Generally, a lot of works were devoted to investigation of these factors' influence against the mechanics of ice destruction, including ice pressure distribution laws subject to contact area of different supports. The completeness of physical-mechanical processes subject to contact ice destruction shall be provided by indenters with pressure sensors. It was used in works of Kamesaki, and others [52], Sodhi and others [53], Frederking and others [54], Takeuchi and others [55], Kryzhevich and others [56]. An integral configuration of the tensile contact field was obtained by applying a plastic strain gage film on the support model as it was described by Höderath and others], and tactile film with different colors depending on the pressure value per each section – Takeuchi and others. [58].

However, in spite of performed investigations, no applicable explanation of resonance phenomena, self or forced vibration subject to dynamic impact due to the interaction between ice and structure were revealed. The reasons for such phenomena can be subdivided into two categories: negative damping (Blenkarn, [4]; Määttänen [8]) and resonance (Sodhi [59]). Ice pressure force due to resonance frequency of structure vibration is described for both cases when the frequency of ice pressure force change due to ice destruction has increased the self-vibration of structure (Yue & Guo [23]; Määttänen [11]; L. Wang, J. Xu [61]; Huang & Liu [62]). Both types of structure vibration are usually considered as self-energizing; the mechanism of forced vibration shall be considered as an alternative. During 50 years, the group of scientists (inclusive of Määttänen and Sodhi respectively) has investigated the nature of structure vibration phenomena in order to define resonance or self-energizing or forced vibrations occurring in front of the structure subject to ice destruction load.

The first approach of scientists for justification of a concept explaining the formation of resonance vibration of the structure was based upon the investigation of the critical combination of parameters subject to ice destruction: i.e. its stability, support diameter, ice cover thickness and drifting velocity. ice strength was always considered as a maximum stability value defined by experiments with small samples for uniaxial compression σ_o. Most scientists have considered the dependency of this parameter from ice volume deformation velocity $\acute{\varepsilon}$ (L_{cr}) in front of the support due to ice field movement as a main feature. However in a series of experiments by some authors, this hypothesis has not found a definite confirmation.

The other approach for the ice destruction model in contact with a support was submitted by Sodhi [59]. His conclusions are based upon the results of full scale laboratory experiments with model ice subject to testing of 50–500 mm model piles against an ice load from a 50–80 mm ice field and a drifting velocity from 10 up to 210 mm/sec. Based upon testing results, Sodhi [59] has suggested to consider the resonance vibrations of flexible structures as a result of ice field action with ice destruction frequency, i.e. forced vibrations.

An idealized diagram of ice destruction due to shear was suggested by Sodhi and Morris [60] for description of the ice destruction as a single peak subject to law velocity of the indenter movement. It shall be noted that almost all ice thickness shall be wasted for chipping of the two prisms. Moreover, the length of the chipped section is equal to one third from the total thickness of ice.

The investigation the destruction of ice by mechanism chipping prior Sodhi and Morris [60] and further was performed by very much scientists [26-47], where the strength features of ice due to shear also were studed [60–62]. Chip is one of the dissipation mechanisms (release) of elastic energy of a compressed material by forming the free surface of new cracks. The chip is formed due to the realization the crack of lateral shear and developed within the compressed volume of ice subject to displacement of crack edges located at a definite angle to direction of compressing force. Usually different authors have explained the parameters of contact force of saw-tooth type during the time of interaction as a manifestation of this mechanism (or as per the length of destructed ice area).

The chips are featured with an unstable character that provides local destruction and loss of contact area. As per some works [42], for example, it provides the decrease of real thickness of ice h up to effective thickness h'. Moreover, these autors associate such decrease is referred with ice deformation velocity of ice field.

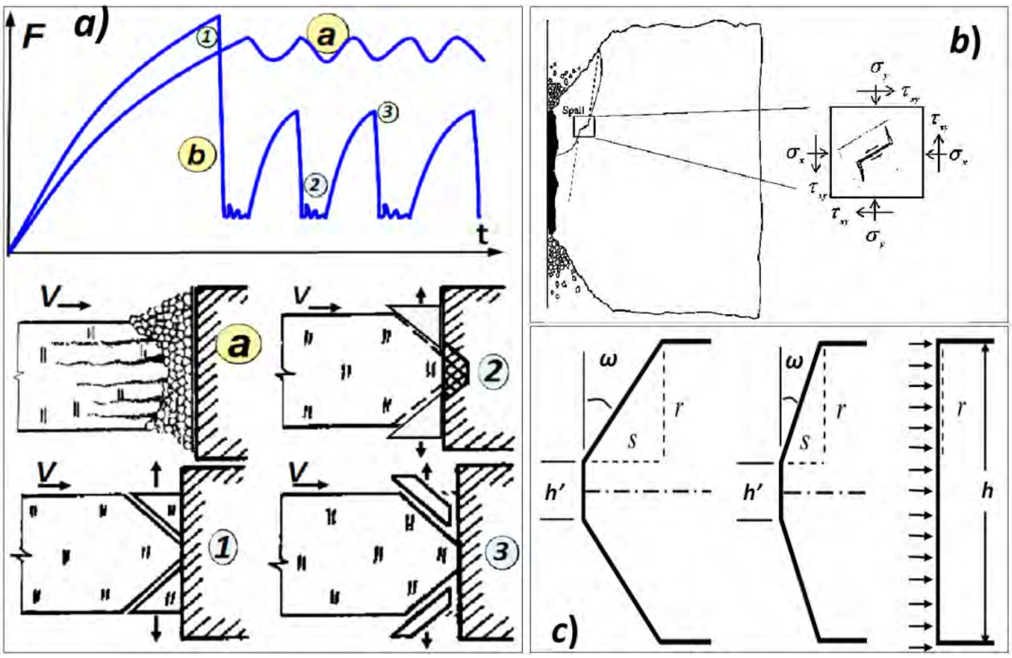

Figure 2. The fracture modes of ice on contact with a leg of structure as per Tsuprik V.G., 1984, [63, 64] a) crushing of ice and extrusion of products breaking the ice from contact area (a); the primary spalls (1) and alternation spalls with crushing of ice in the central part of the ice sheet (2-3). Formation of spall crack within the compressed area of a contact (a) and the diagram of edge leveling due to local spalls and crushing of compressed ice (d) at the central point of wedge as per Taylor and Jordaan, 2012 [65]

The Fig. 2-a shows the types of fracture of the contact edge ice field with the leg of the structure, proposed in 1984 by V.G. Tsuprik [63, 64] based on known results of the few research works done at the time, including studies of the author (Fig. 1). Depending on the strength and speed of THE ice field and the rigidity the legs of the structure, different modes of ice destruction may be experienced: beginning from a continuous soft crushing and extrusion of acrumpled mass of ice to the pure brittle mechanism of spalls of the blocks of ice or alternation spalls with crushing and extrusion of products breaking the ice in the contact area.

Considering the results of different investigations, Taylor and Jordaan [65] have suggested the probabilistic model of ice field edge fracture mechanism (PFM model - probabilistic fracture mechanics). It consists of a probabilistic approach for the initial process of ice field destruction associated with different defects of ice providing chipping of areas within the contact zone of the structure surface (see Fig. 2-b).

The results of all the above-mentioned investigations provides the possible explanation of the relationship between processes of spalling and crushing, when following one after another chipping, which creates a wedge in the ice field edge, where process develops of compressing and crushing i.e. leveling process of the edge line and formation of new large spalls (see Fig. 1; 2-c). Thus the process of crushing is a sequence of small spalls formed within the middle part of the contact area, with their release on the free surface or it occurs in the middle of the contact area in the high pressure zones. All these striped and mutually complementary processes represent the full process fracture of ice in contact with a structure.

Investigation of the parameters of cyclical ice load for real structures in natural conditions

The direct measurement of ice pressure forces using panels provides important initial information for the development of theoretical models for structure design. The first scientists applying such methods were Peyton [3] and Blenkarn [4], who in 1966-1970 obtained the records of ice loads acting upon structures located within the Cook Inlet in Alaska. Määttänen [8,11] has investigated ice forces providing the vibration of lighthouses within the Gulf of Bothnia. Engelbrektson [9, 67] has performed full scale measurements of ice pressure against the Norströmsgrund lighthouse located within the Gulf of Bothnia. He noted that the ice pressure against the support depends on the ice destruction character, i.e. the ice field drifting velocity. Kärnä and Turunen (1990) have suggested the four types of models for an identification of the ice pressure force; they provide different types of structural measures.

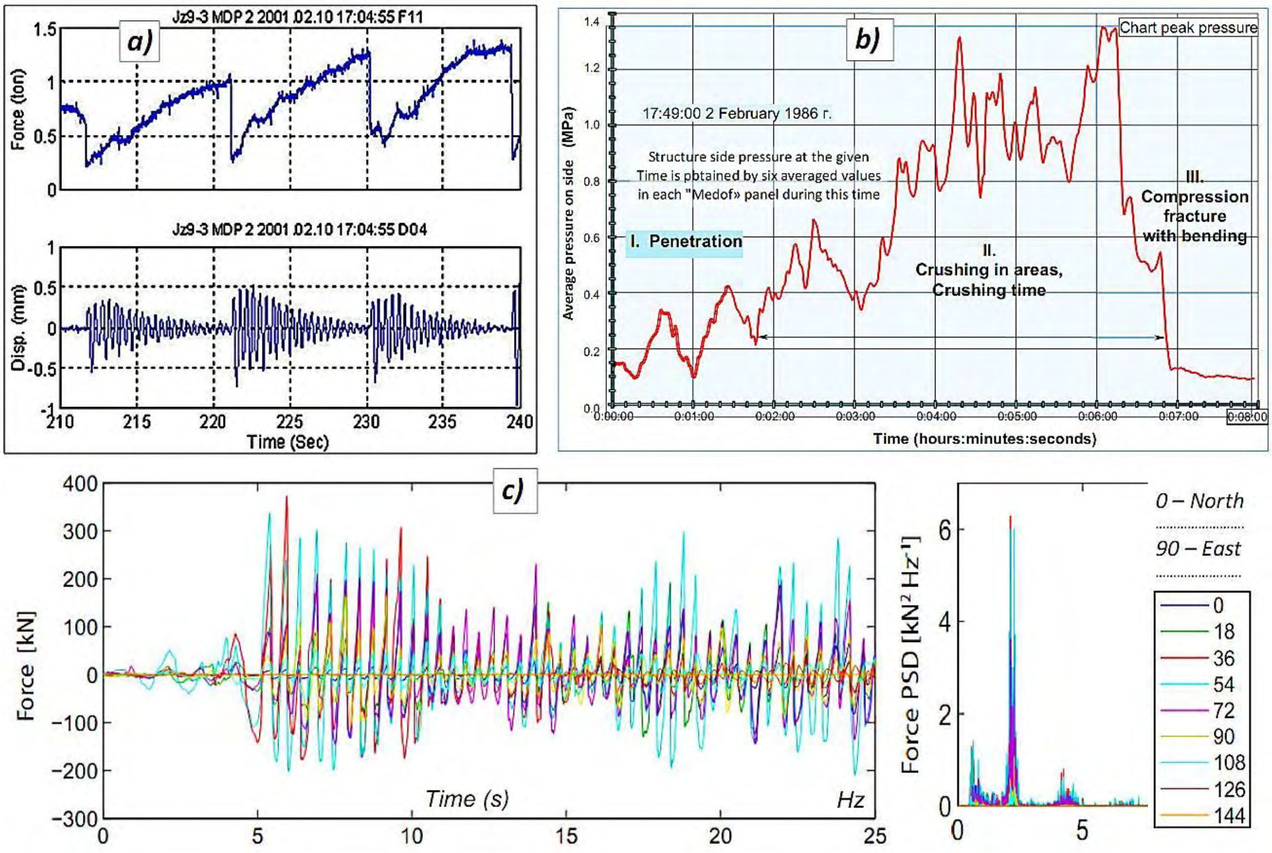

Figure 3. Record of ice loads on legs and vibration of structure subject to cycle destruction of ice: a) - as per Yue et al. [69], b) - as per Vershinin et al. [48], c) - as per Nord et al. [25]

In order to develop this idea D.S. Sodhi [68] in 2000 at the Bohai Gulf and Yue and others [69] have performed the investigation of ice thickness and temperature influence against the upper conversion velocity (***V₂***). These investigations were purposed in qualitative and quantitative analysis of conversion between continuous crushing (CC) and interrupted crushing (IC) on the basis of the model's reaction measurement. These authors have performed full-scale investigations of ice field and structure interaction. These investigations were featured with a simultaneous recording of the ice impact time, its velocity and structure movement. The authors of this investigation [69] have concluded that the contact force shall represent the function of relative shear of structure and relative velocity between structure and ice field edge; moreover, time shall be constant.

Besides the special strain gage panels, in order to perform the investigation of structure vibration, acceleration indicators, tilt indicators, seismographs, etc. were used. They provide the possibility to record the detailed distribution of contact pressure of ice in the contact area, to investigate the functional dependency of peak values of ice force and frequency subject to conditions of ice field and structure interaction. Among these factors area ice field velocity, ice thickness and ice strength. Such methods were used for structures at the Gulf of Bothnia and the Bohai Gulf, as well as the Molikpaq Platform. Some results are given on Figure 3.

This figure shows a static impact of ice and the corresponding vibrations of the platform foundation structure within the Bohai Gulf (Fig. 3-a) as per Yue and others [70], Fig. 3-b shows the typical destruction of an ice field for the Molikpaq platform [48]. Fig.3-c shows the records of ice load acting upon strain gage panels located at the foundation of a lighthouse subject to different angles of ice field drifting and the diagram of ice destruction frequency distribution within the Gulf of Bothnia (see Fig. 3-c) as per [25].

Based upon the brief investigation of ice load cycle parameters for real structures in natural conditions it can be noted that structure vibrations occur as its reaction to ice destruction until a certain depth. In the case of small velocity ice field movement, the transfer of kinetic energy from the ice field to the structure happens as a separate impulse (see Fig. 3-a) that causes the deviation of the structure from equilibrium state and accumulation of elastic potential energy in the contact zone of ice. Ice destruction in this volume release support of structure from ice pressure and construction reconstitutes the statically equilibrium due to elastic potential energy in material of structure support. In the time reconstitutes of happens extruding of ice destruction products from the contact area. Until to new contact can to pass the time depends from ice field velocity and the ice destruction depth. In the case of high velocity of ice field, depending on structure rigidity and strength of ice, the transfer of kinetic energy into potential energy of ice compression with further destruction can provide an increase in structure deviation (see Fig. 3-b), i.e. vibration. In this period of IF-IRS interaction, free fluctuations of the structure are possible. If the frequency of ice destruction with the same parameters is will close to one of the self-vibration frequency of the structure, resonance phenomena can occur (see Fig. 3-c) and such situation can cause loss of stability and destruction. Practically, such phenomena can occur for structures with different rigidity as reaction structure to different combination of main parameters, such as ice field thickness, its velocity and ice strength (Fig. 4).

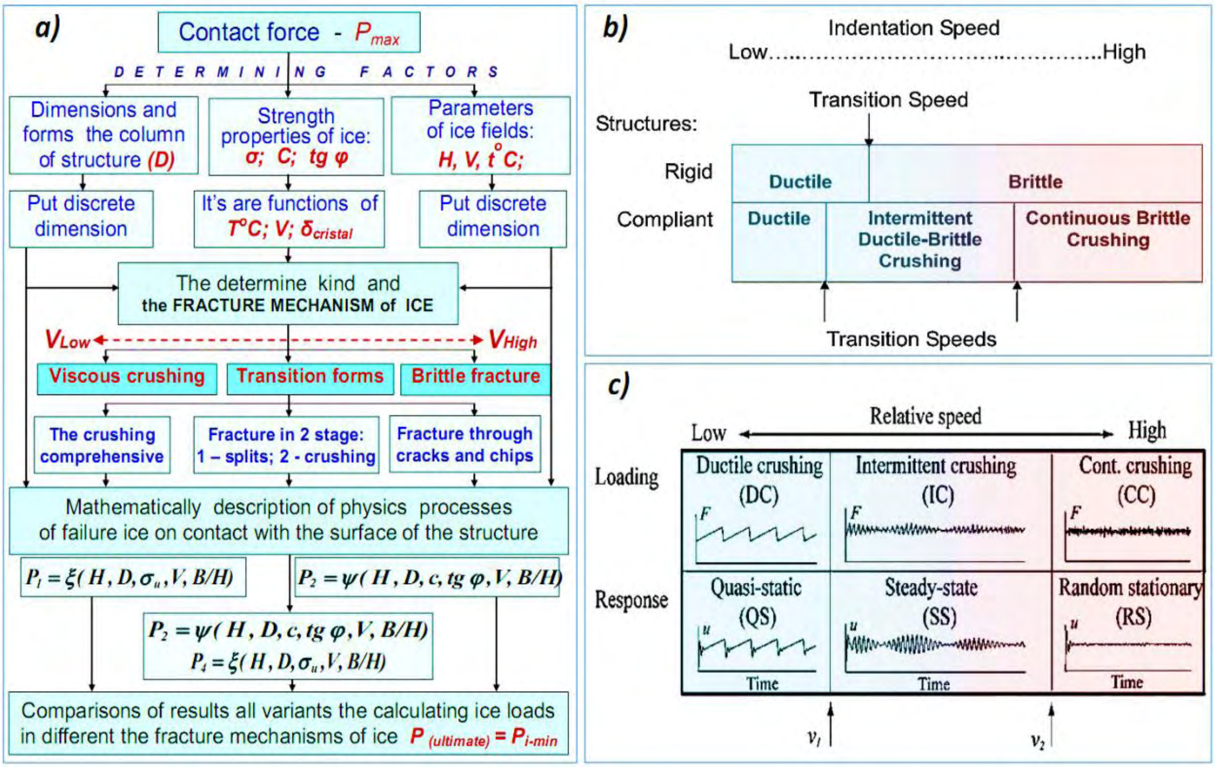

Figure 4 The classification scheme of possible types of destruction of ice with different combinations of factors that determine the fracture properties of ice in the process of interaction of IL-IRS: a) By on studies of Tsuprik.G., 1984 [63,64]; b) –by D. Sodhi, 2000, [68]; c) –by Bjerkås M. and Skiple A., 2005, [66]

Thus, the analysis of the results of the studies of all the phenomena occurring in the process of interaction between IF and IRS both in natural and experimental conditions showed that it can be proven that, depending on the speed of the IF, the rigidity design of IPC and the stiffness (strength) of ice, all possible modes of IF-IRS interaction can be divided into three types. An integrated approach to the classification of all the phenomena described here was submitted in 1984 in the works of V.G. Tsuprik [63, 64]. This provision was later recognized by the majority of researchers, except at very low speed mode when there is creep (fluidity) of ice, and adequate schemes were presented in the works Sodhi [68] (Fig. 4-b) and Bjerkås and Skiple [66] (Fig. 4).

The methods of theoretical modeling of the ice-structure interaction process

The first model of ice fracture in contact with the ice field is the "classic" model, created back in the first half of the 20th century and is currently represented in normative instruments [1, 2] in the form of the " K.T. Korzhavin formula". This model represents the most elemental method of calculation of the maximum value of the contact force of rigid motionless structures with the edge of a drifting ice field.

But, as shown above in this paper, the interaction of ice field and structure can develop according to different scenarios, which are determined by the peculiarities of the fracture of ice depending on its hardness (strength) and loading conditions in each particular case, given the flexibility of the legs of the structure. In terms of methodology and organization, the IRS design should be elaborated by algorithms for ice load calculations, understandable and adequate to all the scenarios of development process of interaction of IF-IRS. Such algorithms should be at least three and they should be based on models that describe the process of interaction between the IF-IRS on three completely different scenarios. For quasi-static processes, peak ice force occurs when the limit is reached, the plasticity of ice and this ice strength criterion is necessary for use in the calculation method of ice load, which should be based on the model of continuous ice fracture and extrusion of the products of ice destruction from the contact area. In other cases, the models of elastic-brittle fracture of ice should apply, or models combining several types of ice fracture. There are possible cases of the emergence of phenomena of autooscillations in the IF-IRS system, caused by the cyclical destruction of ice. To calculate the force of the impact of ice on the structure and its period of oscillation, dynamic equations should be obtained where the limit value of ice strength parameter necessarily should be taken into account, which regulates the transition to the beginning crushing of ice in a stress volume in edge ice field and load-shedding on the structure in case of an excess of the limit value for this parameter.

Data from many experimental observations becomes the basis for the development of an analytical description of the oscillation processes and the structure vibration during its interaction with a drifting ice field. Presently, there are a lot of theoretical models describing the dynamic interaction of ice and structure. Now many models are known: Interaction model subject to insignificant displacement; brittle fracture model; model of continuous crushing and displacement of ice; deformation’s models, for example those with deactivating ligaments; elastic-brittle models based upon Hooke's Law; Mohr-Coulomb model of bulk material; hydrodynamic and spectrum models; negative friction models and relative displacement; model of vortex-induced vibration (VIV); et al. [4, 10–12, 20–26, 31, 48, 49, 74, 80].

For a full and adequate representation of all the possible variants of the mechanical processes occurring during interaction of a drifting ice field with structure, it is probably enough to explore the three "benchmark" types of theoretical models proposed by different authors as a basis for using algorithms of ice load calculations. These three classes of models are very briefly discussed below.

Model of periodical crushing with spalls

Ice fracture by periodic crushing mode is characterized by the formation spalls on the ice field edge and a reduction of the ice thickness up to the effective – $h^{/}$ (as opposed to actual ***h***, Figs. 1 , 2), which depends on the ice deformation speed. As the speed of the ice field V_{if} increases, the value $h^{/}$ decreases, as the size of the spalls grows in the zone of ice fracture in contact with the surface of the leg. During alternation of processes of spalls-crushing are occurring recession and increase of the ice load and it has a saw-tooth type because the contact area is changing. Such models have been developed since the late 1960's and the complex interaction process of between IF-IRS was effectively described by the model of a system with one degree of freedom. At the base of such models lies the unified concept of periodic fragmentation of ice at the leg of structure, proposed by H.R. Peyton [3] in the years 1968 and 1969. Matlok and co-authors [69] had used Peyton’s concept and proposed a revolutionary idea that "the fracture of ice occurrs at a certain size” and they presented a model that can describe the reaction of the structure upon impact of an ice field acting at low and high speeds.

In order to demonstrate their hypothesis, many authors apply the Matlock model [69], which describes well enough the fluctuations of the structure close to the relaxation oscillations. A mechanical analogy of this well-known model is shown in Figure 5-a. In this model, moving ice field is presented in the form of a simple beam with many elastic cantilever teeths, that moving with a speed V_{IF} in the direction of a single-mass model of the structure (***M***) with elements of elasticity (***K***) and damping (***C***).The teeths are in contact with a cantilevered elastic-pliable model of support rigidly fixed at its base.This model has the ability to receive "sawtooth" loads on the structure (fig. 5-b), because the destruction of the teeth occurs only for the critical deformation of S_{cr}. The S_{cr} value can depend on the speed of the ice field, and the thickness and height of the teeth (fig. 5-a) allows to simulate the strength and elastic properties of ice. Changing the distance between the tines can simulate the length of the breaking ice zone L_{cr} before thecontact surface of the leg of the structure. The length L_{cr} determines the frequency of the ice fracture and, consequently, the period of oscillation structures ***T*** in the models of some authors, such as Yue et al. [70] and some others.

Variations of these parameters on this model, a different character (type) of fracture the ice can be obtained, which can vary from visco-plastic to brittle (fig. 5-b) and mainly depends on the speed of the ice field V_{LP} and the stiffness of the ice. The equation of this mechanical process, implemented this model in [69] is written in the form:

$$M\ddot{x} + C\dot{x} + Kx = F(t), \tag{1}$$

This non-inertial model of elastic-brittle type ice fracture simulates the relaxational oscillations of the structure and allows to obtain the ice load by numerical methods in the form of a sawtooth curve, where each peak starts to grow from zero load. This effect is achieved by the fact that the limit value of the deformation of each tooth S_{cr} must be entered in advance in the calculation. The model of Matlok et al. [73], does not allow to "grab" the resonant frequency of the structures because in its mathematical interpretation, the periodicity of the forces as a function of time is not entered.

Significant development of the theory of ice self-induced vibrations in the process of interaction between IF and IRS was achieved by the research of K.A. Blenkarn [4], who in 1970 stated that the structure and ice field must be seen as a system of related elements. Additionally, this researcher, based on the results of the experiments of Peyton [3], who researched the reduction of ice strength by increasing its loading rate (Рис. 5-d), proposed to "consider the ice forces to be a function of the relative velocity between the far-field ice V_{if} and the structure $\dot{X}$". Using these three hypotheses, K.A. Blenkarn [4] proposed to describe the oscillation process in the IF-IRS system under the influence of the force F(v) to apply the known theory of oscillations that uses the equation of motion of the body with "negative damping " [71], which is a function of the relative velocity $V_r = (V_{if} - \dot{x})$ of the two interacting system elements LP-IPC. His model is described mathematically as follows:

$$(M/g)/\ddot{x} + C\dot{x} + Kx = F(V_{if} - \dot{x}), \tag{2}$$

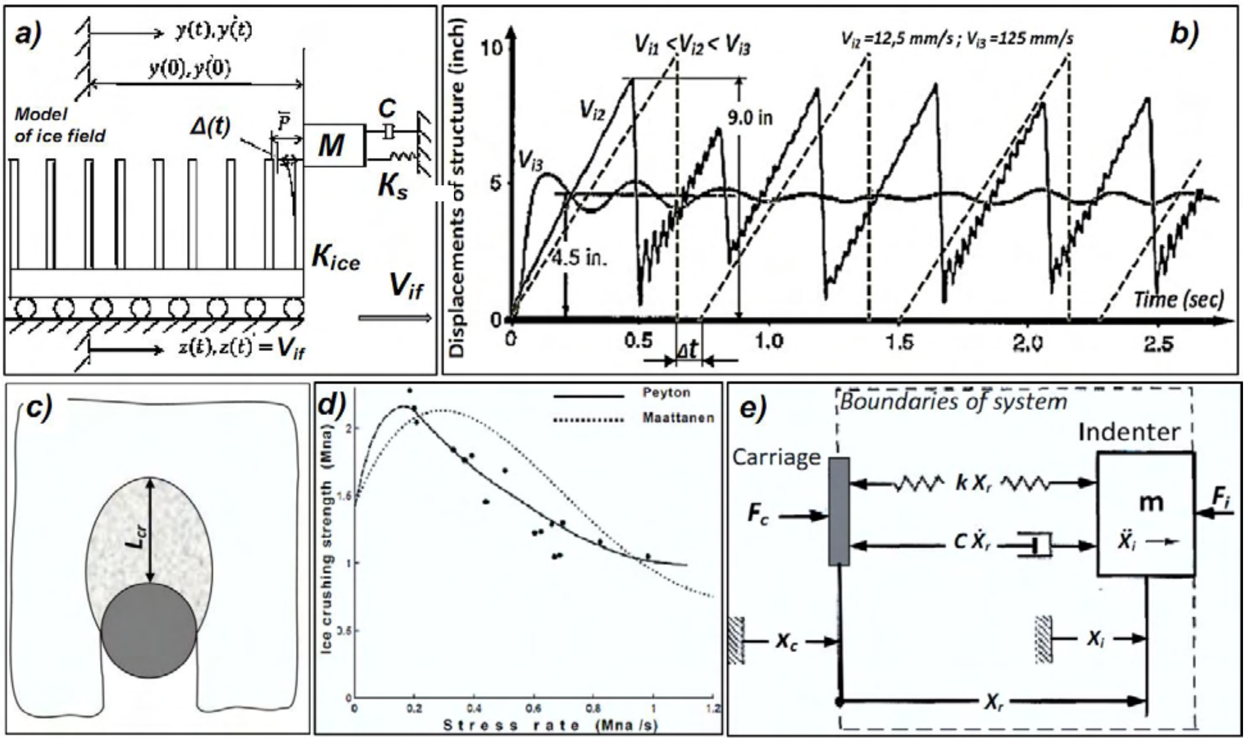

Fig. 5 Models of interaction for IF - IRS system: a, b) –Matlock et al. [69]; c) –Yue et al. [70]; d) –Dependence of strength of ice loading speed as per Peyton [3] and Määttänen [11]; e) –Sodhi model [72]

Next, given the low values of displacements of structures and deformations of ice, K.A. Blenkarn [4] rewrote the force function F as the formula (3), which then was subsituted in formula (2) and formula (4) was obtained:

$$F(V_{if} - \dot{x}) = F(V) - \dot{x}\,\frac{\partial F(V)}{\partial V} \tag{3}$$

$$M\ddot{x} + \left(C + \frac{\partial F}{\partial v}\right)\dot{x} + Kx = F(v) \tag{4}$$

Thus, the "negative damping” concept entered by K.A. Blenkarn [4] for the system IF-IRS based on the use of the dependencies of ice strength and its download speeds, proposed by H.R. Peyton [3] (Fig. 5-c), explains the emergence of autooscillations in the IF-IRS system. The ice self-excited oscillations in the system occur if the friction coefficient $\partial F/\partial v$ becomes negative and is numerically greater than the structure damping factor $\boldsymbol{C}$. Then the equation 4 will be the equation for "negative net damping”, and the preponderance of negative friction ($\partial F/\partial v$) over positive ($\boldsymbol{C}$) over time will lead to an increase in amplitude of the structure. In addition, K.A. Blenkarn [4] experimentally determined that the frequency of ice load peaks corresponding to the points of ice fracture, is governed by the ice field speed $\boldsymbol{V_{if}}$, the structure flexibility $\boldsymbol{K}$ and the rigidity $\boldsymbol{K_{ice}}$**,** depending on the relative velocity of the structure and the ice fields $\boldsymbol{V_r}$ (download speed of ice). Blenkarn K.A. [4] also confirmed that a simple case of "intermittent" interaction can be described by the model presented by Matlock et al. [69].

The concept of "negative damping” is received quite widespread among researchers. M. Määttänen in 1977 [11] proposed a mathematical model for the description of autooscillations in the IF-IRS system, which has many degrees of freedom. Here, the model has also been obtained by combining the equation of structure motion and ice load as the relative velocity function $\boldsymbol{F(V_r)}$ in the form of the external friction characteristic. The load was adopted as on Fig. 5-d, where each point on the curve is the limit strength of one sample tested on uniaxial compression with a constant loading speed. This model was further developed by Wang & Xu [61], Vershinin et al. [48] and other researchers. But the concept of "negative damping and self-excited vibration" was constantly subjected to criticism and disagreement by another researcher of this problem Sodhi D.S. [59] for many years. This author considers the oscillations, emerging in the process of IF-IRS interaction and explains its position by the existence of a number of inconsistencies, which challenges the concept of Blenkarn and his followers. The following discrepancies are noted:

– The model with "negative damping" describes an idealized physical process in which at each moment of time is has a place the maximum stress state on the eve of the beginning of the ice crushing in the contact zone, and the initial contact force cannibalizing is determined by the value $\boldsymbol{V_r}$ and the specified strength sample $\boldsymbol{R_c(\dot{\sigma})}$;

– mathematically not permissible, when we are looking for a solution to the time-dependent interaction between solids, but the strength of ice is taken only as point on the "stress-deformation" curve, obtained at the time of the ice sample destruction during testing;

– physically, it means ignoring the real physical-mechanical properties of ice, described by the curve of tests on strength of ice with respect to time when determining a power function $\boldsymbol{F(t)}$ for the equation (1) as a similar dependency curve by Peyton R. [3] (fig. 5- d);

– the concept is not a confirmed hypothesis, because it is based on estimates of the negative damping, rather than specific measurements of key parameters of the process.

Sodhi D.S. [72] offered its interaction model IF-IRS (fig. 5-e). He held very carefully prepared experiments in the "closed" mechanical system that controlled all the factors and ***measured changes of energy*** and values of all variable parameters that could influence the parameters of the interaction model IF and the leg of the IRS. The results of these experiments have shown that the process of interaction between IF-IRS is always a process of dissipation (transfer) of kinetic energy of the IF in ice array and no transfer of energy from the ice field to the structure. On this basis, Sodhi D.S. [72] excludes any possibility of oscillations induced by ice as a result of the negative damping, as proposed Blenkarn [4] and Maattanen M. [11].

Despite the existence of contradictions, considered by the two points of view on a single phenomenon, offering new models as the type considered here, that are formed using the hypothesis of negative damping. In every model, the instant ice crushing strength parameter is considered, and isdefined by tests of small specimens for uniaxial compression and the $\boldsymbol{\sigma_o}$ parameter of this strength depends on the speed of sample loading, as shown in Fig. 5-d.

The "continuous” and ”layer-by-layer” crushing models

The model identified in the header, made up of a separate group of LF-IRS interaction models, was formulated at the beginning of the ice fracture modeling, developed during a long period and used at the present time. First, based onmodels of such type was a "hydrodynamic model" for the fracture of ice by Kurdumov and Heisin, proposed in 1976 [73], shown in Figure 6-a. These authors’ model was based on the concept of extruding products of ice fracture from contact zone. Here, a mechanism for breaking the ice is not considered, and the model is based on the hypothesis of the continuous change of the physical state of the ice from the solid phase of the rear sight (intact) of ice to the destructed state in the form of an ice crumb.

In a work of the author [74], it is also represented a developed model of layer-by-layer fracture of ice during dynamic interaction between IF and the supports of the IRS (fig. 6-b). Products destruction of ice occur as the result of the transition of "solid ice" by in a layer-by-layer mode from a pre-fractured layer, located before the frontal boundary (front) of destruction in to new state as a layer of crushed ice (crumb), which extrudes from the contact area. This transformation is occurring in end process increase of contact pressures in moment reached limit of the volume potential energy deformation accumulated in the pre-fractured layer.

In models of such type is not direct contact with the intact ice during interaction and at least, most of the interaction forces transferred through the layer of crushed ice or ice-crumb, as shown on Figure 6-a,b,c. In the moment where peak pressure will achieved in a compressed layer of damaged ice, occurs crushing this layer and followed by an instantaneous drop of the contact forces, the crushing phase ends and occurs change the type of process on to new process - phase of the clearing. In these types of models the contact force during process interaction variate in accordance with the phase of the crushing and clearing. The effort, required to extruding the fragmented ice In such models, are increased synchronously with the approaching to zero thickness layer of ice crumbs.

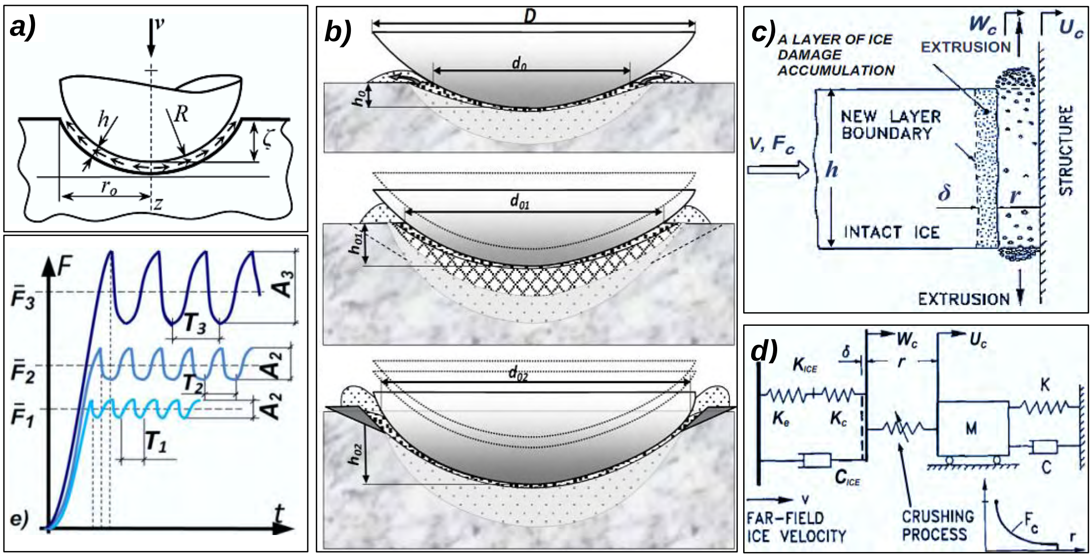

Figure 6. Models continuous crushing: a) – representation of a hydrodynamic model Kheisin et al. [73]; b) – layer-by-layer model of ice fracture by Tsuprik [74]; d),c) – model continuous crushing by Kärnä and Turunen [75]; d) – model destruction of the ice layer by Jordaan and Timco [76]; e) – different of contact force graphics for model of continuous crushing of ice for one speed ice field, but different values ice rigid

The authors of the work [76] use the same approach as in [73-75], introducing the body of ice field in several areas: far from the surface, the ice is in pristine condition (intact ice); closer to the contact surface, ice has a layer badly damaged by cracking; between this layer and the surface, structures are formed by a layer of fractured ice (ice crumbs).

The contact force during the process of interaction IF-IRS in models of this type are weakly changing when the transition fracture process from the phase of crushing to the phase of cleaning, if the strength of ice is low. But with the increasing strength of ice, such models can describe the periodic process of the ice fracture and, consequently, periodic change of amplitude (***A***) and the period (***T***) of the peaks of ice load ***F*** on the structure (Fig. 6-e). Thus, the layer-by-layer mechanism of breaking the ice with a relatively high strength can generate a cyclical ice load on the structure, causing it to wobble. Amplitude and period of oscillation of structure are defined by its rigidity K_D and the rigidity of ice K_{ice}, which depends from the strength of ice R_c and from the conditions of its contact with the structure.

Experimental-theoretical method for dispensing of energy consumption by the destruction of ice

Given that the considered system is closed, the most complete processes of element interaction within this system can be described by using the law of conservation of energy. In such approach, the main energetical processes in the phenomena of oscillations of the IRS are processes of moving the kinetic energy of the ice field into elastic energy deviation of the structure inequilibrium and the elastic energy of compressed volume ice and potential energy dissipated in this part of the ice. At the same time, on the basis of conservation laws, it is clear that in the process of the interaction, part of the kinetic energy of the drifting IF is spent irretrievably on the fracture of ice.

As far as we know, the solutions of task of relaxational oscillations in the IF-IRS system by method for solving the equation of energy balance has not yet been cited. In paper [48] the scheme of energy consumption in the "ice-structure" system was viewed, but in the mathematical description of the dry friction model, the dynamic processes for the ice field and in the structure is described by of two differential equations of motion, related through a common for these elements of unified system by force their contact interaction. But the strength of ice in explicitly form in to the equations is not included. At the same time, in different years a number of researchers have suggested the use of the specific energy of ice fracture ε_{cr} as a parameter of the strength in the calculation of ice load [72, 78–80].

The mechanism of oscillation generation in the system IF-IRS

Consider IF and IRS not as two separate objects, but as a system in which those objects are interacting among themselves, new phenomena are spawned, which are not characteristic for each of these objects outside the system. Such phenomena are the process of the ice fracture and the structure oscillation process. We assume that the size of the ice field is large, its mass and its velocity change slightly during interaction and in the calculation of the values of these parameters, the kinetic energy IF can be considered as unchanged, and its mass and speed as constant values. With these assumptions, the interaction of the elements in the system IF- IRS can be regarded as a function of the active, autonomous, conservative self-excited autooscillation and self-adjusting system of the relaxational type (fig. 7). Usually, the mechanical behavior of this system is described by linear differential equations. But this approach does not take into account the cause of the hesitation, i.e. the nature or source of the emergence of a periodical force.

Previously, the possible scenarios of development of the process of interaction of the elements of the system IF-IRS were analysed. So, if the speed of movement of the ice field VIF= Vi1 is small (fig. 5-b), and ice has high strength RC, the ice load on reliance will have the appearance of individual peaks with gradual rise of force and abrupt it decline in moment of ice fracture. Breach of contact may occur after shift wedge-shaped blocks of ice on the bottom and top surfaces of the ice field (fig. 2-b,c). The structure, freed from the pressure of the ice field will begin to reverse movement towards the ice field, which continues to move, and then all processes in the system reoccur. The beginning of the next contact may come through the time interval Δt (fig. 5-b). When the speed of the ice field (IF) monotonically increases $V_{ij}>\ldots > V_{i3} > V_{i2} > V_{i1}$,load peaks are followed more frequently and at high speed IF and smaller ice strength, the ice load curve has slightly noticeable extremes (a variant of the curve in Fig. 5-b V_{i3}).

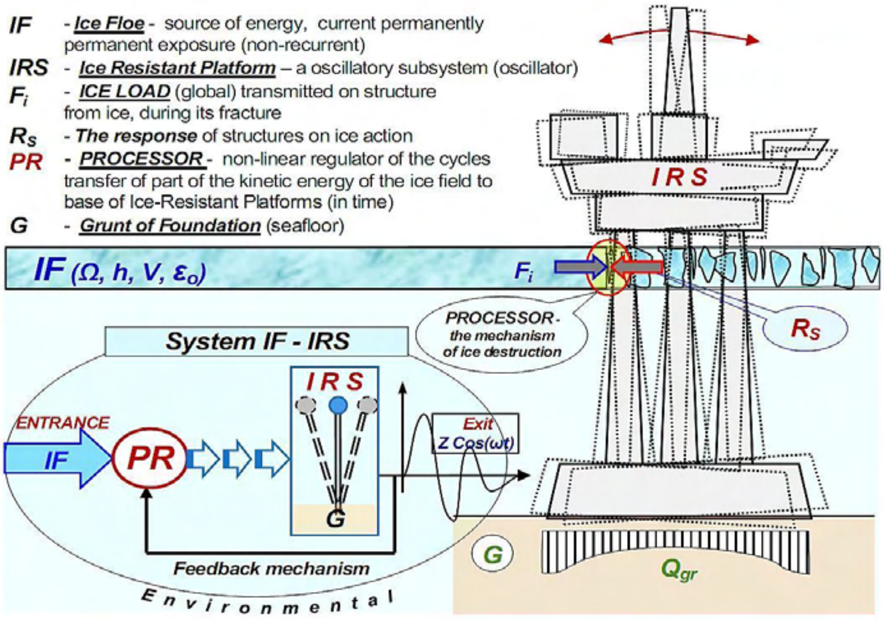

Figure 7 Image and functional scheme of “IF – IRS” system and subsystem “IRS”, in their emergence the autooscillations

Namely, such nature of mechanical processes and such alternation in the IF- IRS system generates a cyclical sequence of increase and decline of ice load on a structure which can lead to a self-exciting oscillation of IRS when exposed to ice fields. At the same time, as can be seen from the theory of vibrations [71], the autooscillation in systems is usually occurring due to periodical transfer of energy from the source to vibrating element of the system, i.e. in our case from IF to IRS.

Therefore, hesitation of the structure will be supported by the injections of energy taken from the moving ice field and there should be a mechanism for dosing of the output kinetic energy of the ice field and its transfer to the structure. Perhaps the authors of work [76] Jordaan I.J. and Timco G.W. speculated in the same manner in their model of ice destruction and therefore they designated the location of the process of transfer of kinetic energy from the ice fields to the structure between the images of these two elements of system IF-IRS. (Fig. 6-d).

Dosing and frequency of transfer of kinetic energy from ice field to structure performed due to the account of the functioning of the processor of the system– during realizing of the mechanism of fracture of ice (PR on Fig. 7), which acting as a ratchet mechanism in a watch or pressure regulator valve a in steam machine – but here as the regulator cycles of hesitation process.

The specific energy of mechanical fracture of ice as a regulator of structure frequency oscillations

Consider the approach to a structure that has the transverse dimension supports (D) and stiffness G_S, an ice field with certain combinations of V_{IF} speed, thickness h and hardness (strength) of ice Gi (Fig. 8-a). Description of the energy transfer process in an array of ice from the leg of structure and the potential energy accumulation mechanism that acting in deformable volume of ice, in this work are taken according to the concept, described in [77, 78].

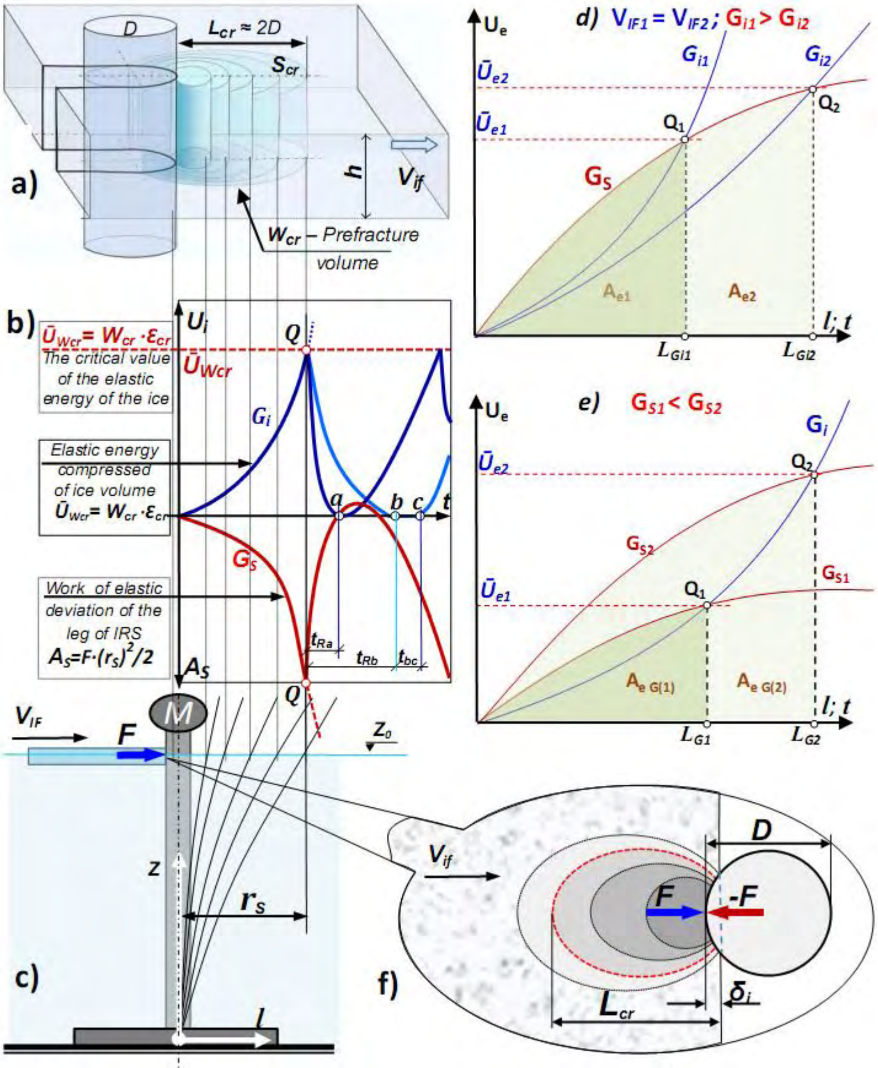

Figure 8. Illustrations the occurrence of cyclic ice loads during process interaction of ice field edge with the surface of leg structure

Tsuprik V.G. The forming cyclic loads on the offshore structures during ice field edge fracture. *Magazine of Civil Engineering*. 2017. No. 6. Pp. 118–139. doi: 10.18720/MCE.74.10.

We write the equation of balance of the ice field kinetic energy consumption $\boldsymbol{\Delta U_{IF}}$ in the contact zone by its transmission into elements of the system IF-IRS, in which it will distributed, in the form of elastic energy ($\boldsymbol{\Delta U_e}$) during the same interval:

$$\Delta\, \boldsymbol{U_{IF}} = \Delta \boldsymbol{U_e}\,. \tag{5}$$

In the active phase of interaction, the influx of the kinetic energy of the ΔU_{IF} from the IF in the contact area during one loading cycle occurs continuously, the level of potential energy U_{Wcr} in the strained volume of ice field W_{cr} increases (Fig. 8-a,b) and at the same time, work A_S is exerted to reject structures (Fig. 8-b,c). From the conservation laws are known that physical sense have not the full numerical value the value of the potential energy , but the change of its numerical value during deformation , only in this case it represents the energy of the elastic deformation. However, considering the condition of additivity, the dissipation energy ΔU_e of the system equals the sum of energy (of work) used on the elastic deviation of the structure ΔU_S, including the dissipation energy in the material and in the constructions of the structure, and the energy ΔU_{Wcr}, stocked within the ice array at its edge area, including the energy dissipated in ice:

$$\Delta \boldsymbol{U_e} = \Delta \boldsymbol{U_S} + \Delta \boldsymbol{U_{Wcr}} \tag{6}$$

In the process of interaction with the IF-IRS at any moment prior to the time of destruction of the ice in a strained volume, according to Newton’s third law, the balance of the changes in the energies of elastic deformations of the curved leg structure and the compressed volume of ice will take place.

$$\boldsymbol{\Delta U_S} = \boldsymbol{\Delta U_{Wcr}}; \quad \boldsymbol{\Delta U_e} = \boldsymbol{2\Delta U_{Wcr}}. \tag{7}$$

Therefore, the balance – equality (5) in the process of interaction between IF and IRS, subject to (7) may be breached only in 2 cases: due destruction of the structure (stability loss) or due destruction of the ice. Staging of the considered problem here assumes to take into the calculation the size and parameters of sustainability or local strength of structures that withstand the possible greatest ice load. This means that a force that causes the destruction of ice, i.e. ice load on structure, needs to be determined on the basis of the requirement of destructing the ice. Therefore, it is necessary to examine the parameters and conditions for the destruction of the ice that must be included in formula for calculating the boundary conditions for the energety state of the strained ice volume W_{cr}.

A mathematical description condition of the beginning of the destruction of the ice in the final stage of its deformation, not only has a great theoretical value for this unique material, but also a practical importance for solving the problem of ice loads, as described in this work. Here, the magnitude ε_{cr} - specific energy of mechanical fracture of ice was adopted as a criterion of ice destruction. The theoretical basis of this criterion is the theoretical model of layer-by-layer destruction of ice and methods for experimental determination of this value are given in the works [74, 79, 80, 83].

Thus, the key parameter governing the cyclicity of the ice destructed is a critical threshold value of potential energy of deformation ε_{cr} accumulated in the unit volume. The exceeding of this threshold energy shall cause the destruction of the ice and breaking of the contact ice-structure for a while. To achieve critical stress state pre-fracture in the strained volume of ice W_{cr} it is necessary to spend energy (Fig. 8-a, b):

$$\boldsymbol{\overline{U}_{Wcr}} = \boldsymbol{W_{cr}} \cdot \boldsymbol{\varepsilon_{cr}}\,. \tag{8}$$

Changes in the energy state of the interacting elements of LP-MLE system, considering full synchronization in time of the consideration processes (6), occur is due perform work by force $\boldsymbol{F}$ as on the deviation of the $\boldsymbol{r_S}$ support structure in the direction of movement of the ice field ($\boldsymbol{A_S}$ - Fig. 8-c), and on embedding of the support into the edge of the ice field in the opposite direction ($\boldsymbol{A_I}$ - Fig. 8-f) on $\boldsymbol{\delta_i}$ depth.

$$\boldsymbol{\overline{U}_S} = \boldsymbol{A_S} = \int_0^{r_S} \boldsymbol{F} \cdot \boldsymbol{d(r_S)} = \boldsymbol{F} \cdot \frac{\boldsymbol{r_S}}{\boldsymbol{2}}; \tag{9}$$

$$\boldsymbol{\overline{U}_{Wcr}} = \boldsymbol{A_i} = \int_0^{\delta_i} \boldsymbol{F} \cdot \boldsymbol{d(\delta_i)} = \boldsymbol{F} \cdot \frac{\boldsymbol{\delta_i}}{\boldsymbol{2}}, \tag{10}$$

The maximum ice load on the IRS can be determined from equation (8) and (10) describes the limiting value of the potential energy of the elastic deformation in ice volume $\boldsymbol{W_{cr}}$ created by the work of the contact force, provided to the embedding leg of structure in the ice at a depth $\boldsymbol{\delta_i}$:

$$\boldsymbol{F} = \boldsymbol{\varepsilon_{cr}} \cdot \boldsymbol{f(W_{cr}/\delta_i)}\,. \tag{11}$$

The dependence of the volume of ice fracture and the depth of an elastic embedding structure in the ice is the subject of a separate study.

Results and Discussion

The important result of all studies should be considered understanding that the phenomenon of fracture of ice is the cause and source of other phenomenon - vibrations of the IRS. The phenomenon of the destruction of the ice during IF-IRS interaction has a dynamic periodic nature and the nature (mechanism) of ice fracture determines the frequency and amplitude of the encountered oscillation in constructions. It is proposed in the work that the experimental-theoretical method of dispensing the energy costs for the destruction of the ice revealed that the essence of the phenomenon of cyclical ice loading is the periodic violations of the energy balance of the two main simultaneous processes of accumulation of elastic energy in the structure deviating and accumulating elastic deformities in ice volume. For the flexible structure by the main parameter, governing the processes of elastic deviation of the IRS and the compression of the limited volume of ice on the front surface of the structure leg is the size of the dose of kinetic energy of the ice field, which is consumed on the work for deviation of the structure and for compression of some amount of ice in the array edge of ice field to its critical level stress state.

According to diagram Fig. 8-b,c, the critical value of ice destruction energy $\bar{U}_i$ in condition of compression ice volume at a contact zone shall be determined for each calculating event by using the ice field thickness h and its velocity V_i (parameters of ice field kinetics) and rigidity (strength) of ice G_i, defined by the parameter specific energy fracture of ice ε_{cr}. A mechanism of regulation of the limiting number of the spent kinetic energy of the ice field, that is, the conditions of equality (5), is based upon the interruption of the energy transfer process from the ice field by a gap of contact IF-IRS after the compressed ice crushed. This mechanism shall be considered as a basic condition for emergence of self-vibration in IF–IRS system. Figure 8-d shows the graphical interpretation of the results obtained for the two different cases of strength parameters of ice fields (stiffness) G_{i1} and G_{i2} interacting with a structure leg with rigidity of G_S. Figure 8-e shows graphs for the case of two structures with varying stiffness (G_{S1}, G_{S2}), interacting with the ice field with constant stiffness ice (G_i). As can be seen in these graphs, the absorption of flux of ice field energy in interaction process in points (Q) interrupting becourse reached of the limit of opportunities its absorption Ue in IF-IRS System. Therefore, the amount of absorbed energy of ice field during the time Δt, i.e. the power transfer of ice field energy is determined by the speed of its movement, V_{IF}, the rigidity of ice G_i, and the stiffness of structures G_s.

Depending on the combinations of all the above parameters, the oscillation mode can be transient, established with constant amplitude and frequency, and random (with random frequency and amplitude).Several scientists have included in the descriptions of their proposed models of interaction between IF with IRS, the processes of energy dissipation in a deformed ice volume and in the material of the leg of the structure [2, 31, 48, 53, 54, et al.], and they considered these processes as independent. They assumed that the probability of the emergence of the critical cycle, i.e. the stabilizing process of auto-oscillation, is related to the fact that in the case of monotonically increasing amplitudes of oscillation in the IF-IRS system, the energy dissipation in the system at the expense of damping is monotonically increased; and through some period of time, the energy dissipation of the system in one cycle must be equal to the energy received by the structure in this period of time from the drifting ice field [48]. Thus, if the frequency of these vibrations match with one of the frequencies of natural oscillations of IRS, the system IF-IRS can present self-exciting oscillation with constant amplitude, and the energy source for these fluctuations is the kinetic energy of the IF.

This mode, in terms of reliability construction, is the most dangerous because of the possibility of resonance phenomena. The combination of the phenomenological events described is a complex cause of dangerous vibrations in offshore structures, which can lead to accidents, and reduced reliability and durability of structures. But for this occurrence, the autooscillation regime must be respected by the two conditions arising from the law of conservation of energy.

Condition A: the amount of the “energy swap ΔU_{IF}" from the ice field in an oscillating element of the system per unit time must not be less than the amount of energy ΔU_e dissipating in the system;

Condition B: the transfer of the "doze energy” must occur synchronously with the frequency of vibrations of IRS, i.e. the power of inertia of IRS in this moment must be zero, or a vector of this force should have the same direction as movement of the ice field and have a value close to zero.

Therefore, emergensing the autooscillations in the IF-IRS system require serious theoretical and experimental evidence, because for their automatic resumption must be require the return of a structure to its neutral position absolutely synchronous with the frequency of the ice fracture. On the basis proposed in this paper, the conception of the energetical description of the interaction process in the system IF-IRS lower an attempt is made to consider the possibility of emergence of autooscillation processes in this system.

Figure 9 shows the diagram of self-excited oscillations in the IF – IRS system subject to an increase of ice field velocity V_{IF} and some decrease of the specific energy of ice destruction ε_{cr} on account of an increased velocity of the ice load. The increase of ice movement velocity V_{IF} leads to an increase in the contribution of “energy swap ΔU_{IF}" through a contact area per time t_s prior to the destruction of the next layer of ice. In this regard, the process of cyclical destruction of ice from an area of a single oscillation (Fig.9-b1) is moving into zone of the intermediate mode (Fig.9-b) and further into an area of stable high speed V_3 (fig.9-b3). Here occurs an almost continuous transformation of the kinetic energy of the field into potential energy of layer compression at a contact zone, its destruction and a displacement of destructed fragments out of a contact zone. The structure obtaining increased energy during a shorter period of time, as per the oscillation theory, shall increase its amplitude.

Implementation of the "Conditions A" is possible for certain combinations of parameters of the ice field and the structure, including: drift speed V_{IF}, its thickness h and the value of ε_{cr}, as well as the stiffness of the IRS G_S and its mass. Given the diversity of the natural environment, this coincidence is always possible because the ice field, which has a very large kinetic energy, will be destroyed in the contact area. Such event always precedes a cycle of accumulating potential energy in the ice array. Energy flux from the ice field will equal to the energy required for fracture of ice because this process is governed by the critical value of the specific elastic energy in an array of ice (Fig. 9-a), which will cause its fracture.

A more complex situation can be with the execution of the "Condition B". Execution of the second condition is possible only if the new contact of the surface structure, after ousting products of ice destruction from the previous cycle of interaction, will begin with the intact ice in point "x" on the Figures 9-b,c. Only in this case, the vector of force pressure ice on his contact with the structure will not receive the resistance from structure which prior to this point was moving against the movement of the ice field. Then the kinetic energy of the ice field will start a smooth segue into the potential energy of the elastic deflection of the structure or "added" to the remnants of the inertial force of a structure, when it returns to the resting state, if was had the transition it oscillation through the resting state (“0”). Therefore, only the execution of events in such order can create conditions for development of the autooscillations in the IF-IRS system.

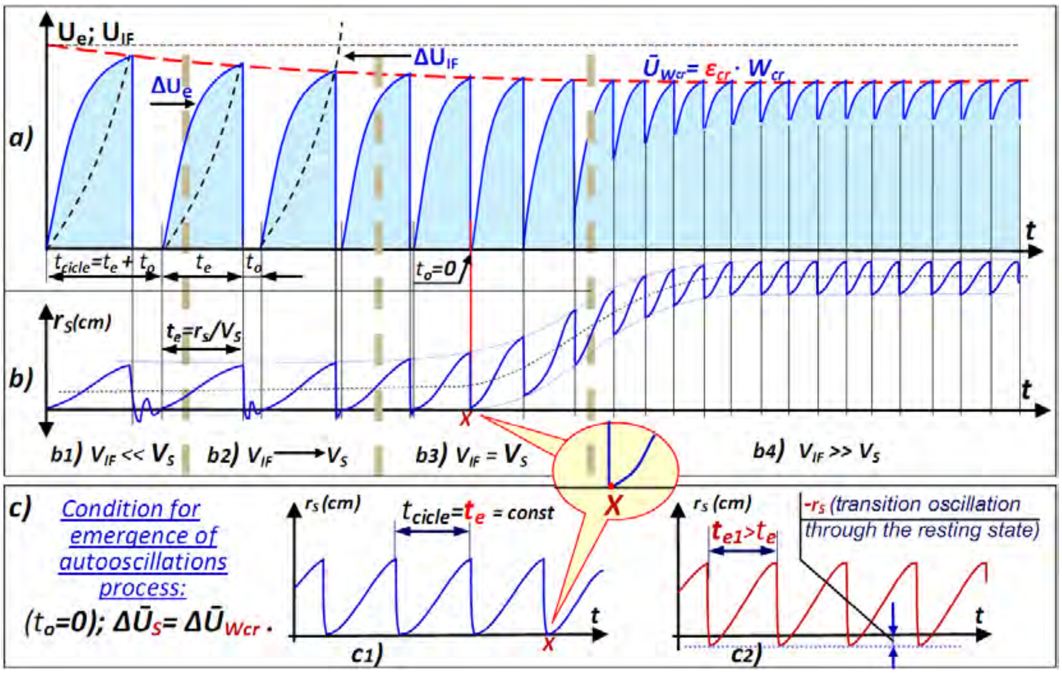

Figure 9 Diagrams of changing of self-excited oscillations of IF-IRS system (a-b) due to increase of velocity movement ice field Vif and view charts of autooscillations process of hard (C1) and flexible structures (C2) according to the theory of oscillations.
Here tcikl is a full time of contact (full cycle); te – a time of active phase load compressed ice and structure; t0 – a time when not contact;

This scenario is also theoretically possible, but in this case, the graph of fluctuations must conform to the type at Fig. 9-c (it can be compared with the schedule of the oscillations of the pendulum in clocks). But it does not correspond to the views of oscillations on the schedules of "self-excited oscillations", recorded in field and laboratory experiments that are listed in many previously published works [4, 9, 11, 13, 25, 70]. At the same time, all these records, possibly, were obtained in the forced vibration mode, as stated in several works of D. Sodhi [60, 72].

Conclusion

In this work, first the energetical concept of the process of emergence of a cyclical load from ice field (IF) to ice resistant structures (IRS) is justified. It is shown that the description of the process of fracture edges of ice fields in the contact zone shall be based on the consideration of energy balance in the system containing these two objects. The process of transferring the kinetic energy from the moving ice field to the structure is presented in this work, in the form of simultaneous development of the two main processes: accumulation of elastic energy in equal shares in deviating of the structure and in the volume of ice in the contact area of the edge the ice field. The essence of the phenomenon of cyclical ice loads on the IRS is shown as periodical interruptions of the monotonous processes of elastic accumulation of energy and its partial dissipation in two elements of the system IF-IRS, caused by the destruction of ice in the contact area and a simultaneous breach of contact between IF and IRS.

The results obtained in the investigations provide a basis for offering the followings conclusions.

1. In phenomenon of the cyclic ice loads the exclusive role plays a fracture mechanism of ice. Presence of such mechanism providing the periodical limitation size (volume) "paging" of energy from ice field to subsystem “IRS” in compliance with the theory of vibration, doing this mechanism as regulator of the period and amplitude oscillation of IRS, and it are limiting increase amplitude during autooscillations. Such mechanism is the main sign of autooscillation system.

2. Periodicity of the ice destruction is defined by the velocity of accumulation of elastic energy deformations of ice at the contact zone of the ice edge and the structure depending on IF velocity, structure’s rigidity and friction force between elements of sistem. The fracture, as a spontaneous process releasing potential energy stored elastically in the strained volume of ice, starts in a local micro-volume, where is achieved the violation of equality speed of adding of energy and power of its scattering.

3. The basic parameter determining the frequency fracture of ice, i.e. periodicity of resets accumulated elastic energy in each next elastically compressed volume of ice in a continuous process of interaction of the elements of the IF-IRS system is threshold of the value of the specific energy of elastic compression of ice required to launch of the fracture mechanism of ice in the ice array of edge ice field.

4. Application of the specific energy of mechanical fracture of ice ε_{cr} for calculation of marine ice-resistant platforms on to cycle ice load, seems completely justified and efficient because the energy has a concrete physical sense and better of another parameters of strength correspond to essence of notions about it as about a complex of potential energetical barriers preventing the develop of kinetic processes in materia. The use of energy as an internal state of the material allows to use mathematical methods of mechanics, physics, thermodynamics, elasticity theory, and other fundamental sciences.

Reference

1. *SP 38.13330.2012.* Nagruzki i vozdeystviya na gidrotekhnicheskiye sooruzheniya (volnovyye, ledovyye i ot sudov). [Russian Set of Rules SP 38.13330.2012. Loads and impacts on hydraulic structures (wave, ice and ships)]. (rus)
2. *ISO/FDIS 19906 (2010).* Petroleum natural gas industries - Arctic offshore structures. ISO TC 67/SC7N. International Organization for Standardization (Draft). 2010.
3. Peyton H.R. Sea ice forces. Ice pressures against structures. *Technical Memorandum, 92.* National Research Council of Canada. Ottawa. Canada. 1966. Pp. 117–123.
4. Blenkarn K.A. Measurement and analysis of ice forces on Cook Inlet structures. *Proceedings of 2nd Offshore Technology Conference.* Houston, TX, OTC 1261. 1970. Vol. II. Pp. 365–378.
5. Neill G. R. Dynamic ice forces on piers and piles: an assessment of design guidelines in the light of resent research. *Canadian Journal of Civil Engineering*. 1970. No. 3. Pp. 305–341.
6. Schwartz J. The Pressure of the floating ice fields on piles. *Proceedings of the International Symposium on Ice (IAHR).* Reykjavik. Iceland. 1970. No. 6-3. Pp. 12.
7. Korenkov V.A. Naturnyye izmereniya dinamicheskogo davleniya lda na bychok nizkonapornoy plotiny [Full-scale measurements of the dynamic pressure of ice on the goby of a low-pressure dam]. *Trudy koordinatsionnykh*

Литература

1. СП 38.13330.2012. Нагрузки и воздействия на гидротехнические сооружения (волновые, ледовые и от судов). Свод правил, актуализированная редакция СНиП 2.06.04-82*.
2. ISO/FDIS 19906 (2010). Petroleum natural gas industries - Arctic offshore structures. ISO TC 67/SC7N. International Organization for Standardization (Draft). 2010.
3. Peyton H.R. Sea ice forces. Ice pressures against structures // Technical Memorandum, 92. National Research Council of Canada. Ottawa. Canada. 1966. Pp. 117–123.
4. Blenkarn K.A. Measurement and analysis of ice forces on Cook Inlet structures // Proceedings of 2nd Offshore Technology Conference. Houston, TX, OTC 1261. 1970. Vol. II. Pp. 365–378.
5. Neill G. R. Dynamic ice forces on piers and piles: an assessment of design guidelines in the light of resent research // Canadian Journal of Civil Engineering. 1970. № 3. Pp. 305–341.
6. Schwartz J. The Pressure of the floating ice fields on piles // Proceedings of the International Symposium on Ice (IAHR). Reykjavik. Iceland. 1970. № 6-3. Pp. 12.
7. Кореньков В.А. Натурные измерения динамического давления льда на бычок низконапорной плотины // Труды координационных совещаний по гидротехнике. Вып. 111. (Регулирование ледовых явлений на каскадах гидроузлов). Л.: Энергия. 1976. С. 148–152.

soveshchaniy po gidrotekhnike. Leningrad: Energiya, 1976. No. 111. Pp. 148–152. (rus)
8. Määttänen M. Experiences of ice forces against a steel lighthouse mounted on the seabed and proposed constructional refinements. *Proceedings of the 3rd Port and Ocean Engineering under Arctic Conditions*. Fairbanks. AK. USA. 1975. Vol. 2. Pp. 857–869.
9. Engelbrektson A. Dynamic ice loads on lighthouse structures. *Proc. 4th Int. Conf. on Port and Ocean Eng. under Arctic Conditions.* St. John's. Canada. 1977. Vol. 2. Pp. 654–864.
10. Bergdahl L. Two lighthouses damaged by ice. *Symposium on Ice and Its Action on Hydraulic Structures.* IAHR. Leningrad. 1972. Pp. 234–238.
11. Määttänen M. Stability of self-excited ice-induced structural vibrations. *Proceedings of 4th International Conference on Port and Ocean Engineering under Arctic Conditions.* Canada, 1977. Vol. II. Pp. 684–694.
12. Azhermachev G. A. O vozdeystvii lda na opory morskikh platform pri yego podvizhke [On the effect of ice on the supports of offshore platforms when it moves]. *Stroitelstvo i tekhnogennaya bezopasnost.* 2005. No. 12. Pp. 6–9. (rus)
13. Yue Q., Bi X. Ice-induced jacket structure vibrations in Bohai Sea. *Journal of Cold Regions Engineering*. 2000. Vol. 14. No. 2. Pp. 81–92.
14. Huang Y., Shi Q., Song S. The interaction between ice and a compliant vertical pile. *Proceedings of the 19th Port and Ocean Engineering under Arctic Conditions.* Dalian. China. 2007. Vol.1. Pp. 142–152.
15. Jefferies M.G., Wright W.H. Dynamic Response of Molikpaq to Ice-Structure Interactions. *Proceedings 7th International Conference on Offshore Mechanics and Arctic Engineering.* Houston. 1988. Vol. IV. Pp. 201–220.
16. Timco G.W., Johnston M.E., Wright B.D. Multi-year ice loads on the Molikpaq: May 12, 1986 Event. *Proceedings 18th International Conference on Port and Ocean Engineering under Arctic Conditions.* POAC'05. Potsdam. USA.2005. Vol. 1. Pp. 453–462.
17. Litonov O.Ye. K voprosu analiza dinamicheskikh modeley vozdeystviya lda na morskiye platform [On the analysis of dynamic models of the effect of ice on marine platforms]. *Rossiyskiy morskoy registr sudokhodstva.* 2011. No. 34. Pp. 237–241. (rus)
18. Belendir Ye.N. *Nauchnoye obosnovaniye proyektirovaniya gravitatsionnykh opornykh blokov morskikh ledostoykikh platform i ikh sopryazheniya s gruntovym osnovaniyem* [Scientific substantiation of the design of gravity support blocks of marine ice-resistant platforms and their interface with the ground base]. Abstract of PhD Thesis. VNIIG. 2006. 45 p. (rus)
19. Barker A., Timco G., Gravesend H., Vølund P. Ice loading on Danish wind turbines. Part 1: Dynamic model tests. *Cold Regions Science and Technology.* 2005. No. 41. Pp. 1–23.
20. Zhang D.Y., Wang G.J., Yue Q.J., Lou C.J. Structural ice-resistant performance evaluation of offshore wind turbine foundation. *Proceedings of the 26th International Ocean and Polar Engineering Conference*. Rhodes. Greece. 2016. Pp. 83–90.
21. Eranti E. Ice forces in dynamic ice structure interaction. theory and applications. *VTT Publications*. 1992. No. 90. P. 81.
22. Kärnä T., Kolari K., Jochmann P., Evers K-U., Xiangjun B., Määttänen M., Martonen P. Tests on dynamic ice-structure interaction. *Proc of OMAE'03 22nd Int Conf on Offshore Mech and Arctic Eng.* Mexico. 2003. Vol. 3. Pp. 823–829.
23. Yue Q., Guo F. Physical mechanism of ice-induced self-excited vibration. *Journal Eng. Mech*. 2011. Vol. 138. Pp. 784–790.
24. Onken G., Evers K., Haase A., Jochmann P. Ice model tests with a cylindrical structure to investigate dynamic ice structure interaction. *Proceedings of the 22nd International Conference on Port and Ocean Engineering under Arctic Conditions (POAC).* Espoo. 2013. Pp. 462–470.
25. Nord T.S., Øiseth O., Lourens E.M. Ice force identification on the Norströmsgrund lighthouse. *Computers and Structures.* 2016. No. 169. Pp. 24–39.

8. Määttänen M. Experiences of ice forces against a steel lighthouse mounted on the seabed and proposed constructional refinements // Proceedings of the 3rd Port and Ocean Engineering under Arctic Conditions. Fairbanks. AK. USA. 1975. Vol. 2. Pp. 857–869.
9. Engelbrektson A. Dynamic ice loads on lighthouse structures // Proc. 4th Int. Conf. on Port and Ocean Eng. under Arctic Conditions. St. John's. Canada. 1977. Vol. 2. Pp. 654–864.
10. Bergdahl L. Two lighthouses damaged by ice // Symposium on Ice and Its Action on Hydraulic Structures. IAHR. Leningrad. 1972. Pp. 234–238.
11. Määttänen M. Stability of self-excited ice-induced structural vibrations // Proceedings of 4th International Conference on Port and Ocean Engineering under Arctic Conditions. Canada, 1977. Vol. II. Pp. 684–694.
12. Ажермачев Г.А. О воздействии льда на опоры морских платформ при его подвижке // Строительство и техногенная безопасность. 2005. № 12. С. 6–9.
13. Yue Q., Bi X. Ice-induced jacket structure vibrations in Bohai Sea // Journal of Cold Regions Engineering. 2000. Vol. 14. № 2. Pp. 81–92.
14. Huang Y., Shi Q., Song S. The interaction between ice and a compliant vertical pile // Proceedings of the 19th Port and Ocean Engineering under Arctic Conditions. Dalian. China. 2007. Vol.1. Pp. 142–152.
15. Jefferies M.G., Wright W.H. Dynamic Response of Molikpaq to Ice-Structure Interactions // Proceedings 7th International Conference on Offshore Mechanics and Arctic Engineering. Houston. 1988. Vol. IV. Pp. 201–220.
16. Timco G.W., Johnston M.E., Wright B.D. Multi-year ice loads on the Molikpaq: May 12, 1986 Event // Proceedings 18th International Conference on Port and Ocean Engineering under Arctic Conditions. POAC'05. Potsdam. USA.2005. Vol. 1. Pp. 453–462.
17. Литонов О.Е. К вопросу анализа динамических моделей воздействия льда на морские платформы // Российский морской регистр судоходства. 2011. № 34. С. 237–241.
18. Белендир Е.Н. Научное обоснование проектирования гравитационных опорных блоков морских ледостойких платформ и их сопряжения с грунтовым основанием. Автореферат диссертации на соискание степени доктора технических наук. ВНИИГ. 2006. 45 с.
19. Barker A., Timco G., Gravesend H., Vølund P. Ice loading on Danish wind turbines. Part 1: Dynamic model tests // Cold Regions Science and Technology. 2005. № 41. Pp. 1–23.
20. Zhang D.Y., Wang G.J., Yue Q.J., Lou C.J. Structural ice-resistant performance evaluation of offshore wind turbine foundation // Proceedings of the Twenty-sixth International Ocean and Polar Engineering Conference. Rhodes. Greece. 2016. Pp. 83–90.
21. Eranti E. Ice forces in dynamic ice structure interaction. theory and applications // VTT Publications. 1992. № 90. P. 81.
22. Kärnä T., Kolari K., Jochmann P., Evers K-U., Xiangjun B., Määttänen M., Martonen P. Tests on dynamic ice-structure interaction // Proc of OMAE'03 22nd Int Conf on Offshore Mech and Arctic Eng, Mexico. 2003. Vol. 3. Pp. 823–829.
23. Yue Q., Guo F. Physical mechanism of ice-induced self-excited vibration // Journal Eng. Mech. 2011. Vol. 138. Pp. 784–790.
24. Onken G., Evers K., Haase A., Jochmann P. Ice model tests with a cylindrical structure to investigate dynamic ice structure interaction // Proceedings of the 22nd International Conference on Port and Ocean Engineering under Arctic Conditions (POAC). Espoo. 2013. Pp. 462–470.
25. Nord T.S., Øiseth O., Lourens E.M. Ice force identification on the Norströmsgrund lighthouse // Computers and Structures. 2016. № 169. Pp. 24–39.
26. Takeuchi T., Akagawa C., Nakazawa N., Sakai M., Terashima T., Saeki H. Ice failure mode and ice load observed in medium-scale field ice indentation test // Proc of The Twelfth International Offshore and Polar Engineering Conference. Kitakyushu. Japan. 2002. Pp. 607–612.
27. Schwarz J. The pressure of floating ice fields on piles //

26. Takeuchi T., Akagawa C., Nakazawa N., Sakai M., Terashima T., Saeki H. Ice failure mode and ice load observed in medium-scale field ice indentation test. *Proc of The Twelfth International Offshore and Polar Engineering Conference.* Kitakyushu. Japan. 2002. Pp. 607–612.
27. Schwarz J. The pressure of floating ice fields on piles. *Proc. IAHR Ice Symp.* Reykjavik. 1970. № 6-3. P. 12 .
28. Groasdale K.E. The Nutcracker ice strength Tester and its operation in the Beaufort sea. *IAHR. Symp. Ice and its Action on Hydraulic structures.* Reykjavik. Iceland. 1970. Pp. 4–6.
29. Croasdale K.R. Ice forces: Current practices. *Proc. OMAE Conf.* Houston. USA, 1977. Vol. 4. Pp. 133–152.
30. Croasdale K.R., Morgenstern N.R., Nuttall J.B. Indentation tests to investigate ice pressures on vertical piers. *Journal Glaciology*. 1977. No. 81. Pp. 301–312.
31. Tryde P. Ice research in Denmark. *Symp. Krig Isfragor*. Stockholm. 1974.
32. Hirayama K., Schwarz J., Wu H.C. Ice forces of vertical pile indentation and penetration. *Proc. IAHR Ice Symp.* Hanover. 1975. Pp. 442–445.
33. Vershinin S.A., Kopaygorodskiy Ye.M., Panov V.V., Shvayshteyn Z.I. Davleniye lda na otdelno stoyashchiye opory po laboratornym i naturnym ispytaniyam [Ice pressure on stand-alone supports for laboratory and full-scale testing]. *Trudy AANII.* Leningrad: Gidrometizdat, 1975. Vol. 326. Pp. 59–65. (rus)
34. Kivisild H.R., Iyer S.H. In city test for ice strength measu-rements. *Ocean Engineering*. 1976. Vol. 3. No. 5. Pp. 329–342.
35. Nevel D.E., Perham R.E., Hogue G.B. Ice forces on vertical piles. *US CRREL Report: 77-10.* Hanover. NH. 1977.
36. Michel B., Toussaint N. Mechanics and theory of indentation of ice plates. *Journal of Glaciology.* 1977. Vol. 19. No. 8. Pp. 285–300.
37. Khrapatyy N.G., Tsuprik V.G. Polunaturnyye issledovaniya dinamicheskogo vozdeystviya lda na opory gidrotekhniches-kikh sooruzheniy [Semi-dynamic studies of the dynamic effect of ice on the supports of hydrotechnical structures]. *Materialy konferentsiy i soveshchaniy po gidrotekhnike* [Materials of conferences and meetings on hydraulic engineering]. Leningrad: Energiya, 1979. Pp. 101–104. (rus)
38. Kry P.R. Ice forces on wide structures. *Canadian Geotech. J.* No. 17. 1980. Pp. 97–113.
39. Taylor T.P. An experimental investigation of the crushing strength of ice. *Proceedings International Conference on Port and Ocean Engineering under Arctic Conditions (POAC).* Quebec. 1981. Pp. 332–345.
40. Ojima T., Matsushima Y., Yamashita S. Some considerations on the designing of Arctic structures. *Proc. OMAE Conf.* NY. 1985. Pp. 128–134.
41. Saeki H., Hamanaka K., Ozaki A. Experimental on ice forces on pile. *Proceedings International Conference on Port and Ocean Engineering under Arctic Conditions*. 1977. Vol. 2. Pp. 195–706.
42. Saeki H., Tanaka S., Ono T. The distribution of ice pressure on offshore pile structure and failure mechanics of ice sheet. *Proc. OTC Conference*. Houston. 1984. Vol. 1. Pp. 349–357.
43. Yamashita M. et al. Model test and analytical simulation on fracture mechanism of ice. *Proceedings International Conference on Port and Ocean Engineering under Arctic Conditions (POAC).* 1985. Pp. 195–204.
44. Bekker A.T. The Ice load formation modeling in the interaction of ice plate with a cylindrical indenter. *Proc of the Twenty-fifth Int Ocean and Polar Eng Conf.* Kona, Hawaii. 2015. Pp. 1723–1729.
45. Karulin E., Marchenko A., Karulina M. et al. Field Indentation Tests of Vertical Semi-Cylinder on First-Year Ice. *Proc 22nd Int Symp on Ice*. Singapore. IAHR. 2014. Pp. 179–186.
46. Sodhi D.S., Takeuchi T., Nakazawa N., Akagawa S., Saeki H. Medium-scale indentation tests on sea ice at various speeds. *Cold Regions Science and Technology.* 1998. Vol. 28. Pp. 161–182.
47. Kujala P. Modelling of the ice edge failure process with curved failure surfaces. *Int Symp on Applied Snow and Ice*

Proc. IAHR Ice Symp. Reykjavik. 1970. № 6-3. P. 12 .
28. Groasdale K.E. The Nutcracker ice strength Tester and its operation in the Beaufort sea // IAHR. Symp. Ice and its Action on Hydraulic structures. Reykjavik. Iceland. 1970. Pp. 4–6.
29. Croasdale K.R. Ice forces: Current practices // Proc. OMAE Conf. Houston, USA, 1977. Vol. 4. Pp. 133–152.
30. Croasdale K.R., Morgenstern N.R., Nuttall J.B. Indentation tests to investigate ice pressures on vertical piers // Journal Glaciology. 1977. No. 81. Pp. 301–312.
31. Tryde P. Ice research in Denmark // Symp. Krig Isfragor. Stockholm. 1974.
32. Hirayama K., Schwarz J., Wu H.C. Ice forces of vertical pile indentation and penetration // Proc. IAHR Ice Symp. Hanover. 1975. Pp. 442–445.
33. Вершинин С.А., Копайгородский Е.М., Панов В.В., Швайштейн З.И. Давление льда на отдельно стоящие опоры по лабораторным и натурным испытаниям // Труды ААНИИ. Л: Гидрометиздат. 1975. Т. 326. С. 59–65.
34. Kivisild H.R., Iyer S.H. In city test for ice strength measu-rements // Ocean Engineering. 1976. Vol. 3. № 5. Pp. 329–342.
35. Nevel D.E., Perham R.E., Hogue G.B. Ice forces on vertical piles // US CRREL Report: 77-10. Hanover. NH. 1977.
36. Michel B., Toussaint N. Mechanics and theory of indentation of ice plates // Journal of Glaciology. 1977. Vol. 19. № 8. Pp. 285–300.
37. Храпатый Н.Г., Цуприк В.Г. Полунатурные исследования динамического воздействия льда на опоры гидротехничес-ких сооружений // Материалы конференций и совещаний по гидротехнике (Ледотермические явления и их учёт при возведении и эксплуатации гидроузлов и гидротехнических сооружений). Л.: Энергия, 1979. С. 101–104.
38. Kry P.R. Ice forces on wide structures // Canadian Geotech. J. No. 17. 1980. Pp. 97–113.
39. Taylor T.P. An experimental investigation of the crushing strength of ice // Proceedings International Conference on Port and Ocean Engineering under Arctic Conditions (POAC). Quebec. 1981. Pp. 332–345.
40. Ojima T., Matsushima Y., Yamashita S. Some considerations on the designing of Arctic structures // Proc. OMAE Conf. NY. 1985. Pp. 128–134.
41. Saeki H., Hamanaka K., Ozaki A. Experimental on ice forces on pile // Proceedings International Conference on Port and Ocean Engineering under Arctic Conditions. 1977. Vol. 2. Pp. 195–706.
42. Saeki H., Tanaka S., Ono T. The distribution of ice pressure on offshore pile structure and failure mechanics of ice sheet // Proc. OTC Conference. Houston. 1984. Vol. 1. Pp. 349–357.
43. Yamashita M. et al. Model test and analytical simulation on fracture mechanism of ice // Proceedings International Conference on Port and Ocean Engineering under Arctic Conditions (POAC). 1985. Pp. 195–204.
44. Bekker A.T. The Ice load formation modeling in the interaction of ice plate with a cylindrical indenter // Proc of the Twenty-fifth Int Ocean and Polar Eng Conf. Kona, Hawaii. 2015. Pp. 1723–1729.
45. Karulin E., Marchenko A., Karulina M. et al. Field Indentation Tests of Vertical Semi-Cylinder on First-Year Ice // Proc 22nd Int Symp on Ice. Singapore. IAHR. 2014. Pp. 179–186.
46. Sodhi D.S., Takeuchi T., Nakazawa N., Akagawa S., Saeki H. Medium-scale indentation tests on sea ice at various speeds // Cold Regions Science and Technology. 1998. Vol. 28. Pp. 161–182.
47. Kujala P. Modelling of the ice edge failure process with curved failure surfaces // Int Symp on Applied Snow and Ice research. Rovaniemi. Finland. 1993. Pp. 1–16.
48. Вершинин С.А., Трусков П.А.. Кузьмечев К.В. Воздействие льда на сооружения Сахалинского шельфа. М.: Институт Гипростроймост, 2006. 208 с.
49. Muhonen A., Kärnä T., Eranti E., Riska K., Jarvinen E., and Lehmus E. Laboratory indentation tests with thick freshwater ice // VTT Research Notes 1370. Espoo, Finland. 1992.

research. Rovaniemi. Finland. 1993. Pp. 1–16.
48. Vershinin S.A., Truskov P.A.. Kuzmechev K.V. *Vozdeystviye lda na sooruzheniya Sakhalinskogo shelfa* [The impact of ice on the structures of the Sakhalin shelf]. Moscow.: Institut Giprostroymost, 2006. 208 p. (rus)
49. Muhonen A., Kärnä T., Eranti E., Riska K., Jarvinen E., and Lehmus E. Laboratory indentation tests with thick freshwater ice. *VTT Research Notes 1370.* Espoo, Finland. 1992.
50. Tsuprik V.G. The fracture laws of ice edge in its interaction with the shaft surface of the structure. *Proc. of the Twenty-fifth International Ocean and Polar Engineering Conference.* Kona. Hawaii. 2015. Pp.1803–1808.
51. Afanasyev V.P., Dolgopolov Yu.V., Shvayshteyn Z.K. Davleniye lda na morskiye otdelno stoyashchiye opory [Ice pressure on marine free-standing towers]. *Trudy. AANII.* Leningrad: Gidrometizdat, 1971. Vol. 300. Pp. 61–80. (rus)
52. Kamesaki K., Yamauchi Y., Kärnä T. Ice force as a function of structural compliance. *Proc. 13th IAHR Ice Symposium.* Beijing. 1996. Vol. I. Pp. 395–402.
53. Sodhi D.S. Nonsimultaneous crushing during edge indentation of freshwater ice sheets. *Cold Regions Science and Technology.* 1998. No. 27. Pp. 179–195.
54. Frederking R., Timco G.W. Sea ice floe impact – large scale basin experiment. *Proc 10th Int Offshore and Polar Eng Con*f. Seattle. ISOPE. 2000. Vol.1. Pp. 640–645.
55. Takeuchi T., Akagawa C., Nakazawa N., Sakai M., Terashima T., Saeki H., Ice failure mode and ice load observed in medium-scale field ice indentation test. *Proc of The Twelfth International Offshore and Polar Engineering Conference.* Kitakyushu. Japan. 2002. Pp. 607–612.
56. Kryzhevich G., Karulina M., Karulin E. Experimental study of ice loads in a test basin under action of granulated and columnar crystal ice on an elastic model. *Proc of the Twenty-fifth Int Ocean and Polar Eng Conf.* Kona. USA. 2015. Pp. 1780–1791.
57. Höderath A., Ziemer G. Local design pressures for fixed offshore structures – utilization of scale model tests. *23rd IAHR Int. Symp. on Ice. Ann Arbor.* Michigan. USA. 2016. Vol. 4872921.
58. Takeuchi T., Soejima A., Sasaki S., Akagawa S. Ice indentation test on consolidated layer model made of saline and freshwater ice blocks. *Proceed. oh the 18th IAHR Intern. Symp. on Ice.* 2006. Pp. 239–246.
59. Sodhi D.S. Ice-induced vibrations of structures. *IAHR Ice Symposium.* Sapporo. 1988. Vol. 2. Pp. 625–657.
60. Sodhi D.S, Morris C.E. Characteristic frequency of force variations in continuous crushing of sheet ice against rigid cylindrical structures. *Cold Regions Science and Technology.* 1986. Vol. 12. Pp. 1–12.
61. Wang L., Xu J. Description of dynamic ice-structure interaction and the ice force oscillator model. *11th International Conference on Port and Ocean Engineering under Arctic Cond.* POAC'91. St. John's. Newfoundland, 1991. Pp.141–154.
62. Huang G., Liu P. A dynamic model for ice-induced vibration of structures. *Journal Offshore Mech. Arct. Eng.* 2009. Vol. 131. Article 011501.
63. Tsuprik V.G. Ob uchete kharaktera kontaktnykh razrusheniy lda pri normirovanii nagruzki na vertikalnyye opory shelfovykh sooruzheniy [On the account of the nature of contact fractures of ice during the normalization of the load on vertical supports of shelf structures.]. *Borba s ledovymi zatrudneniyami na rekakh i vodokhranilishchakh pri stroitelstve i ekspluatatsii GTS. Trudy soveshchaniy po gidrotekhnike* [Combating the ice difficulties on the rivers and reservoirs during the construction and operation of the GTS. Proceedings of meetings on hydraulic engineering]. Leningrad: Energiya, 1984. Pp. 176–180. (rus)
64. Tsuprik V.G. Consideration of the mode of contact ice failure in determining ice forces action on offshore structures. *Proc. of the Second International Offshore and Polar Engineering Conference, (PACOMS-92).* San-Francisco, USA. 1992. Pp. 790–794.
65. Taylor R.S., Jordaan I.J. Probabilistic fracture mechanics applied to compressive ice failure. *Proceed. 22nd Int.*

50. Tsuprik V.G. The fracture laws of ice edge in its interaction with the shaft surface of the structure // Proc. of the Twenty-fifth International Ocean and Polar Engineering Conference. Kona. Hawaii. 2015. Pp.1803–1808.
51. Афанасьев В.П., Долгополов Ю.В., Швайштейн З.К. Давление льда на морские отдельно стоящие опоры // Тр. ААНИИ. Т.300 (Физико-технические исследования льда). Л.: Гидрометиздат, 1971. С. 61–80.
52. Kamesaki K., Yamauchi Y., Kärnä T. Ice force as a function of structural compliance // Proc. 13th IAHR Ice Symposium. Beijing. 1996. Vol. I. Pp. 395–402.
53. Sodhi D.S. Nonsimultaneous crushing during edge indentation of freshwater ice sheets // Cold Regions Science and Technology. 1998. № 27. Pp. 179–195.
54. Frederking R., Timco G.W. Sea ice floe impact – large scale basin experiment // Proc 10th Int Offshore and Polar Eng Conf. Seattle. ISOPE. 2000. Vol.1. Pp. 640–645.
55. Takeuchi T., Akagawa C., Nakazawa N., Sakai M., Terashima T., Saeki H., Ice failure mode and ice load observed in medium-scale field ice indentation test // Proc of The Twelfth International Offshore and Polar Engineering Conference. Kitakyushu. Japan. 2002. Pp. 607–612.
56. Kryzhevich G., Karulina M., Karulin E. Experimental study of ice loads in a test basin under action of granulated and columnar crystal ice on an elastic model // Proc of the Twenty-fifth Int Ocean and Polar Eng Conf. Kona. USA. 2015. Pp. 1780–1791.
57. Höderath A., Ziemer G. Local design pressures for fixed offshore structures – utilization of scale model tests // 23rd IAHR Int. Symp. on Ice. Ann Arbor. Michigan. USA. 2016. Vol. 4872921.
58. Takeuchi T., Soejima A., Sasaki S., Akagawa S. Ice indentation test on consolidated layer model made of saline and freshwater ice blocks // Proceed. oh the 18th IAHR Intern. Symp. on Ice. 2006. Pp. 239–246.
59. Sodhi D.S. Ice-induced vibrations of structures // IAHR Ice Symposium. Sapporo. 1988. Vol. 2. Pp. 625–657.
60. Sodhi D.S, Morris C.E. Characteristic frequency of force variations in continuous crushing of sheet ice against rigid cylindrical structures // Cold Regions Science and Technology. 1986. Vol. 12. Pp. 1–12.
61. Wang L., Xu J. Description of dynamic ice-structure interaction and the ice force oscillator model // 11th International Conference on Port and Ocean Engineering under Arctic Cond. POAC'91. St. John's. Newfoundland, 1991. Pp.141–154.
62. Huang G., Liu P. A dynamic model for ice-induced vibration of structures // Journal Offshore Mech. Arct. Eng. 2009. Vol. 131. Article 011501.
63. Цуприк В.Г. Об учете характера контактных разрушений льда при нормировании нагрузки на вертикальные опоры шельфовых сооружений. В кн.: "Борьба с ледовыми затруднениями на реках и водохранилищах при строительстве и эксплуатации ГТС". Тр. совещаний по гидротехнике. Л.: Энергия, 1984. С. 176–180.
64. Tsuprik V.G. Consideration of the mode of contact ice failure in determining ice forces action on offshore structures // Proc. of the Second International Offshore and Polar Engineering Conference, (PACOMS-92). San-Francisco, USA. 1992. Pp. 790–794.
65. Taylor R.S., Jordaan I.J. Probabilistic fracture mechanics applied to compressive ice failure // Proceed. 22nd Int. Offshore and Polar Eng. Conf. Rhodes. ISOPE. 2012. Pp. 1235–1229.
66. Bjerkås M. Skiple A. Occurrence of continuous and intermediate crushing during ice-structure interaction // Proceedings, Eighteenth International Conference on Port and Ocean Engineering under Arctic Conditions, POAC05. St. John's. 2005. Pp. 1–10.
67. Engelbrektson A. An ice-structure interaction model based on observations in the Gulf of Bothnia // Proceedings, Eighteenth International Conference on Port and Ocean Engineering under Arctic Conditions. POAC'89. 1989. Vol. 1. Pp. 504–517.
68. Sodhi D.S. Crushing failure during ice-structure interaction // Engineering Fracture Mechanics. 2001. Vol. 68.

Offshore and Polar Eng. Conf. Rhodes. ISOPE. 2012. Pp. 1235–1229.
66. Bjerkås M. Skiple A. Occurrence of continuous and intermediate crushing during ice-structure interaction. *Proceedings, Eighteenth International Conference on Port and Ocean Engineering under Arctic Conditions, POAC05.* St. John's. 2005. Pp. 1–10.
67. Engelbrektson A. An ice-structure interaction model based on observations in the Gulf of Bothnia. *Proc. 18th In. Conference on Port and Ocean Engineering under Arctic Conditions. POAC'89.* 1989. Vol. 1. Pp. 504–517.
68. Sodhi D.S. Crushing failure during ice-structure interaction. *Engineering Fracture Mechanics.* 2001. Vol. 68. Pp. 1889-1921.
69. Matlock H., Dawkins W., Panak J. A model for the prediction of ice -structure interaction. *Journal of Engineering Mechanics. ASCE, EM4*. 1969. Pp. 1083–1092.
70. Yue Q., Guo F., and Kärnä,T. Dynamic ice forces of slender vertical structures due to ice crushing. *Cold Regions Science and Technology.* 2009. Vol. 56. Pp. 77–83.
71. Andronov A.A., Vitt A.A., Khaykin S.E. *Teoriya kolebaniy* [Theory of oscillations]. Moscow: Nauka, 1981. 918 p. (rus)
72. Sodhi D.S. Energy exchanges during indentation tests in freshwater ice. *Annals of Glaciology.* 1991. Vol. 15. Pp. 247–253.
73. Kurdyumov V.A., Kheysin D.Ye. Gidrodinamicheskaya model udara tverdogo tela o led [Hydrodynamic model of impact of a solid on ice] *Prikladnaya mekhanika.* 1976. No. 10. Pp. 103–109. (rus)
74. Tsuprik V.G. Model razrusheniya morskogo lda pri dinamicheskom szhatii [The model of the destruction of sea ice under dynamic compression]. *Sbornik statey. Vladivostok: DPI.* 1986. Pp. 76–84. (rus)
75. Kärnä T., Turnunen R. Dynamic response of narrow structures to ice crushing. *Cold Regions Science and Tech.* No. 17. 1989. Pp. 173–187
76. Jordaan I.J., Timco G.W. Dynamics of the ice-crushing process. *Journal of Glaciology.* 1988. Vol. 34. No. 118. Pp. 318–326.
77. McKenna R.F., Jordaan J., Xiao J. Analysis of damage and energy flow in the crushed layer during rapid ice loading. *IAHR Ice Symposium*. Espoo, 1990. Pp. 231–245.
78. Singh S.K., Jordaan I.J. Constitutive behaviour of crushed ice. *Proceedings of the Symposium on Inelasticity and Damage in Solids subject to Microstructural Change*. Memorial University of Newfoundland. 1997. Pp. 367–379.
79. Khrapatyy N.G., Tsuprik V.G. K voprosu rascheta beskonechnykh plit na uprugom osnovanii na udar s uchetom kontaktnykh yavleniy [On the problem of calculating infinite plates on an elastic foundation for impact with allowance for contact phenomena] // *Gidrotekhnika i gidravlika.* Vladivostok: DPI, 1976. Pp. 41–54. (rus)
80. Tsuprik V.G. Theoretical and experimental studies of specific energy of mechanical failure of sea ice. *Proc. 22nd Int. Offshore and Polar Eng. Conf. (ISOPE).* Rhodes, Greece, 2012. Pp. 1242–1246.
81. Iyer S.H. Existing ice codes and suggested criteria. *Proc. 5th IAHR Symp. on Ice Probl., Part 1.* Lulea, Sweden, 1978. Pp. 363–375.
82. Dolgopolov Yu.V., Marchenko D.V. K raschetu ledovykh nagruzok na statsionarnyye i podvizhnyye morskiye GTS s uchetom ikh podatlivosti [To the calculation of ice loads on stationary and mobile marine gas turbines, taking into account their compliance.]. *Gidrotekhnicheskiye sooruzheniya.* Vladivostok: DPI, 1980. Pp. 38–42.
83. Bekker A.T., Tsuprik V.G., Pomnikov E.E. Studies of specific energy fracture of ice using method test samples on uniaxial compression. *Proc 27th Int Ocean and Polar Eng Conf.* San Francisco, CA, USA, (ISOPE). 2017. Pp. 1319–1325.

Pp. 1889-1921.
69. Matlock H., Dawkins W., Panak J. A model for the prediction of ice -structure interaction // Journal of Engineering Mechanics. ASCE, EM4. 1969. Pp. 1083–1092.
70. Yue Q., Guo F., and Kärnä,T. Dynamic ice forces of slender vertical structures due to ice crushing // Cold Regions Science and Technology. 2009. Vol. 56. Pp. 77–83.
71. Андронов А.А., Витт А.А., Хайкин С.Э. Теория колебаний. 2-е изд. М.: Наука, 1981. 918 с.
72. Sodhi D.S. Energy exchanges during indentation tests in freshwater ice // Annals of Glaciology. 1991. Vol. 15. Pp. 247–253.
73. Курдюмов В.А., Хейсин Д.Е. Гидродинамическая модель удара твердого тела о лед // Прикладная механика. 1976. № 10. С. 103–109.
74. Цуприк В.Г. Модель разрушения морского льда при динамическом сжатии // Сборник статей. Владивосток: ДПИ, 1986. С. 76–84.
75. Kärnä T., Turnunen R. Dynamic response of narrow structures to ice crushing // Cold Regions Science and Tech. № 17. 1989. Pp. 173–187
76. Jordaan I.J., Timco G.W. Dynamics of the ice-crushing process // Journal of Glaciology. 1988. Vol. 34. № 118. Pp. 318–326.
77. McKenna R.F., Jordaan J., Xiao J. Analysis of damage and energy flow in the crushed layer during rapid ice loading // IAHR Ice Symposium. Espoo, 1990. Pp. 231–245.
78. Singh S.K., Jordaan I.J. Constitutive behaviour of crushed ice // Proceedings of the Symposium on Inelasticity and Damage in Solids subject to Microstructural Change. Memorial University of Newfoundland. 1997. Pp. 367–379.
79. Храпатый Н.Г., Цуприк В.Г. К вопросу расчета бесконечных плит на упругом основании на удар с учетом контактных явлений. В кн. Гидротехника и гидравлика. Владивосток: Дальневосточный политехнический институт, 1976. С. 41–54.
80. Tsuprik V.G. Theoretical and experimental studies of specific energy of mechanical failure of sea ice // Proc. 22nd Int. Offshore and Polar Eng. Conf. (ISOPE). Rhodes, Greece, 2012. Pp. 1242–1246.
81. Iyer S.H. Existing ice codes and suggested criteria // Proc. 5th IAHR Symp. on Ice Probl., Part 1. Lulea, Sweden, 1978. Pp. 363–375.
82. Долгополов Ю.В., Марченко Д.В. К расчету ледовых нагрузок на стационарные и подвижные морские ГТС с учетом их податливости. В кн. Гидротехнические сооружения. Владивосток: Дальневосточный государственный университет, 1980. С. 38–42.
83. Bekker A.T., Tsuprik V.G., Pomnikov E.E. Studies of specific energy fracture of ice using method test samples on uniaxial compression // Proc Twenty-seventh Int Ocean and Polar Eng Conf. San Francisco, CA, USA, (ISOPE). 2017. Pp. 1319–1325.

Vladimir Tsuprik,
+7(924)1212374; tsuprik.vg@dvfu.ru

Владимир Григорьевич Цуприк,
+7(924)1212374; эл. почта: tsuprik.vg@dvfu.ru

Tsuprik V.G. The forming cyclic loads on the offshore structures during ice field edge fracture. *Magazine of Civil Engineering*. 2017. No. 6. Pp. 118–139. doi: 10.18720/MCE.74.10.

doi: 10.18720/MCE.74.11

Influence of superplasticizers on the concrete mix properties

Влияние суперпластификаторов на свойства бетонной смеси

Yu.G. Barabanshchikov,
S.V. Belyaeva,
I.E. Arkhipov,
M.V. Antonova,
A.A. Shkol'nikova,
K.S. Lebedeva,
Peter the Great St. Petersburg Polytechnic University, St. Petersburg, Russia

Д-р техн. наук, профессор Ю.Г. Барабанщиков,
старший преподаватель С.В. Беляева,
студент И.Е. Архипов,
студент М.В. Антонова,
студент А.А. Школьникова,
студент К.С. Лебедева,
Санкт-Петербургский политехнический университет Петра Великого, г. Санкт-Петербург, Россия

Key words: buildings; construction; civil engineering; water reducing admixtures; polycarboxylate; superplasticizers; additives; cement-water paste

Ключевые слова: здания; строительство; гражданское строительство; водоредуцирующие добавки; поликарбоксилат; суперпластификаторы; добавки; бетонная смесь

Abstract. The most important technological properties of concrete mix are its workability, waterproof capacity, immutability of the properties and air-entrainment. The task of increasing the efficiency and quality of concrete and reinforced concrete is still very relevant and it cannot be successfully solved without the use of special chemical additives. The purpose of the research is to obtain workable concrete mix using special additives. The plasticizers based on polycarboxylate esters: Power Flow PF-2695, Power Flow PF-1130 and Power Flow PF-2237 have been determined as the most effective. It was found that some additives after the addition cause the creation of defects.

Аннотация. Наиболее важными технологическими свойствами бетонной смеси являются удобоукладываемость, водонепроницаемость, неизменность свойств во времени и воздухововлечение. Проблема повышения эффективности и качества бетона и железобетона остается актуальной, однако без использования химических добавок ее невозможно решить успешно. Данная работа нацелена на получение удобоукладываемой бетонной смеси путем применения специальных добавок. Пластификаторы на основе эфиров поликарбоксилатов такие, как Power Flow PF-2695, Power Flow PF-1130 и Power Flow PF-2237, по результатам работы были определены, как наиболее эффективные. Также было выявлено, что некоторые добавки способны вызвать появление дефектов.

Introduction

The most important technological properties of concrete mix are its workability, waterproof capacity, immutability of the properties and air-entrainment.

The possibility of obtaining self-compensating high workability concrete mix allows to lay it down in hard-to-get, densely reinforced, thin-shell concrete construction, which is especially important in the construction of unique buildings and structures, such as thermal and nuclear power structures [1-5]. Nowadays additives improving placeability of concrete are widely used. Depending on the effectiveness, they are called plasticizers and superplasticizers.

The use of these additives allows reducing material costs and avoiding complicated construction works in severe climate conditions.

The subject of this research is plasticizers – additives that increase plastic properties of the concrete mixture and cement spreadability at the same water-cement ratio. The use of plasticizers allows

Барабанщиков Ю.Г., Беляева С.В., Архипов И.Е., Антонова М.В., Школьникова А.А., Лебедева К.С. Влияние суперпластификаторов на свойства бетонной смеси // Инженерно-строительный журнал. 2017. № 6(74). С. 140-146.

increasing the workability without any changes in strength of the resulting concrete and increasing adhesion to the reinforcement. Usually excess water is added to maintain plastic properties of the concrete mixture, which reduces the strength of the structure. Such situations can be avoided by using a plasticizer [6].

The most common plasticizers are polycarboxylates, lignosulphonates and naphthalenesulfonates [7].

Lignosulphonates are the product of sulfonation of natural polymer lignin, contained in the wood. Therefore, woodworks waste is a possible source for their production. However, non-treated lignosulphonate contains wood sugar, which slows down concrete setting, and promotes air entrainment. Last modified lignosulphonates have similar side effects in less degree, but have a restriction on dosage and relatively low efficiency. Lignosulphonate relates to strong plasticizers, increase workability of the concrete mixtures from P1 to P4, reduces water requirement up to 15 %.

Naphthalenesulfonate works well together with the lignosulphonate. It belongs to the superplasticizers, reduces water requirement up to 25% and it does not slow down the hydration process. In large doses, it slows the setting and does not work well in low cement consumption.

Currently most effective additives are plasticizers based on polycarboxylate esters. They do not prevent hydration, but you cannot use them at low cement consumption without stabilizer.

Polycarboxylates have a quite flexible chemical structure that allows to model molecules for accurate set properties [7, 8].

The same materials are used in the manufacture of self-compacting concrete mixture, but to obtain stable results tighter control and decrease in the values of limiting deviations are essential [9]. The basic requirements for self-compensating concrete are high plasticity and concrete disintegration minimizing. For this purpose superplasticizers based on polycarboxylates are used, and strict quality control is carried out at all stages – during the selection of materials, in the production process and the process of concrete casting.

The task of increasing the efficiency and quality of concrete and reinforced concrete is still very relevant and it cannot be successfully solved without the use of chemical additives [10-12]. Chemical additives are one of the simplest and accessible ways of improving the properties of concrete, which can significantly reduce the cost per unit of output. They allow to improve the quality and efficiency of a large range of reinforced concrete structures and to increase the working life of structures and buildings. Therefore, enormous attention is paid to the use of chemical additives in concrete technology all over the world. For example, by the end of 90ths the share of concrete additives for different purposes in Japan accounted for more than 80%, in the US, Germany, France and Italy - more than 70%. In Russia in the same period, the share of concrete with chemical additives was about 40%.

The problem of using additives for concrete modification is versatile [13, 14]. In global practice, there is currently no standard classification for additives for cement and concrete. Different countries have developed their own classification schemes. In view of the large differences of chemical additives depending on the material composition and the specific properties, the nature of their impact on the concrete mix and concrete may differ significantly, and sometimes even be selective [15].

In accordance with the classification of the additives introduced in [16], the term superplasticizer is applied to additives, which regulate the properties of concrete mixtures, and have gained the leading position in the group of water reducing admixtures due to extremely high effect of liquefaction of concrete mixture without reducing concrete strength in all terms of testing. Superplasticizers appeared in the early 70th because of research of Japanese and German scientists. The basic idea of such additives was to receive concrete mixtures that can be placed into shapes without applying mechanical action, or used them with respective sharp decrease in the level of intensity of mechanical action impacts [17, 18].

The purpose of the research is to obtain workable concrete mix using special additives.

The most advanced third generation water reducing admixtures, so called superplasticizers, which are oligomers based on polycarboxylate, are used in order to improve waterproof qualities of concrete. Polycarboxylates are sensitive to the properties of cement, so the choice of the most effective admixture was made with account of the chemical and mineralogical composition of the cement [19, 20].

Research methods

Preliminary selection of the concrete compositions was performed to satisfy specified requirements for water resistance, strength, class of aggressiveness of environment [21]. In the appointment of concrete composition ingredients (cement [22], aggregates of different fractional composition [23], additives [24]) were selected in accordance with the European standards.

Comparing a number of cements was carried out five cements, which satisfy the requirements to the greatest extent were selected:

1. Portland cement with mineral additives CEM II/B-M(S-LL)-42.5 N, Finnsementi (Finland);
2. Sulfate-resisting portland cement CEM I 42.5 N-SR3, Finnsementi (Finland);
3. Sulfate-resisting portland cement CEM I 32.5 N SR-3, Mordovtsement (Russia);
4. Portland cement CEM I 42.5 N, Belarusian Cement Plant (Belarus);
5. Sulfate-resisting portland cement CEM I-42.5 N-SR3, Sukhoy Log (Russia) [25].

These cements were tested as part of the cement-water paste in accordance with European standards to determine their normal consistency.

The effectiveness of additives in relation to each of the cement determined by Suttard's viscometer. Paste quality was visually evaluated (the presence of water separation, air bubbles, spreading of cement-water paste).

The production of cement-water paste normal density was carried out according to EN 196-3 [26]. The density of the cement-water paste is determined using a Vicat apparatus and various accessories to it.

A comparative tests were carried out to select a new additive to assess the effectiveness of various modifiers with the use of Suttard's viscometer:

1. The glass with marked concentric circles and polished cylinder 100 mm height and 50 mm in diameter were moistened with water;
2. The cement-water paste was prepared in a spherical bowl. The desired dosage was measured in advance;
3. The resulting mixture had been stirring for 30 seconds, then it was left at rest for 1 minute;
4. The resulting substance was stirred using two quick circular motions and poured into the cylinder pressed to the glass in the center of the circles. The excess paste was cut with a knife and the paste was aligned with the surface of the cylinder;
5. The cylinder was raised in a strictly vertical direction, and the paste was poured in a cone-shaped pat;
6. The lower base cake reached a certain diameter, marked on the glass. That was the result of the first part of the experiment;
7. The same actions were carried out with a paste, but with a plasticizer in it;
8. The result of the experiment depended on the difference between the diameters of the base of the resulting pats.

Test results

The results of tests of additives with various cements are shown in Figures 1–5.

Our research was aimed to design workable concrete mix. To achieve the required results it is necessary to identify the plasticizers, which will be used to further concrete design and recommended for use in concrete mixture. As you can see from our study, plasticizing agents works very selectively with each kind of cement, which confirms the idea of the effect of the chemical and mineralogical composition of cement on water-reducing action of additives [11].

The results of the study also showed that superplasticizers based on polycarboxylate are more effective, which is expressed in comparatively low optimal doses and low sensitivity to the type and composition of cement [14].

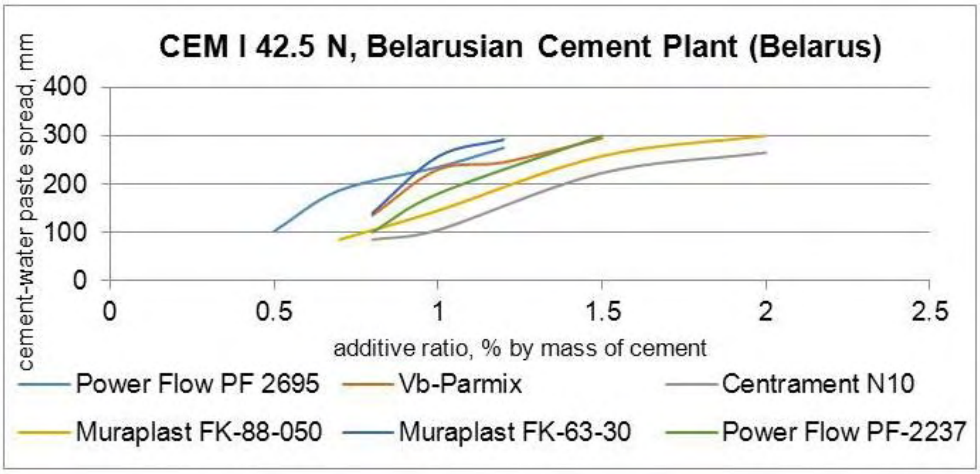

Figure 1. The results of tests of additives with CEM I 42.5 N, Belarusian Cement Plant

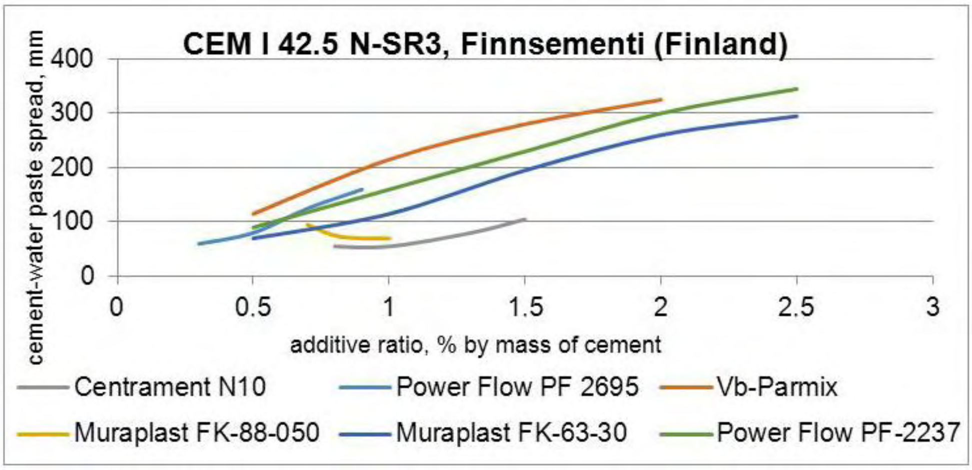

Figure 2. The results of tests of additives with CEM I 42.5 N-SR3, Finnsementi

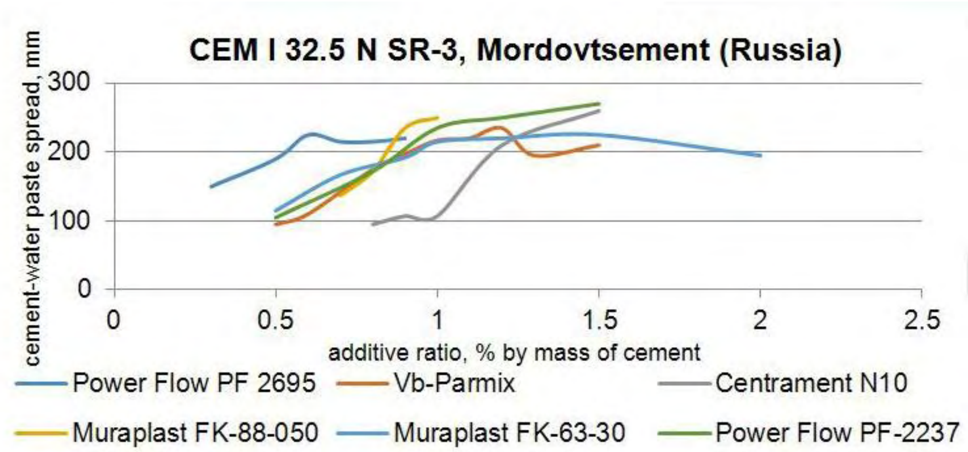

Figure 3. The results of tests of additives with CEM I 32.5 N SR-3, Mordovtsement

Barabanshchikov Yu.G., Belyaeva S.V., Arkhipov I.E., Antonova M.V., Shkol'nikova A.A., Lebedeva K.S. Influence of superplasticizers on the concrete mix properties. *Magazine of Civil Engineering*. 2017. No. 6. Pp. 140–146. doi: 10.18720/MCE.74.11.

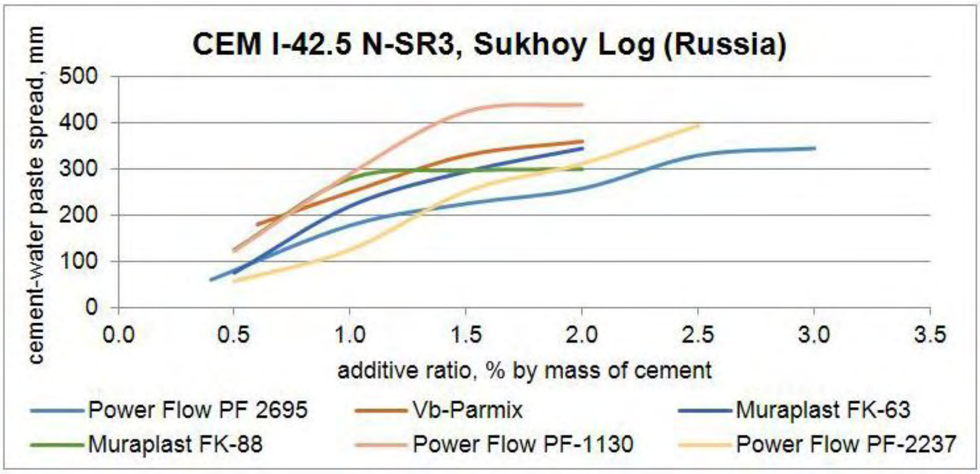

Figure 4. The results of tests of additives with CEM I-42.5 N-SR3, Sukhoy Log

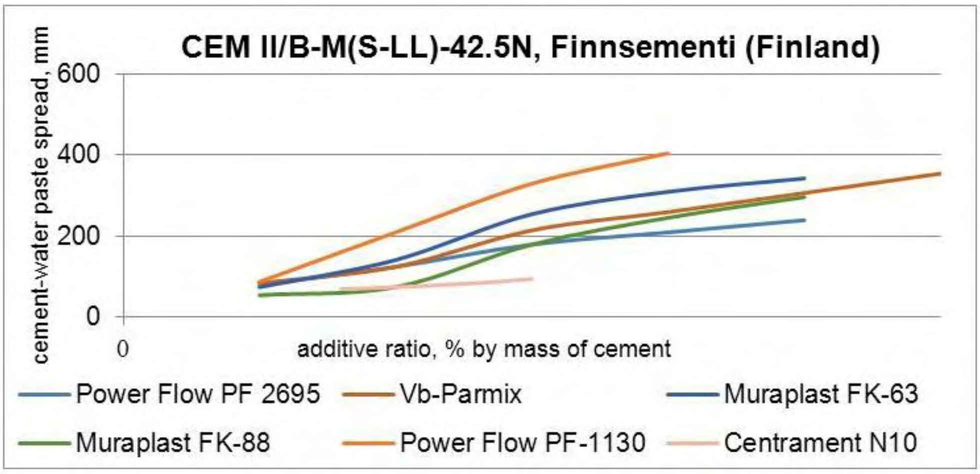

Figure 5. The results of tests of additives with CEM II/B-M(S-LL)-42.5N, Finnsementi

Conclusions

As a result of the experiment the following conclusions were made:

1. All tested additives showed the expected effect: an increase of cement-water paste spread after the addition of the plasticizer;
2. The same plasticizer showed different results with different cements;
3. A number of additives after the addition cause the creation of defects, such as oily stains, blistering, water gain;
4. One of the additives (TF 76) showed a negative effect when it was added at the same time with the silica fume – the concrete structure changed, gaining curdled consistency;
5. Some additives showed the desired effect when added up to 3% – cement-water paste spread achieved more than 30 cm with no defects.

According to test results, the following additives were selected as the most effective: PF 2695, PF 1130, and PF 2237.

Reference

1. Komarinsky M.V. A productivity of reciprocating concrete pump. *Construction of Unique Buildings and Structures.* 2013. No. 6(11). Pp. 43-49. (rus)
2. Zeng C., Gong M., Gui M. Influence of superplasticizer on anti-carbonation property of concrete (Conference Paper). *Applied Mechanics and Materials International.* 2012. Vol. 204-208. Pp. 3790-3794.
3. El-Didamony H., Heikal M., Aiad I. Behavior of delayed

Литература

1. Комаринский М.В. Производительность поршневого бетононаноса // Строительство уникальных зданий и сооружений. 2013. № 6(11). С. 43-49.
2. Zeng C., Gong M., Gui M. Influence of superplasticizer on anti-carbonation property of concrete (Conference Paper) // Applied Mechanics and Materials International. 2012. Vols. 204-208. Pp. 3790-3794.
3. El-Didamony H., Heikal M., Aiad I. Behavior of delayed

addition time of SNF superplasticizer on microsilica-sulphate resisting cements. *Ceramics – Silikaty.* 2013. Vol. 57. No. 3. Pp. 232-242

4. El-Didamony H., Aiad I., Heikal M. Impact of delayed addition time of SNF condensate on the fire resistance and durability of SRC-SF composite cement pastes. *Construction and Building Materials.* 2014. Vol. 50. Pp. 281-290.
5. Solobaj A.Yu., Voronkova V.S. Demchenko V.N., Kudajbergenova Zh.B. Influence of super-plasticizer on workability concrete mix in the hot earthquake-prone regions. *Construction of Unique Buildings and Structures.* 2014. No. 11(26). Pp. 95-101. (rus)
6. Larsen L.O., Naruts V.V. Self-compacting concrete with limestone powder for transport infrastructure. *Magazine of Civil Engineering.* 2016. No. 8. Pp. 76-85. (rus)
7. Fan W., Stoffelbach F., Rieger J. A new class of organosilane-modified polycarboxylate superplasticizers with low sulfate sensiyivity. *Cement and Concrete Research.* 2012. Vol. 42. Pp. 166-172.
8. Bouharoun S., De Caro P., Dubois I., Djelal C., Vanhove Y. Effect of a superplasticizer on the properties of the concrete oil formwork interface. *Construction and Building Materials.* 2013. No. 47. Pp. 1137-1144.
9. *Russian State Standard GOST 22266-94*: Sulfate-resistant cement. Specifications (rus)
10. Barabanshikov Yu., Belyaeva S., Antonova M., Vasiutina S. Calculation of the temperature in ventilated air gap of reinforced concrete cooling tower. *Creative Construction Conference 2015 (CCC2015). Procedia Engineering.* 2015. Vol. 123. Pp. 41–49.
11. 11. Smirnova O., Makarevich O. Vybor vodoreduciruyushchih dobavok i ih raskhodov dlya vysokoprochnyh betonov sbornyh konstrukcij [Selection of water-reducing additives and their rate for the high-strength concrete prefabricated]. Energy-Efficient Technologies in the Regional Building Complex. 2014. Vol. 4. Pp. 70-74 (rus)
12. Kosukhin M.M., Poluektova V.A., Malinovker V.M., Shapovalov N.A. Polifunkcional'nyj superplastifikator dlya betonov na osnove othodov proizvodstva pirokatekhina [Polyfunctional superplasticizer for concretes based on pyrocatechin production waste products]. *Fundamental'nye issledovaniya.* 2013. No. 1-3. Pp. 718-722. (rus)
13. Gołaszewski J. Influence of cement properties on new generation superplasticizers performance. *Construction and Building Materials.* 2012. Vol. 35. Pp. 586-596
14. Izotov V.S., Sokolov Y.A. *Himicheskie dobavki dlya modifikacii betona* [Chemical additives for concrete modifications]. Moscow: Kazan State Architectural University, "Paleotypes". 2006. 244 p. (rus)
15. *Russian State Standard GOST 24211-2008*: Additives for concrete and mortar. General specifications (rus)
16. Barabanshchikov Yu.G., Komarinskiy M.V. Influence of superplasticizer S-3 on the technological properties of concrete mixtures. *Advanced Materials Research.* 2014. Vol. 941-944. Pp. 780-785.
17. Collepardi M. Superplasticizers and Air Entraining Agents: state of the art and future needs. Concrete Technology Past Present and Future. *Proceedings of V. Mohan Malhotra Symposium.* 1994. Pp. 399-416.
18. Bian R.B., Miao C.W., Shen J. Review of chemical structures and synthetic methods for polycarboxylate superplasticizers. *Eighth CANMET/ACI International Conference.* Sorrento. Italy. 2006. Suppl. Papers. Pp. 133-144.
19. Smirnova O.M. Compatibility of portland cement and polycarboxylate-based superplasticizers in high-strength concrete for precast constructions. *Magazine of Civil Engineering.* 2016. No. 6. Pp. 12-22.

addition time of SNF superplasticizer on microsilica-sulphate resisting cements // Ceramics – Silikaty. 2013. Vol. 57. № 3. Pp. 232–242.

4. El-Didamony H., Aiad I., Heikal M. Impact of delayed addition time of SNF condensate on the fire resistance and durability of SRC-SF composite cement pastes // Construction and Building Materials. 2014. Vol. 50. Pp. 281–290.
5. Солобай А.Ю., Воронкова В.С., Демченко В.Н., Кудайбергенова Н.А. Влияние суперпластификатора на удобоукладываемость бетонной смеси в жарких сейсмоопасных регионах // Строительство уникальных зданий и сооружений. 2014. № 11 (26). С. 95–101.
6. Ларсен О.А., Наруть В.В. Самоуплотняющийся бетон с карбонатным наполнителем для объектов транспортной инфраструктуры // Инженерно-строительный журнал. 2016. № 8. С. 76–85.
7. Fan W., Stoffelbach F., Rieger J. A new class of organosilane-modified polycarboxylate superplasticizers with low sulfate sensiyivity // Cement and concrete Research. 2012. Vol. 42. Pp. 166–172.
8. Bouharoun S., De Caro P., Dubois I., Djelal C., Vanhove Y. Effect of a superplasticizer on the properties of the concrete oil formwork interface // Construction and Building Materials. 2013. No. 47. pp. 1137-1144.
9. ГОСТ 22266-94 «Цементы сульфатостойкие».
10. Barabanshikov Yu., Belyaeva S., Antonova M., Vasiutina S. Calculation of the temperature in ventilated air gap of reinforced concrete cooling tower // Creative Construction Conference 2015 (CCC2015). Procedia Engineering. 2015. Vol.123. Pp. 41–49.
11. Смирнова О., Макаревич О. Выбор водоредуцирующих добавок и их расходов для высокопрочных бетонов сборных конструкций // Ресурсоэнергоэффективные технологии в строительном комплексе региона. 2014. № 4. С. 70–74.
12. Косухин М.М., Полуэктова В.А., Малиновкер В.М., Шаповалов Н.А. Полифункциональный суперпластификатор для бетонов на основе отходов производства пирокатехина // Фундаментальные исследования 2013. № 1-3. С. 718–722.
13. Gołaszewski J. Influence of cement properties on new generation superplasticizers performance // Construction and Building Materials. 2012. Vol. 35. Pp. 586–596.
14. Изотов В.С., Соколова Ю.А. Химические добавки для модификации бетона М.: ПАЛЕОТИП. 2006. 244 с.
15. ГОСТ 24211-2008 «Добавки для бетонов и строительных растворов. Общие технические условия».
16. Barabanshchikov Yu.G., Komarinskiy M.V. Influence of superplasticizer S-3 on the technological properties of concrete mixtures // Advanced Materials Research. 2014. Vol. 941-944. Pp. 780–785.
17. Collepardi M. Superplasticizers and Air Entraining Agents: state of the art and future needs // Concrete Technology Past Present and Future. Proceedings of V. Mohan Malhotra Symposium. 1994. Pp. 399–416.
18. Bian R.B., Miao C.W., Shen J. Review of chemical structures and synthetic methods for polycarboxylate superplasticizers // Eighth CANMET/ACI International Conference. Sorrento. Italy. 2006. Suppl. Papers. Pp. 133–144.
19. Смирнова О.М. Совместимость портландцемента и суперпластификаторов на поликарбоксилатной основе для получения высокопрочного бетона сборных конструкций // Инженерно-строительный журнал. 2016. № 6. С. 12–22.
20. Коровкин М.О., Ерошкина Н.А., Покшин В.Р., Кошкин А.Г. Сравнительные исследования эффективности суперпластификаторов // Образование и наука в современном мире. Инновации. 2016. №. 6-1.

Barabanshchikov Yu.G., Belyaeva S.V., Arkhipov I.E., Antonova M.V., Shkol'nikova A.A., Lebedeva K.S. Influence of superplasticizers on the concrete mix properties. *Magazine of Civil Engineering*. 2017. No. 6. Pp. 140–146. doi: 10.18720/MCE.74.11.

20. Korovkin M.O., Eroshkina N.A., Pokshin V.R., Koshkin A.G. Sravnitel'nye issledovaniya ehffektivnosti superplastifikatorov [Comparative research on the effectiveness of superplasticizer*]. Obrazovanie i nauka v sovremennom mire. Innovacii.* 2016. No. 6-1. Pp. 149-157. (rus)
21. *European Standard EN 206-1:2000.* Concrete – Part 1: Specification, performance, production and conformity
22. *European Standard EN 197-1:2011*. Cement – Part 1: Composition, specifications and conformity criteria for common cements
23. *European Standard EN 12620:2013.* Aggregates for concrete
24. *European Standard EN 934-2:2009.* Admixtures for concrete, mortar and grout – Part 2: Concrete admixtures. Definitions, requirements, conformity, marking and labelling
25. Strelenya L.S. K ocenke rastekaemosti stroitel'nogo rastvora [To the assessment of spreadability of building mortar]. *Construction Materials.* 2001. Vol. 9. Pp. 34-35. (rus)
26. *European Standard YeN 196-3:2009.* Methods of testing cement. Part 3: Determination of setting times and soundness.

С. 149–157.
21. EN 206-1:2000 “Concrete – Part 1: Specification, performance, production and conformity”.
22. EN 197-1:2011 “Cement – Part 1: Composition, specifications and conformity criteria for common cements”.
23. EN 12620:2013 “Aggregates for concrete”.
24. EN 934-2:2009 “Admixtures for concrete, mortar and grout – Part 2: Concrete admixtures. Definitions, requirements, conformity, marking and labeling”.
25. Стреленя Л.С. К оценке растекаемости строительного раствора // Строительные материалы. 2001. № 9. С. 34–35.
26. EN 196-3:2009 “Methods of testing cement. Part 3: Determination of setting times and soundness”.

Yuriy Barabanshchikov,
+7(812)5341286; ugb@mail.ru

Svetlana Belyaeva,
+7(921)9056310; sbelaeva@gmail.com

Ivan Arkhipov,
+7(967)5526391; ivan-arhipov-95@mail.ru

Maria Antonova,
+7(921)-552-70-39; m-antonova@mail.ru

Anna Shkol'nikova,
+7(964)3272753; annashkolnikova@inbox.ru

Kseniya Lebedeva,
+7(951)6584897; ksenialebedeva8@gmail.com

Юрий Германович Барабанщиков,
+7(812)5341286; эл. почта: ugb@mail.ru

Светлана Вячеславовна Беляева,
+7(921)9056310; эл. почта: sbelaeva@gmail.com

Иван Евгеньевич Архипов,
+7(967)5526391;
эл. почта: ivan-arhipov-95@mail.ru

Мария Валерьевна Антонова,
+7(921)-552-70-39;
эл. почта: m-antonova@mail.ru

Анна Андреевна Школьникова,
+7(964)3272753;
эл. почта: annashkolnikova@inbox.ru

Ксения Сергеевна Лебедева,
+7(951)6584897;
эл. почта: ksenialebedeva8@gmail.com

doi: 10.18720/MCE.74.12

The stress-strain state of ribbed shell structures

Напряженно-деформированное состояние ребристых оболочечных конструкций

V.V. Karpov,
St. Petersburg State University of Architecture and Civil Engineering, St. Petersburg, Russia
O.V. Ignat'ev,
Peoples Friendship University of Russia (RUDN University), Moscow, Russia
A.A. Semenov,
St. Petersburg State University of Architecture and Civil Engineering, St. Petersburg, Russia

Д-р техн. наук, профессор В.В. Карпов,
Санкт-Петербургский государственный архитектурно-строительный университет, г. Санкт-Петербург, Россия,
д-р техн. наук, заведующий кафедрой О.В. Игнатьев,
Российский университет дружбы народов, г. Москва, Россия,
канд. техн. наук, доцент А.А. Семенов,
Санкт-Петербургский государственный архитектурно-строительный университет, г. Санкт-Петербург, Россия

Key words: shells; stiffened shells; stiffening ribs; stresses; deformation

Ключевые слова: оболочки; подкрепленные оболочки; ребра жесткости; напряжения; деформирование

Abstract. The paper presents an analysis of the stress-strain state of shallow shell structures of double curvature, reinforced from the concave side by a various number of stiffeners. Mindlin–Reissner shell deformation theory is used, which accounts for geometrical nonlinearity and transverse shears, as well as for discrete introduction of stiffeners with contact between the stiffener and the shell along the strip. The mathematical model is written in the form of a functional of full potential deformation energy. The algorithm of the analysis is based on the application of the Ritz method to the functional, which is used for reducing the problem to a system of nonlinear algebraic equations. The resulting system is solved by the parameter continuation method. Structural variations that are considered in the paper are fastened with fixed-pin joints along the contour and are subject to external uniformly distributed transverse loading. The values of stresses, forces, and moments in the stiffeners and in the shell skin are obtained and analyzed. Specific features of their distribution are revealed. All values are given in dimensionless parameters. It is shown that accounting for the contact of the stiffener with the shell skin along the strip allows one to investigate the stress-strain state in the stiffeners, which are not possible using delta functions with the introduction of stiffeners along the line.

Аннотация. В работе проводится анализ напряженно-деформированного состояния пологих оболочечных конструкций двоякой кривизны, подкрепленных со стороны вогнутости различным числом ребер. Используется теория деформирования оболочек Миндлина–Рейснера, учитывающая геометрическую нелинейность, поперечные сдвиги, а также дискретное введение ребер жесткости с контактом ребра и обшивки по полосе. Математическая модель записана в виде функционала полной потенциальной энергии деформации. Алгоритм расчета основан на применении к функционалу метода Ритца для сведения задачи к системе нелинейных алгебраических уравнений. Полученная система решается методом продолжения решения по параметру. Рассматриваемые варианты конструкций шарнирно неподвижно закреплены по контуру и находятся под действием внешней равномерно распределенной поперечной нагрузки. Анализируются полученные данные о значениях напряжений, усилий и моментов в ребрах жесткости и в обшивке. Выявлены особенности их распределения. Значения приведены в безразмерных параметрах. Показано, что учет контакта ребра с обшивкой по полосе позволяет исследовать напряженно-деформированное состояние в ребрах, что невозможно при введении ребер по линии с помощью дельта-функций.

Карпов В.В., Игнатьев О.В., Семенов А.А. Напряженно-деформированное состояние ребристых оболочечных конструкций // Инженерно-строительный журнал. 2017. № 6(74). С. 147-160.

Introduction

The study of the behavior of shell structures is essential for different sectors of industry [1–4], including Civil Engineering [5–6]. For thin-walled shells, it is important to account for the reinforcement with stiffeners [7–35], which make it possible to significantly increase the critical load value, redistribute hazardous stresses, and thus increase the robustness of the structure.

Most of the stability studies of reinforced shells were carried out for closed cylindrical shells [10, 11, 17, 20, 21, 29–31], because such structures are the most widely used in practice. In addition, due to their symmetry, they can be analyzed using simplified models (as an axisymmetric problem).

According to the type of external action, structures under axial compression are more frequently investigated [11–22, 27–29, 32], whereas structures under uniformly distributed transverse loading are studied less often [15–18, 26, 27].

Stability of shells under static loading is considered in [16–24], and the vibrations of such structures in [7, 8, 13–15, 32]. Optimization issues of reinforced shells for solving specific practical problems were discussed in [26–30].

In most cases the stiffeners are located on the side of the concavity of the shell, but the cases where the stiffeners are located on the external side of the shell are also of interest [17, 18, 28, 31].

The finite element method for calculating reinforced thin-walled shells was used in [4, 7, 8, 11, 17, 20, 25, 26, 34, 35].

In most studies it is assumed that stiffeners interact with the shell skin along the line: thus, for example, A.I. Lurie [36] and V.Z. Vlasov [37] considered the stiffeners as Kirchhoff–Klebsch bars, where the locations of stiffeners were defined with the aid of delta functions. With this approach, it is assumed [38] that the effect of shell-reinforcing stiffeners on the shear and torsion of the median surface of the shell skin can be neglected, and deformation of reinforcements is described by the relations of a linear stress state without accounting for their interaction.

The most accurate approach is when the contact between the stiffener and the shell skin occurs along the strip [39]. Also, for reinforced shells, it is essential to account for transverse shears [40].

The purpose of this paper is to analyze the stress-strain state of stiffened shell structures and to identify the features of their deformation process.

The objective of the study is to perform a computational experiment to determine the stress-strain state of shallow shells of rectangular base with a varying number of shell-reinforcing stiffeners.

Methods

Let us consider shallow isotropic shell structures of double curvature, of square base (Figure 1), with fixed-pin joints along the contour and subjected to external uniformly distributed transverse loading q. The load is oriented along the normal to the median surface. The shell is reinforced from the concave side by an orthogonal grid of stiffeners, parallel to the coordinate lines.

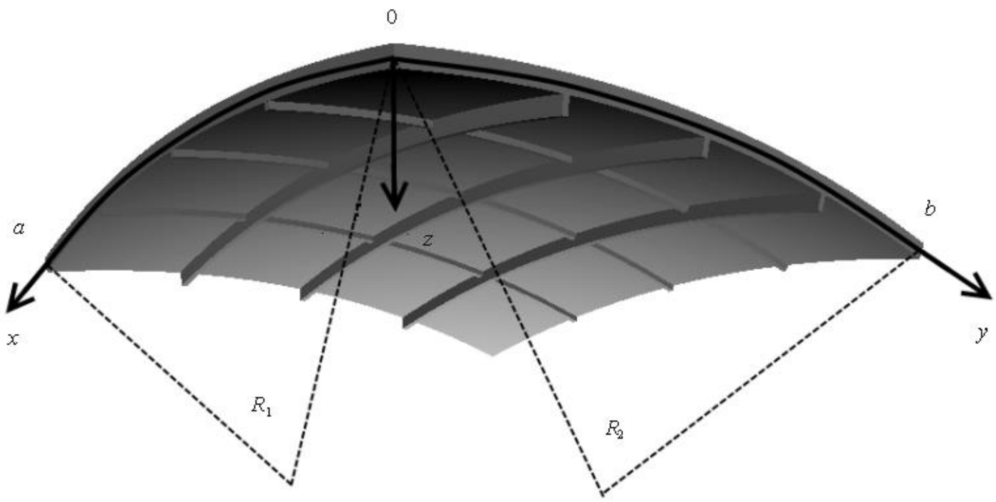

Figure 1. Schematic representation of a shallow shell structure of double curvature, of square base

Mathematical model

The mathematical model of deformation of such structures is constructed from three groups of relations: geometric (associating displacements and strains), physical (associating stresses and strains), and the functional of the total potential deformation energy.

Let us consider a geometrically nonlinear version of the model, which also takes into account transverse shears (the Mindlin–Reissner model), and the possibility of discrete introduction of stiffeners, taking into account the contact of the stiffener and the shell skin along the strip and accounting for the shear and torsional rigidity of the stiffeners. In this case, the unknown functions are three displacement functions $U = U(x, y)$, $V = V(x, y)$, and $W = W(x, y)$ and two functions of the angles of rotation of the normal, $\Psi_x = \Psi_x(x, y)$, and $\Psi_y = \Psi_y(x, y)$; and the geometric relations will have the form:

$$\varepsilon_x = \frac{\partial U}{\partial x} - k_x W + \frac{1}{2}\theta_1^2,\ \varepsilon_y = \frac{\partial V}{\partial y} - k_y W + \frac{1}{2}\theta_2^2,\ \gamma_{xy} = \frac{\partial V}{\partial x} + \frac{\partial U}{\partial y} + \theta_1\theta_2,$$
$$\chi_1 = \frac{\partial \Psi_x}{\partial x},\ \chi_2 = \frac{\partial \Psi_y}{\partial y},\ 2\chi_{12} = \frac{\partial \Psi_y}{\partial x} + \frac{\partial \Psi_x}{\partial y}, \tag{1}$$

where $\varepsilon_x, \varepsilon_y$ are axial strains along the x and y coordinates of the median surface; γ_{xy} is the shear strain in the $x\mathrm{O}y$ plane; $\chi_1, \chi_2, \chi_{12}$ are functions of change of curvatures and torsion; $k_x = 1/R_1, k_y = 1/R_2$ are primary curvatures of the shell along the x and y axes; R_1, R_2 are the principal radii of curvature; and

$$\theta_1 = -\frac{\partial W}{\partial x},\quad \theta_2 = -\frac{\partial W}{\partial y}. \tag{2}$$

The physical relations for linearly elastic deformation of an isotropic material under a plane stress state will have the form

$$\sigma_x = \frac{E}{1-\mu^2}\left[\varepsilon_x + \mu\varepsilon_y + z(\chi_1 + \mu\chi_2)\right];\ \sigma_y = \frac{E}{1-\mu^2}\left[\varepsilon_y + \mu\varepsilon_x + z(\chi_2 + \mu\chi_1)\right];$$
$$\tau_{xy} = G_{12}\left[\gamma_{xy} + 2z\chi_{12}\right], \tag{3}$$

where E is the elastic modulus of an isotropic material; μ is the Poisson's ratio; and G_{12} is the shear modulus.

Expressions for forces and moments are separated into components acting in the shell skin (index 0), and in the stiffeners (index R). Consequently, we have

$$N_x = N_x^0 + N_x^R,\quad N_y = N_y^0 + N_y^R,\quad N_{xy} = N_{xy}^0 + N_{xy}^R,\quad N_{yx} = N_{yx}^0 + N_{yx}^R,$$
$$M_x = M_x^0 + M_x^R,\quad M_y = M_y^0 + M_y^R,\quad M_{xy} = M_{xy}^0 + M_{xy}^R,\quad M_{yx} = M_{yx}^0 + M_{yx}^R, \tag{4}$$
$$Q_x = Q_x^0 + Q_x^R,\quad Q_y = Q_y^0 + Q_y^R.$$

If the stiffeners are introduced discretely, then in the expressions (4) one should take [35]

$$N_x^0 = G_1 h(\varepsilon_x + \mu\varepsilon_y),\quad N_y^0 = G_1 h(\varepsilon_y + \mu\varepsilon_x),\quad N_{xy}^0 = N_{yx}^0 = G_{12} h\gamma_{xy},$$
$$M_x^0 = G_1\frac{h^3}{12}(\chi_1 + \mu\chi_2),\quad M_y^0 = G_1\frac{h^3}{12}(\chi_2 + \mu\chi_1),\quad M_{xy}^0 = M_{yx}^0 = 2G_{12}\frac{h^3}{12}\chi_{12},$$
$$Q_x^0 = G_{13}kh(\Psi_x - \theta_1),\qquad Q_y^0 = G_{23}kh(\Psi_y - \theta_2), \tag{5}$$
$$N_x^R = G_1\left[F(\varepsilon_x + \mu\varepsilon_y) + S(\chi_1 + \mu\chi_2)\right],\quad N_y^R = G_1\left[\bar{F}(\varepsilon_y + \mu\varepsilon_x) + \bar{S}(\chi_2 + \mu\chi_1)\right],$$
$$N_{xy}^R = N_{yx}^R = G_{12}\left[F\gamma_{xy} + 2\bar{S}\chi_{12}\right],$$

$$M_x^R = G_1\left[\bar{S}\left(\varepsilon_x + \mu\varepsilon_y\right) + \bar{J}\left(\chi_1 + \mu\chi_2\right)\right], \quad M_y^R = G_1\left[\bar{S}\left(\varepsilon_y + \mu\varepsilon_x\right) + \bar{J}\left(\chi_2 + \mu\chi_1\right)\right],$$
$$M_{xy}^R = M_{yx}^R = G_{12}\left[\bar{S}\gamma_{xy} + 2\bar{J}\chi_{12}\right],$$
$$Q_x^R = G_{13}k\bar{F}\left(\Psi_x - \theta_1\right), \qquad Q_y^R = G_{23}k\bar{F}\left(\Psi_y - \theta_2\right), \; G_1 = \frac{E}{1-\mu^2}.$$

Here h is the thickness of the shell skin; $\bar{F}$, $\bar{S}$, and $\bar{J}$ are the area of the cross-sectional or longitudinal section of the stiffener per unit length of the cross-section; the static moment of the area; and the moment of inertia of this cross-section. In the discrete approach, it is taken into account that the contact of the stiffener with the shell skin occurs along the strip, the shear and torsional rigidity of the stiffeners are taken into account, and then these characteristics are calculated as follows [41]:

$$\bar{F} = \sum_{j=1}^{m} F^j \bar{\delta}\left(x - x_j\right) + \sum_{i=1}^{n} F^i \bar{\delta}\left(y - y_i\right) - \sum_{i=1}^{n}\sum_{j=1}^{m} F^{ij}\bar{\delta}\left(x - x_j\right)\bar{\delta}\left(y - y_i\right);$$
$$\bar{S} = \sum_{j=1}^{m} S^j \bar{\delta}\left(x - x_j\right) + \sum_{i=1}^{n} S^i \bar{\delta}\left(y - y_i\right) - \sum_{i=1}^{n}\sum_{j=1}^{m} S^{ij}\bar{\delta}\left(x - x_j\right)\bar{\delta}\left(y - y_i\right); \tag{6}$$
$$\bar{J} = \sum_{j=1}^{m} J^j \bar{\delta}\left(x - x_j\right) + \sum_{i=1}^{n} J^i \bar{\delta}\left(y - y_i\right) - \sum_{i=1}^{n}\sum_{j=1}^{m} J^{ij}\bar{\delta}\left(x - x_j\right)\bar{\delta}\left(y - y_i\right),$$

where

$$F^i = h^i, \; F^j = h^j, \; F^{ij} = h^{ij}, \; S^i = h^i\left(h + h^i\right)/2, \; S^j = h^j\left(h + h^j\right)/2, \; S^{ij} = h^{ij}\left(h + h^{ij}\right)/2,$$
$$J^i = 0.25h^2h^i + 0.5h\left(h^i\right)^2 + \frac{1}{3}\left(h^i\right)^3, \tag{7}$$
$$J^j = 0.25h^2h^j + 0.5h\left(h^j\right)^2 + \frac{1}{3}\left(h^j\right)^3, \quad J^{ij} = 0.25h^2h^{ij} + 0.5h\left(h^{ij}\right)^2 + \frac{1}{3}\left(h^{ij}\right)^3.$$

Here h^i, h^j are the height of the stiffener; indices i and j indicate the order number of the stiffener located parallel to the x and y axes, respectively; n, m are the number of stiffeners; $h^{ij} = \min\left\{h^i, h^j\right\}$; and $\bar{\delta}\left(x - x_j\right)$, $\bar{\delta}\left(y - y_j\right)$ are unit bar graph functions equal to 1 in places where stiffeners are connected, which are equal to the difference of two unit functions:

$$\bar{\delta}\left(x - x_j\right) = U\left(x - a_j\right) - U\left(x - b_j\right), \quad \bar{\delta}\left(y - y_i\right) = U\left(y - c_i\right) - U\left(y - d_i\right). \tag{8}$$

Moreover, $a_j = x_j - r_j/2, \quad b_j = x_j + r_j/2, \quad c_i = y_i - r_i/2, \quad d_i = y_i + r_i/2$, where r_i, r_j are the width of the stiffener; and indices i and j indicate the order number of the stiffeners located parallel to the x and y axes, respectively.

The total potential deformation energy of a shallow shell of double curvature can be written with the aid of a functional E_p that represents the difference of the potential deformation energy of the system and the work of external forces:

$$E_p = \frac{1}{2}\int_0^a\int_0^b \left\{ N_x\varepsilon_x + N_y\varepsilon_y + \frac{1}{2}\left(N_{xy} + N_{yx}\right)\gamma_{xy} + M_x\chi_1 + M_y\chi_2 + \left(M_{xy} + M_{yx}\right)\chi_{12} + \right. \tag{9}$$
$$\left. + Q_x\left(\Psi_x - \theta_1\right) + Q_y\left(\Psi_y - \theta_2\right) - 2qW \right\} dxdy.$$

Representing this functional as the sum of two functionals, individually corresponding to the shell skin and the stiffeners, we obtain

$$E_p = E_p^0 + E_p^R, \tag{10}$$

where [41]

$$E_p^0=\frac{1}{2}\int_0^a\int_0^b\Big\{N_x^0\varepsilon_x+N_y^0\varepsilon_y+\frac{1}{2}\left(N_{xy}^0+N_{yx}^0\right)\gamma_{xy}+M_x^0\chi_1+M_y^0\chi_2+\left(M_{xy}^0+M_{yx}^0\right)\chi_{12}+$$

$$+Q_x^0\left(\Psi_x-\theta_1\right)+Q_y^0\left(\Psi_y-\theta_2\right)-2qW\Big\}dxdy=$$

$$=\frac{Eh}{2\left(1-\mu^2\right)}\int_0^a\int_0^b\Big\{\varepsilon_x^2+2\mu\varepsilon_y\varepsilon_x+\varepsilon_y^2+\overline{G}_{12}\gamma_{xy}^2+\frac{h^2}{12}\left(\chi_1^2+2\mu\chi_1\chi_2+\chi_2^2+4\overline{G}_{12}\chi_{12}^2\right)+ \qquad (11)$$

$$+\overline{G}_{13}k\left(\Psi_x-\theta_1\right)^2+\overline{G}_{23}k\left(\Psi_y-\theta_2\right)^2-\frac{2\left(1-\mu^2\right)qW}{Eh}\Big\}dxdy,$$

$$\overline{G}_{12}=\frac{G_{12}\left(1-\mu^2\right)}{E},\overline{G}_{13}=\frac{G_{13}\left(1-\mu^2\right)}{E},\overline{G}_{23}=\frac{G_{23}\left(1-\mu^2\right)}{E},$$

An expression for E_p^R is obtained analogously:

$$E_p^R=\frac{1}{2}\int_0^a\int_0^b\Big\{N_x^R\varepsilon_x+N_y^R\varepsilon_y+\frac{1}{2}\left(N_{xy}^R+N_{yx}^R\right)\gamma_{xy}+M_x^R\chi_1+M_y^R\chi_2+\left(M_{xy}^R+M_{yx}^R\right)\chi_{12}+$$

$$+Q_x^R\left(\Psi_x-\theta_1\right)+Q_y^R\left(\Psi_y-\theta_2\right)\Big\}dxdy= \qquad (12)$$

$$=\frac{E}{2\left(1-\mu^2\right)}\int_0^a\int_0^b\Big\{\Big[F\left(\varepsilon_x^2+2\mu\varepsilon_y\varepsilon_x+\varepsilon_y^2+\overline{G}_{12}\gamma_{xy}^2+\overline{G}_{13}k\left(\Psi_x-\theta_1\right)^2+\overline{G}_{23}k\left(\Psi_y-\theta_2\right)^2\right)+$$

$$+2\overline{S}\left(\varepsilon_x\chi_1+\mu\varepsilon_y\chi_1+\varepsilon_y\chi_2+\mu\varepsilon_x\chi_2+2\overline{G}_{12}\gamma_{xy}\chi_{12}\right)+J\left(\chi_1^2+\chi_2^2+2\mu\chi_1\chi_2+4\chi_{12}^2\right)\Big]\Big\}dxdy.$$

Algorithm

In this paper, it is proposed to use an algorithm based on the Ritz method and the method of parameter continuation for the study of shell structures.

According to this algorithm, the Ritz method is applied to the functional in order to reduce the variational problem to a system of nonlinear algebraic equations. For this, the required functions are represented in the form

$$U(x,y)=\sum_{I=1}^{N}U(I)Z1(I);\; V(x,y)=\sum_{I=1}^{N}V(I)Z2(I);\; W(x,y)=\sum_{I=1}^{N}W(I)Z3(I);$$

$$\Psi_x(x,y)=\sum_{I=1}^{N}PS(I)Z4(I);\; \Psi_y(x,y)=\sum_{I=1}^{N}PN(I)Z5(I), \qquad (13)$$

and the system of nonlinear algebraic equations is obtained relative to the unknown numerical parameters $U(I)$, $V(I)$, $W(I)$, $PS(I)$, and $PN(I)$.

The convergence of the Ritz method in solving the problems of stability of thin-walled reinforced shells was shown in [40], where for problems with symmetric shells the difference in the critical load values for $N=9$ and $N=16$ was minimal. In this paper, all the results were obtained with $N=9$.

Various numerical methods can be used to solve this system [40, 42, 43]. In this paper we use the parameter continuation method [40].

Approximation functions in (13) are selected depending on the method of fixing the shell contour, and must satisfy the boundary conditions. With the fixed-pin joint along the contour, we obtain the following boundary conditions:

for $x=0,\, x=a$:

$$U = V = W = 0, \; M_x = 0, \; \Psi_y = 0;$$

for $y = 0, \; y = b$:

$$U = V = W = 0, \; M_y = 0, \; \Psi_x = 0.$$

Taking into account the fact that shallow shells of double curvature of square base have symmetry, the approximation functions for this type of fastening can be taken in the form:

$$U(x,y) = \sum_{k=1}^{\sqrt{N}} \sum_{l=1}^{\sqrt{N}} U_{kl} \sin\left(2k\pi \frac{x}{a}\right) \sin\left((2l-1)\pi \frac{y}{b}\right),$$

$$V(x,y) = \sum_{k=1}^{\sqrt{N}} \sum_{l=1}^{\sqrt{N}} V_{kl} \sin\left((2k-1)\pi \frac{x}{a}\right) \sin\left(2l\pi \frac{y}{b}\right),$$

$$W(x,y) = \sum_{k=1}^{\sqrt{N}} \sum_{l=1}^{\sqrt{N}} W_{kl} \sin\left((2k-1)\pi \frac{x}{a}\right) \sin\left((2l-1)\pi \frac{y}{b}\right),$$

$$\Psi_x(x,y) = \sum_{k=1}^{\sqrt{N}} \sum_{l=1}^{\sqrt{N}} PS_{kl} \cos\left((2k-1)\pi \frac{x}{a}\right) \sin\left((2l-1)\pi \frac{y}{b}\right),$$

$$\Psi_y(x,y) = \sum_{k=1}^{\sqrt{N}} \sum_{l=1}^{\sqrt{N}} PN_{kl} \sin\left((2k-1)\pi \frac{x}{a}\right) \cos\left((2l-1)\pi \frac{y}{b}\right).$$

Results and Discussion

Calculations are carried out for shallow shells of double curvature of square base with $a = b$, and $R_1 = R_2$, with fixed-pin joint along the contour and subjected to uniformly distributed transverse loading.

Let us introduce the dimensionless parameters

$$\xi = \frac{x}{a}, \; \eta = \frac{y}{b}, \; \overline{U} = \frac{aU}{h^2}, \; \overline{V} = \frac{bV}{h^2}, \; \overline{W} = \frac{W}{h}, \; k_\xi = \frac{a^2 k_x}{h}, \; k_\eta = \frac{b^2 k_y}{h}, \; \overline{\Psi}_x = \frac{a\Psi_x}{h},$$
$$\overline{\Psi}_y = \frac{b\Psi_y}{h}, \; \overline{P} = \frac{a^4 q}{Eh^4}, \quad \sigma_\eta = \frac{a^2 \sigma_y}{Eh^2}, \; N_\eta = \frac{a^2 N_y}{Eh^3}, M_\eta = \frac{a^2 M_y}{Eh^4}, \tag{14}$$

We will investigate the nature of stress distribution on the outer surface of the shells for different numbers of shell-reinforcing stiffeners with height $3h$ and width $2h$ for $a{=}60h$ and $R_1 = R_2 = 225h$ $\left(k_\xi = k_\eta = 16\right)$.

Figure 2 shows the stress diagrams σ_η for $\overline{P} = 150,$ reinforced with four stiffeners (Figure 2, a) and two stiffeners (Figure 2, b). The curve with number 1 corresponds to the cross-section $\xi = 0.1,$ curve 2 to the cross-section $\xi = 0.2,$ curve 3 to the cross-section $\xi = 0.3,$ curve 4 to the cross-section $\xi = 0.4,$ and curve 5 to the cross-section $\xi = 0.5.$

As can be seen from Figure 2, the stresses on the stiffener decrease substantially, but closer to the central cross-section $(\xi = 0.5)$, the character of the stress becomes smoother.

For shells reinforced with two wide stiffeners (width $12h$), the stress pattern remains the same (Figure 2, c).

Now let us investigate the nature of the distribution of forces and moments in the stiffeners and in the shell skin.

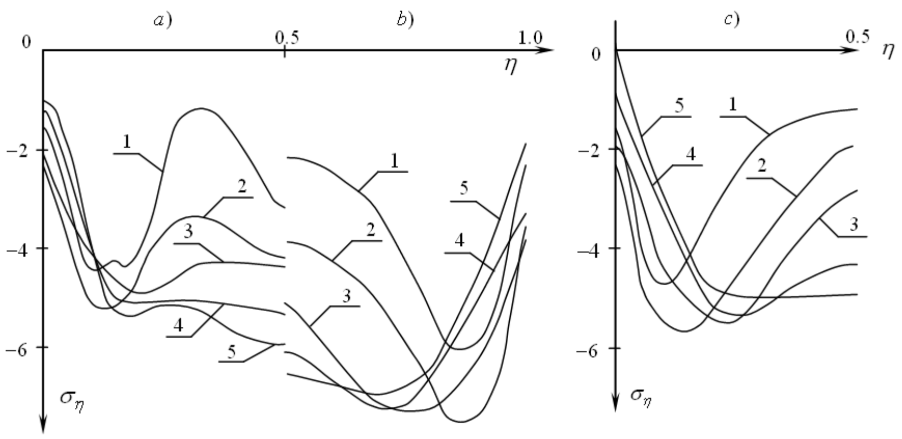

Figure 2. Diagram of stresses σ_η of a shallow shell with various cross-sections

Figure 3 shows diagrams of forces N_η^R and moments M_η^R acting in the stiffener (Figure 3, a) and along the stiffener (Figure 3, b); and N_η^0 and M_η^0 (Figures 3, c and 3, d) in the shell skin along the stiffener (for the shell reinforced by two stiffeners intersecting in the center with height $3h$ and various widths for $\overline{P}=150$, $\xi=0.5$).

Curve 1 corresponds to the width of the stiffener $2h$, curve 2 to width $12h$, and curve 3 to width $24h$. As can be seen from Figure 3, the forces and moments in the cross-section of the stiffener are much larger than in the shell skin. Moreover, the fibers in the shell skin are compressed, and the fibers in the stiffener are elongated, because N_η^R and N_η^0 have opposite signs.

Figures 3,e and 3,f show the diagrams of moments M_η^0 and forces N_η^0 in the cross-section of a shell skin $\eta = 0.1$ (between the stiffeners). All values presented in Figure 3 are related to the unit length of the cross-section.

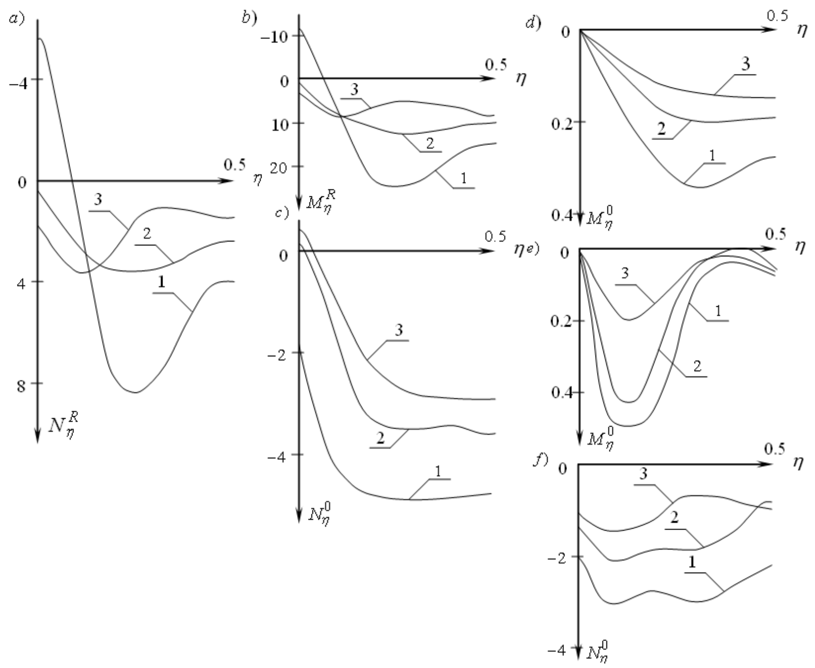

Figure 3. Diagrams of forces N_η and moments M_η of a shallow shell in the cross-section $\xi = 0.5$

As can be seen from Figure 3, as the width of the stiffener decreases, the forces and moments in the stiffeners increase. Let us consider shells reinforced with two and four intersecting stiffeners of height $3h$ and width h. In Figures 4 and 5, the curve number indicates the number of shell-reinforcing stiffeners.

Figure 4 shows the "load $\overline{P}$ - deflection $\overline{W}$ in the center of the shell" dependencies and diagrams of the angles of rotation of the normal $\overline{\Psi}_x$ along the axis ξ for $\overline{P}=150$ and $\eta=0.1$. As can be seen from this figure, at the point where the stiffener is attached to the shell skin, the angles of rotation $\overline{\Psi}_x$ become practically equal to zero.

Figure 5 shows the diagrams of forces N_η^R (Figure 5, a) and N_η^0 (Figure 5, b), and moments M_η^R (Figure 5, c) and M_η^0 (Figure 5, d) per unit length of the cross-section, for $\overline{P}=150$ along the stiffener (parallel to the *y* axis).

Since the force and moment diagrams are given along the stiffener, then for the shells reinforced with two stiffeners, the stiffener is located at $\xi=0.5$, and for the shells reinforced with four stiffeners at $\xi=0.35$.

As can be seen from Figure 5, in the cross section of the stiffener, significant forces and moments appear along the stiffener, while these values are much smaller in the shell skin. Near the edge, the stiffener is subject to compression, and further from the edge, to elongation. At the place of intersection of the stiffeners, the forces are reduced. A smooth change in the forces is observed in the shell skin.

Since the model of the stiffened shell, taking into account the transverse shears, permits the out-of-plane bending of the stiffener, let us analyze this point.

Figure 6 shows the diagrams of bending moments M_η^R (in the direction of the axis η) in the cross-section of the stiffener $(\xi=0.5)$ and the longitudinal section of the stiffener $(\eta=0.5)$ which are mutually orthogonal, for the shells reinforced with a different number of stiffeners: 2 stiffeners (curve 2) and 6 stiffeners (curve 6), with height 3*h* and width *h*. The index "1" in Figure 6 designates that the height of the stiffeners is $6h$ and the width is h. A shallow shell of square base with parameters $a=120h,\ k_\xi=32$ is subject to uniformly distributed transverse loading, $\overline{P}=500$.

As can be seen from Figure 6, the bending of a stiffener in cross-section is somewhat larger than in longitudinal section, but is of the same order. As the height of the stiffener increases, bending moments also increase. At the intersections of the stiffeners, their bending (out-of-plane) decreases. The direction of bending of the stiffener out of its plane differs for a shell that has only one stiffener in the direction being examined and a shell that has several stiffeners in the direction being examined.

Next, let us study the character of the normal stress distribution along the stiffener in different layers of the stiffened shell along the thickness of the stiffener.

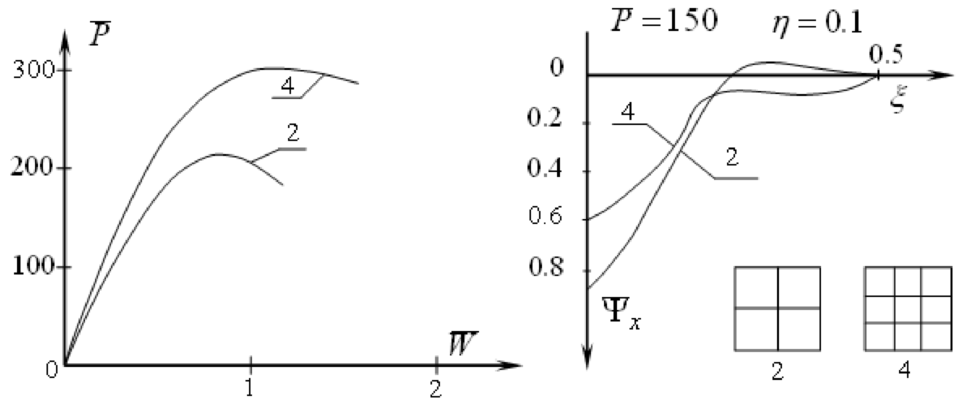

Figure 4. "Load-deflection" graphs for a shallow shell reinforced with two and four stiffeners, and diagrams of the angles of rotation of the normal $\overline{\Psi}_x$

Karpov V.V., Ignat'ev O.V., Semenov A.A. The stress-strain state of ribbed shell structures. *Magazine of Civil Engineering*. 2017. No. 6. Pp. 147–160. doi: 10.18720/MCE.74.12.

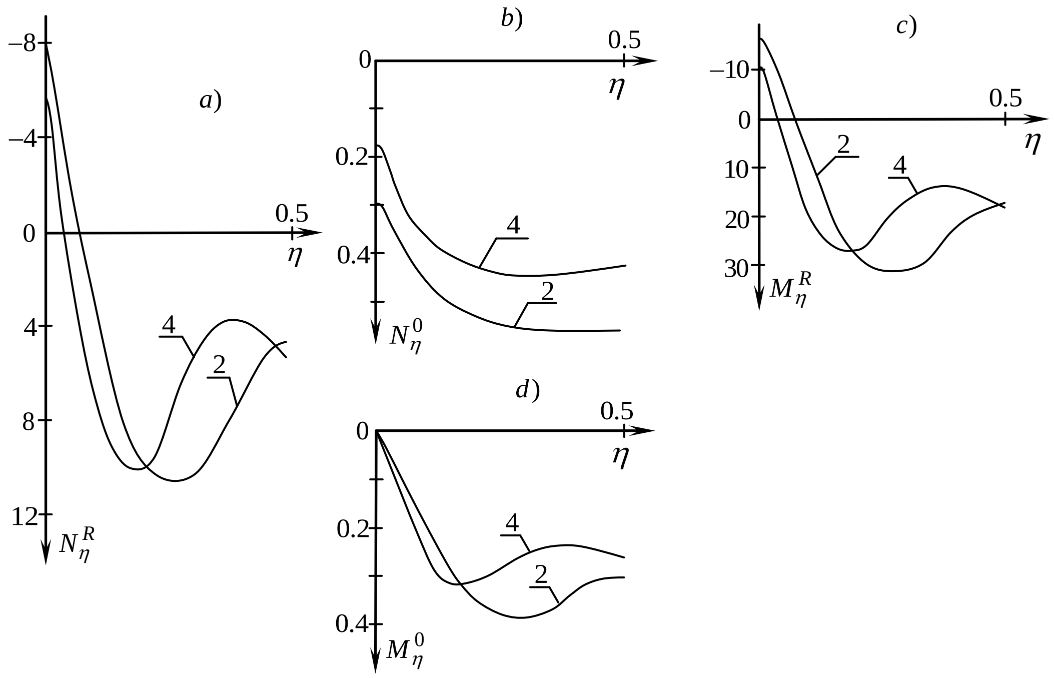

Figure 5. Diagrams of forces and moments in the shell skin and in the stiffeners of a shallow shell reinforced with two and four stiffeners

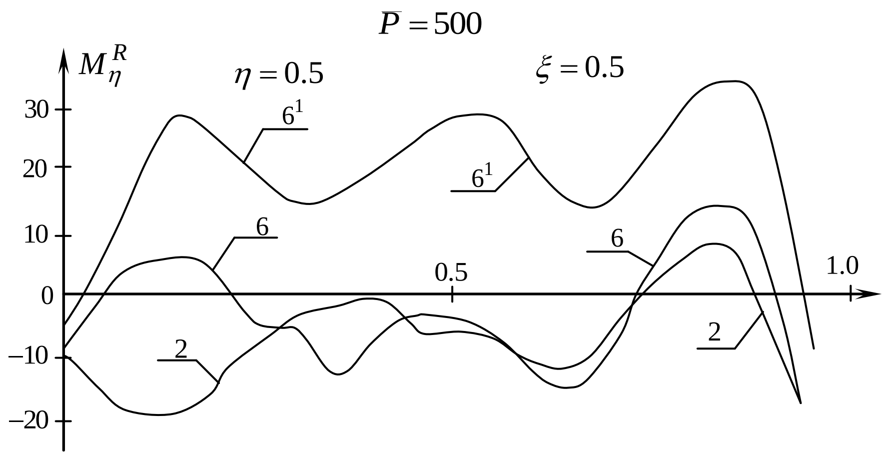

Figure 6. Diagrams of moments M_η^R in different cross-sections for a shallow shell reinforced with a different number of stiffeners

Let us examine the stress distribution in the shell skin and in the stiffener under critical load. Figure 7 shows the stress diagrams σ_η for $\xi = 0.5$ along the η axis for the shell with $a = 60h, k_\xi = 16$: curve 1 for $z = -h/2$, curve 2 for $z = 0$, curve 3 for $z = h/2$, curve 4 for $z = h/2 + 3h$ (at the center of the stiffener), and curve 5 for $z = h/2 + 6h$ (bottom part of the stiffener). Figure 8 shows similar results for shells with parameters $k_\xi = 32$, $a = 120h$ (index "1"), and $a = 240h$ (index "2") near the critical load value (for the shell with $a = 120h$, $\bar{P}_{kr} = 1860$, and for the shell with $a = 240h$, $\bar{P}_{kr} = 1580$). The shells are reinforced with six stiffeners with height $3h$ and width $2h$.

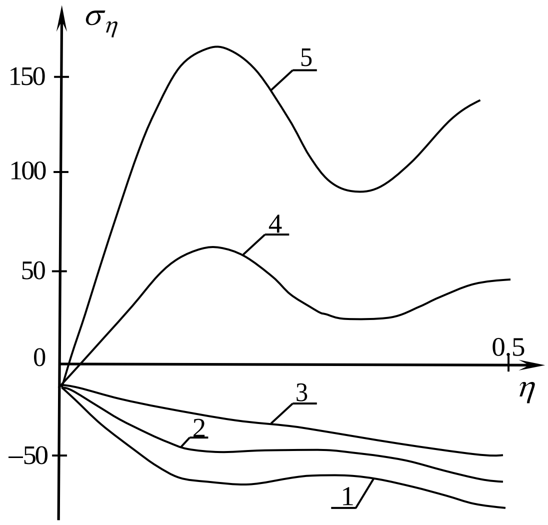

Figure 7. Diagram of stresses σ_η in different cross-sections of the stiffener for $a = 60h, k_\xi = 16$

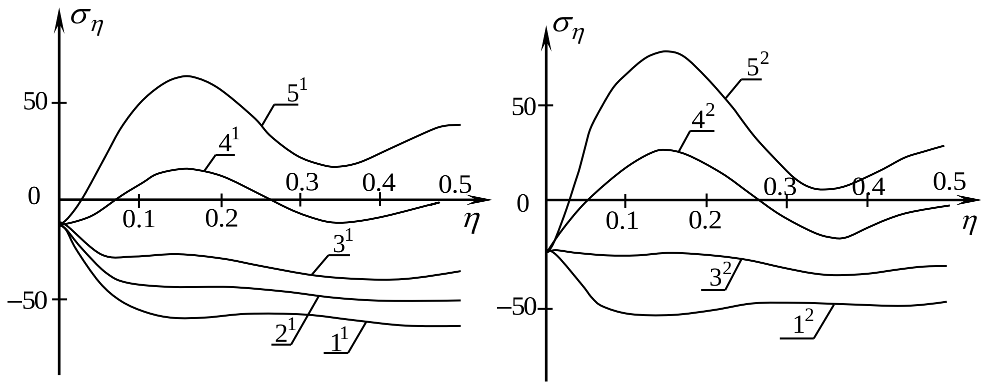

Figure 8. Diagram of stresses σ_η in different cross-sections of the stiffener for $a = 120h, k_\xi = 32$

As can be seen from Figures 7 and 8, stresses occurring in the stiffener significantly exceed stresses in the shell skin. These stresses increase with the height of the stiffener. Therefore, plastic deformations will appear in the stiffener first, and only afterwards in the shell skin. When plastic deformations occur in the stiffener, the moment of stability loss may occur earlier.

Therefore, it is necessary to analyze the maximum stresses in the shell and stiffeners for comparison with the maximum allowable values in order to remain in the elastic zone.

To confirm the reliability of this approach to the introduction of stiffeners, let us consider the results of an experimental study of the stability of stiffened shells, performed at the Ural Scientific Center of the USSR Academy of Sciences and described in the work of V. I. Klimanov and S. A. Timashev [43]. Tests were carried out on 18 samples of shallow shells of square base from plexiglass, the parameters of which are $a = b = 0.6$ m, $R_1 = R_2 = 1.51$ m, $h = 0.001$ m, reinforced by an orthogonal grid of stiffeners with a cross-sectional area 0.0033×0.0092 m² ($3.3h \times 9.2h$) and step size for stiffener arrangement 0.075 m (9×9 stiffeners). The dimensionless parameters of the curvature of such shells are $k_\xi = k_\eta = 238$. The load was assumed to be uniformly distributed over the area of the shell.

As a result of the experiment, the authors of Ref. [43] obtained critical load values that ranged from $0.411 \cdot 10^{-2}$ MPa to $0.703 \cdot 10^{-2}$ MPa. According to the method of calculation of reinforced shells proposed by us, a study of similar structure was conducted: when reinforced with stiffeners ($3.3h \times 9.2h$), the critical load value is $0.72 \cdot 10^{-2}$ MPa (the difference in values is explained by the fact that during calculations, the ideal structure is considered, as well as the possibility of plastic deformations and other factors), and when reinforced with stiffeners ($2h \times 3h$) the critical load value is $0.3 \cdot 10^{-2}$ MPa.

It is also noted in [43] that the shells were initially exposed to cavities, which, under further loading, developed to a depth of $0.55h$. On average, under load $q = 0.195 \cdot 10^{-2}$ MPa, deflections of the model centers are $2.5h$. For a load $q = 0.389 \cdot 10^{-2}$ MPa, they were equal to $7h$ [43]. Similar qualitative results of the process of stability loss of the shell were obtained in this work.

Conclusions

As a result of the calculations and analysis of the data obtained, the following features of the stress-strain state of stiffened shallow shell structures of double curvature can be outlined:

– when the shell is reinforced with a small number of stiffeners, stresses in the area of their connection to the shell skin decrease quickly, and their redistribution occurs in comparison with the smooth shell, but closer to the central cross-section $(\xi = 0.5)$ the character of stresses becomes smoother. Moreover, as the width of the stiffeners increases, the nature of the stresses remains the same;

– as the number of stiffeners increases, the distribution of stresses on the outer surface of the shell skin becomes smoother;

– as the width of the stiffener decreases, the forces and moments in the stiffeners increase;

– at the places where the stiffeners are connected to the shell skin, the angles of rotation of the normal Ψ_x become close to zero, but in the other part of the shell they increase, so that, in comparison with smooth shells, accounting for transverse shears significantly affects the stress-strain state of the stiffened shell;

– in the cross-section of the stiffener there are significant forces and moments, whereas in the shell skin these values are much less than in the stiffener itself. Near the contour of the shell, the stiffener is subject to compression, and closer to the center it is under tension.

– as the height of the stiffener increases, bending moments in the stiffener increase;

– at the intersection of the stiffeners, their bending (out of the plane of the stiffener) decreases, which proves the necessity to take into account the joint action of the stiffeners at their intersection. With the introduction of stiffeners along the line, this effect is not taken into account;

– stresses occurring in the stiffener significantly exceed stresses in the shell skin. These stresses increase with the height of the stiffener. Therefore, plastic deformations will occur first in the stiffener, and then in the shell skin. When plastic deformations develop in the stiffener, the moment of stability loss may occur earlier.

Thus, taking into account the contact of the stiffener with the shell skin along the strip makes it possible to investigate the stress-strain state in the stiffeners, which is not possible using delta functions with the introduction of stiffeners along the line.

Reference

1. Smerdov A.A. A computational study in optimum formulations of optimization problems on laminated cylindrical shells for buckling II. Shells under external pressure. *Composites Science and Technology.* 2000. Vol. 60. No. 11. Pp. 2067–2076.
2. Lutskaya I.V., Maksimyuk V.A., Storozhuk E.A., Chernyshenko I.S. Nonlinear elastic deformation of thin composite shells of discretely variable thickness. *International Applied Mechanics.* 2016. Vol. 52. No. 6. Pp. 616–623.
3. Leonenko D.V., Starovoitov E.I. Vibrations of cylindrical sandwich shells with elastic core under local loads. *International Applied Mechanics.* 2016. Vol. 52. No. 4. Pp. 359–367.
4. Kopecki T., Święch Ł. Experimental and numerical analysis of post-buckling deformation states of integrally stiffened thin-walled components of load-bearing aircraft structures. *Journal of Theoretical and Applied Mechanics.* 2014.

Литература

1. Smerdov A.A. A computational study in optimum formulations of optimization problems on laminated cylindrical shells for buckling II. Shells under external pressure // Composites Science and Technology. 2000. Vol. 60. № 11. Pp. 2067–2076.
2. Lutskaya I.V., Maksimyuk V.A., Storozhuk E.A., Chernyshenko I.S. Nonlinear elastic deformation of thin composite shells of discretely variable thickness // International Applied Mechanics. 2016. Vol. 52. № 6. Pp. 616–623.
3. Leonenko D.V., Starovoitov E.I. Vibrations of cylindrical sandwich shells with elastic core under local loads // International Applied Mechanics. 2016. Vol. 52. № 4. Pp. 359–367.
4. Kopecki T., Święch Ł. Experimental and numerical analysis of post-buckling deformation states of integrally stiffened thin-walled components of load-bearing aircraft structures // Journal of Theoretical and Applied Mechanics. 2014.

Vol. 52. No. 4. Pp. 905–915.

5. Krivoshapko S.N. Research on General and Axisymmetric Ellipsoidal Shells Used as Domes, Pressure Vessels, and Tanks. *Applied Mechanics Reviews.* 2007. Vol. 60. No. 6. Pp. 336–355.
6. Kondratyeva L.N., Routman Y.L., Maslennikov A.M., Golykh O.V. Analytical Method of Determining Folded Depressed Shells Free Oscillation Frequency. *Advanced Materials Research.* 2014. Vol. 1020. Pp. 291–296.
7. Li D., Qing G., Liu Y. A layerwise/solid-element method for the composite stiffened laminated cylindrical shell structures. *Composite Structures.* 2013. Vol. 98. Pp. 215-227.
8. Shi P., Kapania R.K., Dong C. Free Vibration Analysis of Curvilinearly Stiffened Cylindrical Shells. American Institute of Aeronautics and Astronautics. *Proceedings of 56th AIAA/ASCE/AHS/ASC Structures, Structural Dynamics, and Materials Conference, AIAA SciTech Forum.* AIAA, 2015. Vols. 2015-2050. Pp. 1–19.
9. Garrido M., Correia J. R., Keller T., Cabral-Fonseca S. Creep of sandwich panels with longitudinal reinforcement ribs for civil engineering applications: experiments and composite creep modeling. *Journal of Composites for Construction.* 2017. Vol. 21. No. 1. Pp. 04016074.
10. Gavrilenko G.D., Matsner V.I. Experimental justification of the analytical method for determining the upper and lower bounds of the critical loads in ribbed shells. *Strength of Materials.* 2006. Vol. 38. No. 2. Pp. 150–165.
11. Wang B., Du K., Hao P., Zhou C., Tian K., Xu S., Ma Y., Zhang X. Numerically and experimentally predicted knockdown factors for stiffened shells under axial compression. *Thin-Walled Structures.* 2016. Vol. 109. Pp. 13–24.
12. Less H., Abramovich H. Dynamic buckling of a laminated composite stringer–stiffened cylindrical panel. *Composites Part B: Engineering.* 2012. Vol. 43. No. 5. Pp. 2348–2358.
13. Qu Y., Chen Y., Long X., Hua H., Meng G. A modified variational approach for vibration analysis of ring-stiffened conical–cylindrical shell combinations. *European Journal of Mechanics - A/Solids.* 2013. Vol. 37. Pp. 200–215.
14. Duc N.D. Corrigendum to “Nonlinear dynamic response of imperfect eccentrically stiffened FGM double curved shallow shells on elastic foundation” [Compos. Struct. 99 (2013) 88–96]. *Composite Structures.* 2013. Vol. 102. Pp. 306–314.
15. Bich D.H., Dung D.V., Nam V.H. Nonlinear dynamic analysis of eccentrically stiffened imperfect functionally graded doubly curved thin shallow shells. *Composite Structures.* 2013. Vol. 96. Pp. 384–395.
16. Dung D.V., Chan D.Q. Analytical investigation on mechanical buckling of FGM truncated conical shells reinforced by orthogonal stiffeners based on FSDT. *Composite Structures.* 2017. Vol. 159. Pp. 827–841.
17. Barlag S., Rothert H. An idealization concept for the stability analysis of ring-reinforced cylindrical shells under external pressure. *International Journal of Non-Linear Mechanics.* 2002. Vol. 37. No. 4–5. Pp. 745–756.
18. Dung D.V., Hoa L.K., Nga N.T., Anh L.T.N. Instability of eccentrically stiffened functionally graded truncated conical shells under mechanical loads. *Composite Structures.* 2013. Vol. 106. Pp. 104–113.
19. Patel S.N., Datta P.K., Sheikh A.H. Buckling and dynamic instability analysis of stiffened shell panels. *Thin-Walled Structures.* 2006. Vol. 44. No. 3. Pp. 321–333.
20. Hilburger M.W., Starnes Jr. J.H. Buckling behavior of compression-loaded composite cylindrical shells with reinforced cutouts. *International Journal of Non-Linear Mechanics.* 2005. Vol. 40. No. 7. Pp. 1005–1021.
21. Xiang Y., Wang C.M., Lim C.W., Kitipornchai S. Buckling of intermediate ring supported cylindrical shells under axial compression. *Thin-Walled Structures.* 2005. Vol. 43. No. 3. Pp. 427–443.

Vol. 52. № 4. P. 905–915.

5. Krivoshapko S.N. Research on general and axisymmetric ellipsoidal shells used as domes, pressure vessels, and tanks // Applied Mechanics Reviews. 2007. Vol. 60. № 6. Pp. 336–355.
6. Kondratyeva L.N., Routman Y.L., Maslennikov A.M., Golykh O.V. Analytical method of determining folded depressed shells free oscillation frequency // Advanced Materials Research. 2014. Vol. 1020. Pp. 291–296.
7. Li D., Qing G., Liu Y. A layerwise/solid-element method for the composite stiffened laminated cylindrical shell structures // Composite Structures. 2013. Vol. 98. Pp. 215–227.
8. Shi P., Kapania R.K., Dong C. Free vibration analysis of curvilinearly stiffened cylindrical shells. american institute of aeronautics and astronautics // Proceedings of 56th AIAA/ASCE/AHS/ASC Structures, Structural Dynamics, and Materials Conference, AIAA SciTech Forum. AIAA, 2015. Vols. 2015-2050. Pp. 1–19.
9. Garrido M., Correia J. R., Keller T., Cabral-Fonseca S. Creep of sandwich panels with longitudinal reinforcement ribs for civil engineering applications: experiments and composite creep modeling // Journal of Composites for Construction. 2017. Vol. 21. № 1. P. 04016074.
10. Gavrilenko G.D., Matsner V.I. Experimental justification of the analytical method for determining the upper and lower bounds of the critical loads in ribbed shells // Strength of Materials. 2006. Vol. 38. № 2. Pp. 150–165.
11. 11. Wang B., Du K., Hao P., Zhou C., Tian K., Xu S., Ma Y., Zhang X. Numerically and experimentally predicted knockdown factors for stiffened shells under axial compression // Thin-Walled Structures. 2016. Vol. 109. Pp. 13–24.
12. Less H., Abramovich H. Dynamic buckling of a laminated composite stringer–stiffened cylindrical panel // Composites Part B: Engineering. 2012. Vol. 43. № 5. Pp. 2348–2358.
13. Qu Y., Chen Y., Long X., Hua H., Meng G. A modified variational approach for vibration analysis of ring-stiffened conical–cylindrical shell combinations // European Journal of Mechanics - A/Solids. 2013. Vol. 37. Pp. 200–215.
14. Duc N.D. Corrigendum to “Nonlinear dynamic response of imperfect eccentrically stiffened FGM double curved shallow shells on elastic foundation” [Compos. Struct. 99 (2013) 88–96] // Composite Structures. 2013. Vol. 102. Pp. 306–314.
15. Bich D.H., Dung D.V., Nam V.H. Nonlinear dynamic analysis of eccentrically stiffened imperfect functionally graded doubly curved thin shallow shells // Composite Structures. 2013. Vol. 96. Pp. 384–395.
16. Dung D.V., Chan D.Q. Analytical investigation on mechanical buckling of FGM truncated conical shells reinforced by orthogonal stiffeners based on FSDT // Composite Structures. 2017. Vol. 159. Pp. 827–841.
17. Barlag S., Rothert H. An idealization concept for the stability analysis of ring-reinforced cylindrical shells under external pressure // International Journal of Non-Linear Mechanics. 2002. Vol. 37. № 4–5. Pp. 745–756.
18. Dung D.V., Hoa L.K., Nga N.T., Anh L.T.N. Instability of eccentrically stiffened functionally graded truncated conical shells under mechanical loads // Composite Structures. 2013. Vol. 106. Pp. 104–113.
19. Patel S.N., Datta P.K., Sheikh A.H. Buckling and dynamic instability analysis of stiffened shell panels // Thin-Walled Structures. 2006. Vol. 44. № 3. Pp. 321–333.
20. Hilburger M.W., Starnes Jr. J.H. Buckling behavior of compression-loaded composite cylindrical shells with reinforced cutouts // International Journal of Non-Linear Mechanics. 2005. Vol. 40. № 7. Pp. 1005–1021.
21. Xiang Y., Wang C.M., Lim C.W., Kitipornchai S. Buckling of intermediate ring supported cylindrical shells under axial compression // Thin-Walled Structures. 2005. Vol. 43. № 3. Pp. 427–443.
22. Mouhat O., Khamlichi A. Effect of loading pulse duration on

22. Mouhat O., Khamlichi A. Effect of loading pulse duration on dynamic buckling of stiffened panels. *MATEC Web of Conferences.* 2014. Vol. 16. Pp. 07006.
23. Dung D.V., Dong D.T. Nonlinear thermo-mechanical stability of eccentrically stiffened functionally graded material sandwich doubly curved shallow shells with general sigmoid law and power law according to third-order shear deformation theory. *Applied Mathematics and Mechanics.* 2017. Vol. 38. No. 2. Pp. 191–216.
24. Weber M.J., Middendorf P. Semi-analytical skin buckling of curved orthotropic grid-stiffened shells. *Composite Structures.* 2014. Vol. 108. Pp. 616–624.
25. Qu Y., Wu S., Chen Y., Hua H. Vibration analysis of ring-stiffened conical–cylindrical–spherical shells based on a modified variational approach. *International Journal of Mechanical Sciences.* 2013. Vol. 69. Pp. 72–84.
26. Siryus V. Minimization of the weight of ribbed cylindrical shells made of a viscoelastic composite. *Mechanics of Composite Materials.* 2011. Vol. 46. No. 6. Pp. 593–598.
27. Jarmai K., Snyman J.A., Farkas J. Minimum cost design of a welded orthogonally stiffened cylindrical shell. *Computers & Structures.* 2006. Vol. 84. No. 12. Pp. 787–797.
28. Simões L.M.C., Farkas J., Jármai K. Reliability-based optimum design of a welded stringer-stiffened steel cylindrical shell subject to axial compression and bending. *Structural and Multidisciplinary Optimization.* 2006. Vol. 31. No. 2. Pp. 147–155.
29. Hao P., Wang B., Tian K., Liu H., Wang Y., Niu F., Zeng D. Simultaneous buckling design of stiffened shells with multiple cutouts. *Engineering Optimization.* 2017. Vol. 49. No. 7. Pp. 1116–1132.
30. Lene F., Duvaut G., Olivier-Mailhe M., Ben Chaabane S., Grihon S. An advanced methodology for optimum design of a composite stiffened cylinder. *Composite Structures*. 2009. Vol. 91. No. 4. Pp. 392–397.
31. Yu W., Li Z.L. Structural Similitude for Prestressed Vibration and Buckling of Eccentrically Stiffened Circular Cylindrical Panels and Shells by Energy Approach. *International Journal of Structural Stability and Dynamics.* 2016. Vol. 16. No. 10. Pp. 1550074.
32. Abramovich H., Zarutskii V.A. Effect of the stiffness of ribs on the vibrations and stability of open cylindrical shells. *International Applied Mechanics*. 2011. Vol. 46. No. 9. Pp. 994–1000.
33. Amiro I.Ya., Zarutskii V.A. *Metody rascheta obolochek. Tom 2. Teoriya rebristykh obolochek* [Theory of Ribbed Shells, Vol. 2 of the five-volume series Methods of Shell Design]. Kiev: Naukova Dumka, 1980. 368 p. (rus)
34. Fialko S.Yu., Ankyaniec E.K. Vibrations of thin cylindrical shells with non-stiff connection between ribs and panelling. *Proceedings of the 8th SSTA Conference*, Jurata, Poland, 12-14 October 2005. Shell Structures: Theory and Applications. Pp. 315–318.
35. Fialko S.Y. Stress–strain analysis of thin-walled shells with massive ribs. *International Applied Mechanics.* 2004. Vol. 40. No. 4. Pp. 432–439.
36. Lurye A.I. *Obshchiye uravneniya obolochki, podkreplennoy rebrami zhestkosti* [General equations of the shell, reinforced by stiffeners]. Leningrad, 1948. 28 p. (rus)
37. Vlasov V.Z. *Kontaktnyye zadachi po teorii obolochek i tonkostennykh sterzhney* [Contact problems on the theory of shells and thin-walled rods]. Izv. AN SSSR. OTN. 1949. No. 6. Pp. 819–939. (rus)
38. Karmishin A.V., Lyaskovets V.A, Myachenkov V.I., Frolov A.N. *Statika i dinamika tonkostennykh obolochechnykh konstruktsiy* [Statics and dynamics of thin-walled shell structures]. Moscow: Mashinostroyeniye, 1975. 376 p. (rus)
39. Karpov V.V., Ignatyev O.V., Salnikov A.Yu. *Nelineynyye matematicheskiye modeli deformirovaniya obolochek peremennoy tolshchiny i algoritmy ikh issledovaniya*

dynamic buckling of stiffened panels // MATEC Web of Conferences / ed. Belhaq M. 2014. Vol. 16. P. 07006.
23. Dung D.V., Dong D.T. Nonlinear thermo-mechanical stability of eccentrically stiffened functionally graded material sandwich doubly curved shallow shells with general sigmoid law and power law according to third-order shear deformation theory // Applied Mathematics and Mechanics. 2017. Vol. 38. № 2. Pp. 191–216.
24. Weber M.J., Middendorf P. Semi-analytical skin buckling of curved orthotropic grid-stiffened shells // Composite Structures. 2014. Vol. 108. P. 616–624.
25. Qu Y., Wu S., Chen Y., Hua H. Vibration analysis of ring-stiffened conical–cylindrical–spherical shells based on a modified variational approach // International Journal of Mechanical Sciences. 2013. Vol. 69. Pp. 72–84.
26. Siryus V. Minimization of the weight of ribbed cylindrical shells made of a viscoelastic composite // Mechanics of Composite Materials. 2011. Vol. 46. № 6. Pp. 593–598.
27. Jarmai K., Snyman J.A., Farkas J. Minimum cost design of a welded orthogonally stiffened cylindrical shell // Computers & Structures. 2006. Vol. 84. № 12. Pp. 787–797.
28. Simões L.M.C., Farkas J., Jármai K. Reliability-based optimum design of a welded stringer-stiffened steel cylindrical shell subject to axial compression and bending // Structural and Multidisciplinary Optimization. 2006. Vol. 31, № 2. P. 147–155.
29. Hao P., Wang B., Tian K., Liu H., Wang Y., Niu F., Zeng D. Simultaneous buckling design of stiffened shells with multiple cutouts // Engineering Optimization. 2017. Vol. 49. № 7. Pp. 1116–1132.
30. Lene F., Duvaut G., Olivier-Mailhe M., Ben Chaabane S., Grihon S. An advanced methodology for optimum design of a composite stiffened cylinder // Composite Structures. 2009. Vol. 91. № 4. Pp. 392–397.
31. Yu W., Li Z.L. Structural Similitude for Prestressed Vibration and Buckling of Eccentrically Stiffened Circular Cylindrical Panels and Shells by Energy Approach // International Journal of Structural Stability and Dynamics. 2016. Vol. 16. № 10. P. 1550074.
32. Abramovich H., Zarutskii V.A. Effect of the stiffness of ribs on the vibrations and stability of open cylindrical shells // International Applied Mechanics. 2011. Vol. 46. № 9. Pp. 994–1000.
33. Амиро И.Я., Заруцкий В.А. Методы расчета оболочек. Том 2. Теория ребристых оболочек. Киев: Наукова думка, 1980. 368 с.
34. Fialko S.Yu., Ankyaniec E.K. Vibrations of thin cylindrical shells with non-stiff connection between ribs and paneling // Proceedings of the 8th SSTA Conference, Jurata, Poland, 12-14 October 2005. Shell Structures: Theory and Applications. Pp. 315–318.
35. Fialko S.Y. Stress–strain analysis of thin-walled shells with massive ribs // International Applied Mechanics. 2004. Vol. 40. № 4. Pp. 432–439.
36. Лурье А.И. Общие уравнения оболочки, подкрепленной ребрами жесткости. Ленинград, 1948. 28 с.
37. Власов В.З. Контактные задачи по теории оболочек и тонкостенных стержней // Изв. АН СССР. ОТН. 1949. № 6. С. 819–939.
38. Кармишин А.В., Лясковец В.А, Мяченков В.И., Фролов А.Н. Статика и динамика тонкостенных оболочечных конструкций. М.: Машиностроение, 1975. 376 с.
39. Карпов В.В., Игнатьев О.В., Сальников А.Ю. Нелинейные математические модели деформирования оболочек переменной толщины и алгоритмы их исследования. М.: Изд-во АСВ; СПб.: СПбГАСУ, 2002. 420 с.
40. Карпов В.В. Прочность и устойчивость подкрепленных оболочек вращения: в 2 ч. Ч.2: Вычислительный эксперимент при статическом механическом

[Nonlinear mathematical models of deformation of shells of variable thickness and algorithms for their investigation]. Moscow: Izd-vo ASV; Saint-Petersburg: SPbGASU, 2002. 420 p. (rus)

40. Karpov V.V. *Prochnost i ustoychivost podkreplennykh obolochek vrashcheniya: v 2 ch. Ch.2: Vychislitelnyy eksperiment pri staticheskom mekhanicheskom vozdeystvii* [Strength and stability of reinforced shells of rotation: in 2 parts. Part 2: Computational experiment with static mechanical action]. Moscow: Fizmatlit, 2011. 248 p. (rus)
41. Trushin S. Numerical algorithm for solving of nonlinear problems of structural mechanics based on the continuation method in combination with the dynamic relaxation method. *MATEC Web of Conferences.* 2016. Vol. 86. Pp. 01006.
42. Kuznetsov E.B., Leonov S.S. Parametrization of the Cauchy Problem for Systems of Ordinary Differential Equations with Limiting Singular Points. *Computational Mathematics and Mathematical Physics.* 2017. Vol. 57. No. 6. Pp. 931–952.
43. Klimanov V.I., Timashev S.A. *Nelineynyye zadachi podkreplennykh obolochek* [Nonlinear problems of supported shells]. Sverdlovsk: UNTs AN SSSR, 1985. 291 p. (rus)

воздействии. М: Физматлит, 2011. 248 с.

41. Trushin S. Numerical algorithm for solving of nonlinear problems of structural mechanics based on the continuation method in combination with the dynamic relaxation method // MATEC Web of Conferences. 2016. Vol. 86. P. 01006.
42. Kuznetsov E.B., Leonov S.S. Parametrization of the Cauchy Problem for Systems of Ordinary Differential Equations with Limiting Singular Points // Computational Mathematics and Mathematical Physics. 2017. Vol. 57. № 6. Pp. 931–952.
43. Климанов В.И., Тимашев С.А. Нелинейные задачи подкрепленных оболочек. Свердловск: УНЦ АН СССР, 1985. 291 с.

Vladimir Karpov,
vvkarpov@lan.spbgasu.ru

Oleg Ignat'ev,
ignatiev.oleg.v@yandex.ru

Alexey Semenov,
+7(812)5750549; sw.semenov@gmail.com

Владимир Васильевич Карпов,
эл. почта: vvkarpov@lan.spbgasu.ru

Олег Владимирович Игнатьев,
эл. почта: ignatiev.oleg.v@yandex.ru

Алексей Александрович Семенов,
+7(812)5750549;
эл. почта: sw.semenov@gmail.com

doi: 10.18720/MCE.74.13

Stress-strain state of composite reinforced concrete slab elements under fire activity

Напряженно-деформированное состояние фрагмента сталежелезобетонного перекрытия в условиях огневого воздействия

V.A. Rybakov,
I.A. Ananeva,
Peter the Great St. Petersburg Polytechnic University, St. Petersburg, Russia
A.O. Rodicheva,
"LenzhilNIIproekt", Co., Ltd, St. Petersburg, Russia
O.T. Ogidan,
Peter the Great St. Petersburg Polytechnic University, St. Petersburg, Russia

Канд. техн. наук, доцент В.А. Рыбаков,
студент И.А. Ананьева,
Санкт-Петербургский политехнический университет Петра Великого, г. Санкт-Петербург, Россия
инженер А.О. Родичева,
ЛенжилНИИпроект, г. Санкт-Петербург, Россия
студент О.Т. Огидан,
Санкт-Петербургский политехнический университет Петра Великого, г. Санкт-Петербург, Россия

Key words: reinforced concrete structures; composite reinforced concrete structures; profiled sheet; rebar; floor; fire resistance; limit of fire resistance, temperature; ultimate moment

Ключевые слова: железобетонные конструкции; температура; сталежелезобетонные конструкции; профилированный лист; арматура; перекрытие; огнестойкость; предел огнестойкости; предельный момент

Abstract. One of the most topical issues (in construction) has become providing fire protection facilities for reinforced concrete. The Eurocode-4 and other recommendations have been applied for more than 10 years in European countries. In Russia we have only one method of analysis - STO 36554501-006-2006. This work is devoted to comparise all these algorithms. 3 methods of analysis of composite reinforced concrete slab elements under fire activity are described. 3 analytical models of structures with different calculation perameters are consedered for determination of corresponding dependences and creating the algorithm of calculation. Partial coefficients were identified for analysis of composite reinforced concrete slab elements according European Standarts for application in Russian Federation.

Аннотация. Одним из наиболее актуальных вопросов является обеспечение огнестойкости и огнесохранности железобетонных конструкций. В Российской Федерации для расчета сталежелезобетонной конструкции на огневое воздействие существует СТО 36554501-006-2006. В европейских странах уже много лет действует технический кодекс Eurocode-4; институты, занимающиеся конструкциями, издают ряд рекомендаций по расчету. В работе описаны 3 методики расчета сталежелезобетонного перекрытия на огнестойкость, проведено их сравнение. Рассмотрены 3 модели перекрытий с различными параметрами для выявления соответствующих зависимостей и создания алгоритма расчета. Выявлены частные коэффициенты для расчета на огневое воздействие по европейским нормам на территории Российской Федерации.

Рыбаков В.А., Ананьева И.А., Родичева А.О., Огидан О.Т. Напряженно-деформированное состояние фрагмента сталежелезобетонного перекрытия в условиях огневого воздействия // Инженерно-строительный журнал. 2017. № 6(74). С. 161–174.

Introduction

Fire is one of the most horrible disasters, which brings enormous losses and destruction, claiming many lives. [1–4] In the history of mankind, there have been fires that destroyed entire cities (Rome (70, B.C.), London (1666), Moscow (1812), Hamburg (1842), San Francisco (1906)). And these days as indicated by statistics, the number of fires not only does not decrease despite the technical progress but sometimes increases because of them. [5–11]

People since ancient times have searched for solutions to the fires buildings preservation problems, whereas many building materials were highly flammable. The search was crowned with success, when it was discovered

Reinforced concrete was launched by Joseph Monier (1861). In 1938, a progressive method of reinforced concrete strength analysis on destruction stages was obtained by scientists such as A.A. Gvozdev, Y.V. Stolyarov, V.I. Murashev and others. Since 1979, the use of profiled sheet as a retained formwork for construction of monolithic reinforced concrete floor slabs on steel beams started.

Authors R.I. Rabinovich, A.A. Bogdanov, M.G. Karpovskiy, in their researches performed in Promzdaniy Central Research Institute of USSR's Gosstroy and the Donetsk Promstroyniiproekt together with the Concrete and Reinforced Concrete Research Institute, experimentally studied the behaviour of composite slabs in an integrated manner, taking into account reinforced concrete and steel beams of floors.

Any structures must be protected against fire exposure. Therefore, there are requirements about the observance of fire safety. [12–14]

Fire-resistance is a global fire-technical characteristics, regulated with the construction codes and rules such as in Russia (the Federal law of the Russian Federation of 22 July 2008 N 123-FZ "Technical regulations on fire safety requirements"), and in the European Union (Directive 89/106/EC, EN 1991-1-2:2002. Eurocode 1. Impact on Structures. Part 1-2. The General Impact. Exposure to Determine fire Resistance, EN 13501-2:2007+A1:2009. Part 2. Classification Using Test Data on the Combustion Reaction When the Fire Resistance Test, Excluding Ventilation). [15–18, 20–22].

Calculation of steel-concrete composite slabs on profiled sheet as a whole is difficult because it does not have fully-fledged techniques regulated with building codes

In Russia, there is only one method of reinforced concrete structures calculation according to the Guidance to STO 36554501-006-2006 by Milovanov [15].

In European countries, Eurocode 4 "Design of Composite Steel and Concrete Structures. Part 1-2. General Rules. Structural Fire Designs" is used for analyses of fire resistance. [24] There are as well various recommendations, including "The Fire Resistance of Composite Floors with Steel Decking" [25], issued by The Steel Construction Institute.

There is a problem of harmonization of European and Russian standarts establishing General requirements for methods of test for fire resistance of building structures. There is a necessity for a global systematization of computational and experimental methods for fire resistance assessing of building structures and harmonize them with the current regulatory framework in Russian Federation in the fire safety field. [19, 23]

When using the three selected methods were considered their advantages and disadvantages. In the Manual by Milovanov the advantage is presence isofields and isolines, but there are disadvantages that the methodology considered a limited number of beams and narrow examples. There are difficulties in extrapolating the solution of problems. In other codes this is not a problem, but they are not applicable in Russia.

In the paper to determine the possibility of European codes harmonization on the territory of Russia three above-mentioned methods were used: according to the Guidance [15] and two European Standards [24, 25]. These techniques are applicable on the territory of the corresponding countries and therefore can be applied in solving design and construction problems.

The aim of this research was to assess the possibility of using European norms for the analysis of fire resistance of composite reinforced concrete floors and their adaptation in the Russian Federation.

The following objectives were set and addressed in order to achieve the goals:

1. Analysis of the ultimate equilibrium of three fragments of composite reinforced concrete joist floors of differing range of parameters, as described; selection of geometrical and physical characteristics of the structure under a specified load;

2. Analysis of the ultimate equilibrium of the above fragments of floors as described in methods proposed in Eurocode-4 [24]; selection of partial coefficients to maximize the correspondence of methods to each other;

3. Analysis of the ultimate equilibrium of the above fragments of floors as described in the methods proposed in the recommendations of the “The Fire Resistance of Composite Floors with Steel Decking” [25], issued by The Steel Construction Institute.

Methods

For ultimate equilibrium analysis of reinforced concrete slabs according to different design standards there were taken 3 different buildings with different load, the class of functional fire hazard and type of premises.

The limits of fire resistance were taken in accordance with the technical regulations based on the fire resistance of the building:

1. Residential 5-storey building, height – 18m, floor area – 1150 m2. It can be concluded from the tables that the grade of fire resistance – I, structural fire hazard class – C1. It follows that the limit of fire resistance of floors for such a building should not be less than REI60.

2. Public office building – 6-storey building, height – 20.5 m, floor area – 2950 m^2. It can be concluded from the tables that the grade of fire resistance – I and limit of fire resistance of intermediate floors for such a building should not be than REI60.

3. Industrial building – 2-storey building, height – 9.6m, fire danger rating – B, grade of fire resistance – I. Limit of fire resistance of floors for such a building should not be less than REI60.

According to Russian Set of Rules SP 20.13330.2016 (Loads and Impacts), which outlines the normative values of evenly distributed loads depending on the type of room, and loads from floor and equipment, we can say that usually the load on the floor may be the minimum of 1.96 kN/m^2 (if we are not dealing with industrial buildings). In industrial buildings sometimes we have to deal with even more load of 19.6 kN/m^2, but in this work for the range of loads was taken from 3.63 m (load in corridors, staircases and hallways of residential and public buildings) to 17.75 kN/m^2 (conditional load for industrial buildings in the case when there is no data about the hardware).

One of the important parameters for composite reinforced concrete floor is the profiled sheet, adopted from Russian State Standard GOST 24045-94. [26–30]. Selected profiled sheets are shown in table 1.

Concrete of classes B15 to B30 are usually used when designing slabs. Since the class of concrete has little effect on the method for calculating the structure, class B25 is adopted for each model.

The following frequently used rebar diameters were taken for this research:

- bottom reinforcement (bars) – with a diameter of 8 to 12 mm.
- upper reinforcement (mesh) – reinforcement bar class – Br-1 (3 mm in diameter) and A400 (from 6 to 10 mm in diameter). Mesh spacing respectively: 3 x 50 x 50, 6 x 100 x 100, 10 x 200 x 200.

Continuous reinforcement is laid, as a more technologically advanced option. In the same way the rebar continuity provides continuity for the structure. [31–34].

Thus, the summary table for all three studied models can provided as follows:

Table 1. Summary table of the models

	Model 1	Model 2	Model 3
Support and moment diagram	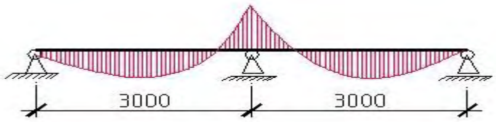		
Functional purpose	Residential	Administrative	Industrial
Type of room	garret	gym	Hydromechanical transmission repair workshop
Limit of fire resistance	REI60	REI60	REI60
Acting load	3.63 kN/m^2	8.04 kN/m^2	17.75 kN/m^2
Profiled sheet	N57-750-0.9 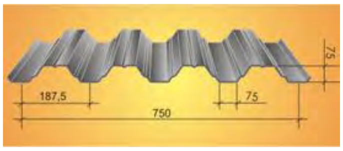	N57-750-0.9 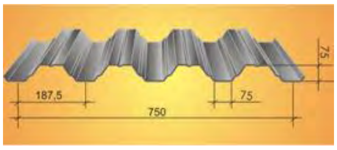	N114-600-0.9 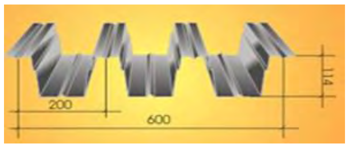
Concrete grade	B25	B25	B25
Method of reinforcements and rebars	Upper: BP-1, 3mm mesh, spacing 50x50 Lower: A-III 8mm	Upper: A-III, 6mm mesh, spacing 100x100 Lower: A-III 10mm	Upper: A-III, 10mm mesh, spacing 200x200 Lower: A-III 12mm
Total floor thickness	107mm	150mm	214mm

Analysis of fire resistance according to STO 36554501-006-2006

The behaviour of reinforced concrete structures under and after standard fire were considered in the "Manual…" of STO, the stress-strain state of structures when briefly exposed to fire before the onset of ultimate fire resistance to loss of carrying capacity were analysed.

The order of analysis of the floors is as follows:

1. Evaluation of fire resistance of the building
2. Evaluation of the bake-out temperature of the section
3. Evaluation of the service factors of the rebars
4. Static analysis of the structure

$$M_u = R_{snt} \cdot A_s \cdot (h_0 - 0.5x) + R_{sct} \cdot A'_s \cdot (0.5x - a') \tag{1}$$

where a' – compressive reinforcement cover, m;

R_{snt} – tensile strength of the reinforcing steel bars under heating, MPa;

R_{sct} – compressive strength of the longitudinal reinforcing steel bars under heating, Mpa;

5. Conclusion of bearing capacity of the section: comparison of the external and ultimate moments.

$$M_0 < M_u \tag{2}$$

Thus, as a result of the analysis on all models the following data were gotten:

Table 2. Summary results of the calculation according to STO

	N57-750-0.9	N57-750-0.9	N114-600-0.9
Ø upper reinforcement	3 mm, 50x50	6 mm, 100x100	10 mm, 200x200
Ø lower reinforcement	8 mm	10 mm	12 mm
h_{prof} (prof. height)	57 mm	75 mm	114 mm
h'_c (comp. zone height)	50 mm	75 mm	100 mm
h_{given} (given height)	85.9 mm	120.9 mm	169.6 mm
q (distributed load)	3.7 KN/m^2	8.2 KN/m^2	18.1KN/m^2
M_0 (bending moment)	4.1 KN·m	9.2 KN·m	20.4 KN·m
A_s (cross-section area of the tensile zone)	50.3 mm^2	78.5 mm^2	113.1 mm^2
A'_s (cross-section area of the comp. zone)	21.3 mm^2	56.6 mm^2	78.5 mm^2
b_{rib} (rib width)	118.25 mm	114.75 mm	122 mm
h_0 (eff. depth of section)	77 mm	120 mm	179 mm
h_t (eff. height under heating)	71.1mm	113mm	179mm
x_{comp} (height of comp. zone of concrete)	4.3мм	5.7мм	9.8мм
M_u (ultimate bending moment)	4.2 KN·m	9.6 KN ·m	29.8KN·m
$M_0 < M_u$	**4.1KN·m<4.2KN·m**	**9.2KN·m<9.6KN·m**	**20.4KN·m<29.8KN·m**

Based on the data from the table, the following conclusions were made:

1. Compressive zone of concrete increases with increasing thickness of the slab in a nonlinear relationship.

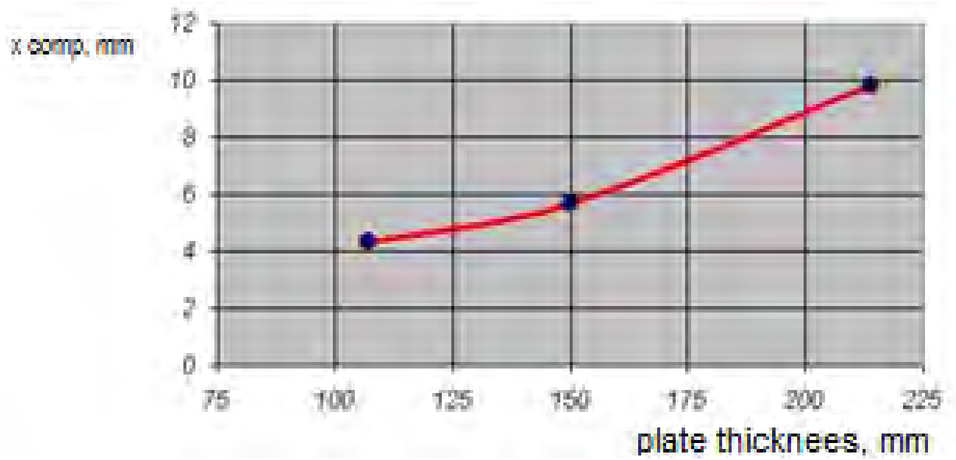

Figure 1. Height of the compressive zone of concrete to slab thickness graph

2. Effective height under heating increases as well with increasing slab thickness.

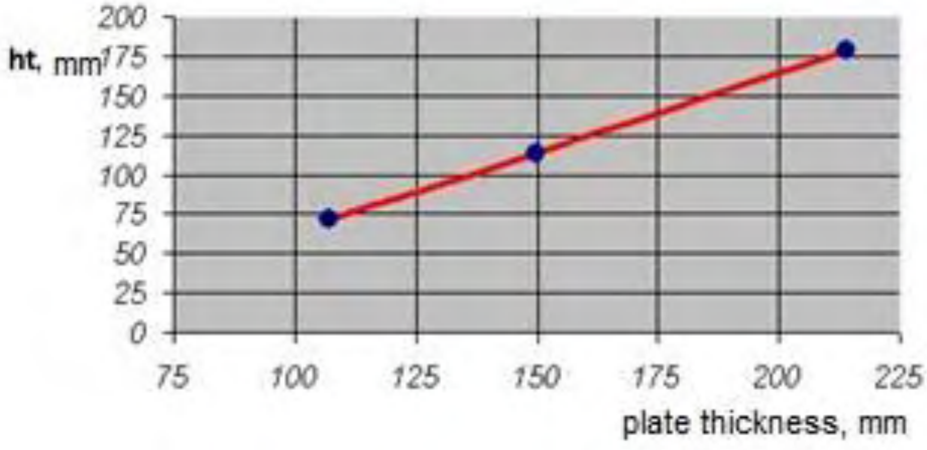

Figure 2. Effective height under heating to slab thickness graph

Fire resistance analysis according to Eurocode-4 "Design of Composite Steel and Concrete Structures – Part 1-2: General Rules – Structural Fire Design"

Fire prevention section of Eurocodes (part 2) determines the characteristics of fire resistance when designing structures that must implement the required functions (bearing and/or enclosure) during the set duration of the regulated impact of the fire at the specified load.

The order of analysis of the floor is as follows:

1. The choice of the design characteristics of materials.
2. Analysis of the structure with a choice of coefficients

$$\eta_{fi} = \frac{G_k + \psi_{fi} Q_{k,1}}{\gamma_G G_k + \gamma_{Q,1} Q_{k,1}} \tag{3}$$

where γ_G – partial factor of variable impact;

$\gamma_{Q,1}$ – partial factor of variable impact 1.

3. Evaluation of the ultimate temperature

$$\theta_{\text{lim}} = d_0 + d_1 \cdot N_s + d_2 \cdot \frac{A}{L_r} + d_3 \cdot \Phi + d_4 \cdot \frac{1}{l_3} \tag{4}$$

where θ_{lim} – limiting temperature [°C];

N_s – axial force in the upper reinforcement [N];

d_i – coefficients, shown in table D.4;

Φ – projection coefficient of top flange.

4. The analysis of bending moments

$$M = z \cdot N_p \tag{5}$$

where z - rib-position indicator [mm$^{-0,5}$];

N_p - tensile force, [кN].

5. Conclusion of bearing capacity of the section: comparison of the external and ultimate moments.

$$M_0 < M_u \tag{6}$$

Thus, as a result of the analysis on all models, the following data were gotten:

Table 3. Summary results of the analysis according to Eurocode-4

	N57-750-0.9	**N57-750-0.9**	**N114-600-0.9**
Ø upper reinforcement	3 mm, 50x50	6 mm, 100x100	10 mm, 200x200
Ø lower reinforcement	8 mm	10 mm	12 mm
$h_{\text{prof.}}$ (prof. height)	57 mm	75 mm	114 mm
E_d (calc. impact)	5.1 KN/m^2	11.67 KN/m^2	26.24 KN/m^2
h_{eff} (eff. height)	85.9 mm	120.9 mm	169.6 mm
G_c (stand. value of const. impact)	3.0 KN/m^2	4.2 KN/m^2	6.1 KN/m^2
Q_c (stand. value of main impact)	0.7 KN/m^2	4.0 KN/m^2	12.0 KN/m^2
M_0 (bending moment)	3.97 KN·m	8.89 KN·m	19.01 KN·m
A_s (cross-section area of the tensile zone)	50.3 mm^2	78.5 mm^2	113.1 mm^2
A'_s (cross-section area of the comp. zone)	21.3 mm^2	56.6 mm^2	78.5 mm^2
$\eta_{\text{f,i}}$ (coeff. of .reduction)	0.66	0.6	0.64
ψ (combination factor)	0.5	0.7	0.9
$\frac{A}{L}$ (given rib thickness)	30.96 mm	34.5 mm	41.6 mm
θ_{top} (top flange temp.)	635.8 C	598.3 C	514.1 C
θ_{mid} (mid flange temp.)	748.7 C	726.8 C	677.3 C
θ_{bot} (bottom flange temp.)	847.5 C	850.8 C	845.3 C
θ_{rod} (rod temp.)	368.7 C	380.9 C	342.4 C
x_{comp} (height of comp. zone of concrete)	4.53 mm	7.1 mm	10.2 mm
M_u (ult. moment)	4.13 KN·m	9,24 KN·m	24.85 KN·m
$M_0 < M_u$	**3.97KN·m<4.13KN·m**	**8.89KN·m<9.24KN·m**	**19.01KN·m<24.85KN·m**

Based on the data from the table, the following graphs were plotted:

1. Compressive zone of concrete increases with increasing slab thickness in a curvilinear relationship, the numerical values are close to the values obtained in the analysis according to STO

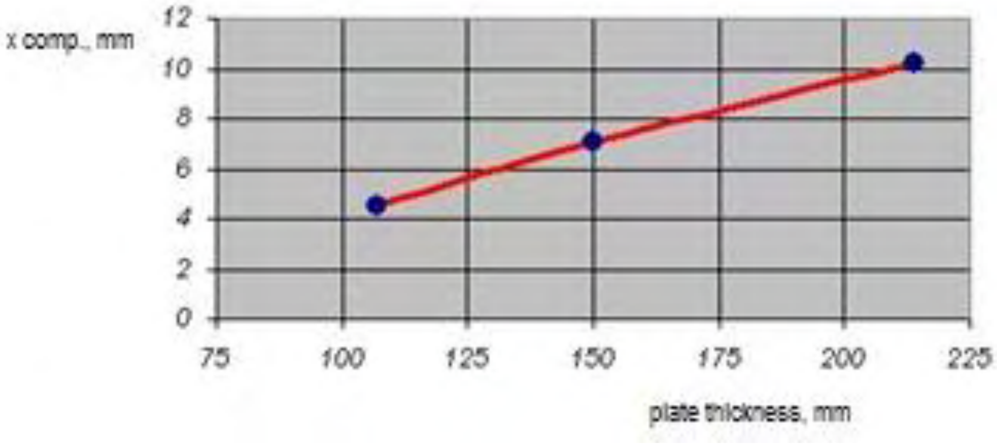

Figure 3. Height of the compressive zone of concrete to slab thickness graph

Fire resistance analysis according to the recommendations of “The Fire Resistance of Composite Floors with Steel Decking”, issued by The Steel Construction Institute

The order of analysis of the floor is as follows:

1. The choice of the design characteristics of materials.
2. Analysis of the bending moments for continuous structures,

$$M_0 = \frac{L^2 \cdot (\gamma_{fd} \cdot W_d + \gamma_{fi} \cdot W_i)}{8} \quad (7)$$

where *L* – span, [м];

γ_{fd}, γ_{fi} – load safety factor;

3. Conclusion of the compliance of limit of fire resistance and the need for additional reinforcement.

Thus, as a result of the analysis on all models, the following data were gotten:

Table 4. Summary results of the analysis according to Eurocode-4

	N57-750-0.9	N57-750-0.9	N114-600-0.9
Ø upper reinforcement	3 mm, 50x50	6 mm, 100x100	10 mm,200x200
Ø lower reinforcement	8 mm	10 mm	12 mm
h_{PROF} (prof. height)	57 mm	75 mm	114 mm
W_d (floor load)	3.0 KN/m2	4.2 KN /m2	6.1 KN /m2
W_i (live load)	0.7 KN /m2	4.0 KN /m2	12.0 KN/m2
M_0 (bending moment)	4.1 KN·m	9.2 KN·m	20.1 KN·m
d_{COMP} (comp. zone of concrete)	4.9 mm	7.8 mm	11.2 mm
M_U (ultimate bending moment)	4.2 KN ·m	10.4 KN·m	25.5 KN·m
$M_0 < M_U$	**4.1KN·m<4.2KN·m**	**9.2KN·m<10.4KN·m**	**20.1KN·m<25.5KN·m**

Based on the data from all models, the following conclusions can be made:

1. The curve of the compressive zone height to the thickness of the floor is a straight-line, when the thickness of the slab increases, the thickness of the compressive zone of the slab increases respectively

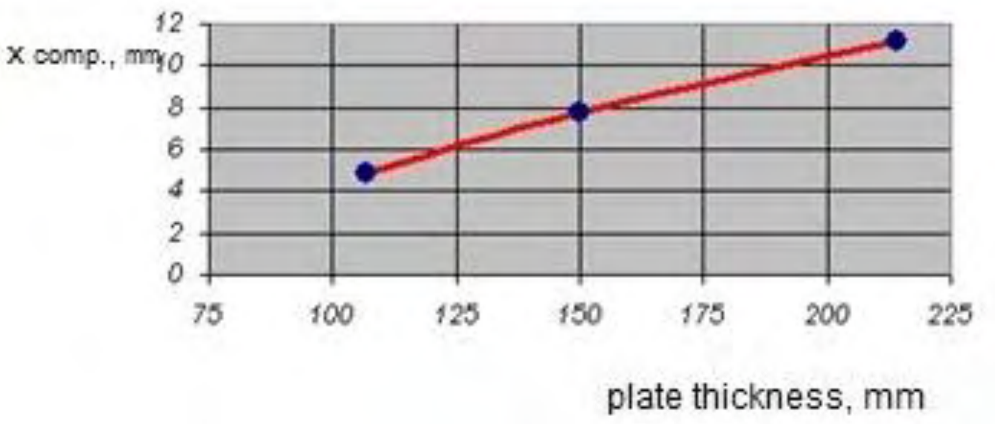

Figure 4. Height of compressive zone of concrete to slab thickness graph

Results and Discussion

To prove the reliability of the results obtained in the calculation for the three above-mentioned methods, the model was calculated by the finite element method (FEM)

The calculation was carried out in the SCAD Office software (version 11.3). For calculation, the third model of the slab with the profiled sheet H114-600-0,9 for the industrial building was adopted. The thickness of this slab is 214 mm.

When calculating by the FEM, the profiled sheet was not modeled. It was taken into account that the stresses of the profiled sheet reach the yield point of steel in conditions of fire action.

Model:

Number of nodes: 252 630;

Number of elements: 224 800;

The size of grid is 15mm;

Boundary conditions - fixing by the X, Y, Z-axes at the beginning, middle and end of the slab.

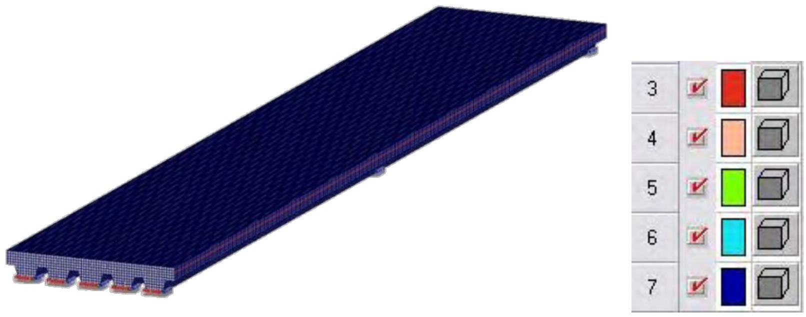

Figure 5. Model of the slab fragment for calculation according to FEM
3 types of elements:

- bars;
- 6-node isoparametric finite elements;
- 8-node isoparametric finite elements.

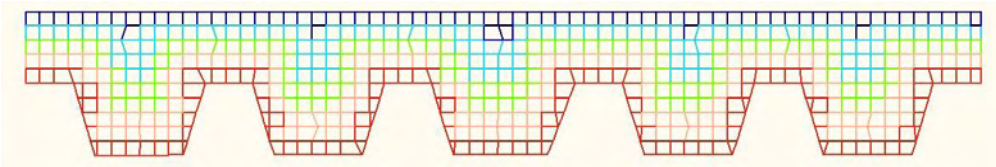

Figure 6. The partitioning into finite elements in cross section of the slab

Fire is a consequence of designed emergency case, according to 1.5.2.5 EN 1990. Possibility of deformational analysis according to Russian and foreign normative documents is considered.

Value of variable force for designed emergency case must be installed pursuant to EN 1990, according to appendix 4.2.1 of EN 1991-1-2. However, as it is stated in A.1.4. appendix, limit state is normed by second group of limit states that does not include any emergency cases such as fire. Emergency load is considered only in bearing capacity calculation (appendix A.1.3). Thus, structural normative documents do not regulate analysis of deformations in fire case. Also, Russian Set of Rule SP.20.13330.2011 and [15] do not consider fire impact deformation analysis.

However, limit state takes place if deformation value reaches 5% of span value, according to Russian State Standard GOST 30247.1.

$$f_{\max} = \frac{l}{20} = \frac{3000}{20} = 150\text{mm} \tag{8}$$

$$f_{slab} = 1.03\text{mm} \tag{9}$$

$$f_{slab} < f_{\max} \tag{10}$$

where, f_{max} – ultimate slab information [mm]

f_{slab} – slab deformation, [mm];

l – length of plate, [mm];

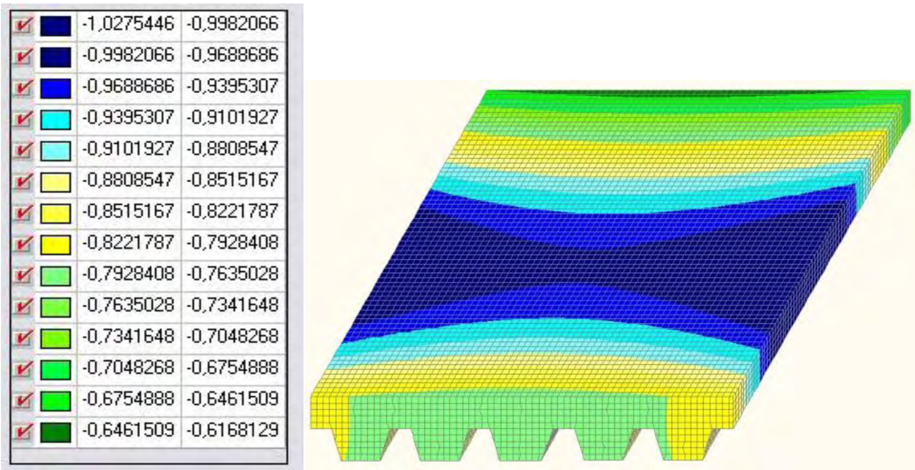

Figure 7. The displacements isofields results by Z-axis of the half-plate (mm)

As all the deflections of the slab are much less than the ultimate, it can be concluded that the steel-reinforced concrete slab should be calculated according to the first group of ultimate fire resistance states only (in strength), because in the calculation of the second group of limiting states the rigidity conditions are satisfied automatically.

The condition for the strength of the slab can be expressed as follows:

$$\sigma_{\max} < R_{bnt} \tag{11}$$

where σ_{max} – maximum normal stress [MPa];

R_{bnt} – characteristic concrete resistance to compression under fire activity, [MPa]

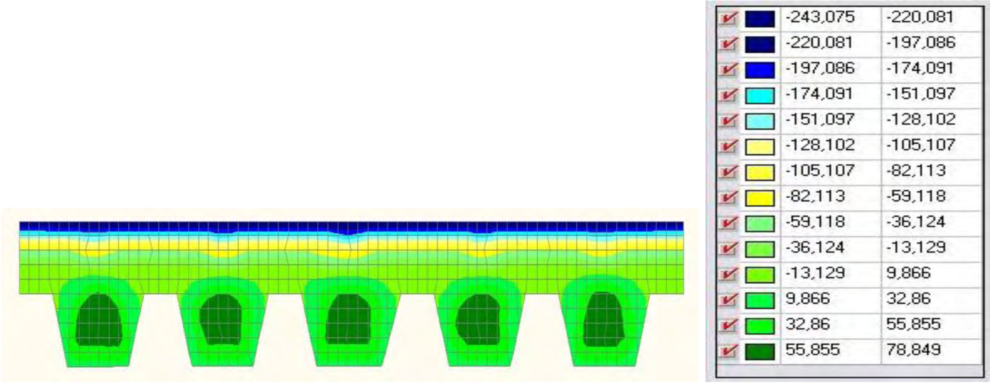

Figure 8. The cross-section normal stresses isofields of the middle span cross-section of the plate (10-2 MPa)

According to this strength calculation, it is possible to draw the conclusions:

• When finite elements method calculating in the elastic stage, the neutral line is sharply shifted;
• The elasto-plastic stage of the concrete operation in the fire activity occurs much earlier than under normal use conditions;
• It is not advisable to calculate the steel reinforced concrete slab for the fire action in the elastic stage.

Also the following strength calculating condition must be satisfied:

$$\sigma_{\max} = N_{\max}/A_s < R_{snt} = R_{sn} * \gamma_{st} \tag{12}$$

where N_{max} – maximum tensile force in the reinforcement bar, [kg];

A_s – reinforcement bar area, [mm^2];

R_{snt} – characteristic tensile resistance of the reinforcement bar under fire activity, [MPa];

R_{sn} – characteristic tensile resistance of the reinforcement bar, [МПа];

γ_{st} – condition load effect factor of the reinforcement bar

Thus, the strength calculation results are shown in Table 5.

Table 5. Results of strength calculating of the slab

reinforcement	Nmax, daN	As, mm2	σmax	Rsn, MPa	ɤst	Rsnt, MPa	Conclusion
top	20	28.3	7.1	400	1.0	400	$\sigma_{\max} < R_{snt}$
bottom	271	78.5	34.5		0.63	252	$\sigma_{\max} < R_{snt}$

When calculating, the upper and lower reinforcement were considered for compliance with the strength condition.

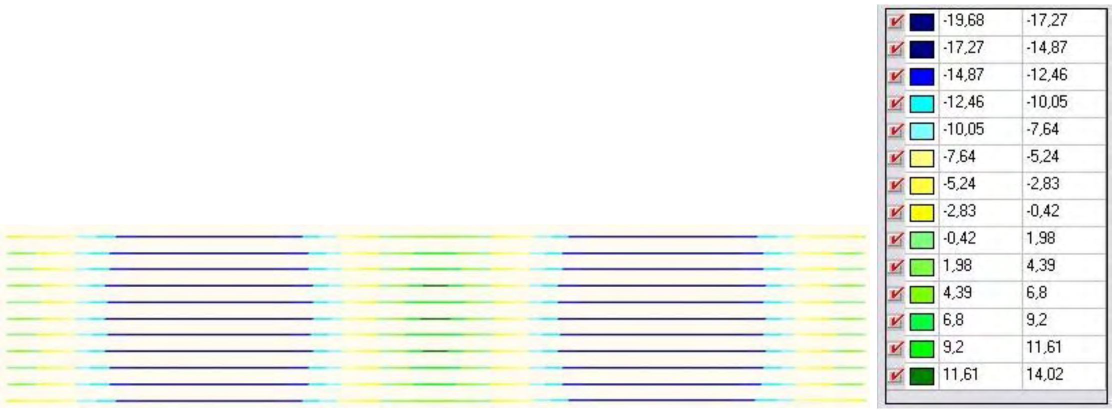

Figure 9. Top reinforcement bar axial force isofields (daN)

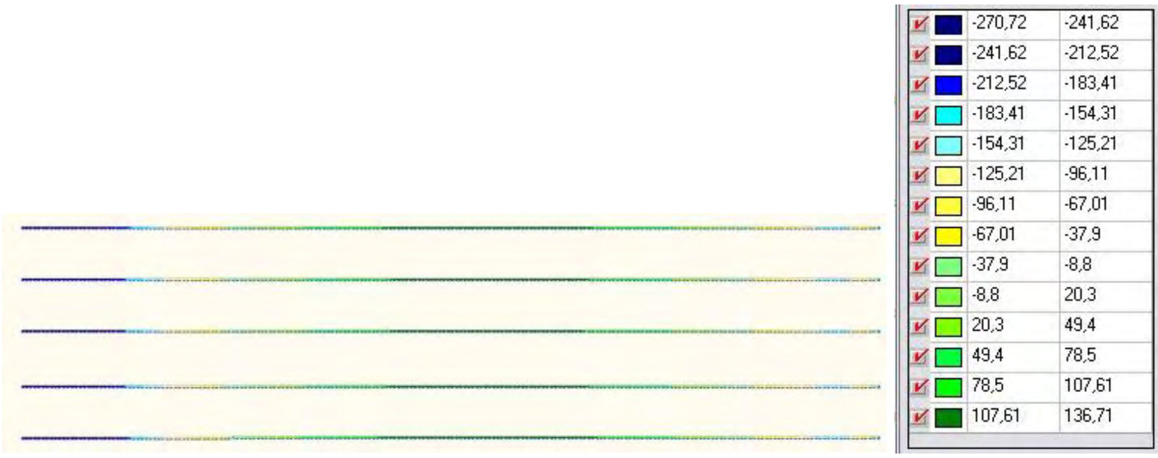

Figure 10. Bottom reinforcement bar axial force isofields (daN)

As can be seen from figures 8, 9, 10 and table 5 stresses in concrete and reinforcement within the allowable. Thus, the slab retains its bearing capacity during fire exposure for 60 minutes.

Conclusions

In the course of this work, the following conclusions were made:

1. It was shown that the compressive zone of concrete is located above the rebars, which means that the floor is a heavily reinforced structure at the time of fire;

2. It was shown that the analysis according to Eurocode-4 corresponds with the analysis according to Milovanov's manual to STO which is confirmed by close results of analysis of external and ultimate moments when exposed to fire;

3. It was shown that the recommendations of the Steel Construction Institute are identical to the fire prevention section of the Eurocode-4 which is confirmed by the same approach of analysis of the positive bending moments and the same results when analyzing the negative moments;

4. It is suggested to use the following partial coefficients of variable impact for the analysis of fire resistance according to Eurocode in the Russian Federation: for dead loads – 1.35, for live loads – 1.5;

5. Reliability of the calculation results for the three methods (Manual for STO, Eurocode, "Recommendations…") is confirmed by the results obtained by the finite element method.

Reference

1. Kolomiytsev D.E., Rodicheva A.O., Rybakov V.A. Eksperimentalnoe opredelenie ognestoykosti mezhduetazhnykh perekrytiy na osnove stalnykh tonkolistovykh profiley [Experimental determination of fire resistance of intermediate floors based on light-gage steel profiles]. *XXXIX SPbSPU science week: Materials of the International Science-Practical Conference.* P.1. Saint-Petersburg, 2010. Pp. 194–197. (rus)
2. Kolomiytsev D.E., Rodicheva A.O., Rybakov V.A. Opredelenie ognestoykosti fragmentov mezhduetazhnogo perekrytiya na osnove stalnykh S-obraznykh profiley [Determination of fire resistance of the fragments of intermediate floors based on C-shaped steel profiles]. *Magazine of Civil Engineering*. 2010. No. 8(18). Pp. 32–37. (rus)
3. Kolomiytsev D.E., Rodicheva A.O., V.V.Feofanov. Ognestoykost mezhduetazhnogo perekrytiya na osnove stalnykh S-obraznykh profiley [Fire resistance of intermediate floors based on C-shaped steel profiles*]. Mir stroitel'stva i nedvizhimosti.* 2011. No. 38. Pp. 46–50. (rus)
4. Roytman V.M. *Ognestoykost konstruktsiy, zdaniy i sooruzheniy: sovremennye problemy otsenki* [Fire

Литература

1. Коломийцев Д.Е., Родичева А.О., Рыбаков В.А. Эксперементальное определение огнейстойкости междуэтажных перекрытий на основе стальных тонколистовых профилей // XXXIX Неделя науки СПбПУ: Материалы международной научно-практической конференции. Ч. 1. Санкт-Петербург: СПбПУ, 2010. С.194–197.
2. Коломийцев Д.Е., Родичева А.О., Рыбаков В.А. Огнестойкость междуэтажного перекрытия на основе стальных С-образных профилей // Инженерно-строительный журнал. 2010. № 8(18). С. 32–37.
3. Коломийцев Д.Е., Родичева А.О., Феофанов В.В. Огнестойкость междуэтажного перекрытия на основе стальных С-образных профилей // Мир строительства и недвижимости. 2011. № 38. С. 46–50.
4. Ройтман В.М. Огнестойкость конструкций, зданий и сооружений: современные проблемы оценки. М.: Стройпрофиль, 2010. 9 с. 4.
5. Федоров В.С., Левицкий В.Е., Молчадский И.С., Александров А.В. Огнестойкость и пожарная опасность строительных конструкций. М.: АСВ, 2009. 360 с.
6. Кривцов Ю.В., Микеев А.К., Пронин Д.Г. Развитие

Rybakov V.A., Ananeva I.A., Rodicheva A.O., Ogidan O.T. Stress-strain state of composite reinforced concrete slab elements under fire activity. *Magazine of Civil Engineering*. 2017. No. 6. Pp. 161–174. doi: 10.18720/MCE.74.13.

resistance of building and structures: Present Problems of Valuation]. Moscow: Stroyprofil, 2010. 9 p. (rus)
5. Fedorov V.S., Levitskiy V.E., Molchadskiy I.S., Aleksandrov A.V. *Ognestoykost i pozharnaya opasnost stroitelnykh konstruktsiy* [Fire resistance and fire hazard of building constructions]. Moscow: ASV, 2009. 360 p. (rus)
6. Krivtsov Yu.V., Mikeev A.K., Pronin D.G. Razvitie trebovaniy pozharnoy bezopasnosti k ognestoykosti konstruktsiy v stroitelnykh normakh i pravilakh, razrabatyvaemykh TsNIISK [The development of fire safety requirements of structures in rules and regulation developed by CRICS. *Industrial and Civil Engineering.* 2009. No. 10. Pp. 25–26. (rus)
7. Krivtcov A., Gravit M., Zimin S., Nedryshkin O., Pershakov V. Calculation of limits of fire resistance for structures with fire retardant coating. *Matec Web of Conferences.* 2016. Pp. 23–27.
8. Ulybin A.V. Inspection methods of reinforcement parameters of concrete structures. *Magazine of Civil Engineering.* 2012. No. 1(27). Pp. 4–13. (rus)
9. Sokolov V.A., Strakhov D.A. Prochnost i treshchinostoykost zhelezobetonnykh konstruktsiy [Strength and crack resistance of reinforced concrete structures]. LAP LAMBERT, 2012. 120 p. (rus)
10. Heinisou M, Jokinen T. Tabular composite columns in a non-symmetrical fire. *Magazine of Civil Engineering.* 2014. No. 5(49). Pp. 107–120.
11. Dry C., Corsaw M. A. Comparison of bending strength between adhesive and steel reinforced concrete with steel only reinforced concrete. *Cement and Concrete Research*. 2003. Pp. 1723–1727.
12. Korsun V., Vatin N., Korsun A., Nemova D. Physical-mechanical properties of the modified fine-grained concrete subjected to thermal effects up to 200 °C. *Applied Mechanics and Materials.* 2014. Pp. 1013–1017.
13. Korsun V., Mashtaler S., Vatin N., Korsun A., Franchi A., Crespi P. The strength and strain of high-strength concrete elements with confinement and steel fiber reinforcement including the conditions of the effect of elevated temperatures. *Procedia Engineering*. 2015. № 117. Pp. 970–979.
14. Korsun V., Korsun A. The influence of precompression on strength and strain properties of concrete under the effect of elevated temperatures. *Applied Mechanics and Materials*. 2015. Pp. 469–474.
15. Milovanov A.F. *Ognestoykost zhelezobetonnykh konstruktsiy* [Fire resistance of reinforced concrete structures]. Moscow: Stroyizdat, 1986. 442 p. (rus)
16. Roytman M.Ya. *Protivopozharnoe normirovanie v stroitelstve* [Fire regulation in construction]. Moscow: Stroyizdat, 1985. 85 p. (rus)
17. Khudikovskiy V.L., Zaytsev A.M., Progrev zhelezobetonnykh konstruktsiy pri pozhare [Heating of reinforced concrete structures under fire]. *Scientific Herald of the Voronezh State University of Architecture and Civil Engineering. Construction and Architecture.* 2008. No. 3. Pp. 188–191.
18. Ilin N.A. Opredelenie ognestoykosti stroitelnykh konstruktsiy zdaniy i sooruzheniy [Determination of fire resistance of buildings and structures]. *Modern High Technologies.* 2009. No. 1. Pp. 34–38. (rus)
19. Gravit M., Gumenyuk V., Nedryshkin O. Fire resistance parameters for glazed non-load-bearing curtain walling structures. Extended application. *Procedia Engineering*. 2015. Pp. 114–118.
20. *EN 1991-1-2:2002 Eurocode 1*: Actions on structures. Part 1-2: General actions. Actions on structures exposed to fire. Brussels: GEN 1991.
21. *Construction Products Directive 89/106/EC (Council Directive 89/106/EC)*, website of European Commission, 1989
22. *EN 13501-2:2007+A1:2009* Fire classification of construction products and building elements – Part 2: Classification using data from fire resistance tests,

требований пожарной безопасности к огнестойкости конструкций в строительных нормах и правилах, разрабатываемых ЦНИИСК // Промышленное и гражданское строительство. 2009. № 10. С. 25–26.
7. Krivtcov A., Gravit M., Zimin S., Nedryshkin O., Pershakov V. Calculation of limits of fire resistance for structures with fire retardant coating // Matec Web of Conferences. 2016. Pp. 23–27.
8. Улыбин А.В. Методы контроля параметров армирования железобетонных конструкций // Инженерно-строительный журнал. 2012. № 1(27). С. 4–13.
9. Соколов В.А., Страхов Д.А. Прочность и трещиностойкость железобетонных конструкций. LAP LAMBERT, 2012. 120 с.
10. Хейнисуо М., Йокинен Т. Асимметричное огневое воздействие на цилиндрические композитные колонны // Инженерно-строительный журнал. 2014. №5(49). С. 107–120.
11. Dry C., Corsaw M.A. Comparison of bending strength between adhesive and steel reinforced concrete with steel only reinforced concrete // Cement and concrete research. 2003. Pp. 1723–1727.
12. Korsun V., Vatin N., Korsun A., Nemova D. Physical-mechanical properties of the modified fine-grained concrete subjected to thermal effects up to 200 °C // Applied Mechanics and Materials. 2014. Pp. 1013–1017.
13. Korsun V., Mashtaler S., Vatin N., Korsun A., Franchi A., Crespi P. The strength and strain of high-strength concrete elements with confinement and steel fiber reinforcement including the conditions of the effect of elevated temperatures // Procedia Engineering. 2015. № 117. Pp. 970–979.
14. Korsun V., Korsun A. The influence of precompression on strength and strain properties of concrete under the effect of elevated temperatures // Applied Mechanics and Materials. 2015. Pp. 469–474.
15. Милованов А.Ф. Огнестойкость железобетонных конструкций. М.: Стройиздат, 1986. 442 с.
16. Ройтман М.Я. Противопожарное нормарование в строительстве. М.: Стройиздат, 1985. 85 с.
17. Худиковский В.Л., Зайцев А.М. Прогрев железобетонных конструкций при пожаре // Научный вестник Воронежского государственного архитектурно-строительного университета. Строительство и архитектура. 2008. № 3. С. 188–191.
18. Ильин Н.А. Определение огнестойкости строительных конструкций зданий и сооружений // Современные наукоёмкие технологии. 2009. № 1. С. 34–38.
19. Gravit M., Gumenyuk V., Nedryshkin O. Fire resistance parameters for glazed non-load-bearing curtain walling structures. Extended application // Procedia Engineering. 2015. Pp. 114–118.
20. EN 1991-1-2:2002 Eurocode 1: Actions on structures. Part 1-2: General actions. Actions on structures exposed to fire. Brussels: GEN 1991.
21. Construction Products Directive 89/106/EC (Council Directive 89/106/EC), website of European Commission, 1989.
22. EN 13501-2:2007+A1:2009 Fire classification of construction products and building elements – Part 2: Classification using data from fire resistance tests, excluding ventilation services. Edition: 2010-02-15, 2008.
23. Хазанов И.Р., Гравит М.В., Косачев А.А., Пехотиков А.В., Павлов В.В. Гармонизация европейских и российских нормативных документов, устанавливающих общие требования к методам испытаний на огнестойкость строительных конструкций и применению температурных режимов, учитывающих реальные условия пожара // Пожаровзрывобезопасность. 2014. С. 49–57.
24. EN 1994-1-2:2005 Eurocode 4: Design of composite steel and concrete structures. Part 1-2: General rules — Structural fire design. Brussels: CEN 1994.

Рыбаков В.А., Ананьева И.А., Родичева А.О., Огидан О.Т. Напряженно-деформированное состояние фрагмента сталежелезобетонного перекрытия в условиях огневого воздействия // Инженерно-строительный журнал. 2017. № 6(74). С. 161–174.

excluding ventilation services. Edition: 2010-02-15, 2008
23. Khasanov I.R., Gravit M.V., Kosachev A.A., Pekhotikov A.V., Pavlov V.V. Garmonizatsiya yevropeyskikh i rossiyskikh normativnykh dokumentov, ustanavlivayushchikh obshchiye trebovaniya k metodam ispytaniy na ognestoykost stroitelnykh konstruktsiy i primeneniyu temperaturnykh rezhimov, uchityvayushchikh realnyye usloviya pozhara [Harmonisation of European and Russian regulatory documents establishing General requirements for methods of test for fire resistance of building structures and application of temperature regimes, taking into account the real conditions of a fire]. *Pozharovzryvobezopasnost*. 2014. Pp. 49–57. (rus)
24. *EN 1994-1-2:2005 Eurocode 4:* Design of composite steel and concrete structures. Part 1-2: General rules — Structural fire design. Brussels: CEN 1994.
25. Newman G.M. *The fire resistance of composite floors with steel decking* (Second Edition). SCI Publication 056, The Steel Construction Institute, Ascot. 1991. 29 p.
26. Kim H.-Y., Jeong Y.-J. Ultimate strength of a steel–concrete composite bridge deck slab with profiled sheeting. *Engineering Structures.* 2010. Vol. 32. No. 2. Pp. 534–546.
27. Mirza O., Uy. B. Behaviour of headed stud shear connectors for composite steel–concrete beams at elevated temperatures. Journal of Constructional Steel Research. 2009. Vol. 65. No. 3. Pp. 662–674.
28. Jiangyuan H., Chung D.D.L. Cathodic protection of steel reinforced concrete facilitated by using carbon fiber reinforced mortar or concrete. *Cement and concrete research.* 1997. Pp. 649–656.
29. Suehrcke H., Daldehog D., Harris J.A., Lowe R.W. Heat transfer across corrugated sheets and honeycomb transparent insulation. *Solar Energy.* 2004. Pp. 351–358
30. Demadis K.D., Papadaki M., Raptis R.G., Zhao H. Corrugated, sheet-like architectures in layered alkaline-earth metal r,s-hydroxyphosphonoacetate frameworks: applications for anticorrosion protection of metal surfaces. *Chemistry of Materials.* 2008. Pp. 4835–4846.
31. Porter M.L., Greimann L.F. Shear-bond strength of studded steel deck slabs. *Seventh International Specialty Conference on Cold-Formed Structures.* St. Louis, Missouri, U.S.A. 1984. Pp. 285–306.
32. Dmitriev A.N. Peculiar calculation of actual fire-resistance limits of steel and reinforced concrete building structures. *Industrial and Civil Engineering.* 2007. No. 6 . Pp. 25–28.
33. Bychkov E. Concrete reinforcement: modern reinforced concrete products in Russia. *Concrete Engineering International.* 2007. 20 p.
34. Beliaev M., Semenov A., Semenov S., Benin A. Simulation of pulling the reinforcing bar from concrete block with account of friction and concrete damage. *MATEC WEB OF CONFERENCES.* 2016. Pp. 4–10.

25. Newman G.M. The fire resistance of composite floors with steel decking (Second Edition). SCI Publication 056, The Steel Construction Institute, Ascot. 1991. 29 p.
26. Kim H.-Y., Jeong Y.-J. Ultimate strength of a steel–concrete composite bridge deck slab with profiled sheeting // Engineering Structures. 2010. Vol. 32. № 2. Pp. 534–546.
27. Mirza O., Uy. B. Behaviour of headed stud shear connectors for composite steel–concrete beams at elevated temperatures // Journal of Constructional Steel Research. 2009. Vol. 65. № 3. Pp. 662–674.
28. Jiangyuan H., Chung D.D.L. Cathodic protection of steel reinforced concrete facilitated by using carbon fiber reinforced mortar or concrete // Cement and concrete research. 1997. Pp. 649–656.
29. Suehrcke H., Daldehog D., Harris J.A., Lowe R.W. Heat transfer across corrugated sheets and honeycomb transparent insulation // Solar Energy. 2004. Pp. 351–358.
30. Demadis K.D., Papadaki M., Raptis R.G., Zhao H. Corrugated, sheet-like architectures in layered alkaline-earth metal r,s-hydroxyphosphonoacetate frameworks: applications for anticorrosion protection of metal surfaces // Chemistry of Materials. 2008. Pp. 4835–4846.
31. Porter M.L., Greimann L.F. Shear-bond strength of studded steel deck slabs // Seventh International Specialty Conference on Cold-Formed Structures. St. Louis, Missouri, U.S.A. 1984. Pp. 285–306.
32. Дмитриев А.Н. Особенности расчета фактических пределов огнестойкости сталежелезобетонных строительных конструкций // Промышленное и гражданское строительство. 2007. № 6. С. 25–28.
33. Bychkov E. Concrete reinforcement: modern reinforced concrete products in Russia // Concrete Engineering International. 2007. 20 p.
34. Beliaev M., Semenov A., Semenov S., Benin A. Simulation of pulling the reinforcing bar from concrete block with account of friction and concrete damage // MATEC WEB OF CONFERENCES. 2016. Pp. 4–10.

Vladimir Rybakov,
+7(964)3312915; fishermanoff@mail.ru

Irina Ananeva,
+7(931)9714391; irina.ananeva94@yandex.ru

Anna Rodicheva,
+7(951)6542356; vse_zdes@mail.ru

Olamipe Ogidan,
+7(911)0967745; ogidano@gmail.com

Владимир Александрович Рыбаков,
+7(964)3312915; эл. почта: fishermanoff@mail.ru

Ирина Александровна Ананьева,
+7(931)9714391;
эл. почта: irina.ananeva94@yandex.ru

Анна Олеговна Родичева,
+7(951)6542356; эл. почта: vse_zdes@mail.ru

Оламипе Тимоти Огидан,
+7(911)0967745; эл. почта: ogidano@gmail.com

Rybakov V.A., Ananeva I.A., Rodicheva A.O., Ogidan O.T. Stress-strain state of composite reinforced concrete slab elements under fire activity. *Magazine of Civil Engineering*. 2017. No. 6. Pp. 161–174. doi: 10.18720/MCE.74.13.

doi: 10.18720/MCE.74.14

Stress-strain state of precast and cast-in place buildings

Напряжённо-деформированное состояние сборно-монолитного здания

A.A. Koyankin,
Siberian Federal University, Krasnoyarsk, Russia
V.M. Mitasov,
Novosibirsk State University of Architecture and Construction, Novosibirsk-8, Russia

Канд. техн. наук, доцент А.А. Коянкин,
Сибирский федеральный университет, г. Красноярск, Россия
д-р техн. наук, профессор В.М. Митасов,
Новосибирский государственный архитектурно-строительный университет, г. Новосибирск-8, Россия

Key words: life cycle; reinforced concrete structures; precast with cast-in place construction; genetic nonlinearity; phasing approach of assembling; phasing of the force application

Ключевые слова: жизненный цикл; железобетонные конструкции; сборно-монолитные конструкции; генетическая нелинейность; поэтапность монтажа; поэтапность приложения нагрузки

Abstract. Based on the stages of the construction period of the life cycle of the building, the authors examined the influence of gradual inclusion in the work, including the editing process, its individual building elements on the stress-strain state of a building and its individual design. Determined the nuances of the existence of the building (a separate structure), which should be taken into account at the design stage. These nuances are present in the real structure, but cannot be determined for calculations in the classical way (without changing the stress-strain state in process of erection and loading). Conducted numerical studies of the stress-strain state of a flat frame made from collapsible-monolithic reinforced concrete with account of the phased construction. Also fulfilled a comparative analysis of the obtained results with data of calculation of the same frame, but not taking into account phasing of construction of the structure.

Аннотация. Авторами статьи, исходя из этапов периода строительства жизненного цикла здания, рассмотрено влияние поэтапности включения в работу, в том числе в процессе монтажа, отдельных его элементов на напряжённо-деформированное состояние, как здания, так и отдельной его конструкции. Определены нюансы существования здания (отдельной конструкции), которые должны учитываться на стадии проектирования, присутствуют в реальном сооружении, но не могут быть определены при выполнении расчётов классическим способом (без учёта изменения напряжённо-деформированного состояния по мере возведения и нагружения). Проведены численные исследования напряжённо-деформированного состояния плоского каркаса из сборно-монолитного железобетона с учётом поэтапности возведения, а также выполнен сравнительный анализ полученных результатов с данными расчёта аналогичного каркаса, но не учитывающего этапность возведения.

Introduction

Modern building has reached a high level of development. Engineers are ready to offer to customer buildings of any form and size, including almost of one kilometer height [1–4]. There is a wide range of building materials for carcass construction and it’s finishing. The choice of these materials is defined by functional and constructive details of the building being erecting and by geographic and hydrogeological location of the construction site. The main types of materials used for load-carrying frame erection [5–10, 26], are reinforced concrete, metal, wood and stone. They can be classified basing on a technology of manufacturing used: cast-in place, precast and precast with cast-in-place reinforced concrete structures; rolled metal products and light steel thin-walled structures; solid wood and laminated wood structures; brick, blocks (various types) etc.

Construction design of buildings (foundations, columns, walls, slabs etc.), and also the constructive system developed from them (carcass, wall, mixed), combined with building materials used for their erection throughout the life cycle of the building, including the period of construction, experience different conditions, separated from each other by the appearing of a new factor. This leads to a quality change of stress-deformed state, as a separate construction, and the entire building as well. We define these states as "stage of the life cycle". To these factors are referred: occurrence of additional, principally different from other forces; change of the structural design; change of mechanical-and-physical properties etc. We point out that the definition "stage of the life cycle" can be applied to a separate construction and the building in general as well.

It should be noted, there are not many works that are devoted to influence of the previous existence of the stress-deformed state at various "stage of the life cycles" on the stress-deformed state of building and/or separate structure. However, there is the conclusion about the impact on the stress-deformed state of construction of the earlier stages of its existence from already carried out works. In particular, Professor Perel'muter indicated in [11] "Most of the action done during assembly, leads to changes of the design scheme and/or the stress and deformed state of the system". This fact was successfully confirmed in number of other scientific papers. In particular in [12, 13] devoted to the reinforcement of building structures under load. Within the individual element (beam), the impact of the stress-deformed state of construction in the previous stage to the stress-deformed state the subsequent stage has been shown not only numerically, but also experimentally. The authors of the works [14, 15] present the results of calculations (in linear statement) structures of buildings, qualitative difference evident between calculations made according to traditional methods. The methods corresponds to finished state of the object, and calculations carried out taking into account the phasing of construction of the building. Based on the calculations (flat bar system, a linear formulation of the problem), in [16–18] shows discrepancies in the efforts of the elements when performing calculations with and without allowance for the assembly process. On this basis, conclusions were made about the necessity of taking into account the stage of construction of the building when performing the structural design. Some foreign scientists [19–25] also conducted studies, which confirmed the necessity of taking into account the phased assembly of building structures when performing the calculation of load-bearing structures of the building.

As an example of time phasing for "the stages of the construction period of the life cycle" of a separate construction existence we consider a single-bay precast with cast-in-place two-story frame, with the following stages of construction:

1. Assembling of 1-st floor columns;
2. Assembling by use of a temporary conductors, unit beams of 1-st floor (pinned connection);
3. Post stressed reinforcement fixing on unit beams of the 1-st floor. Laying of high-tensile reinforcement on according channels of assembled part with its post tensioning "on concrete". Unit beam is still pinned on the columns, but with tight clamping its ends by vertical lead-carrying elements. Additional load – force of clamping at the level of unit beams of 1-st floor;
4. Assembling of 2-nd floor columns;
5. Assembling by use of temporary conductors of 2-nd floor unit beams (pinned connection);
6. Stressed reinforcement fixing on 2-nd floor unit beams, similarly as in the 1-st floor beam. Additional load – force of prestressing clamping at the level of 2-nd floor unit beam.
7. Fixing of slab unit elements (slab-casing) and laying of cast-in-place concrete of 1-st and 2-nd floor. At this phase freshly placed cast-in-place concrete has not yet gained the required resistibility and, accordingly, as the load-carrying element is not considered. Unit beam pinned on the columns with tight clamping of the ends. Additional load – weight of built-up construction and weight of cast-in-place concrete.
8. Gaining of the required strength by the cast-in-place concrete. Cast-in-place concrete has gained strength, but until the moment additional force application, is unloaded and no tension occurs from external loads. Structural design of precast with cast-in-place beam does not change, and it becomes rigidly restrained beam;
9. Additional assembling load application (floor construction weight, dividing walls, load-bearing walls) and operation load on the slabs of 1-st and 2-nd floors.

Similarly there is a division into stages and other periods (exploitation, reconstruction, repair, dismantling, etc.) life cycle of the building.

Consideration of the existence of the building based on individual stages from different periods of the life cycle and including them in the design allows:

– to define the real stress deformed state (separate construction) at each stage of its life considering tension and deformation, occurred earlier. In practice [11] the professor Perelmunter A.V., using the definition “genetic nonlinearity”, clearly demonstrated a significant influence of assembly staging on stress deformed state of the building frame;

– to estimate the sufficiency of the load carrying ability, strength and crack resistance of a building (a separate construction) at each separate cycle considering phase by phase accumulated tensions and deformations;

– to use effectively the possibility of building constructions and developing from them at the stage of building systems erection with the purpose of labor and financial expenses minimization for construction, and also reducing the construction period. This effect is achieved by reducing the quantity of casing, reinforcement (more effective location considering the assembling), lack of necessity of waiting for required strength development of cast-in-place concrete of the lower floors for the assembling of the higher floors (common for hybrid precast/cast-in-place building) etc.;

– to regulate stress deformed state of the building (a separate construction) by means of assembling phasing, sequence of loading of erected constructions, change of structural design during strength development etc., that is addition to already known force regulators (reinforcement and its preliminary tension, prior arranged cracks).

Based on the above arguments and taking into account the earlier research [11–21] of various foreign and domestic scientists, the authors of this article defined the goal of studying the impact of the construction period of the life cycle of the building in its stress-deformed state. To achieve this goal have been formulated the following tasks, including: numerical study of a flat frame precast and cast-in place structure, carried out with and without taking into account the phased process of construction; analysis the stress-deformed state precast and cast-in place structure; analysis of phased "viability" of the frame construction for the possibility of perception of current loads.

Methods

The numerical investigations (taking into account the physical nonlinearity) were carried using the software package "Lira” out of the model above mentioned plane frame of precast and cast in place casing including (Figure 1): built-up column of cross-section 100x100 mm (concrete cl. B25) and precast and cast-in-place beams. Which are consisting from assembled part of cross-section 100x100(h) mm (concrete cl.B25) and cast-in-place part of cross-section 100x60(h) mm (concrete cl. B15). For allowance of work nonlinearity of the concrete and reinforcement, bi- and trilinear diagrams of deformation have been used, put to Russian Set of Rules SP 63.13330.2012. Calculations were performed in the following variants: with division for phasing of the construction according to above mentioned algorithm (P-1) and without division for stages of assembling, that is calculation of completely erected construction of the cross frame was performed. As a result of the subsequent analysis, in addition to the consideration of the strain state, considerable attention was given to consideration of the stress state in the body of the frame construction (in the above studies [11–21] analysis of efforts was carried out mostly in rod and flat items).

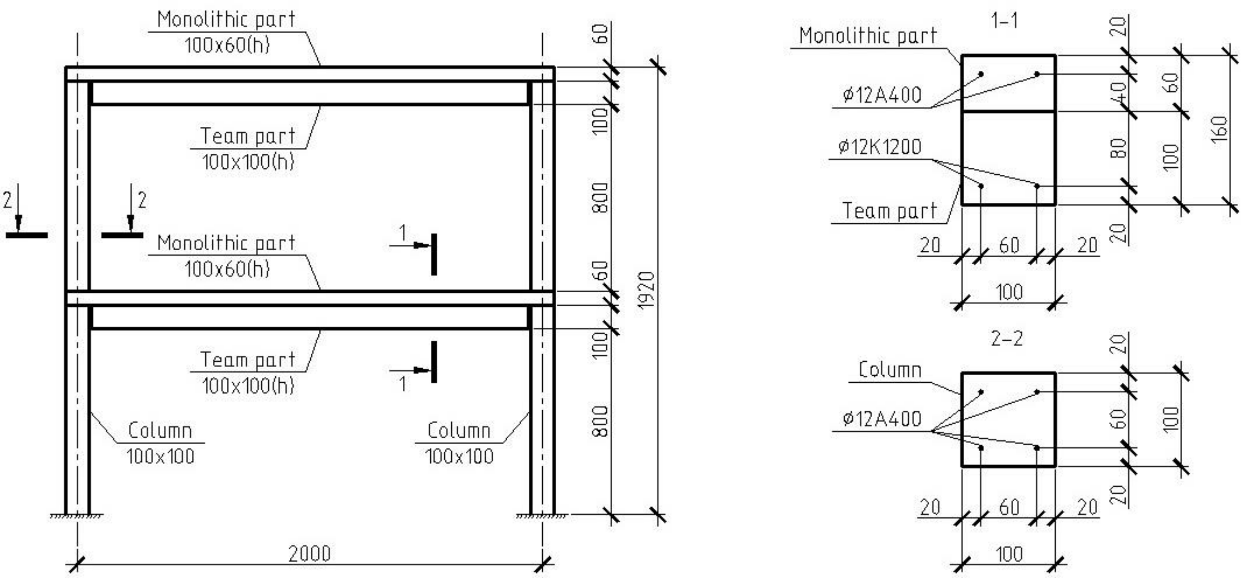

Figure1. The drawing of the numerical model

Results

Let us trace the character of the changes of a stress-deformed state of a precast with cast-in-place frame during its life at the example of model P-1. In the process of unit beams erection of a building upcoming framework, first of all floor-by-floor prefabricated frame construction is made, which consists from columns and leaned on them prefabricated beam parts. The prefabricated beam parts due to posttensioned reinforcement become pretensioned (Figure.2). Precast beam part initially bows under the effect of its own weight, and then bows outward in proportion to the preliminary tensioned steel stress. As the result, in the end of all framework unit beams erection and tensioning of the steel (stage 6), the cross section of the unit beam of the1-st floor is almost centrally pressed with a small difference in the tension at the upper and lower border at the bay center (1.98–2.03 MPa). The cross section of the upper beam is off-center pressed and bowed upwards with the most pressed lower zone in the center of the bay – 2.2 MPa and the less pressed upward zone – 1.68 MPa.

The stress rate in the frame elements do not exceed the admissible limit value, which is quite expectable, considering the fact of the construction loading only with the own weight and preliminary clamping. However, the pulling stress in the column, after the completion of the steel posttensioning have reached 1 MPa. It indicates the possibility of cracks development on the columns internal border at any tiny changes of the parameters of structural design (concrete class lowering, change of the steel posttension, change geometrical parameters of the scheme etc.). Due to that, it is required to pay attention to forces developing in the construction during the erection process, but unfortunately, the project designers do not always observe this.

It should be pointed out that at this stage despite not complete readiness of the frame construction, constructive scheme is already statically indeterminate and geometrically unchangeable system with rigidly restrained columns and pinned connection of beams with columns. This allows to use it successfully (frame) for further erection loads without any special holding equipment.

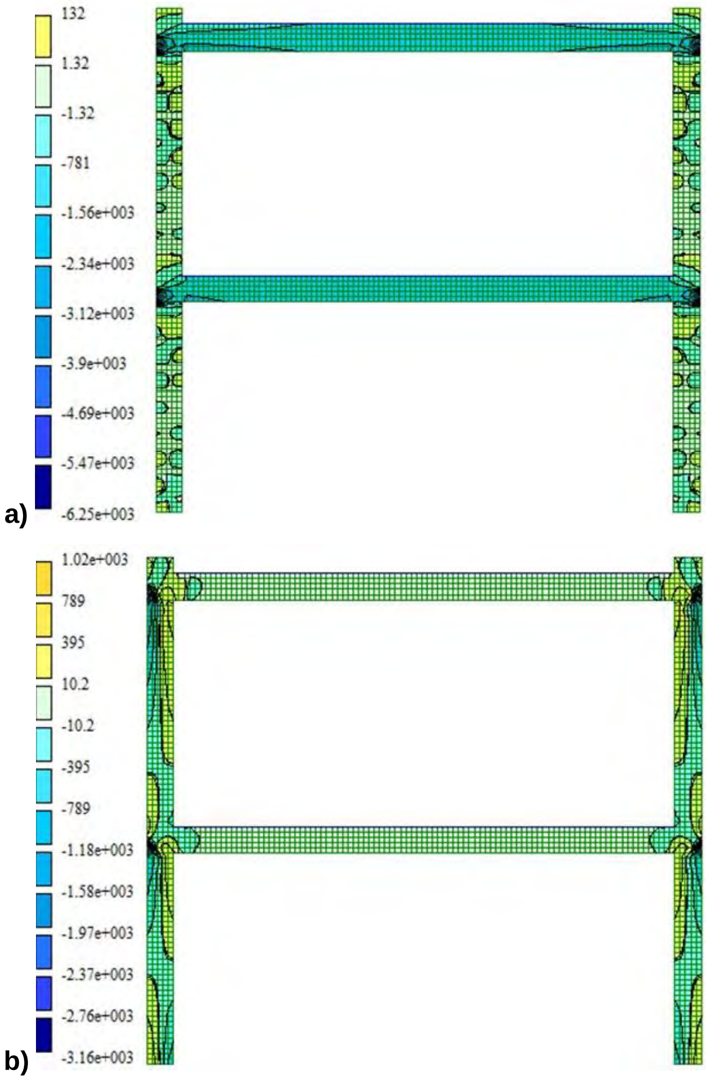

Figure 2. Strain state of the model P-1 at 6-th cycle loading a – Nx; b – Nz

Koyankin A.A., Mitasov V.M. Stress-strain state of precast and cast-in place buildings. *Magazine of Civil Engineering*. 2017. No. 6. Pp. 175–184. doi: 10.18720/MCE.74.14.

Applied further (stage 7) erection loads (weight of unit floor slab, weight of newly laid cast-in-place concrete etc.) lead to new change of strain distribution in the frame construction elements. Unit beams work already as flexible elements with strained and pressed zones (at the bottom strain reaching up to 0.2 MPa, on the top pressing together reaching 4.9 MPa). Upon that, their connection with the column is still pinned (Figure 3). The force of thrust and tight pressing by means of column pretension steel to the beam, force the column to deform from the flat area with development of exposed face strain up to 0.8 MPa and inner face press up to 2.4 MPa. The force in the lower longitudinal reinforcement are 11.6 kH. As the maximum tension stress in the concrete of the frame elements have not been reached, it can be concluded that cracks at this stage are not developed. Before additional erection load beams had upward bend – 0.15 mm, with further bend up to +0.61 mm.

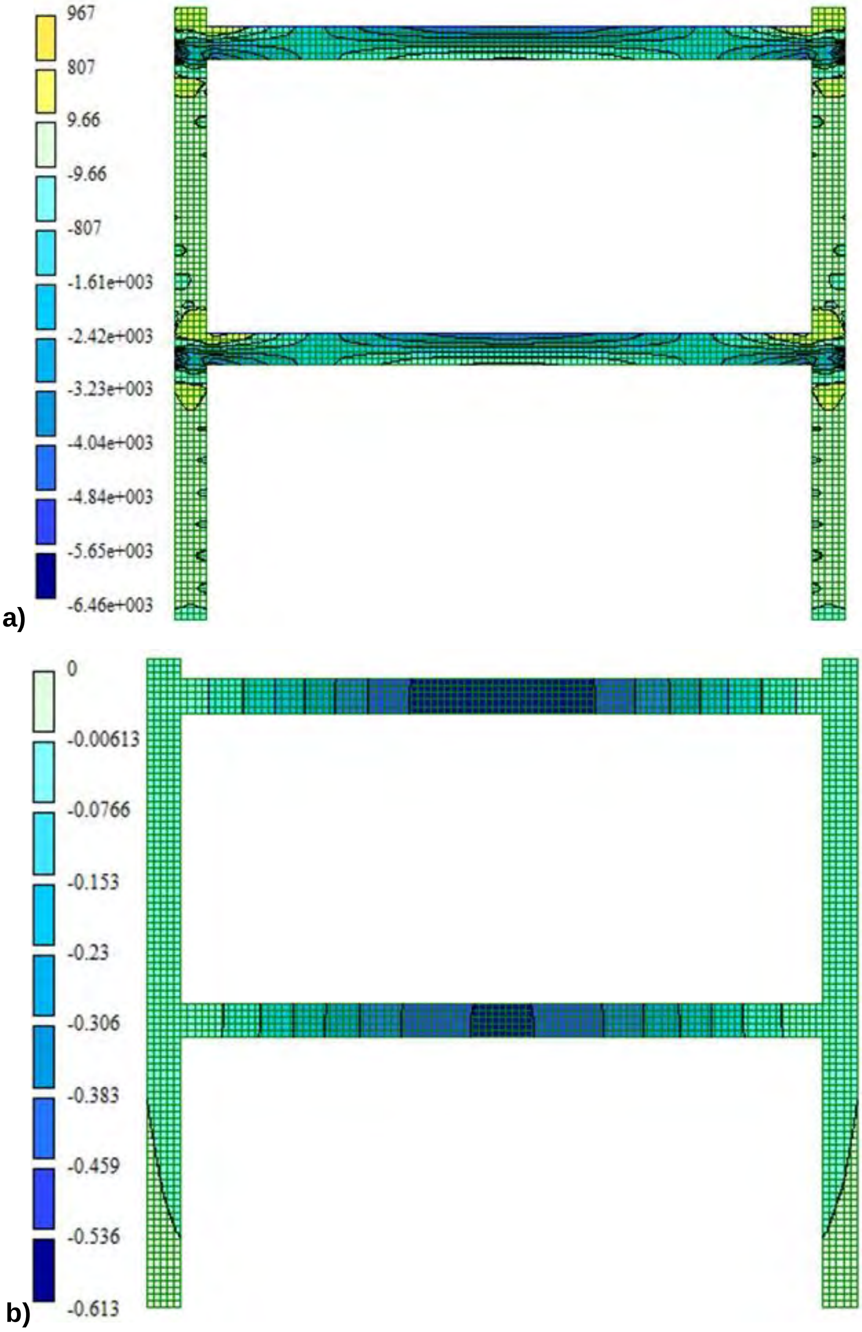

Figure 3. Stress deformed state of model P-1 at 7-th loading cycle: a – Nx; б – sags

From the moment of gaining of required resistibility, but without additional loading (stage 8), stress deformed state at precast parts of columns and beams is still kept. Meanwhile at site concrete tensioning has not yet developed (shrinkage-related and other primary stress are not taken into consideration). From this moment, the frame construction is also statically indeterminable system but with more rate of static indeterminateness by means of rigid connection of precast with cast-in-place beams with column. This frame is in full construction readiness can bear additional erection loading (weight of the floor, walls, carrying wall etc.), and also operational loads as well.

With the more loading (stage 9) stress deformed state again will be different from the previous stage and this results in complex stressed state of bending precast with cast-in-place element. Particularly, precast part with compressive stress, developed earlier, bears more stress (beam of the 1-st floor – 5.45 MPa and beams of the 2-nd floor – 6.6 MPa), than cast-in-place (beam of the 1-st floor – 4.51 MPa and the beam of the2-nd floor – 5.25 MPa). Despite the location of its outer compression area, inside of cross section (closer to the center) of precast with cast-in-place element. Similarly, basing on earlier involvement into operation of precast part and post strain availability, more stress is in the lower longitudinal reinforcement of the precast part (the beam of the 1-st floor – 16.5 kN and the beam of the 2-nd floor – 18.4 kN). Than in the higher pier support reinforcement of the cast-in-place part (the beam of the 1-st floor – 5.1 kN and the beam of the 2-nd floor – 1.4 kN).

Tensile stress in the support zone of the precast part of the beam cross section have not exceeded the limit value 1.05 MPa, that indicates of lack of cracks in this part (Figure 4). At the same time in the center of the bay of precast element cracks develop. Beams bending at this cycle reach up to 2 mm.

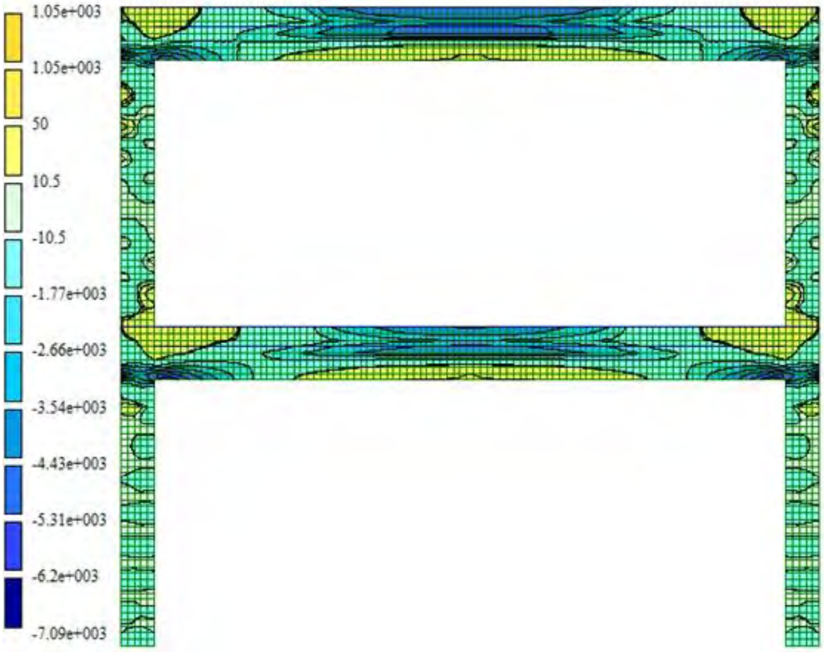

a)

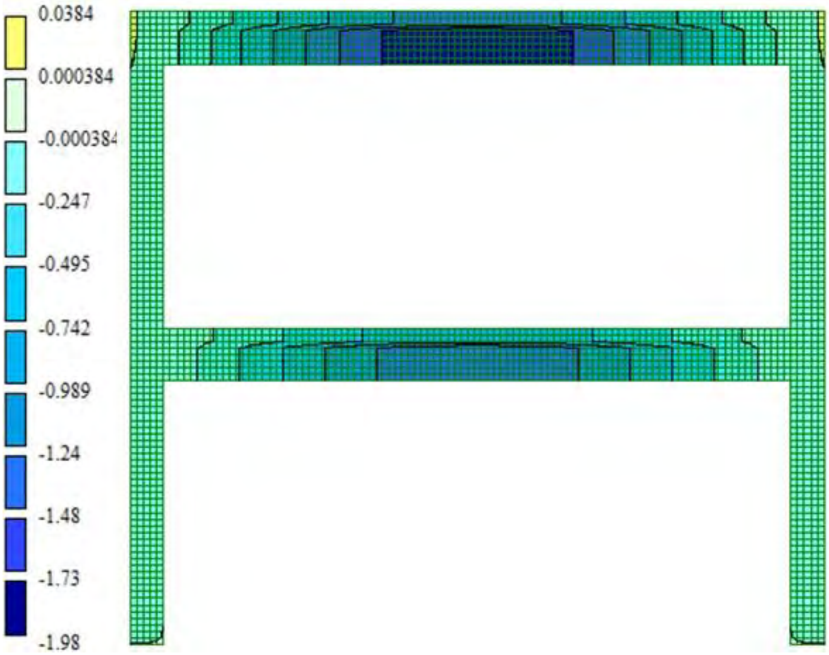

b)

Figure 4. Stress deformed state of model P-1 with full loading : a – Nx; б – sags

Comparing the picture of stress in the models P-1 and P-2, but not analyzing at the level of numeral value, there is a considerate quality difference at stress deformed state of frame beams. It is indicated in that maximal strain, considering gradual construction in the concrete, is focused in the farthest compressed fiber of the precast unit. Meanwhile at standard classic estimation that is without assembling and with once applied loadings, maximal strain values will be in the farthest fiber of the cast-in place part (Figure 5). As in the model P-1 and in the model P-2 the strained is the lower edging of the precast part, where the extreme tension stress are 1.05 MPa. This indicates for the cracks development under the full loading of construction.

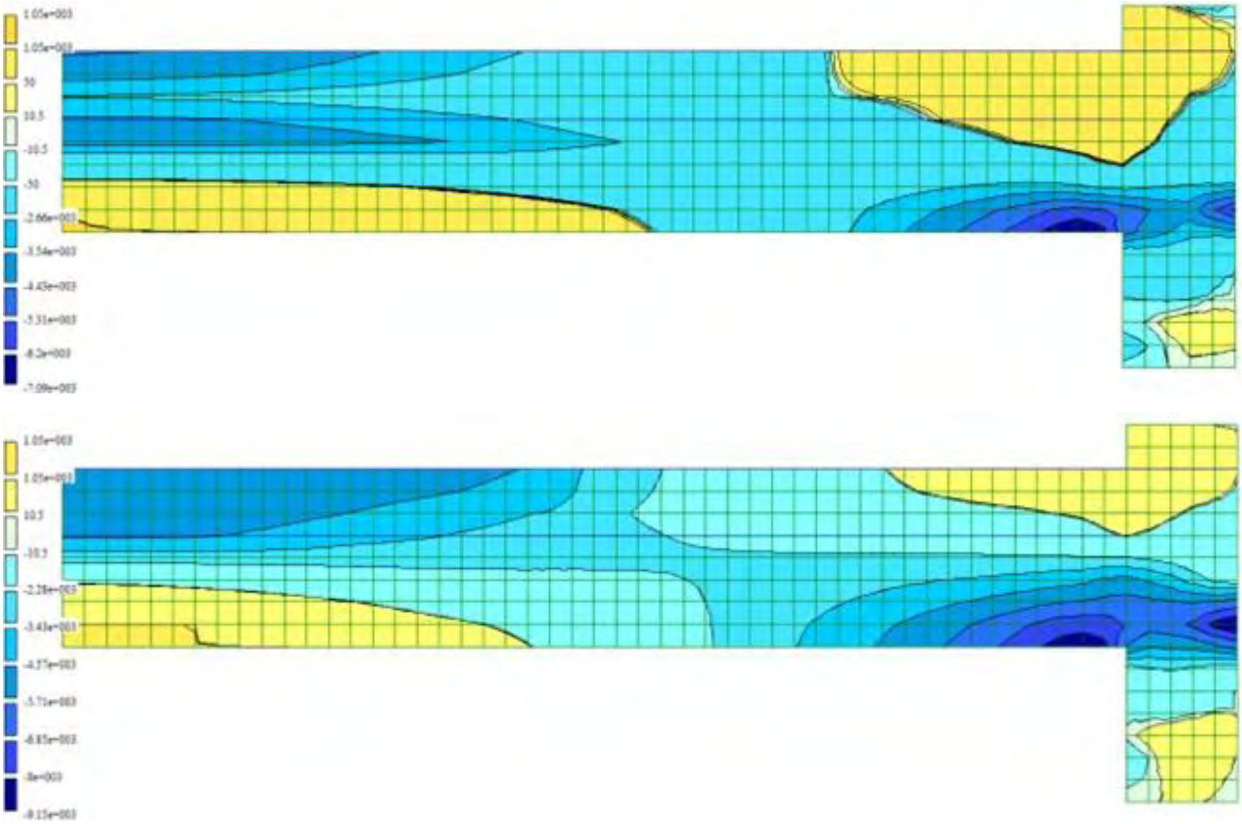

Figure 5. Stress deformed state of the 1-st floor under the full loading: a – P-1; b – P-2

In the model P-2 the maximal stress, developed on the surface of the upper edging of the cast-in place part, has reached the value of 0.6 MPa, meanwhile in the precast part the stress reach 4.53 MPa. In the case of dividing the construction existence for the individual stages of the life cycle the extreme values in the precast part of the beam reach 6.6 MPa, while in the cast-in place concrete the stress is lower and are 4.2 MPa. This fact is caused by that the precast concrete is involved into the process earlier, rather than cast-in place and by the time of gaining of the required strength by the cast-in place concrete and the beginning of the load bearing, in the precast concrete strong stress have already developed. Further, in the course of loading of the precast with cast-in place element, the strain in the precast part is increasing, although with the lower intensity. Thus the precast part is more stressed, that is demanding the proper engineering, and that forces in the cast-in place concrete are of the lower value considering the construction period, indicates the possibility of use of the concrete of the lower strength, including light concrete.

On the supporting structure the stretching forces in the upper zone, using the classic type of calculation and considering “life cycles” are approximately 0.7–0.8 MPa. Compressing stress in the beam concrete of the columns in the model P-1 are 8.7 MPa, and in the model P-2–7.27 MPa.

The real bendings in the construction while making estimations considering stages of the construction period are larger, than bendings, which were calculated at simultaneous readiness of the whole building and simultaneousness of the whole loading application. Particularly, considering the gradual assembling the extreme bendings have reached 1.98 mm, while without “life cycles” – 1.73 mm. This difference is explained by the earlier involvement into the process of the precast part, which has the lesser strength, than precast with cast-in place edging that leads to the accumulation of more size of the bendings until the moment of gaining the strength by the cast-in place concrete (this value in the example is 0.61 mm). Hereafter after the gaining of the required strength by the cast-in place concrete, the increase of the bending is not so significant, as the bending stiffness of the cross section has become higher (bending gain is 1.12 mm).

Comparing the results obtained by the authors of this article in the course of the study with the results obtained by other scientists [11–21], it is possible to note the generality of the conclusion about the execution of the calculation according to the classical technology. When the object is in a ready state, it introduces significant distortion in the stress and deformed state of the design scheme as the building as a whole and its individual structural elements. In particular, the pilot studies carried out in the framework of [12], showed a similar pattern of distribution of deformations along the height of the section, as the numerical study presented in this article. Namely, the later inclusion of the cast-in place concrete leads to the difference of deformations at the interface concretes. In this case, compressive stresses in the precast part is greater than in the monolithic part bending precast and cast-in place element.

Conclusions

1. In the calculations of bearing structures of buildings and subsequent design must take into account the prehistory of the work of the structure at an earlier stage, i.e. to develop the project of the building (a separate structure) taking into account the period of its life cycle. Otherwise, there is a significant distortion of the actual stress-deformed state of the building as a whole and its separate structures.
2. By analogy with requirements to precast concrete structures to make calculations at all stages (production, clamping, transportation, construction etc.) at precast with cast-in place frame erection, it is required to make checkup tests at each stage of the life cycle of the construction.
3. Considering the phasing of constructions erection will allow to avoid initial mistakes at estimation of stress calculation in the body, separate elements and the whole building as well.
4. The real picture of the stress state of precast with cast-in place (especially bending) element, received taking into account the prehistory of the existence of structure in the earlier stages, differs from the pattern of stress distribution. Moreover, these differences are not only quantitative but also qualitative (the maximum compression in the precast with cast-in place girders at the account stages of the life cycle is observed in precast part of the element, while in the traditional calculation – in cast-in place part).

Reference

1. Kruzhkov N.N. *Vysotki stalinskoy Moskvy. Naslediye epokhi* [Tall buildings of Stalin's Moscow. Heritage of epoch]. Moscow: Tsentrpoligraf, 2014. 365 p. (rus)
2. *Vysotnoye stroitelstvo Rossii na rubezhe vekov* [Tall building of Russia on the border of ages] [Online]. URL: http://www.forum-100.ru/pressroom/vysotnoe-stroitelstvo-rossii-na-rubezhe-vekov/ (date of application: 22.12.2016). (rus)
3. Shumeyko V.I., Kudinov O.A. Ob osobennostyakh proyektirovaniya unikalnykh, bolsheproletnykh i vysotnykh zdaniy i sooruzheniy [About the design features of unique, long-span and high-rise buildings and structures]. *Inzhenernyy vestnik Dona.* 2013. No. 4. (rus)
4. Akimov P.A. *Osobennosti proyektirovaniya i vozvedeni-ya. Vysotnyye zdaniya i drugiye unikalnyye sooruzheniya Kitaya* [The features of design and construction. The high-rise buildings and other unique structures China]. Moscow: ASV, 2009. 816 p. (rus)
5. Voylokov I.A. Razvitiye rynka sbornykh zhelezobet-onnykh konstruktsiy i yego perspektivy [The development of the market of precast concrete structures and its prospects]. *Infstroy.* 2008. No. 1/2 (37/38). Pp. 50–53. (rus)
6. Stashevskaya N.A., Malov A.N., Nikolenko Yu.V. Ekspluatatsiya zdaniy na osnove legkikh metallicheskikh konstruktsiy [Operation of buildings based on light metal structures]. *Vestnik RUDN. Seriya: Inzhenernyye issledo-vaniya.* 2011. No. 2. Pp. 18–22. (rus)
7. Packer J.A., Wardenier J., Zhao X., Van der Vegte A., Kurobane Y. *Design Guide for Rectangular Hollow Section (RHS) Joints.* Second Edition. Toronto, 2009. 149 p.
8. Calavera J. *Manual for Detailing Reinforced Concrete Structures to EC2.* London, 2012. 495 p.
9. Shembakov V.A. *Sborno-monolitnoye karkasnoye*

Литература

1. Кружков Н.Н. Высотки сталинской Москвы. Наследие эпохи. М.: Центрполиграф, 2014. 365 с.
2. Высотное строительство России на рубеже веков [Электронный ресурс]. URL: http://www.forum-100.ru/pressroom/vysotnoe-stroitelstvo-rossii-na-rubezhe-vekov/ (дата обращения: 22.12.2016).
3. Шумейко В.И., Кудинов О.А. Об особенностях проектирования уникальных, большепролётных и высотных зданий и сооружений // Инженерный вестник Дона. 2013. № 4.
4. Акимов П.А. Особенности проектирования и возведения. Высотные здания и другие уникальные сооружения Китая. М.: АСВ, 2009. 816 с.
5. Войлоков И.А. Развитие рынка сборных железобетонных конструкций и его перспективы // Инфстрой. 2008. № 1/2 (37/38). С. 50–53.
6. Сташевская Н.А., Малов А.Н., Николенко Ю.В. Эксплуатация зданий на основе лёгких металлических конструкций // Вестник РУДН. Серия: Инженерные исследования. 2011. № 2. С. 18–22.
7. Packer J.A., Wardenier J., Zhao X., Van der Vegte A., Kurobane Y. Design Guide for Rectangular Hollow Section (RHS) Joints. Second Edition. Toronto, 2009. 149 p.
8. Calavera J. Manual for Detailing Reinforced Concrete Structures to EC2. London, 2012. 495 p.
9. Шембаков В.А. Сборно-монолитное каркасное домостроение. Руководство к принятию решения. Чебоксары: ООО «Чебоксарская типография № 1», 2005. 119 с.
10. Мордич А.И., Белевич В.Н., Симбиркин В.Н., Навой Д.И. Опыт практического применения и основные результаты натурных испытаний сборно-монолитного каркаса БелНИИС // Бюллетень строительной техники. 2004.

domostroyeniye. Rukovodstvo k prinyatiyu resheniya [Prefabricated monolithic frame house construction. A guide to decision making]. Cheboksary: OOO "Cheboksarskaya tipografiya № 1", 2005. 119 p. (rus)
10. Mordich A.I., Belevich V.N., Simbirkin V.N., Navoy D.I. Opyt prakticheskogo primeneniya i osnovnyye rezultaty naturnykh ispytaniy sborno-monolitnogo karkasa BelNIIS [Experience of practical application and the main results of field tests of prefabricated monolithic frame. Belgorod scientific research institute for construction]. *Byulleten stroitelnoy tekhniki.* 2004. №8. Pp. 8–12. (rus)
11. Perelmuter A.V. *Besedy o stroitelnoy mekhaniki* [Talk about building mechanics]. Moscow: ASV, 2014. 251 p. (rus)
12. Povetkin M.S. *Napryazhenno-deformirovannoye sostoyaniye usilennykh pod nagruzkoy zhelezobetonnykh izgibayemykh prednapryazhennykh elementov* [The stress-deformed state of reinforced under load of prestressed concrete bending elements]. PhD thesis 05.23.01. Kursk, 2009. 187 p. (rus)
13. Skobeleva Ye.A. *Deformirovaniye prednapryazhennykh zhelezobetonnykh izgibayemykh ele-mentov sostavnogo secheniya* [Deformation of prestressed concrete bending elements of composite sections]. PhD thesis 05.23.01. Orel, 2008. 208 p. (rus)
14. Kabantsev O.V., Karlin A.V. Raschet nesushchikh konstruktsiy zdaniy s uchetom istorii voz-vedeniya i poetapnogo izmeneniya osnovnykh parametrov raschetnoy modeli [Calculation of bearing structures of buildings with account for the history of the erection and the gradual changes of the main parameters of the analysis model]. *Promyshlennoye i grazhdanskoye stroitelstvo.* 2012. No. 7. Pp. 33–35. (rus)
15. Kabantsev O.V., Tamrazyan A.G. Allowing for changes in the calculated scheme during the analysis of structural behavior. *Magazine of Civil Engineering.* 2014. No. 5. Pp. 15–28. (rus)
16. Gorodetskiy A.S., Yevzerov I.D. *Kompyuternyye modeli konstruktsiy* [Computer Models of Designs]. Kiyev: Fakt, 2007. 394 p. (rus)
17. Gorodetskiy A.S., Batrak L.G., Gorodetskiy D.A., Laznyuk M.V., Yusipenko S.V. *Raschet i proyektirovaniye konstruktsiy vysotnykh zdaniy iz monolitnogo zhelezo-betona* [Calculation and design of structures of high-rise buildings of reinforced concrete]. Kiyev: Fakt, 2004. 106 p. (rus)
18. Perelmuter A.V., Slivker V.I. *Raschetnyye modeli sooruzheniy i vozmozhnost ikh analiza* [Rated models of constructions and possibility of their analysis]. Kiyev: Izd-vo «Stal», 2002. 600 p. (rus)
19. Kim H.S., Shin A.K. Column shortening analysis with lumped construction sequences. *Procedia Engineering.* 2011. Vol. 14. Pp. 1791–1798.
20. Pan B., Li G. Finite element simulation of cantilever construction structure. *International Conference on Innovations in Electrical and Civic Engineering (ICIECE 2012).* Phuket. 2012. Pp. 181–186.
21. Shi Q., Lu A., Zhao H., Wu A. Development and application of the adaptive mesh technique in the three-dimensional numerical simulation of the welding process. *Journal of Materials Processing Technology.* 2002. Vol. 121. No. 2-3. Pp. 167–172.
22. Capriccioli A., Frosi P. Multipurpose ANSYS FE procedure for welding processes simulation. *Fusion Engineering and Design.* 2009. Vol. 84. No. 2–6. Pp. 546–553.
23. Song J.Y. Simulation and analysis of construction process of Juancheng Yellow River Highway. *Journal of Harbin Institute of Technology.* 2010. Vol. 42. No. 1. Pp. 266–269.
24. Ates S. Numerical modeling of continuous concrete box girder bridges considering construction stages. *Applied Mathematical Modeling.* 2011. Vol. 35. No. 8. Pp. 3809–3820.

№ 8. С. 8–12.
11. Перельмутер А.В. Беседы о строительной механики. М.: АСВ, 2014. 251 с.
12. Поветкин М.С. Напряжённо-деформированное состояние усиленных под нагрузкой железобетонных изгибаемых преднапряжённых элементов: Дис. … канд. техн. Наук: 05.23.01. Курск, 2009. 187 с.
13. Скобелева Е.А. Деформирование преднапряжённых железобетонных изгибаемых эле-ментов составного сечения: Дис. … канд. техн. Наук: 05.23.01. Орёл, 2008. 208 с.
14. Кабанцев О.В., Карлин А.В. Расчёт несущих конструкций зданий с учётом истории воз-ведения и поэтапного изменения основных параметров расчётной модели // Промышленное и гражданское строительство. 2012. № 7. С. 33–35.
15. Кабанцев О.В., Тамразян А.Г. Учёт изменений расчётной схемы при анализе работы конструкции // Инженерно-строительный журнал. 2014. № 5. С. 15–28.
16. Городецкий А.С., Евзеров И.Д. Компьютерные модели конструкций. Киев: Факт, 2007. 394 с.
17. Городецкий А.С., Батрак Л.Г., Городецкий Д.А., Лазнюк М.В., Юсипенко С.В. Расчёт и проектирование конструкций высотных зданий из монолитного железобетона. Киев: Факт, 2004. 106 с.
18. Перельмутер А.В., Сливкер В.И. Расчётные модели сооружений и возможность их анализа. Киев: Изд-во «Сталь», 2002. 600 с.
19. Kim H.S., Shin A.K. Column Shortening Analysis with Lumped Construction Sequences // Procedia Engineering. 2011. Vol. 14. Pp. 1791-1798.
20. Pan B., Li G. Finite element simulation of cantilever construction structure // International Conference on Innovations in Electrical and Civic Engineering (ICIECE 2012) Phuket, 2012. Pp. 181–186.
21. Shi Q., Lu A., Zhao H., Wu A. Development and application of the adaptive mesh technique in the three-dimensional numerical simulation of the welding process // Journal of Materials Processing Technology. 2002. Vol. 121. № 2-3. Pp. 167–172.
22. Capriccioli A., Frosi P. Multipurpose ANSYS FE procedure for welding processes simulation // Fusion Engineering and Design. 2009. Vol. 84. № 2–6. Pp. 546–553.
23. Song J.Y. Simulation and analysis of construction process of Juancheng Yellow River Highway // Journal of Harbin Institute of Technology. 2010. Vol. 42. No. 1. Pp. 266–269.
24. Ates S. Numerical modeling of continuous concrete box girder bridges considering construction stages // Applied Mathematical Modeling. 2011. Vol. 35. № 8. Pp. 3809–3820.
25. Mitsui K., Kanemitsu T. Construction process analysis for structure by genetic algorithm // Proceedings of the 40 Anniversary Congress "Shell and Structures: From recent Past to the next Millennium". Madrid, 1999. Pp. 31–36.
26. Aoyama H. Design of Modern Ighrise Reinforced Concrete Structures. London, 2001. 462 p.

25. Mitsui K., Kanemitsu T. Construction process analysis for structure by genetic algorithm. *Proceedings of the 40 Anniversary Congress "Shell and Structures: From recent Past to the next Millennium".* Madrid, 1999. Pp. 31–36.

26. Aoyama H. *Design of Modern Ighrise Reinforced Concrete Structures.* London, 2001. 462 p.

Alexander Koyankin,
+7(391)2934711; KoyankinAA@mail.ru

Valery Mitasov,
+7(913)9122364; эл. почта: mitassovv@mail.ru

Александр Александрович Коянкин,
+7(391)2934711; эл. почта: KoyankinAA@mail.ru

Валерий Михайлович Митасов,
+7(913)9122364; эл. почта: mitassovv@mail.ru

Koyankin A.A., Mitasov V.M. Stress-strain state of precast and cast-in place buildings. *Magazine of Civil Engineering*. 2017. No. 6. Pp. 175–184. doi: 10.18720/MCE.74.14.